SYNTHESIS AND DEVELOPMENT OF PROTEASOME AND KINASE FLUORESCENT ASSAYS FOR QUANTITATION OF ENZYME ACTIVITY

Finith E. Jernigan, III

A dissertation submitted to the faculty of the University of North Carolina at Chapel Hill in partial fulfillment of the requirements for the degree of Doctor of Philosophy in the Department of Chemistry.

Chapel Hill
2013

Approved by:

David Lawrence

Nancy Allbritton

Eric Brustad

Klaus Hahn

Marcey Waters

ABSTRACT

FINITH E. JERNIGAN, III: Synthesis and Development of Proteasome and Kinase Fluorescent Assays for Quantitation of Enzyme Activity.

Under the direction of David S. Lawrence.

Enzyme activity is a major component of signal transduction. However, many current methods of enzyme detection, such as fluorophore-labeled antibodies or western blotting, quantitate enzyme concentration and lack the ability to determinate activity levels. This can lead to imprecise depictions of signal transduction pathways. For example, the cyclic-AMP dependent protein kinase (PKA) is ubiquitously expressed, but activity is highly regulated. Near the mitochondria, PKA activity is responsible for the activation of apoptotic pathways and as a consequence is highly regulated. For a complete understanding of apoptotic signal transduction, it is necessary to precisely define PKA activity. Gaining an increased understanding of enzyme activity is the goal of this thesis.

In pursuit of this goal, we have developed chemical tools for the quantitation of PKA activity, as well as the activities of the proteasome. An assay for PKA activity was developed termed “deep quench” using primarily electrostatic interactions between a positively charged fluorescently-labeled PKA substrate and a negatively charged non-fluorescent quenching dye. Upon phosphorylation of the fluorescently-labeled peptide substrate by PKA, interaction between the positively charged residues of the substrate and the negatively charged dye weaken, causing a lower affinity for quenching dye. Since the quenching dye has an

absorbance near the emission of the PKA-substrate fluorophore, the energy transfer between the fluorophore and dye weakens as well, producing extraordinary fluorescent enhancements (up to 150-fold).

Using the "deep quench" system, suborganelle mitochondrial PKA activity was revealed as a relative matrix/intermembrane space/outer membrane (85:6:9) distribution of PKAin bovine heart mitochondria. While this sensor works beautifully *in vitro*, applying the system in an intracellular fashion has proven difficult due to the system's bimolecular nature. We have attempted to solve this problem by covalently linking the non-fluorescent dye carboxy Acid Blue 40 (cAB40) to the fluorescently labeled PKA substrate. However, due to the FRET mechanism of fluorescent quenching, no fluorescent increase was observed upon substrate phosphorylation. To solve this problem, the cAB40 and fluorescent PKA substrate were attached to 100 nm silica nanoparticles. Upon phosphorylation, a 2.2-fold fluorescent increase was observed. cAB40 was more completely characterized and found to quench fluorophores with a wide range of spectral properties. In further studies, Trypsin substrates were assembled, as well as a photolabile cassette, which furnished up to 110-fold enhancements in fluorescence. After demonstrating the utility of the cAB40 quenching dye, the technology was applied to biosensors for the Caspase-like (proteasome β1-subunit), Trypsin-like (proteasome β2-subunit), and Chymotrypsin-like (proteasome β5-subunit) activities of the proteasome. The specificity for the Caspase-like (proteasome β1-subunit) and Chymotrypsin-like (proteasome β5-subunit) activities of the proteasome was demonstrated. Overall this body of work demonstrates the utility of the "deep quench" PKA and proteasome sensors towards the goal of quantifying enzyme activity.

ACKNOWLEDGEMENTS

I would like to thank David Lawrence for his outstanding support, mentorship, and creativity.

I would like to thank my thesis committee for their guidance and insight: Nancy Allbritton, Eric Brustad, Klaus Hahn, and Marcy Waters.

I would also like to thank David Smalley of the UNC proteomics centers for help obtaining all high resolution mass spectrometry.

Last, but most importantly, I would like to thank my family for all their support: Beth Jernigan, Finith Jernigan II, Devin Jernigan and my fiancée Holly Travis.

TABLE OF CONTENTS

LIST OF TABLES

LIST OF FIGURES

LIST OF SCHEMES

ABBREVIATIONS

A	Alanine
AB40	Acid Blue 40
ACN	Acetonitrile
AKAP	A-kinase anchor protein
AKAR	A-kinase activity reporter
Arg	Arginine
Asn	Asparagine
Asp	Aspartic Acid
Boc	t-Butoxycarbonyl
C	Cysteine
cAB40	Carboxy Acid Blue 40
cAMP	Cyclic adenosine monophosphate
CHX	Cycloheximide
Cys	Cysteine
D	Aspartic Acid
Dab	Diaminobutyric Acid
DCM	Dichloromethane
DIPEA	Diisopropylethyl amine
DMF	Dimethylformamide
DMNB-cAMP	P-(4,5-dimethoxy-2-nitrobenzyl) cAMP
Fmoc	N-9-Fluorenylmethyloxycarbonyl
FRET	Förster resonance energy transfer
FRAP	Fluorescence Recovery After Photobleaching

FsK	Forskolin
G	Glycine
GFP	Green Fluorescent Protein
Gln	Glutamine
Glu	Glutamic Acid
Gly	Glycine
H	Histidine
HBTU	2-(1H-Benzotriazole-1-yl)-1,1,3,3-tetramethyluronium hexafluorophosphate
HCTU	2-(6-Chloro-1-H-benzotriazole-1-yl)-1,1,3,3-tetramethylaminium haxafluorophosphate
HDAC	Histone Deacetylase
His	Histidine
HOBT	N-hydroxybenzotriazole H_2O
HPLC	High Pressure Liquid Chromatography
Ile	Isoleucine
K	Lysine
Leu	Leucine
Lys	Lysine
Met	Methionine
Mtt	4-methyltrityl
NEB	Nuclear Envelop Breakdown
Nle	Norleucine
NP	Nanoparticle
P	Proline
Pbf	2, 2, 4, 6, 7-Pentamethyl-dihydrobenzofurane-5-sulfonyl
PEG	Polyethylene glycol

Phe	Phenylalanine
PKA	cyclic-AMP Dependent Protein Kinase
PKG	Protein kinase G
Pro	Proline
Q	Glutamine
R	Arginine
S	Serine
Ser	Serine
SPPS	Solid Phase Peptide Synthesis
T	Threonine
tBu	t-Butyl
TFA	Trifluoroacetic acid
Thr	Threonine
TIPS	Triisopropyl silane
Trp	Tryptophan
Trt	Trityl
Tyr	Tyrosine
V	Valine
Val	Valine
W	Tryptophan
Y	Tyrosine

CHAPTER 1

INTRACELLULAR KINASE AND PROTEASOME ACTIVITY: AN INTRODUCTION

SIGNIFICANCE

Intracellular enzyme activity plays a key role in the coordination of cell processes such as mitosis, apoptosis, and cytotaxis. For example, the activity of the small nuclear GTPase Ran is responsible for control of assembly of the mitotic spindle, nuclear-envelope dynamics, and the timing of cell-cycle transitions during mitosis.[1] Additionally, cyclic-AMP dependent protein kinase (PKA) activity near the mitochondria regulates apoptosis through phosphorylation of the proapoptotic factor BAD (a BCL-2 family member protein).[2] Many methods provide a way to quantitate protein expression, such as antibody labeling or western blotting, among others. However, assessments of protein expression do not provide information on activity, which is generally responsible for signal transduction. For example, PKA is ubiquitously expressed, but PKA activity near the mitochondria is responsible for regulation of apoptosis.[3] Quantitative assessments of enzyme activity are essential for further understanding of signal transduction pathways. Unfortunately, few chemical probes exist with robust enzyme activity

[1] Clarke, P. R.; Zhang, C. *Nature reviews. Molecular cell biology* **2008**, *9*, 464–77.

[2] Harada, H.; Becknell, B.; Wilm, M.; Mann, M.; Huang, L. J.; Taylor, S. S.; Scott, J. D.; Korsmeyer, S. J. *Molecular cell* **1999**, *3*, 413–22.

[3] Pidoux, G.; Taskén, K. *Journal of molecular endocrinology* **2010**, *44*, 271–84.

measurement capabilities that are easily delivered to the cytoplasm. During this investigation we focused on development of chemical fluorescent biosensors capable of PKA activity quantitation and quantitation of the catalytic activities of the proteasome. As mentioned above, mitochondrial PKA activity is involved in the regulation of apoptosis through phosphorylation of the cytosolic protein Bcl-2-associated death promoter (BAD). The proteasome plays a large role in signal transduction through digestion of signaling proteins, therefore preventing participation of the digested proteins in signal transduction pathways. Due to this, measurement of intracellular proteasome activity can provide information on the regulation of a wide range of proteins. It has already been demonstrated that unusual fluctuations of proteasome activity are telltale sign of malignancies, making the proteasome an attractive target of chemotherapeutics.[4] Through this work, we have developed chemical biosensors of PKA and the proteasome and employed them towards the measurement of PKA and proteasome activity.

AN OVERVIEW OF BIOSENSORS FOR INTRACELLULAR IMAGING

Cells rely on vast signal transduction networks to respond to stimuli such as external force,[5] oxidative stress,[6] and chemotaxis.[7] Through study of cellular responses to stimuli, it has become abundantly clear that study of signal transduction requires quantitation of enzyme

[4] Yang, H.; Zonder, J. A.; Dou, Q. P. *Expert opinion on investigational drugs* **2009**, *18*, 957–71.

[5] Janmey, P.; McCulloch, C. *Annual review of biomedical engineering* **2007**, *9*, 1–34.

[6] Cataldi, A. *Current pharmaceutical design* **2010**, *16*, 1387–95.

[7] Emonet, T.; Cluzel, P. *Proceedings of the National Academy of Sciences of the United States of America* **2008**, *105*, 3304–9.

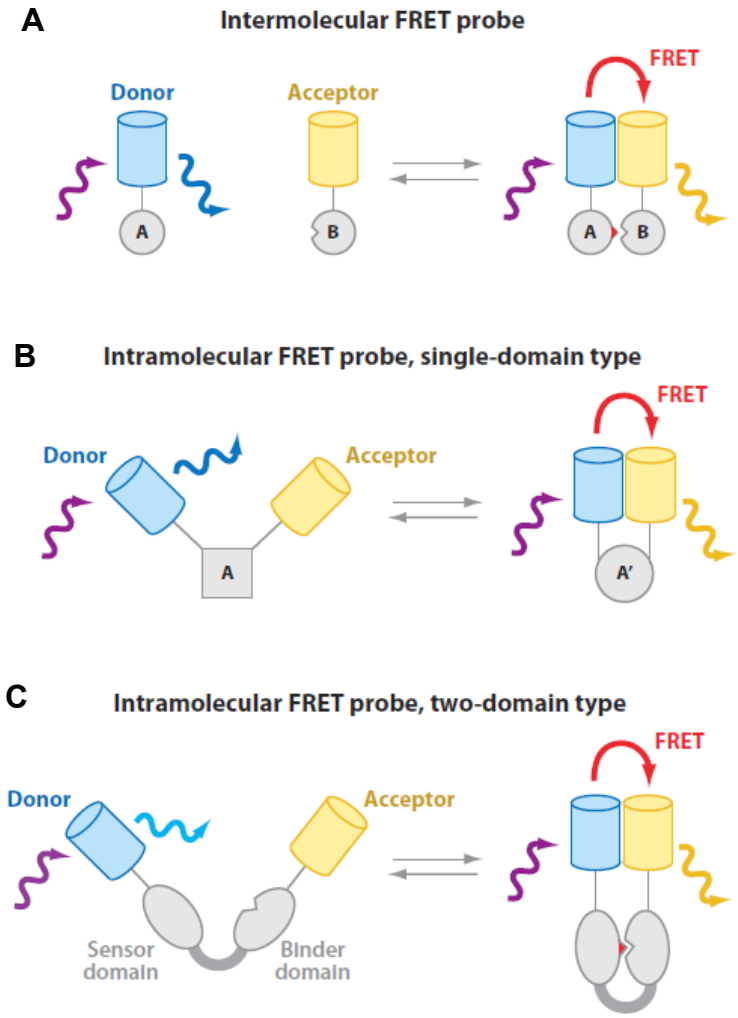

Figure 1.1 Reprinted from Kiyokawa, E.; Aoki, K.; Nakamura, T.; Matsuda, M. *Annual review of pharmacology and toxicology* **2011**, *51*, 337–58. with permission from *Annual Reviews*. Structure of genetically encoded Förster resonance energy transfer (FRET) probes. (*a*) Intermolecular FRET probes are designed to detect the protein-protein interaction. The donor and acceptor fluorophores are fused to the pair of proteins. When they form a complex, the distance between the donor and acceptor becomes close enough to cause FRET. (*b*) FRET can be used to detect the conformational change of proteins. In the simplest design of the intramolecular FRET probe, donor and acceptor fluorophores are fused to the proper position of the proteins of interest so that conformational change of the proteins alters the distance and/or topology of the donor and acceptor fluorophores, thereby resulting in an increase or a decrease in FRET efficiency. (*c*) The conformational change of the proteins of interest is often minute. Typical examples are the GTP-GDP exchange of small GTPases and phosphorylation of proteins. The domain that displays minimal conformational change upon signal perception is termed the sensor domain. This sensor domain is linked to the binder domain, which binds only when the sensor domain exhibits conformational change. The donor and acceptor sandwich the sensor domain–linker–binder domain complex so that the binding increases FRET.

activity. Activity/functional relationships have been discovered in a wide range of enzymes including kinases,[8] the proteasome,[9] GTPases,[10] and caspases.[11] Sensors capable of elucidating activity/function relationships have followed one of two distinct techniques: (1) FRET Green Fluorescent Protein (GFP)-based sensors employing phosphopeptide binding domains to yield measureable changes in fluorescence or (2) chemical probes employing bond cleavage, metal chelation, electrostatic interactions or environmentally-sensitive fluorophores to yield measurable changes in fluorescence upon enzyme action.

GFP-based sensors function through changes in Förster resonance energy transfer between a donor and acceptor fluorescent protein of properly selected photophysical properties. Changes in energy transfer efficiencies modulate the fluorescence of a donor and an acceptor GFP, resulting in a measurable signal. Actions resulting in measureable fluorescent changes of GFP-based sensors include: (a) protein-protein interactions, (b) conformational changes of a substrate, or (c) conformational changes between a fusion protein containing a sensor domain and binding domain (Figure 1.1).[12] Intermolecular GFP sensors of the first type are primarily used as sensors of protein-protein interaction, which is beyond the scope of this work (Figure 1.1a). Typical FRET-based GFP sensors for enzyme catalyzed reactions function via conformational change of the protein after catalysis (Figure 1.1b) or in the case of lack of conformation change, a change induced after interaction with a binding domain (Figure 1.1c).

[8] (1) Scott, J. D.; Newton, A. C. *BMC biology* **2012**, *10*, 61. (2) Yudushkin, I.; Schleifenbaum, A.; Kinkhabwala, A.; Neel, B. G.; Schultz, C.; Bastiaens, P. I. H. *Science* **2007**, *315*, 115–9.

[9] Finley, D. *Annual review of biochemistry* **2009**, *78*, 477–513.

[10] Kiyokawa, E.; Aoki, K.; Nakamura, T.; Matsuda, M. *Annual review of pharmacology and toxicology* **2011**, *51*, 337–58.

[11] Cataldi, A. *Current pharmaceutical design* **2010**, *16*, 1387–95.

[12] Kiyokawa, E.; Aoki, K.; Nakamura, T.; Matsuda, M. *Annual review of pharmacology and toxicology* **2011**, *51*, 337–58.

As an example (Figure 1.1b), the cyclic-AMP (cAMP) FRET sensor ICUE1 (Indicator for cAMP using Epac) functions using the Epac1 (Exchange Protein Activated by cAMP) binding domain located between a FRET GFP pair. A conformational change occurs upon cAMP binding resulting in a fluorescence change.[13] This strategy has been widely employed in many cases where proteins undergo a large conformational change upon activation.[14] However, many proteins do not undergo conformational changes upon activation. In this case, an additional binder domain is necessary to produce a conformational change (Figure 1.1c).[15] This strategy has been employed in the case of FRET reporters of glycosylation,[16] methylation,[17] phosphorylation,[18] and ubiquitination.[19] Although GFP-based FRET reporters are useful tools for enzyme activity imaging, the system does have disadvantages including: (1) difficulties establishing mammalian cells lines expressing the reporter, (2) the small dynamic range of the fluorescent readout, and (3) difficulty using multiple probes in microscopy due to spectrophotometric overlap.[20]

Chemical probes offer many advantages over GFP-based FRET sensors. Chemical probes

---

[13] DiPilato, L. M.; Cheng, X.; Zhang, J. *Proceedings of the National Academy of Sciences of the United States of America* **2004**, *101*, 16513–8.

[14] (1) Calleja, V.; Alcor, D.; Laguerre, M.; Park, J.; Vojnovic, B.; Hemmings, B. a; Downward, J.; Parker, P. J.; Larijani, B. *PLoS biology* **2007**, *5*, e95. (2) Fujioka, A.; Terai, K.; Itoh, R. E.; Aoki, K.; Nakamura, T.; Kuroda, S.; Nishida, E.; Matsuda, M. *The Journal of biological chemistry* **2006**, *281*, 8917–26. (3) Ananthanarayanan, B.; Fosbrink, M.; Rahdar, M.; Zhang, J. *The Journal of biological chemistry* **2007**, *282*, 36634–41.

[15] Aye-Han, N.-N.; Ni, Q.; Zhang, J. *Current opinion in chemical biology* **2009**, *13*, 392–7.

[16] Carrillo, L. D.; Krishnamoorthy, L.; Mahal, L. K. *Journal of the American Chemical Society* **2006**, *128*, 14768–9.

[17] Lin, C.-W.; Jao, C. Y.; Ting, A. Y. *Journal of the American Chemical Society* **2004**, *126*, 5982–3.

[18] Zhang, J.; Allen, M. D. *Molecular bioSystems* **2007**, *3*, 759–65.

[19] Perroy, J.; Pontier, S.; Charest, P. G.; Aubry, M.; Bouvier, M. *Nature methods* **2004**, *1*, 203–8.

[20] Kiyokawa, E.; Aoki, K.; Nakamura, T.; Matsuda, M. *Annual review of pharmacology and toxicology* **2011**, *51*, 337–58.

are: (1) capable of modification and use with a wide variety of commercially available fluorophores, (2) applicable to a wide variety of cell lines, and (3) can be used as part of a multicolor system capable of monitoring the activity of multiple enzymes. However, it can be difficult to devise an activation strategy that yields a fluorescent change upon enzymatic action. A recent review catalogs six methods of fluorescent quenching of small molecule fluorophores capable of producing a fluorescent increase upon action[21]:

(1) Fluorophore self-quenching (homo-FRET)

(2) Quencher-fluorophore FRET quenching

(3) Autoquenching via attached protein/peptide residues

(4) H-type dimer formation

(5) Photon induced electron transfer (PeT)

(6) A dual function activable fluorophore based on a combination of mechanisms

Using these methods of small-molecule fluorophore fluorescent quenching, a variety of chemical probes have been synthesized according to common paradigms. A recent review identified four common paradigms used in chemical-based approaches to fluorescent assays (Figure 1.2).[22] Four common examples include: (1) sensors for proteolysis[23] which rely on bond cleavage to abrogate

[21] Kobayashi, H.; Choyke, P. L. *Accounts of chemical research* **2011**, *44*, 83–90.

[22] Morris, M. C. *Cell biochemistry and biophysics* **2010**, *56*, 19–37.

[23] (1) Chen, J. *Circulation* **2002**, *105*, 2766–2771. (2) Jaffer, F. a; Kim, D.-E.; Quinti, L.; Tung, C.-H.; Aikawa, E.; Pande, A. N.; Kohler, R. H.; Shi, G.-P.; Libby, P.; Weissleder, R. *Circulation* **2007**, *115*, 2292–8. (3) Kozloff, K. M.; Quinti, L.; Patntirapong, S.; Hauschka, P. V.; Tung, C.-H.; Weissleder, R.; Mahmood, U. *Bone* **2009**, *44*, 190–8. (4) Neefjes, J.; Dantuma, N. P. *Nature reviews. Drug discovery* **2004**, *3*, 58–69. (5) Wunder, A.; Tung, C.-H.; Müller-Ladner, U.; Weissleder, R.; Mahmood, U. *Arthritis and rheumatism* **2004**, *50*, 2459–65.

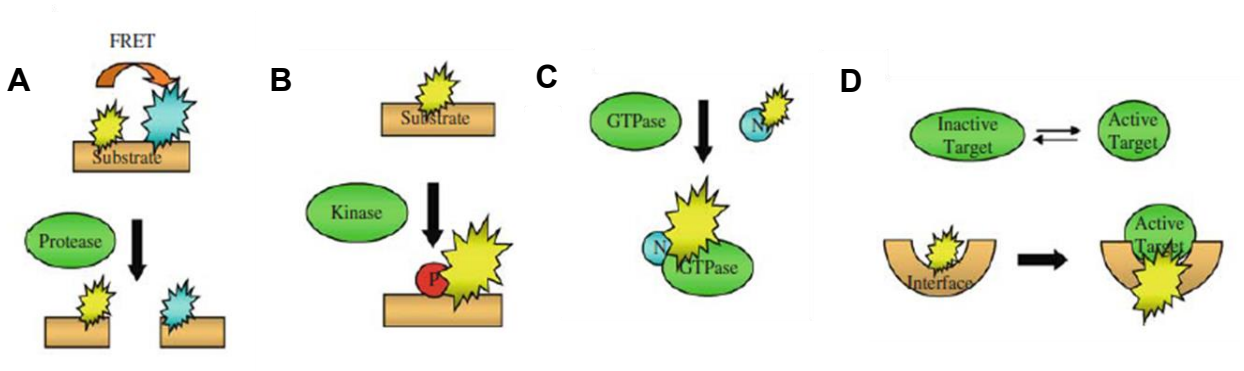

Figure 1.2 Reprinted with permission from Kobayashi, H.; Choyke, P. L. *Accounts of chemical research* **2011**, *44*, 83–90. Copyright 2011 American Chemical Society. Common examples of fluorescence-based biosensors. (a) peptide-based biosensor of proteolytic activity through cleavage-induced abrogation of intramolecular FRET, (b) peptide-based biosensor of protein phosphorylation thorough enhancement of environmentally sensitive fluorophore fluorescence, (c) Nucleotide-based sensors consist of fluorescently labeled nucleotide analogs whos fluorescence is enhanced upon incorporation into DNA. (d) interfacial biosensors consist of polypeptide domains or sequences that bind to a specific target, thereby generating an enhancement in fluorescence.

intramolecular FRET (2) kinase sensors[24] with attached environmentally sensitive fluorophores causing a fluorescence change upon addition of a negatively charged phosphate (3) nucleotide sensors[25] that show enhancement of fluoresce upon incorporation into DNA and (4) interfacial sensors that show enhancements in fluorescence upon binding to an active target. Although many fluorescent probes seem promising for *in vitro* work, difficulties do exist with probe delivery to the cytoplasm and selective activation of the biosensor by the observer, which are not issues in

[24] (1) Chen, C.-A.; Yeh, R.-H.; Yan, X.; Lawrence, D. S. *Biochimica et biophysica acta* **2004**, *1697*, 39–51. (2) Sharma, V.; Wang, Q.; Lawrence, D. S. *Biochimica et biophysica acta* **2008**, *1784*, 94–9. (3) Wang, Q.; Cahill, S. M.; Blumenstein, M.; Lawrence, D. S. *Journal of the American Chemical Society* **2006**, *128*, 1808–9. (4) Wang, Q.; Lawrence, D. S. *Journal of the American Chemical Society* **2005**, *127*, 7684–5. (5) Chen, C.-A.; Yeh, R.-H.; Lawrence, D. S. *Journal of the American Chemical Society* **2002**, *124*, 3840–1. (6) Yeh, R.-H.; Yan, X.; Cammer, M.; Bresnick, A. R.; Lawrence, D. S. *The Journal of biological chemistry* **2002**, *277*, 11527–32. (7) Lawrence, D. S.; Wang, Q. *Chembiochem : a European journal of chemical biology* **2007**, *8*, 373–8.

[25] (1) Cochran, J. C.; Sontag, C. a; Maliga, Z.; Kapoor, T. M.; Correia, J. J.; Gilbert, S. P. *The Journal of biological chemistry* **2004**, *279*, 38861–70. (2) Webb, M. R.; Corrie, J. E. *Biophysical journal* **2001**, *81*, 1562–9. (3) Webb, M. R. *Molecular bioSystems* **2007**, *3*, 249–56. (4) Webb, M. R.; Reid, G. P.; Munasinghe, V. R. N.; Corrie, J. E. T. *Biochemistry* **2004**, *43*, 14463–71.

the case of FRET-based GFP probes (although plasmid transfection with the corresponding GFP-based sensor can sometimes be difficult). Today, cytoplasmic biosensor delivery relies on the use of protein transduction domains (PTDs)[26] or cell penetrating peptides (CPPs),[27] along with mechanical or physical techniques.[28] Once delivered, the biosensor must be in an inert form to prevent enzymatic action before observation. Photodeprotection,[29] through incorporation of a photolabile protecting group, provides the observer with control of the t = 0 observation point. Using these techniques, many disadvantages of chemical probes have been overcome, yet many challenges remain.

MITOCHONDRIAL CYCLIC-AMP DEPENDENT PROTEIN KINASE ACTIVITY NEAR THE CYTOPLASM

Mitochondria are often referred to as the "energy power house" of the cell due to the key role they play in cell respiration. However, signal transduction pathways near mitochondria have been linked to the regulation of the cell-cycle, cellular development and maturation, antiviral responses, cell death, among other cell processes, making the mitochondria much more integral

[26](1) Schwarze, S. R.; Hruska, K. a; Dowdy, S. F. *Trends in cell biology* **2000**, *10*, 290–5. (2) Snyder, E. L.; Dowdy, S. F. *Expert opinion on drug delivery* **2005**, *2*, 43–51.

[27] (1) Deshayes, S.; Morris, M. C.; Divita, G.; Heitz, F. *Cellular and molecular life sciences : CMLS* **2005**, *62*, 1839–49. (2) Morris, M. C.; Deshayes, S.; Heitz, F.; Divita, G. *Biology of the cell / under the auspices of the European Cell Biology Organization* **2008**, *100*, 201–17.

[28] McNeil P. L. *Current Protocol in Cell Biology* **2001**, Chapter 20:Unit 20.1.

[29] (1) Mayer, G.; Heckel, A. *Angewandte Chemie (International ed. in English)* **2006**, *45*, 4900–21. (2) Lawrence, D. S. *Current opinion in chemical biology* **2005**, *9*, 570–5. (3) Ellis-Davies, G. C. R. *Nature methods* **2007**, *4*, 619–28. (4) Li, H.; Hah, J.; Lawrence, D. S. *Journal of the American Chemical Society* **2008**, *130*, 10474–5.

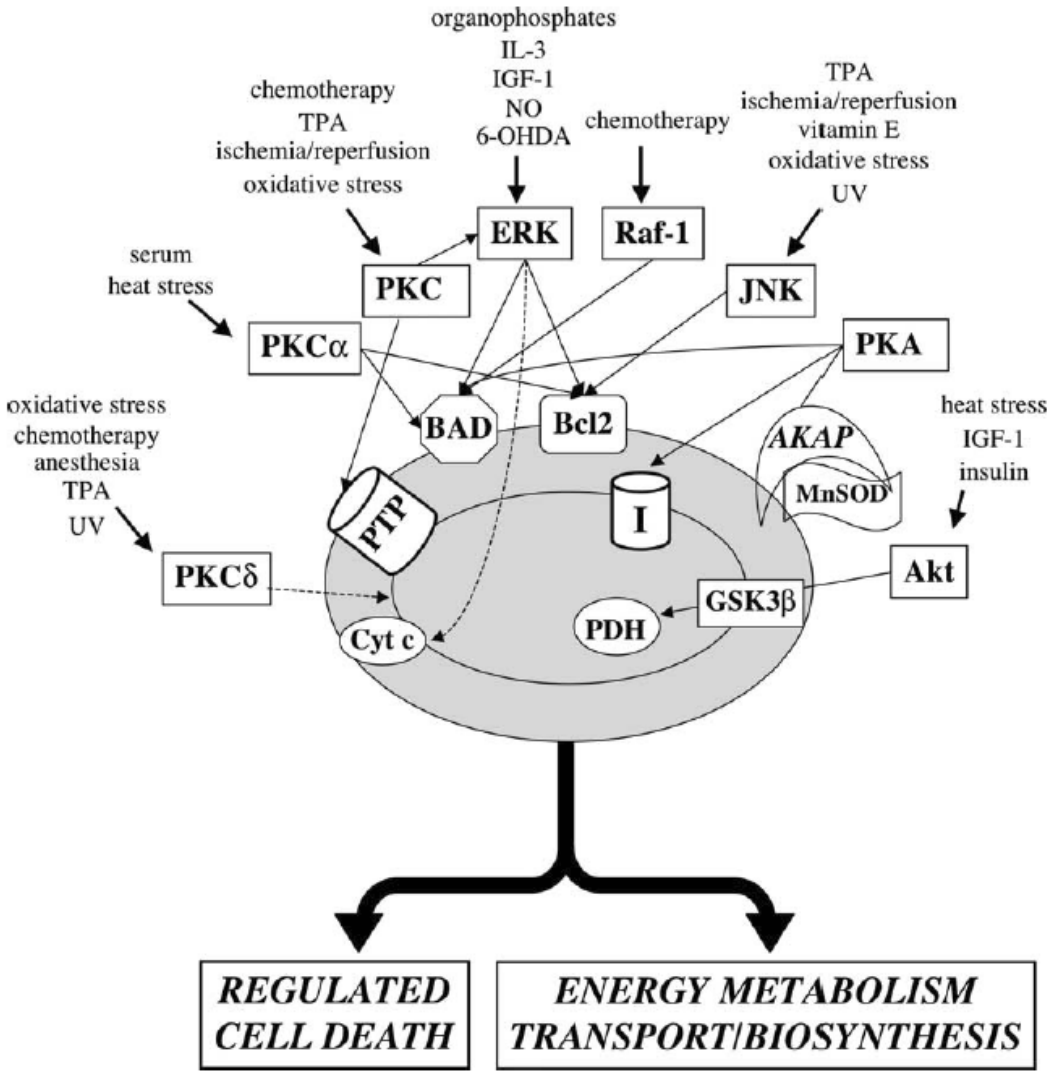

Figure 1.3 Reprinted from McBride, H. M.; Neuspiel, M.; Wasiak, S. *Current biology : CB* **2006**, *16*, R551–60, with permission from *Elsevier*. Schematic summarizing major kinase pathways that converge on the mitochondrion. A growing body of data indicate that activated versions of each of these kinases (rectangles) are targeted directly to mitochondria, resulting in phosphorylation of mitochondrial proteins that regulate cell death (PTP, BAD, Bcl-2) and metabolic function (complex I, GSK3h, PDH). Phospho-ERK and PKC may also influence cytochrome c (Cyt c) release or membrane potential through other mechanisms (dotted arrows). In addition, kinases and mitochondrial anchoring proteins may participate in a novel mechanism for regulating mitochondrial protein expression, as illustrated by PKA- and AKAP-dependent targeting of MnSOD mRNA to the mitochondrion for local translation. Abbreviations not defined elsewhere: IGF-1, insulin-like growth factor 1; IL-3, interleukin-3; NO, nitric oxide; PDH, pyruvate dehydrogenase; PTP, permeability transition pore; TPA, 12-O-tetradecanoylphorbol-13-acetate; UV, ultraviolet radiation; 6-OHDA, 6-hydroxydopamine.

to signal transduction than is generally understood.[30] Mitochondrial signal transduction pathways have been found to involve many kinases, including PKC, PKCδ, PKCα, ERK, Raf-1, JNK, PKA, and Akt (Figure 1.3).[31] Although a wide variety of pathways are worthy of attention, this study chooses to focus on PKA-mediated signaling of apoptosis, of which PKA has been identified as a central mediator.[32]

PKA is composed of a heterotetramer containing two regulatory (R) and two catalytic (C) subunits that are differentially expressed and regulated throughout various subcellular locations and cell lines.[33] Regulation of PKA occurs through the localized production and degradation of the second messenger cAMP.[34] PKA-mediated signaling begins via activation of adenylyl cyclase by an extracellular ligand, which increases the intracellular concentration of cAMP.[35] The second messenger cAMP then binds to the regulatory subunit of PKA (PKA-R), inducing a dissociation of the catalytic subunit (PKA-C), causing PKA-C activation. Phosphodiesterases provide a negative regulator of PKA activity, through degradation of cAMP to AMP.[36] A kinase anchoring proteins (AKAPs) provide a further degree of sophistication by anchoring PKA-R to

[30] McBride, H. M.; Neuspiel, M.; Wasiak, S. *Current biology : CB* **2006**, *16*, R551–60.

[31] Horbinski, C.; Chu, C. T. *Free radical biology & medicine* **2005**, *38*, 2–11.

[32] Orrenius, S. *Toxicology letters* **2004**, *149*, 19–23.

[33] (1) Tasken K, Skalhegg BS, Tasken KA, Solberg R, Knutsen HK, Levy FO, Sandberg M, Orstavik S, Larsen T, Johansen AK, Vang T, Schrader HP, Reinton NT, Torgersen KM, Hansson V, and Jahnsen T. *Adv Second Messenger Phosphoprotein Res* **1997**, *1*, 191–204. (2) Skalhegg BS and Tasken K. *Front Biosci* 5: D678–D693, 2000.

[34] (1) Taskén, K.; Aandahl, E. M. *Physiological reviews* **2004**, *84*, 137–67. (2) Feliciello, A.; Gottesman, M. E.; Avvedimento, E. V. *Cellular signalling* **2005**, *17*, 279–87.

[35] Sunahara, R. K.; Dessauer, C. W.; Gilman, A. G. *Annual review of pharmacology and toxicology* **1996**, *36*, 461–80.

[36] Soderling, S. H.; Beavo, J. *Current opinion in cell biology* **2000**, *12*, 174–9.

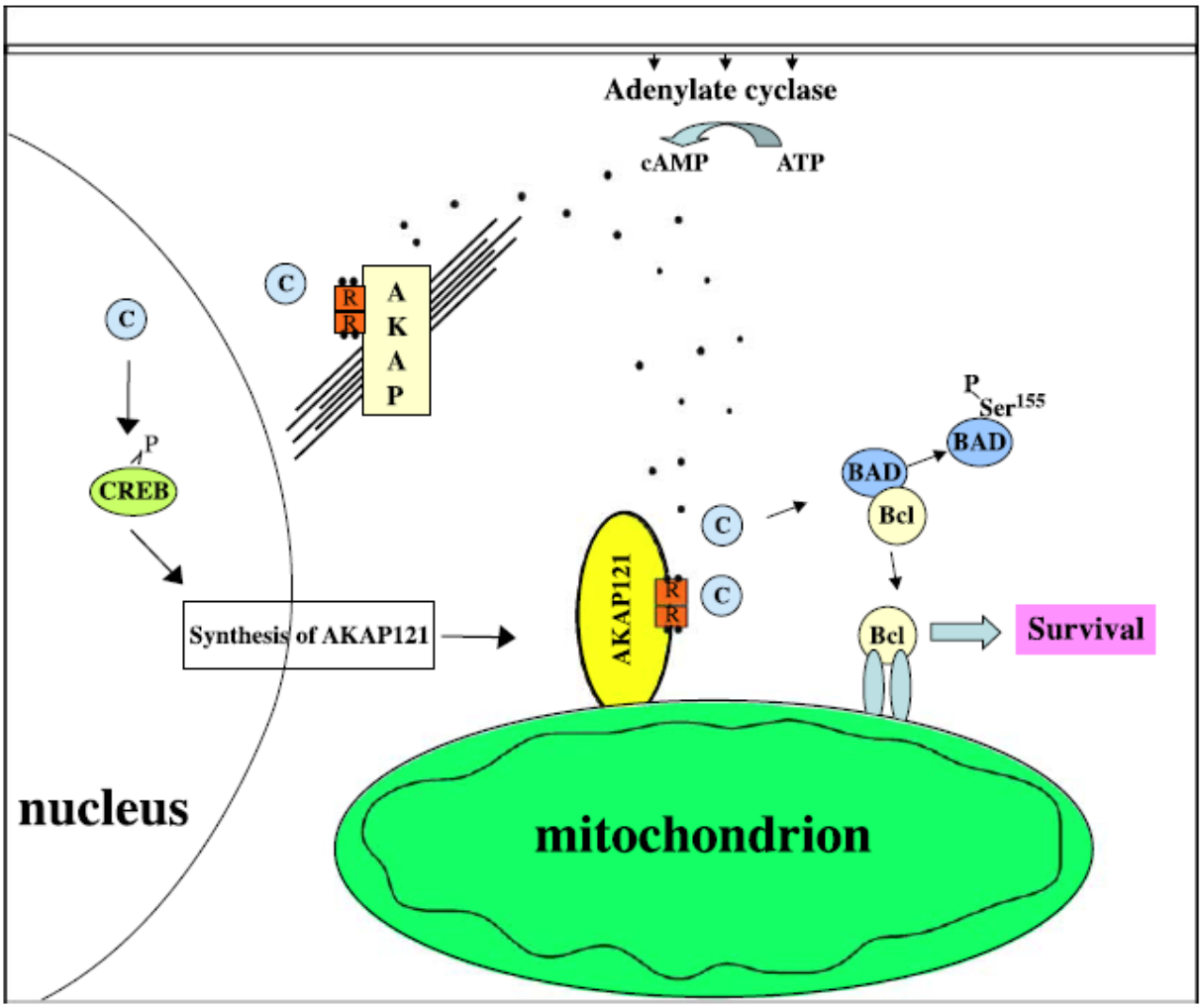

Figure 1.4 Reproduced from Feliciello, A.; Gottesman, M. E.; Avvedimento, E. V. *Cellular signaling* **2005**, *17*, 279–87. with permission from *Cellular Signaling*. cAMP stimulates the expression of AKAP121. AKAP121-PKA inhibits the mitochondrial apoptotic pathway. Cartoon showing the regulation of AKAP121 levels by cAMP. A cAMP increase following adenylyl cyclase stimulation activates a membrane-anchored PKA (included Golgi-centrosome PKA, indicated as AKAP). PKA catalytic subunit (C) dissociated from the holoenzyme enters the nucleus and phosphorylates CREB1. Transcription of AKAP121 is induced by cAMP. Higher AKAP121 levels target more PKA molecules to the outer wall of the mitochondria. The rise in cAMP concentrations dissociates mitochondrial-anchored PKA, PKA phosphorylates serine 155 of the proapoptotic protein BAD. BAD, a BH3-proapoptotic Bcl-2 family member, acts at a key nodal point in the mitochondrial apoptotic pathway. Unphosphorylated BAD binds and inactivates antiapoptotic Bcl-2 homologs, favoring release of cytochrome C from mitochondria and apoptosis. Phosphorylation by PKA blocks BAD association with Bcl-2 and inhibits apoptosis. Membrane bound PKA in other compartments cannot substitute for mitochondrial PKA.

membranes and providing spatial resolution.[37] The coordination of adenylyl cyclases and phosphodiesterases, combined with AKAPs localizing PKA-R, enables signal transduction through the PKA pathway with high spatiotemporal definition.

Intracellular PKA-mediated signal transduction plays large role in regulation of apoptosis at the mitochondria.[38] This was first described by Papa et al., as it was discovered all PKA isoforms were present in purified mitochondria.[39] Several mitochondrial proteins known to be PKA substrates were also present, including nuclear-encoded 18-kd subunit of complex I (NDUFS4), the proapoptotic BAD protein, and the steroidogenic acute regulatory protein (StAR), among others. The most important pathway component to this work is proapoptotic protein BAD, a Bcl-2 family member, and a key part of the proapoptotic pathway (Figure 1.4). Phosphorylation of BAD is known to inhibit apoptosis, playing a key role in cellular survival and death. It has been demonstrated that mitochondrial PKA-C activity is required for phosphorylation of BAD.[40] The pathway begins with cAMP signals from adenylyl cyclase near cell membrane diffuse to cytosomal AKAPs and release PKA-C into the cytosol. PKA-C then diffuses into the nucleus causing phosphorylation of CREB1. CREB1 is responsible for activating transcription of AKAP121, which translocates to the mitochondrial membrane and binds PKA-R. Endogenous PKA-C is then recruited to the mitochondria via PKA-R binding. Simulation via cAMP then causes mitochondrial PKA-C to phosphorylate BAD and prevent

[37] (1) Diviani, D.; Scott, J. D. *Journal of cell science* **2001**, *114*, 1431–7. (2) Michel, J. J. C.; Scott, J. D. *Annual review of pharmacology and toxicology* **2002**, *42*, 235–57.

[38] Feliciello, A.; Gottesman, M. E.; Avvedimento, E. V. *Cellular signaling* **2005**, *17*, 279–87.

[39] Papa, S.; Sardanelli, a M.; Scacco, S.; Technikova-Dobrova, Z. *FEBS letters* **1999**, *444*, 245–9.

[40] Affaitati, A.; Cardone, L.; de Cristofaro, T.; Carlucci, A.; Ginsberg, M. D.; Varrone, S.; Gottesman, M. E.; Avvedimento, E. V.; Feliciello, A. *The Journal of biological chemistry* **2003**, *278*, 4286–94.

apoptosis.

CURRENT CAPABILITIES OF PROTEIN KINASE BIOSENSORS

Our goal is to quantify PKA activity near the mitochondria, with the aim of studying the mitochondrial apoptotic pathway. To accomplish this, new biosensors are needed with improved activity measurement capabilities. Current biosensors for intracellular imaging rely primarily on GFP-based FRET sensors, yet chemical probes are becoming more prevalent. The first PKA biosensor for intracellular use was described in 1991 by Adams et al.[41] At the time, fluorescent sensors were only available for metal ions, and few tools existed for quantitation of PKA activity in real time. Since this publication, the field has been greatly expanded to include sensors with various excitation/emissions wavelengths and for a wide range of protein kinases.

Genetically-encoded reporters of PKA activity typically rely on a ratiometric FRET mode of imaging. A report by Zhang et al., described the use of a genetically encoded FRET PKA biosensor, named AKAR1, capable of targeting via tethering to a PKA holoenzyme (Figure 1.5(A)).[42] The four component biosensor is constructed by sandwiching a PKA substrate and the phosphopeptide binding domain 14-3-3τ between a YFP/CFP FRET pair (Figure 1.5(B)). The consensus sequence of the sensor relies on a previously described sequence specific to 14-3-3τ.[43] Flexible linkers were inserted between the C-terminal tail of 14-3-3τ and between the substrate

[41] Adams, S. R.; Harootunian, A. T.; Buechler, Y. J.; Taylor, S. S.; Tsien, R. Y. *Nature* **1991**, *349*, 694–7.

[42] Zhang, J.; Ma, Y.; Taylor, S. S.; Tsien, R. Y. *Proceedings of the National Academy of Sciences of the United States of America* **2001**, *98*, 14997–5002.

[43] Yaffe, M. B.; Rittinger, K.; Volinia, S.; Caron, P. R.; Aitken, A.; Leffers, H.; Gamblin, S. J.; Smerdon, S. J.; Cantley, L. C. *Cell* **1997**, *91*, 961–971.

peptide and YFP. Mutants were constructed with varying substrate sequences and linkers to find the analog with the best fluorescent enhancement. Upon stimulation with FsK (Forskolin, 50 μM), the phosphopeptide binding domain bound to the phosphorylated substrate peptide causing a change in the FRET ratio by 30% over 5-10 minutes (Figure 1.5 (C)). This sensor demonstrates good substrate specificity versus four related kinases *in vitro* with a small amount of activity towards PKG at longer time frames (Figure 1.5(c)).

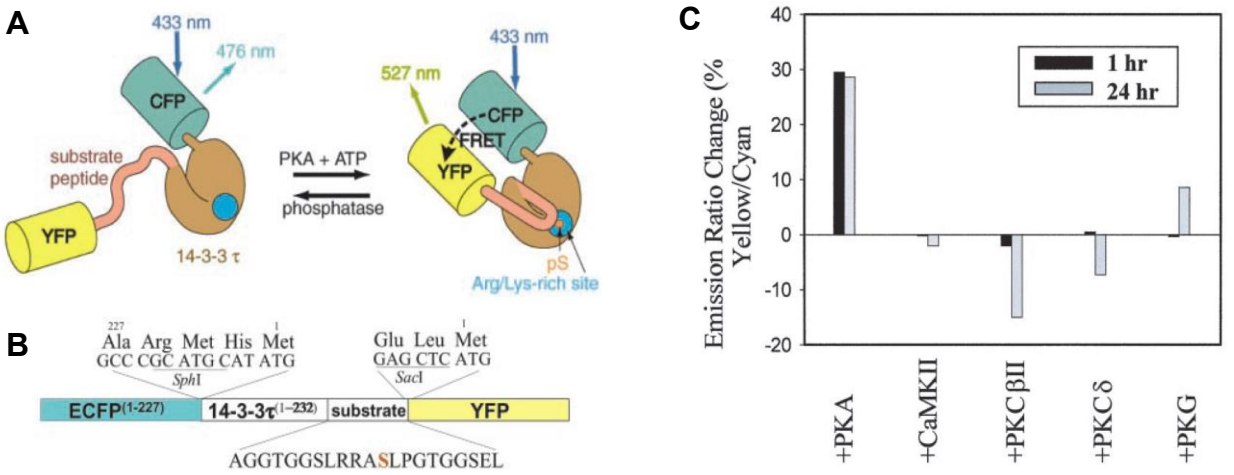

Figure 1.5 Reproduced with permission from Zhang, J.; Ma, Y.; Taylor, S. S.; Tsien, R. Y. *PNAS* **2001**, *98*, 14997–5002. AKAR1 sensor described by Zhang et al. (A) Mechanism of biosensor. Upon phosphorylation, the phosphopeptide binding domain 14-3-3τ binds to the phosphorylated substrate peptide changing the FRET ratio. (B) Construction of the biosensor (C) Specificity of AKAR1.

After all *in vitro* work was performed, AKAR1 was transfected into a variety of cell lines including HeLa, COS-7, HEK293, and Chinese hamster ovary cells and found to be evenly distributed throughout the cytosol (for expression in HeLa cells, see Figure 1.6(A)). Upon transfection, responses to FsK (50 μM) occurred in a shorter 3-5 minute time frame and occurred evenly throughout the cytoplasm (Figure 1.6 (A)). Antiphospho-PKA substrate western blot analysis of AKAR1 from HeLa cells demonstrates FsK selective phosphorylation (Figure 1.6

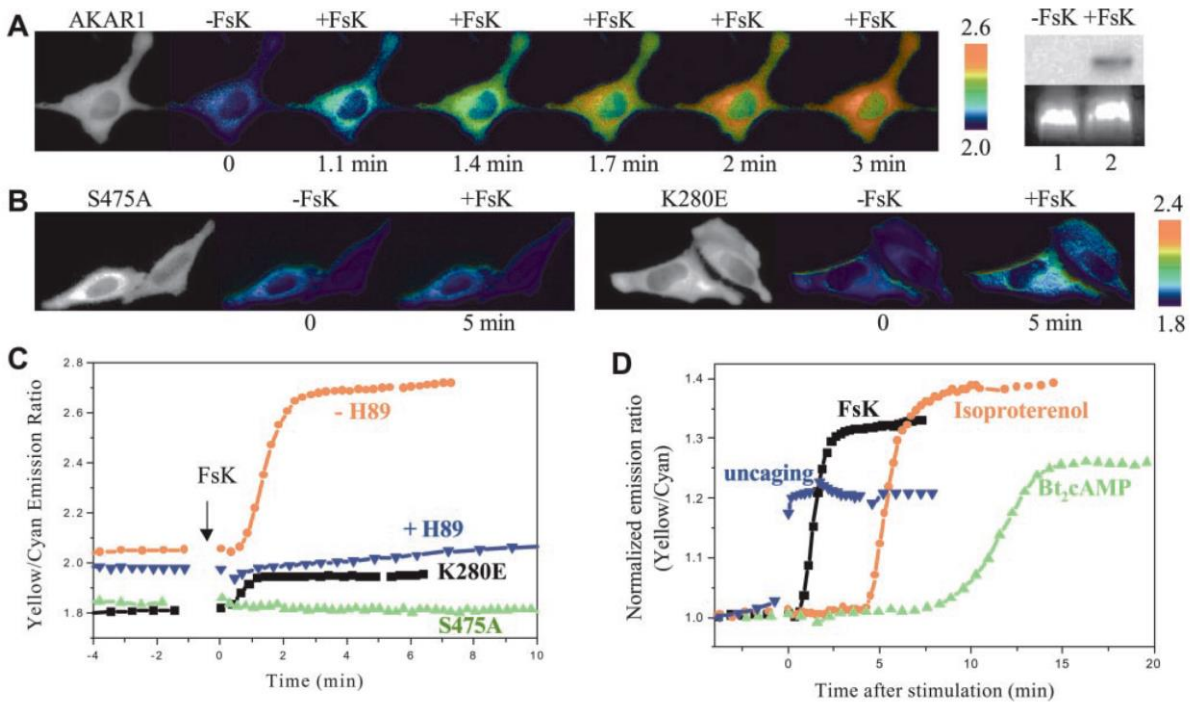

Figure 1.6 Reproduced with permission from Zhang, J.; Ma, Y.; Taylor, S. S.; Tsien, R. Y. *PNAS* **2001**, *98*, 14997–5002. Cellular responses of AKAR1. (A) FRET response of HeLa cells transfected (24 h) with AKAR1. (*Left*) The CFP-only image on the far left shows that the reporter distributes evenly throughout the cytosol. Pseudo color images depict the FRET response of the reporter to FsK stimulation. (*Right*) (*Upper*) The antiphospho-PKAsubstrate Western blot analysis of AKAR1 from HeLa cells; (*Lower*) the fluorescence image [470 ± 20 nm excitation, 530 ± 20 nm emission (YFP only)] of the same gel. Lane 1:AKAR1 from unstimulated cells. Lane 2: Treatment with 50 μM FsK for 30 min increases the phosphorylation level of the reporter. (B) FRET response of the S475A mutant (*Left*) and the K280E mutant (*Right*) of AKAR1. The height of the frames in *A* corresponds to 69 μm. Similar magnifications apply to B. (C) Emission ratio time courses for AKAR1 stimulated with 50MFsK in the absence and presence of the PKA inhibitor H89 (25 μM), and the S475A mutant and the K280E mutant stimulated with FsK (50 μM) in the absence of the inhibitor. (D) Emission ratio time courses of AKAR1 stimulated with 50 μM FsK, 1 mM Bt_2cAMP, 100 μM isoproterenol, and 50 μM of DMNB-cAMP followed by UV uncaging.

(A), on right). AKAR1 mutants were constructed (S475A and K280E) and found to greatly decrease the FRET ratio upon stimulation with FsK (50 μM, Figure 1.6(B)). One major problem with kinase biosensors is specificity, due to the large number of kinases and similarity of kinase consensus sequences. Although specificity was successfully demonstrated *in vitro*, intracellular selectivity is more difficult to achieve. However, AKAR1 was demonstrated to be

unphosphorylated upon treatment with the PKA specific inhibitor H89, demonstrating specificity to PKA (Figure 1.6(C)).

Since publication of Zhang et al. in 2001, similar sensors have been described with similar properties as AKAR1.[44] However, the most important example appeared in Nature in 2005.[45] This work describes the construction of an improved PKA biosensor AKAR2. A major problem with the AKAR1 biosensor is the lack of control of the assay by the observer. The protein must be incubated for 24-48 hours before observation to allow time for expression.[42] During this time, the protein is free to be phosphorylated by endogenous PKA. In the case of AKAR1, binding with the phosphoserine binding domain 14-3-3τ is tight enough to prevent dephosphorylation by phosphodiesterases, rendering the sensor non-reversible. This creates a problem as the sensor may be fully phosphorylated by endogenous PKA and unable to be used by the observer. With chemical probes, control can be obtained using a DMNB protecting group (4,5-dimethoxy-2-nitrobenzyl) attached to a specific location on a chemical probe as to render the probe inert until selective removal by the observer at a precise moment in time. No such precise control currently exists with expressed FRET-based GFP biosensors. To address this problem, AKAR1 was reengineered to include FHA1 (forkhead associated domain 1), instead of the phosphoserine binding domain 14-3-3τ, due to the order of magnitude lower binding affinity.[46] Due to the change in phosphoserine binding domain, the included PKA consensus sequence was modified to enhance FHA1 binding. The lower affinity of phosphoserine binding

[44] (1) Saucerman, J. J.; Zhang, J.; Martin, J. C.; Peng, L. X.; Stenbit, A. E.; Tsien, R. Y.; McCulloch, A. D. *Proceedings of the National Academy of Sciences of the United States of America* **2006**, *103*, 12923–8. (2) Hu, E.; Demmou, L.; Cauli, B.; Gallopin, T.; Geoffroy, H.; Harris-Warrick, R. M.; Paupardin-Tritsch, D.; Lambolez, B.; Vincent, P.; Hepp, R. *Cerebral cortex (New York, N.Y. : 1991)* **2011**, *21*, 708–18.

[45] Zhang, J.; Hupfeld, C. J.; Taylor, S. S.; Olefsky, J. M.; Tsien, R. Y. *Nature* **2005**, *437*, 569–73.

[46] Durocher, D.; Taylor, I. a; Sarbassova, D.; Haire, L. F.; Westcott, S. L.; Jackson, S. P.; Smerdon, S. J.; Yaffe, M. B. *Molecular cell* **2000**, *6*, 1169–82.

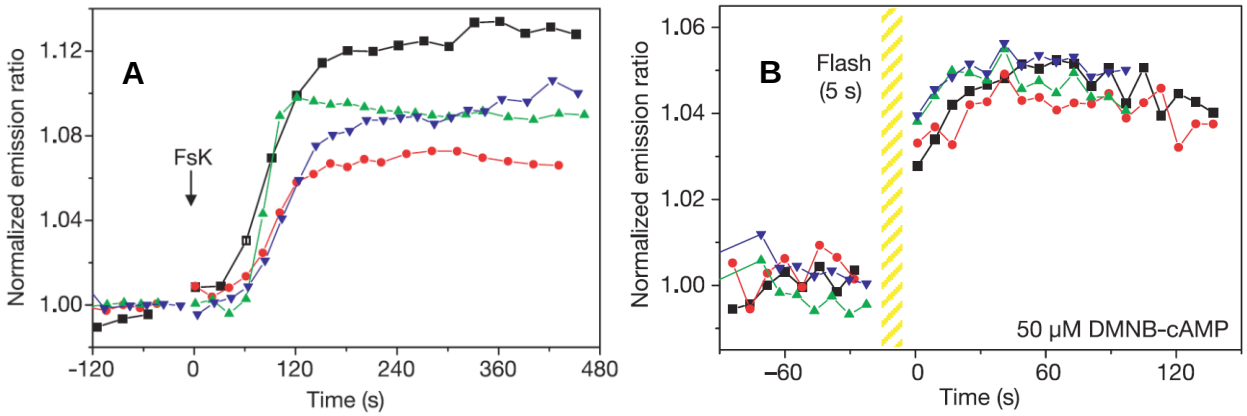

Figure 1.7 Reproduced from Zhang, J.; Hupfeld, C. J.; Taylor, S. S.; Olefsky, J. M.; Tsien, R. Y. *Nature* **2005**, *437*, 569–73. with permission from *Nature Publishing Group*. The insulin-induced delay in PKA activity is specific for a b-adrenergic-coupled pool of PKA. (A) Cells were stimulated acutely by the addition of forskolin. Insulin-treated cells in blue and green triangles; control cells in black squares and red circles. (B) Cells were stimulated acutely by ultraviolet uncaging of DMNB-cAMP. Insulin-treated cells in blue and green triangles; control cells in black squares and red circles.

in the biosensor AKAR2 makes the system susceptible to dephosphorylation by phosphodiesterases at the expense of biosensor dynamic range. Specificity of AKAR2 to PKA was demonstrated in the same manner as AKAR1 (see above). AKAR2 was used to investigate the effect of chronically high insulin levels on PKA activation. The authors demonstrated that chronic hyperinsulinaemia did not delay AKAR2 phosphorylation induced by FsK or by cAMP uncaging, which suggests that insulin treatment does not affect the entire pool of free PKA in 3T3-L1 fibroblasts. These results, although important, are outside the focus of this work. The use of the AKAR2 biosensor is most important, as it demonstrates the need for a reversible system when using FRET-based GFP biosensors. The system also has a small dynamic range compared to AKAR1 (30%), which is, in the case of FsK induced phosphorylation 12% (Figure 1.7(A)), and in the case of cyclic-AMP induced phosphorylation 6% (Figure 1.7(B)).

Although FRET-based GFP biosensors have major advantages (e.g. ease of delivery into cells via transfection and reliance on molecular biology rather than chemistry for biosensor

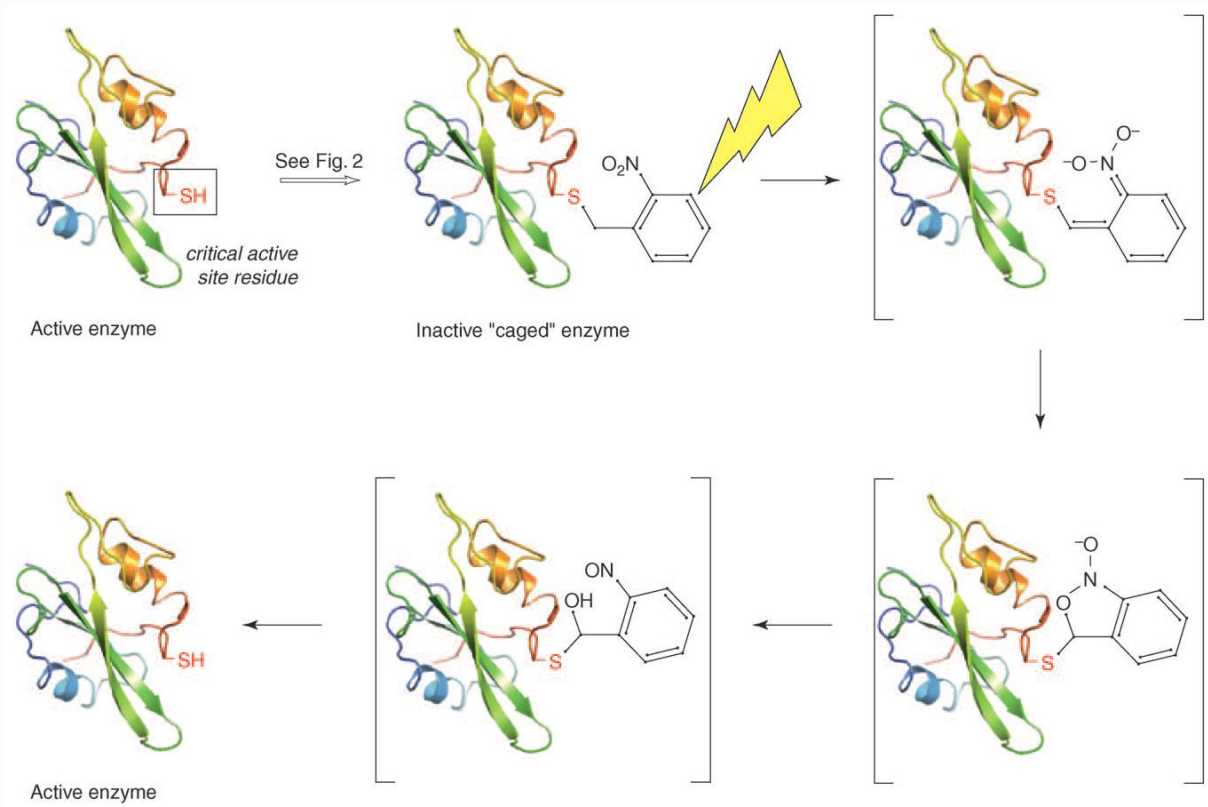

Figure 1.8 Reproduced from Lawrence, D. S. *Current opinion in chemical biology* **2005**, *9*, 570–5. with permission from *Elsevier*. Design and photoactivation of a caged peptide/protein. A key residue in a peptide or protein is identified and transformed (see Fig. 2) into a photo-cleavable analogue that blocks biochemical activity. Subsequent irradiation at the appropriate wavelength regenerates the active species.

construction), major disadvantages exist. Major problems with the above FRET-based GFP kinase biosensors including:

1) Lack of observer control of the starting point of the assay
2) Small dynamic range
3) Use of FRET requires two microscopy channels for observation
4) Limited spectral window for multiple FRET pairs

These problems can largely be overcome through the use of chemical probes. For example, the

UV labile DMNB (4,5-dimethoxy-2-nitrobenzyl) protecting group has been used in the design, use, and synthesis of light-responsive bioreagents.[47] Cyclic-AMP was the first bioreagent to be used in this manner,[48] although many other small molecules, peptides and proteins have also been rendered light responsive.[49] As an example of the paradigm, a small peptide or proteins can be DMNB protected on a cysteine residue critical for protein/peptide function (Figure 1.8).[50] Nitrobenzyl labeling can be accomplished via treatment with 2-nitrobenzyl bromide or through incorporation during peptide synthesis. Upon illumination with ultraviolet light, a reaction occurs passing through an acetal intermediate to yield the unprotected cysteine. The peptide/protein is then activated.

Secondly, the small dynamic range of FRET-based GFP biosensors is of considerable importance if the goal is to measure intercellular enzyme activity. Without a large dynamic range, it is difficult to precisely measure the initial rate of enzyme activity, as the assay can elapse before observation. For example Zhang et al.,[45] incorporated caged ATP to initiate the assay. However, with a short five second flash, most of the initial rate data was unable to be collected (Figure 1.7(B)).

Finally, a limited number of FRET pairs are capable of use intracellularly due to each FRET pair requiring multiple channels for observation. For example, two FRET pairs, ECFP/Venus and TagRFP/mPlum have recently been used for monitoring (1) small Ras GTP-ase activation in live cells after epidermal growth factor stimulation and (2) calcium gradients

[47] Lee, H.-M.; Larson, D. R.; Lawrence, D. S. *ACS chemical biology* **2009**, *4*, 409–27.

[48] Engels, J.; Schlaeger, E. J. *Journal of Medicinal Chemistry* **1977**, *20*, 907–911.

[49] Mayer, G.; Heckel, A. *Angewandte Chemie (International ed. in English)* **2006**, *45*, 4900–21.

[50] Lawrence, D. S. *Current opinion in chemical biology* **2005**, *9*, 570–5.

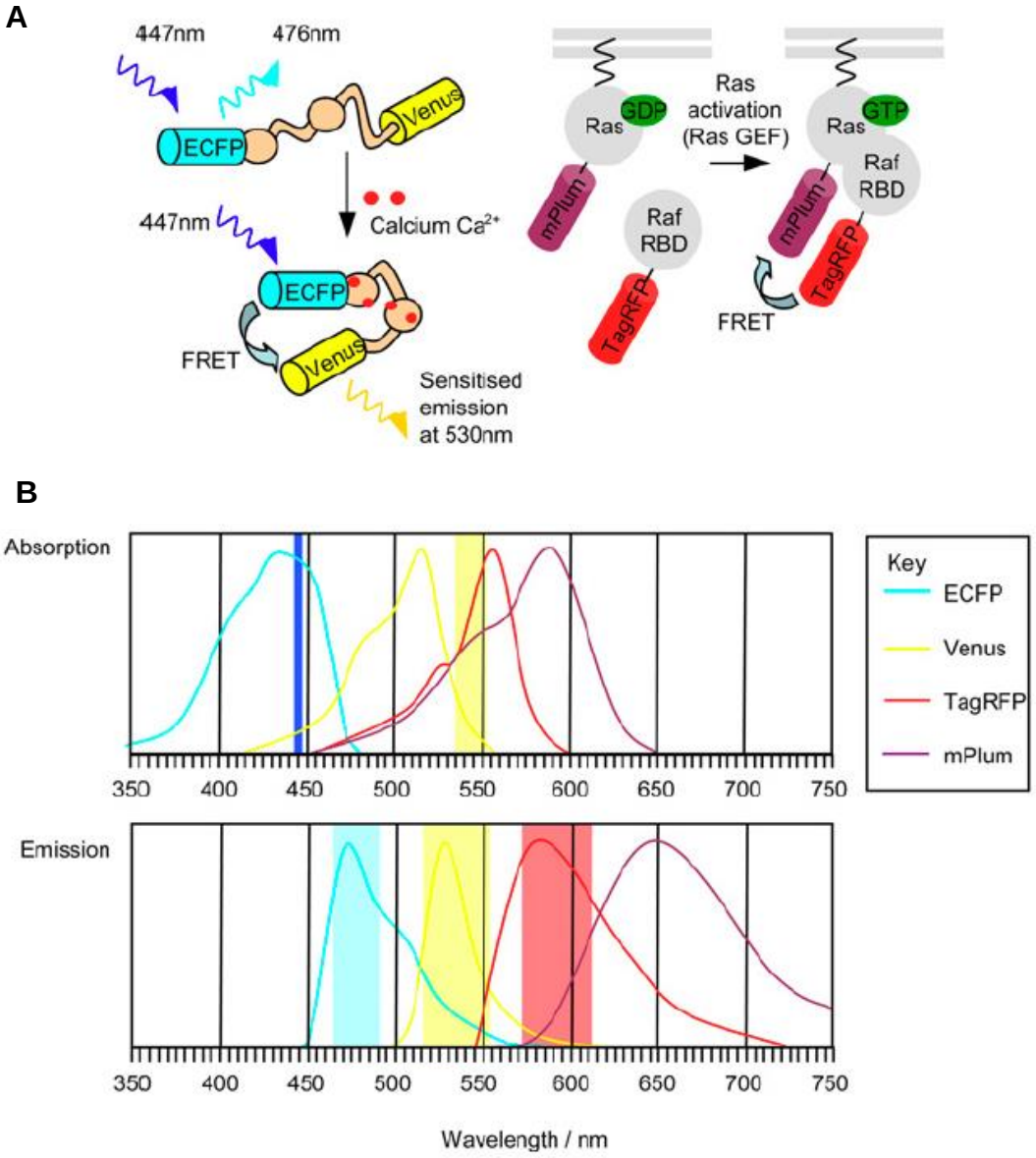

Figure 1.9 Reproduced from Grant, D. M.; Zhang, W.; McGhee, E. J.; Bunney, T. D.; Talbot, C. B.; Kumar, S.; Munro, I.; Dunsby, C.; Neil, M. a a; Katan, M.; French, P. M. W. B*iophysical journal* **2008**, *95*, L69–71.with permission from *Elsevier*. FRET constructs and spectral channels used. (A) Binding of calcium to calmodulin domain of the YCAM3.6 Cameleon results in a conformational change and FRET from ECFP to Venus. Activation of mPlum labeled H-Ras (exchange of GDP for GTP catalyzed by guanonucleotide exchange factor (GEF)) results in recruitment of Tag-RFP labeled Raf-Ras Binding Domain to the membrane and FRET between TagRFP/mPlum. (B) Absorption and emission spectra of the 4 fluorophores. Shaded areas indicate excitation and emission bands used for imaging multiplexed FRET.

simultaneously.[51] This was accomplished by careful selection of GFP mutants so as not to cause cross talk between microscope channels, and reliance on fluorescence lifetime imaging (FLIM) for the TagFRP/mPlum pair instead of spectral ratioing (as was used for the ECFP/Venus pair) (Figure 1.9A). Instead of spectral ratio imaging, which relies on monitoring changes in fluorescence intensity, monitoring via FLIM is indicated by a decrease in the fluorescent lifetime between the FRET pair. Briefly, COS-7 cells were stimulated with epidermal growth factor and spectral ratiometric imaging was used to monitor changes in calcium flux using the ECFP/Venus FRET pair. Observation of FRET between a TagRFP labeled Ras binding domain from C-Raf-Kinase (Raf-Ras Binding Domain) and mPlum labeled H-Ras was accomplished via FLIM. As shown in Figure 1.9(B), use of two FRET pairs requires most of the visible imaging spectrum, leaving no room for imaging of additional intracellular processes. This example demonstrates the problems with attempting to image multiple processes simultaneously using FRET-based GFP biosensors.

Chemical probes of PKA activity have advantages over FRET-based GFP PKA sensors, such as precise control by the observer and wide range of fluorohpores available for imaging. The first peptide biosensor described relied on environmentally-sensitive solvatochromic fluorophores to produce a fluorescent enhancement.[52] A report from Veldhuyzen et al., describes the use of the fluorophore NBD in the creation of a closely related PKC sensor, which could theoretically be applied to PKA.[53] The sensor was constructed via solid phase peptide synthesis

[51] Grant, D. M.; Zhang, W.; McGhee, E. J.; Bunney, T. D.; Talbot, C. B.; Kumar, S.; Munro, I.; Dunsby, C.; Neil, M. A.; Katan, M.; French, P. M. W. *Biophysical journal* **2008**, *95*, L69–71.

[52] Loving, G. S.; Sainlos, M.; Imperiali, B. *Trends in biotechnology* **2010**, *28*, 73–83.

[53] Veldhuyzen, W. F.; Nguyen, Q.; McMaster, G.; Lawrence, D. S. *Journal of the American Chemical Society* **2003**, *125*, 13358–9.

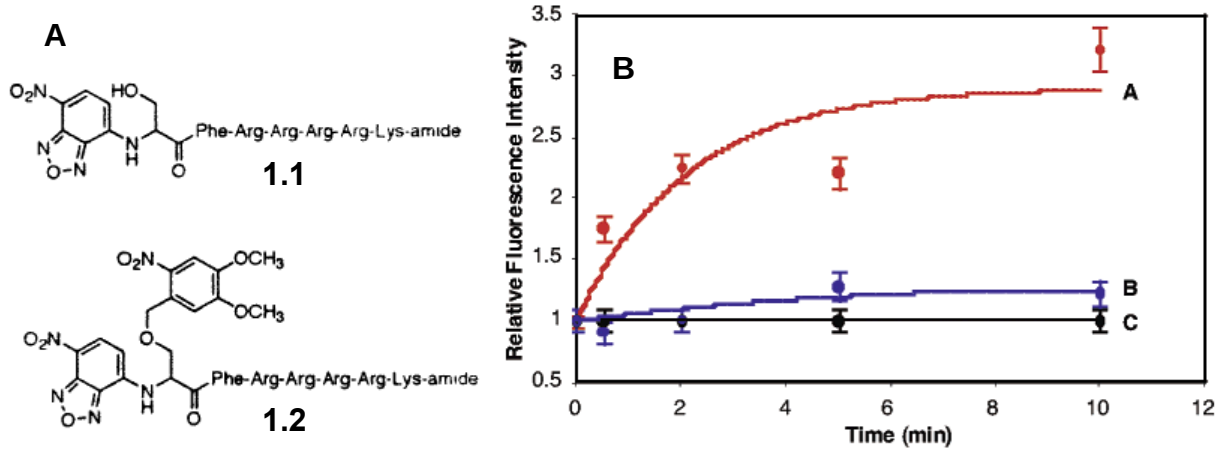

Figure 1.10 Reproduced with permission from Veldhuyzen, W. F.; Nguyen, Q.; McMaster, G.; Lawrence, D. S. *Journal of the American Chemical Society* **2003**, *125*, 13358–9. Copyright 2003 American Chemical Society. (A) **1.1** NBD-labeled fluorescent PKC sensor **1.2** A dimethoxy-2-nitrobenzyl protecting group was added to "cage" the substrate, rendering it inert until photolysis via UV light. (B) Intracellular fluorescence as a function of time following irradiation. **A** Sensor **1.2** irritated intracellularly. **B** Intracellular fluorescence of (B) in the absence of UV light. **C** Sensor irradiated in the absence of intracellular PKC.

(SPPS) to include a PKC consensus sequence, as well as an N-terminally attached NBD fluorophore (Figure 1.10(a)). The NBD fluorophore has appropriate excitation and emission wavelengths (ex 520, em 560) for microscopy. Upon phosphorylation, the biosensor yielded a 3-fold enhancement in fluorescence, which is 10x the maximum response of AKAR1. The addition of a 4,5-dimethoxy-2-nitrobenzyl protecting group is necessary for intracellular work to "cage" the substrate and render it inert prior to photolysis (Figure 1.10(B)). Using the control gained from nitrobenzyl caging, substrates **1.1** and **1.2** (Figure 1.10(A)) were used to investigate Protein Kinase C activity during Nuclear Envelope Breakdown (NEB, Figure 1.11).[54] Using the larger dynamic range, PKC activity was monitored before and after NEB, via microinjection of substrates **1.1** and **1.2**, along with 70 kD Texas red-dextran to provide a standard for ratiometric

[54] Dai, Z.; Dulyaninova, N. G.; Kumar, S.; Bresnick, A. R.; Lawrence, D. S. *Chemistry & biology* **2007**, *14*, 1254–60.

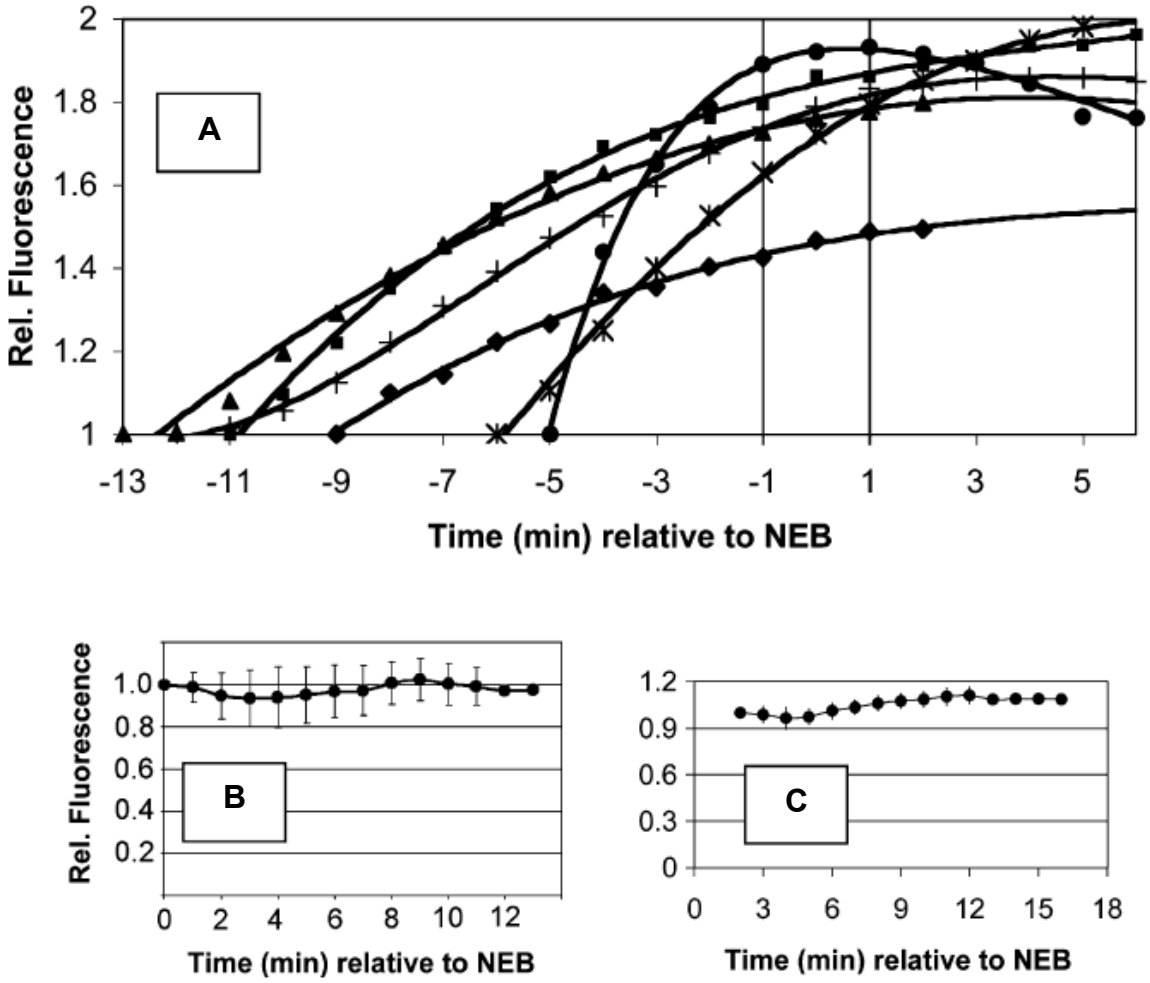

Figure 1.11 Reproduced from Dai, Z.; Dulyaninova, N. G.; Kumar, S.; Bresnick, A. R.; Lawrence, D. S. *Chemistry & biology* **2007**, *14*, 1254–60. with permission from *Elsevier*. Protein Kinase Activity prior to and after Nuclear Envelope Breakdown (A) Time course of the phosphorylation of peptide **1.1** (Figure 1.10) prior to NEB. The nonphosphorylatable analog, **1.2** (Figure 1.10), and 70 kD Texas red-dextran were simultaneously microinjected into PtK2 cells. Cells were illuminated (1 s) during prophase (i.e., prior to NEB) to convert the inert sensor, **1.2** (Figure 1.10), to its active form, **1.1** (Figure 1.10), and the fluorescence change as a function of time was recorded with respect to NEB. Each progress curve is derived from a single cell, and a total of 18 cells were examined (6 of the progress curves are shown here). (B) Time course of the phosphorylation of peptide **1.1** (Figure 1.10) after NEB. PtK2 cells were treated as in Figure 2A, except that photolysis was performed after NEB. The progress curve represents the average fluorescence change of 16 cells (each data point represents the mean ± SD). (C) Fluorescence change after NEB in the presence of okadaic acid (1.5 mM).

imaging (Figure 1.11A). Substrate **1.1** monitored PKC activity before NEB, as it lacked the DMNB protecting group. After NEB, substrate **1.2** was converted into substrate **1.1** via photocleavage for monitoring of PKC activity after NEB. Before NEB, fluorescent enhancements of between 1.4-fold and 2-fold were observed depending on the cell. After NEB, no PKC activity was observed after photolysis of substrate **1.2**, leading the authors' conclusion that PKC activity is present before, but not after, NEB (Figure 1.11B). This type of experiment would be extremely difficult without observer control of the intercellular assay, and a larger dynamic range than is possible with current FRET-based GFP PKC biosensors.

Since the reports by Veldhuyzen et al. and Dai et al., a range of biosensors capable of kinase detection have been synthesized and applied to biological systems including:

(1) Self-quenched micelles which disperse upon phosphorylation[55]

(2) Genetically encoded Lanthanide-binding peptides[56]

(3) "deep-quench" kinase sensors which rely on binding to a 14-3-3τ domain[57]

(4) Lanthanide binding peptides relying on FRET transfer from an attached fluorophore[58]

(5) Peptide substrates that rely on chelation of Ca^{2+} [59]

(6) Sox fluorophore-based Mg^{2+} chelating kinase sensors[60]

---

[55] Sun, H.; Low, K. E.; Woo, S.; Noble, R. L.; Graham, R. J.; Connaughton, S. S.; Gee, M. a; Lee, L. G. *Analytical chemistry* **2005**, *77*, 2043–9.

[56] (1) Zondlo, S. C.; Gao, F.; Zondlo, N. J. *Journal of the American Chemical Society* **2010**, *132*, 5619–21. (2) Balakrishnan, S.; Zondlo, N. J. *Journal of the American Chemical Society* **2006**, *128*, 5590–1.

[57] Sharma, V.; Agnes, R. S.; Lawrence, D. S. *Journal of the American Chemical Society* **2007**, *129*, 2742–3.

[58] (1) Tremblay, M. S.; Lee, M.; Sames, D. *Organic letters* **2008**, *10*, 5–8. (2) Tremblay, M. S.; Zhu, Q.; Martí, A. a; Dyer, J.; Halim, M.; Jockusch, S.; Turro, N. J.; Sames, D. *Organic letters* **2006**, *8*, 2723–6.

[59] Chen, C.-A.; Yeh, R.-H.; Lawrence, D. S. *Journal of the American Chemical Society* **2002**, *124*, 3840–1.

[60] (1) Luković, E.; González-Vera, J. a; Imperiali, B. *Journal of the American Chemical Society* **2008**, *130*, 12821–7. (2) Shults, M. D.; Carrico-Moniz, D.; Imperiali, B. *Analytical biochemistry* **2006**, *352*, 198–207. (3) Luković, E.;

(7) Zn^{2+}-DPA-based kinase biosensors[61]

(8) Ratiometric coumarin kinase biosensors relying on a Cd^{II}-cycle moiety[62]

(9) Quantum dot-based kinase biosensors[63]

Although all nine systems have distinct advantages over FRET-based GFP biosensors, unfortunately none have found as wide spread of use as FRET-based GFP biosensors. The biggest shortcomings with the above probes are (1) the reliance on multiple chemical components and (2) intracellular delivery. In most cases, a metal cation, an antibody, or Zn^{2+}-DPA moiety must be present to produce a fluorescent enhancement. For intracellular use, delivery of multiple components to the cytosol would be required for intracellular measurement. Delivery of one component is non-trivial, and topic of a large body of research.[64] An interesting unimolecular sensor paradigm was described by Kikuchi et al.[62] The biosensor relies on phosphate displacement of a Cd^{II}-cyclen(1,4,7,10-tetraazacyclododecane) moiety to produce a fluorescent enhancement, which could be an issue at physiological ATP concentrations (Figure 1.12). However, if the photophysical properties of the sensor were optimized for imaging and higher concentrations of ATP was demonstrated to have little effect on biosensor fluorescence, it would be easier to deliver than other two component systems. However, like FRET-based GFP

Vogel Taylor, E.; Imperiali, B. *Angewandte Chemie (International ed. in English)* **2009**, *48*, 6828–31. (4) Shults, M. D.; Imperiali, B. *Journal of the American Chemical Society* **2003**, *125*, 14248–9.

[61] (1) Rhee, H.-W.; Choi, S. J.; Yoo, S. H.; Jang, Y. O.; Park, H. H.; Pinto, R. M.; Cameselle, J. C.; Sandoval, F. J.; Roje, S.; Han, K.; Chung, D. S.; Suh, J.; Hong, J.-I. *Journal of the American Chemical Society* **2009**, *131*, 10107–12. (2) Rhee, H.-W.; Lee, S. H.; Shin, I.-S.; Choi, S. J.; Park, H. H.; Han, K.; Park, T. H.; Hong, J.-I. *Angewandte Chemie (International ed. in English)* **2010**, *49*, 4919–23.

[62] Kikuchi, K.; Hashimoto, S.; Mizukami, S.; Nagano, T. *Organic letters* **2009**, *11*, 2732–5.

[63] Freeman, R.; Finder, T.; Gill, R.; Willner, I. *Nano letters* **2010**, *10*, 2192–6.

[64] (1) Rajendran, L.; Udayar, V.; Goodger, Z. V. *Trends in pharmacological sciences* **2012**, *33*, 215–22. (2) Elsabahy, M.; Wooley, K. L. *Chemical Society reviews* **2012**, *41*, 2545–61. (3) Kamaly, N.; Xiao, Z.; Valencia, P. M.; Radovic-Moreno, A. F.; Farokhzad, O. C. *Chemical Society reviews* **2012**, *41*, 2971–3010.

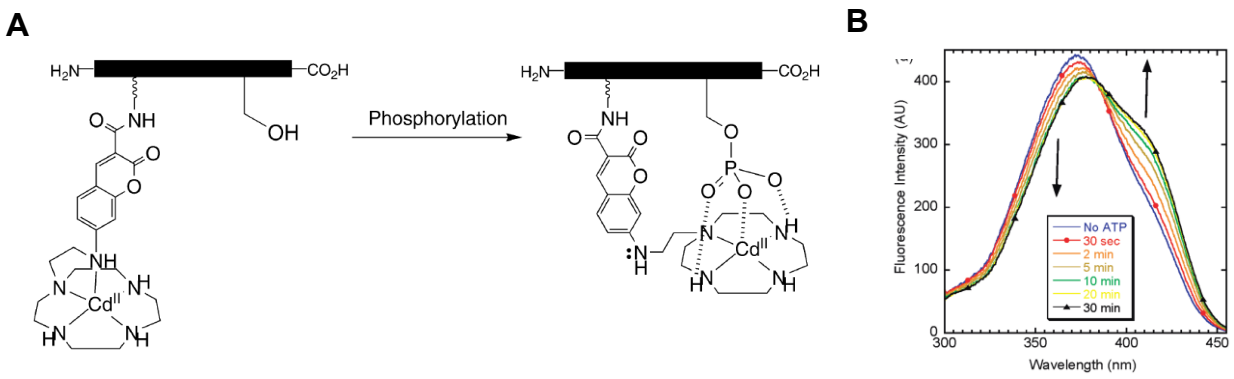

Figure 1.12 Reproduced with permission from Kikuchi, K.; Hashimoto, S.; Mizukami, S.; Nagano, T. *Organic letters* **2009**, *11*, 2732–5. Copyright 2009 American Chemical Society. (a) Mechanism of Peptide Biosensor of PKA. Binding of phosphate causes dissociation of coordinated amine, creating a change in fluorescence of coumarin fluorophore. (b) Ratiometric change observed upon phosphorylation of biosensor.

sensors, a major drawback with this system is reliance upon FRET, the disadvantages of which have been discussed above.

Unfortunately, chemical probes of kinase activity have not widely been adopted by the biological community.[65] In order for widespread adoption of chemical probes to occur, kinase probes must be as easy to use as FRET-based GFP kinase biosensors without requiring expertise in chemistry. This is currently not the case as very few kinase probes (1) are cell permeable (the large majority requiring microinjection) and (2) are available commercially without relying on the synthesis expertise of a chemist. However, chemical kinase probes have distinct advantages over genetically-encoded kinase reporters, including larger dynamic range, better photophysical properties of the fluorophores, and no reliance on multichannel FRET during microscopy. Using these advantages, future development of chemical kinase probes will be very promising if delivery can be improved.

[65] Pazos, E.; Vázquez, O.; Mascareñas, J. L.; Vázquez, M. E. *Chemical Society reviews* **2009**, *38*, 3348–59.

THE PROTEASOME AND REGULATION OF CELLULAR PROTEINS

The proteasome is often referred to as the "garbage can" of the cell due to its primary function in protein degradation.[66] The 2.5 megadalton enzyme complex (often referred to as the 26S proteasome complex) is a part of the ubiquitin–protease system, specifically digesting proteins marked for degradation with the small protein ubiquitin.[67] Protein degradation occurs via a multi-step process including: (1) recognition of substrate, (2) protein unfolding, (3) translocation, (4) deubiquitination, (5) peptide-bond cleavage.[68] The 26S proteasome complex consists of a 28-subunit barrel-like core particle (CP, also referred to as the 20S particle) and two 19-subunit regulatory particles (RPs, also referred to as the 19S particle) on each end of the CP channel (Figure 1.13).[69] The 20S core particle is responsible for polypeptide degradation after substrate recognition and processing by the 19S regulatory particle. Regulation of the proteasome by the 19S particle is of prime importance since an uncontrolled proteasome would degrade a range of intracellular proteins. Fortunately, the substrate channel is narrow and prevents the majority of folded proteins from entering.[70] Once recognized and unfolded, proteins are not degraded in single amino acids but instead exit the proteasome as

[66] Dalton, W. S. *Seminars in oncology* **2004**, *31*, 3–9; discussion 33.

[67] (1) Coux, O.; Tanaka, K.; Goldberg, a L. *Annual review of biochemistry* **1996**, *65*, 801–47. (2) Pickart, C. M.; Cohen, R. E. *Nature reviews. Molecular cell biology* **2004**, *5*, 177–87.

[68] Finley, D. *Annual review of biochemistry* **2009**, *78*, 477–513.

[69] Reyes-Turcu, F. E.; Ventii, K. H.; Wilkinson, K. D. *Annual review of biochemistry* **2009**, *78*, 363–97.

[70] (1) Förster, A.; Masters, E. I.; Whitby, F. G.; Robinson, H.; Hill, C. P. *Molecular cell* **2005**, *18*, 589–99. (2) Groll, M.; Bajorek, M.; Köhler, a; Moroder, L.; Rubin, D. M.; Huber, R.; Glickman, M. H.; Finley, D. *Nature structural biology* **2000**, *7*, 1062–7. (3) Whitby, F. G.; Masters, E. I.; Kramer, L.; Knowlton, J. R.; Yao, Y.; Wang, C. C.; Hill, C. P. *Nature* **2000**, *408*, 115–20. (4) Lee, C.; Prakash, S.; Matouschek, A. *The Journal of biological chemistry* **2002**, *277*, 34760–5.

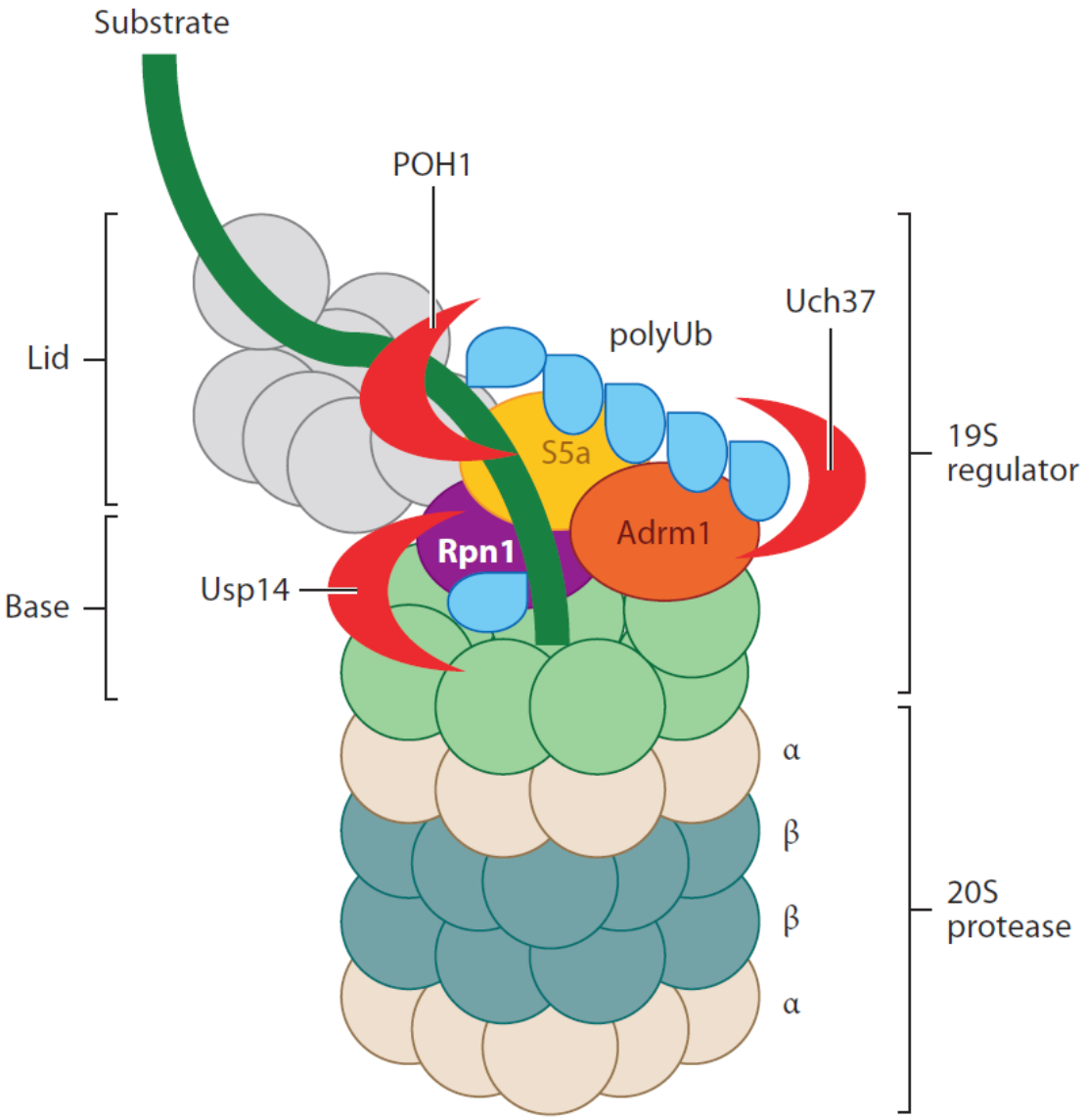

Figure 1.13 Reproduced from Reyes-Turcu, F. E.; Ventii, K. H.; Wilkinson, K. D. *Annual review of biochemistry* **2009**, *78*, 363–97. with permission from *Annual Reviews of Biochemistry*. Structure of the proteasome including deubiquitinating enzymes. Deubiquitinating enzymes shown as red crescents, substrate polypeptide chain as a green line, and ubiquitin as blue ovals. POH1 catalyzes the release of a polyubiquitin chain en bloc as the substrate is engaged and translocated through the gate pore of the 20S protease. S5a binds the polyubiquitin chain, and the distal end of the chain can be removed by the action of Uch37 bound to Adrm1. Usp14 is bound to the proteasome via interactions with the S2 subunit, also known as Rpn1 and probably removes monoubiquitin attached to the substrate.

small peptides.[71]

Although study of the structure and mechanism is indeed important, this study is focused on the study of intracellular signal transduction. Our interest in the proteasome stems from recent reports implicating proteases in signal transduction pathways and a large variety of physiological processes.[72] Intracellular protease activity has been demonstrated to be highly regulated, and activity imbalances are known causes of disease.[73] The proteasome, as a protease, is highly regulated by the 19S subunit and has been implicated in number diseases as a result of changes in proteasome activity.[74] Cell processes known to be regulated by the ubitiquin-proteasome system include:

(1) Cell cycle progression[75]

(2) Self-regulation of the ubitiquin-proteasome pathway[76]

(3) JNK signaling pathway[77]

(4) Calcineurin/NFAT signaling pathways[77]

(5) Gene Transcription[78]

---

[71] (1) Kisselev, A. F.; Akopian, T. N.; Woo, K. M.; Goldberg, A. L. **1999**, *274*, 3363–3371. (2) Goldberg, A. L.; Cascio, P.; Saric, T.; Rock, K. L. *Molecular immunology* **2002**, *39*, 147–64.

[72] Turk, B.; Turk, D. S. A.; Turk, V. *The EMBO journal* **2012**, *31*, 1630–43.

[73] Quesada, V.; Ordóñez, G. R.; Sánchez, L. M.; Puente, X. S.; López-Otín, C. *Nucleic acids research* **2009**, *37*, D239–43.

[74] Dahlmann, B. *BMC biochemistry* **2007**, *8 Suppl 1*, S3.

[75] (1) Lopes, U. G.; Erhardt, P.; Yao, R.; Cooper, G. M. *The Journal of biological chemistry* **1997**, *272*, 12893–6. (2) Votano, J. R.; Parham, M.; Hall, L. H.; Kier, L. B.; Hall, L. M. *Chemistry & biodiversity* **2004**, *1*, 1829–41. (3) An, B.; Goldfarb, R. H.; Siman, R.; Dou, Q. P. *Cell death and differentiation* **1998**, *5*, 1062–75. (4) Blagosklonny, M. V.; Wu, G. S.; Omura, S.; El-Deiry, W. S. *Biochemical and biophysical research communications* **1996**, *227*, 564–9.

[76] Weissman, A. M.; Shabek, N.; Ciechanover, A. *Nature reviews. Molecular cell biology* **2011**, *12*, 605–20.

[77] Portbury, A. L.; Ronnebaum, S. M.; Zungu, M.; Patterson, C.; Willis, M. S. *Journal of molecular and cellular cardiology* **2012**, *52*, 526–37.

(6) Cell polarity of neurons[79]

(7) 5'-AMP-activated protein kinase pathway[80]

However, reports linking the intracellular distribution of proteasome activity with cellular function are lacking. Proteasome biosensors capable of intracellular use could shine light on location/function relationships.

CURRENT CAPABILITIES OF PROTEASOME SENSORS

Due to the wide variety of reports linking changes in protease activity to diseases and disorders,[72] interest is developing in fluorescent reporters that can accurately and precisely measure protease activity. Fluorescent protease substrates have been developed for proteases such as the proteasome,[81] metalloproteases,[82] and cysteine proteases,[83] among others. Generally

---

[78] Geng, F.; Wenzel, S.; Tansey, W. P. *Annual review of biochemistry* **2012**, *81*, 177–201.

[79] Bórquez, D. a; González-Billault, C. *Biological research* **2011**, *44*, 35–41.

[80] Zungu, M.; Schisler, J. C.; Essop, M. F.; McCudden, C.; Patterson, C.; Willis, M. S. *The American journal of pathology* **2011**, *178*, 4–11.

[81] (1) Urru, S. a M.; Veglianese, P.; De Luigi, A.; Fumagalli, E.; Erba, E.; Gonella Diaza, R.; Carrà, A.; Davoli, E.; Borsello, T.; Forloni, G.; Pengo, N.; Monzani, E.; Cascio, P.; Cenci, S.; Sitia, R.; Salmona, M. *Journal of medicinal chemistry* **2010**, *53*, 7452–60. (2) Carmony, K. C.; Lee, D.-M.; Wu, Y.; Lee, N.-R.; Wehenkel, M.; Lee, J.; Lei, B.; Zhan, C.-G.; Kim, K.-B. *Bioorganic & medicinal chemistry* **2012**, *20*, 607–13. (3) Wakata, A.; Lee, H.-M.; Rommel, P.; Toutchkine, A.; Schmidt, M.; Lawrence, D. S. *Journal of the American Chemical Society* **2010**, *132*, 1578–82. (4) Edgington, L. E.; Verdoes, M.; Bogyo, M. *Current opinion in chemical biology* **2011**, *15*, 798–805.

[82] (1) Meyer, B. S.; Rademann, J. *The Journal of biological chemistry* **2012**, *11*. in press. (2) Poras, H.; Duquesnoy, S.; Dange, E.; Pinon, A.; Vialette, M.; Fournié-Zaluski, M.-C.; Ouimet, T. *The Journal of biological chemistry* **2012**, *287*, 20221–30.

[83] (1) Edgington, L. E.; Verdoes, M.; Bogyo, M. *Current opinion in chemical biology* **2011**, *15*, 798–805. (2) Jaffer, F. a; Kim, D.-E.; Quinti, L.; Tung, C.-H.; Aikawa, E.; Pande, A. N.; Kohler, R. H.; Shi, G.-P.; Libby, P.; Weissleder, R. *Circulation* **2007**, *115*, 2292–8. (3) Chen, J.; Tung, C.-H.; Mahmood, U.; Ntziachristos, V.; Gyurko, R.; Fishman, M. C.; Huang, P. L.; Weissleder, R. *Circulation* **2002**, *105*, 2766–71.

protease sensors function via degradation of a substrate labeled with multiple fluorophores and/or fluorescent quenchers (Figure 1.14).[84] This contrasts with the difficulties associated with finding a mechanism of action for development of unimolecular kinase sensors, as phosphorylation has been more difficult for chemists to convert into a fluorescent response. Using polypeptide degradation mechanisms, protease sensors have been constructed of fluorescent proteasome substrates[84] including:

1) Degradation of a GFP protease substrate
2) Ratiometric FRET using two fluorophores with an excitation emission overlap
3) Fluorophore unquenching using a fluorophore and non-fluorescent quencher
4) Fluorophore unquenching via fluorophore self-quenching.
5) Ratiometric FRET using two GFP mutants with overlapping spectral properties

Like kinase biosensors, sensors for the proteasome fall into two categories (1) expressed GFP probes and (2) chemical probes. Li et al. described an expressed enhanced green fluorescent protein (EGFP) probe as a transcription reporter in 1998.[85] Although this system was demonstrated as an example of transcription assay, the reporter was constructed to include elements known to be susceptible to proteasome degradation to decrease cytosol half-life. Mutations of EGFP enhanced protein stability to allow cytosolic EGFP accumulation and therefore easy intracellular detection. However, to construct a biosensor, the authors required

---

[84] Neefjes, J.; Dantuma, N. P. *Nature reviews. Drug discovery* **2004**, *3*, 58–69.

[85] Li, X.; Zhao, X.; Fang, Y.; Jiang, X.; Duong, T.; Fan, C.; Huang, C. C.; Kain, S. R. *The Journal of biological chemistry* **1998**, *273*, 34970–5.

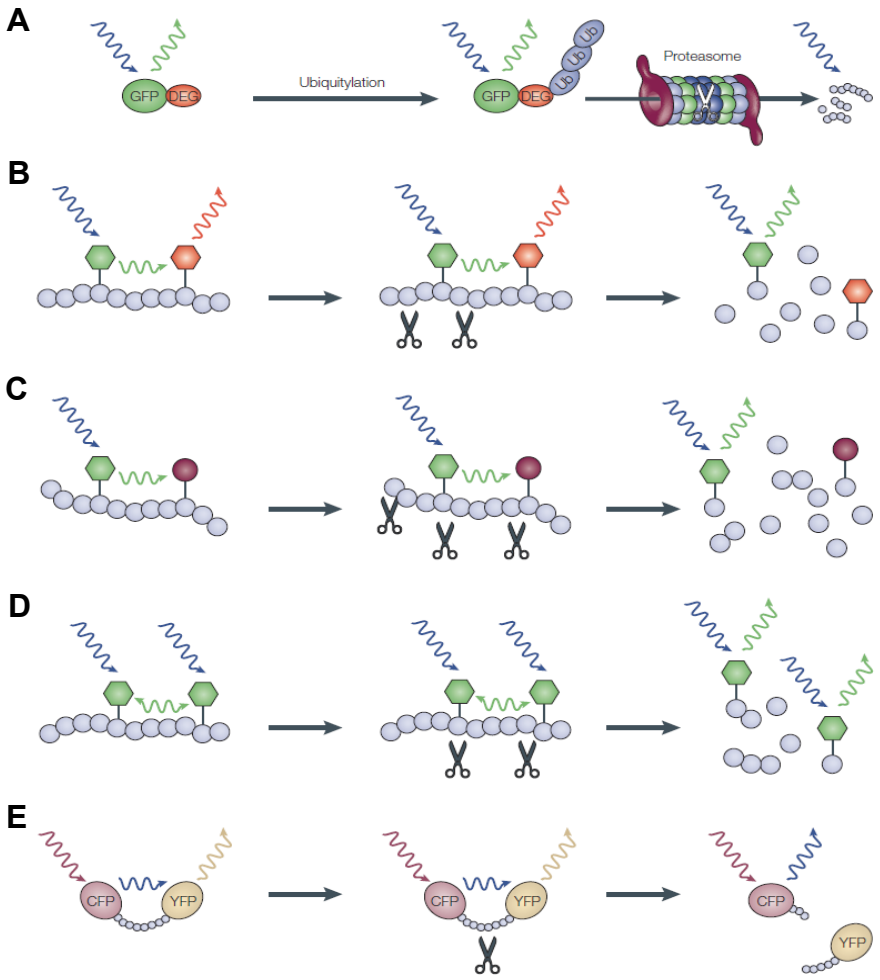

Figure 1.14 Reprinted with permission from Neefjes, J.; Dantuma, N. P. *Nature reviews. Drug discovery* **2004**, *3*, 58–69. Copyright 2004 Nature Publishing Group. (A) Destruction. Coupling of a degradation signal (DEG) to GFP will result in targeting of the GFP for ubiquitylation followed by proteasomal degradation. Degradation of the GFP substrate results in loss of fluorescence. (B) Fluorescence resonance energy transfer (FRET) fluorophore peptide substrate. A FRET peptide substrate contains a donor and acceptor fluorophore with spectral overlap. When the FRET probe is intact and excited with the optimal wavelength for the donor, acceptor fluorescence will be emitted at the expense of donor fluorescence. Cleavage of the FRET probe results in separation of donor and acceptor fluorophores and increased emission from the donor with a concomitant loss of acceptor fluorescence. (C) Quenching with fluorophore/quencher pair in peptide substrate. Small peptide fragments containing a fluorophore and a corresponding quencher will be essentially non-fluorescent. After cleavage, when the quencher is spatially separated from the fluorophore, the fluorophore will emit fluorescence. (D) Quenching with identical fluorophores in peptide substrate. Two identical fluorophores will quench each other. Principle as in (B). (E) FRET fluorescent proteins. With CFP and YFP as donor and acceptor fluorophore, respectively. Principle as in (B). CFP, cyan fluorescent protein; GFP, green fluorescent protein; YFP, yellow fluorescent protein.

rapid turnover of EGFP in the cytoplasm to prevent accumulation and provide a fluorescent readout on an hourly time frame. The long half-life of EGFP was reduced through incorporation of a PEST sequence ($MODC_{(422-461)}$) on the EGFP C-terminus, which is known to enhance proteasomal protein degradation without ubiquitination.[86] After incorporation of the PEST sequence, the authors demonstrated the utility of the biosensor in transfected CHO Tet-off cells using flow cytometry (Figure 1.15(A)). A comparison between EGFP and EGFP-$MODC_{(422-461)}$ before and after treatment with the transcription inhibitor cycloheximide (CHX). Over time after treatment with CHX, EGFP-$MODC_{(422-461)}$ fluorescence decreased whereas EGFP fluoresce remained constant (Figure 1.15(B)). Although this biosensor was demonstrated for use as a reporter of transcription, this system could easily be used as a proteasome reporter by following the proteasome degradation used to decrease EGFP half-life.

A similar protein construct, ZsProSensor-1 was used as a biosensor for the measurement of proteasome activity in MBEC and HepG2 cells.[87] The ZsProSensor-1 consists of a specific degradation motif of ornithine decarboxylase fused to the ZsGreen fluorescent protein.[85] Like the EGFP-$MODC_{(422-461)}$ protein transcription biosensor, the ZsProSensor-1 fusion protein is rapidly degraded by the proteasome without ubiquitylation. First, ZsProSensor-1 was transfected into MBEC and HepG2 cells and intracellular fluorescence was monitored with, and without, the proteasome inhibitor MG132 (Figure 1.16 (A)). With inhibition of the proteasome using MG132, fluorescence was stabilized by the accumulation of ZsProSensor-1. In the absence of MG132, different levels of fluoresce are observed between each cell line, indicated differing levels of

[86] (1) Rogers, S.; Wells, R.; Rechsteiner, M. *Science (New York, N.Y.)* **1986**, *234*, 364–8. (2) Murakami, Y.; Matsufuji, S.; Kameji, T.; Hayashi, S.; Igarashi, K.; Tamura, T.; Tanaka, K.; Ichihara, A. *Nature* **1992**, *360*, 597–9.

[87] Zheng, X.; Ruas, J. L.; Cao, R.; Salomons, F. a; Cao, Y.; Poellinger, L.; Pereira, T. *Molecular and cellular biology* **2006**, *26*, 4628–41.

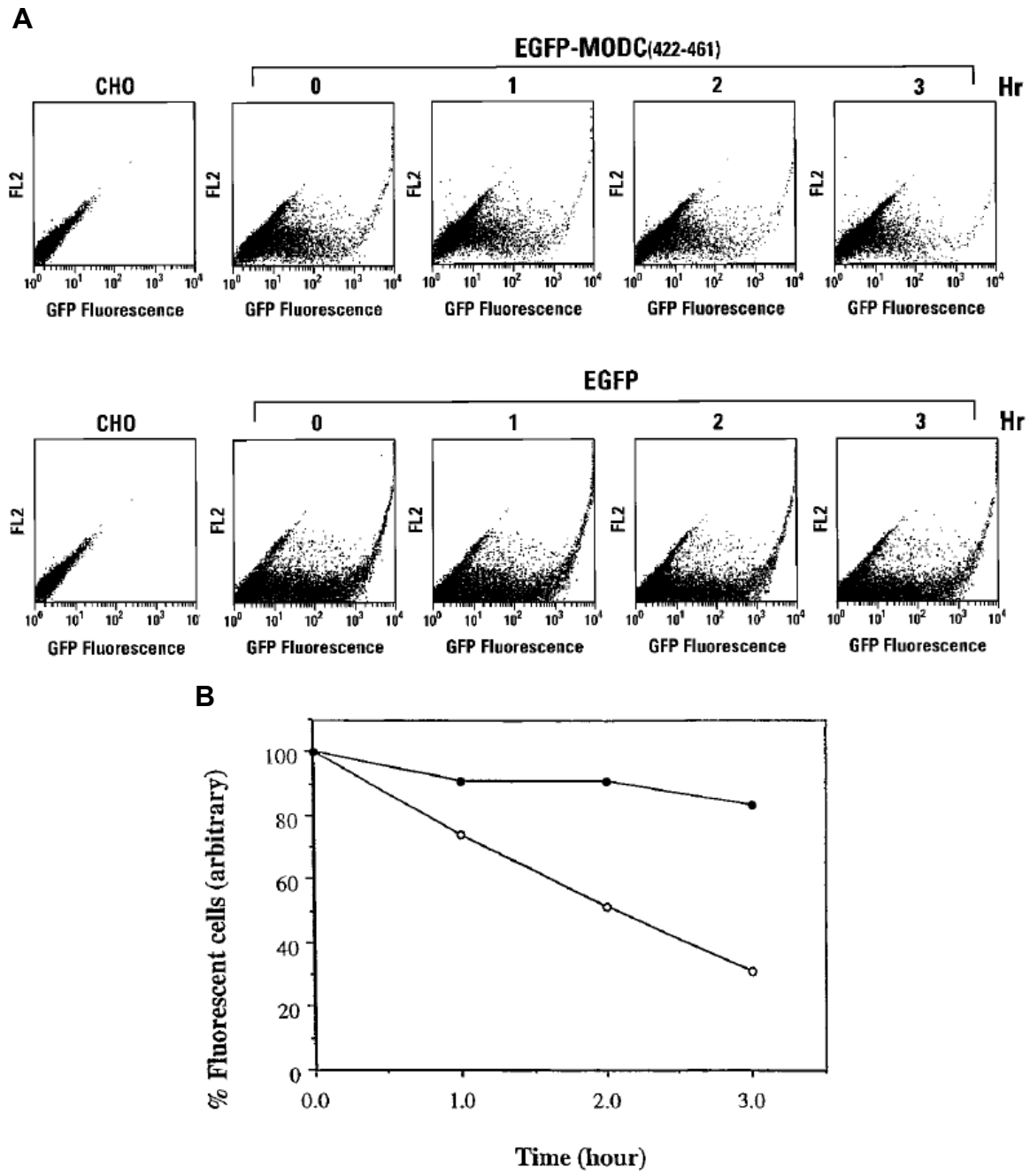

Figure 1.15 Reprinted with permission from Li, X.; Zhao, X.; Fang, Y.; Jiang, X.; Duong, T.; Fan, C.; Huang, C. C.; Kain, S. R. *The Journal of biological chemistry* **1998**, *273*, 34970–5. (A), flow cytometric analysis of the fluorescence stabilities of EGFP and EGFP-MODC-(422–461). CHO K1 Tet-off cells were transfected with the two constructs used in Fig. 1. After 24 h, the transfected cells were treated with 100 mg/ml CHX for 0, 1, 2, and 3 h. The treated cells were collected with EDTA, and 10,000 cells were subjected to FACS analysis. (B) The percentage of the fluorescent cells was plotted. *Solid circles*, EGFP; *open circles*, EGFP-MODC-(422–461).

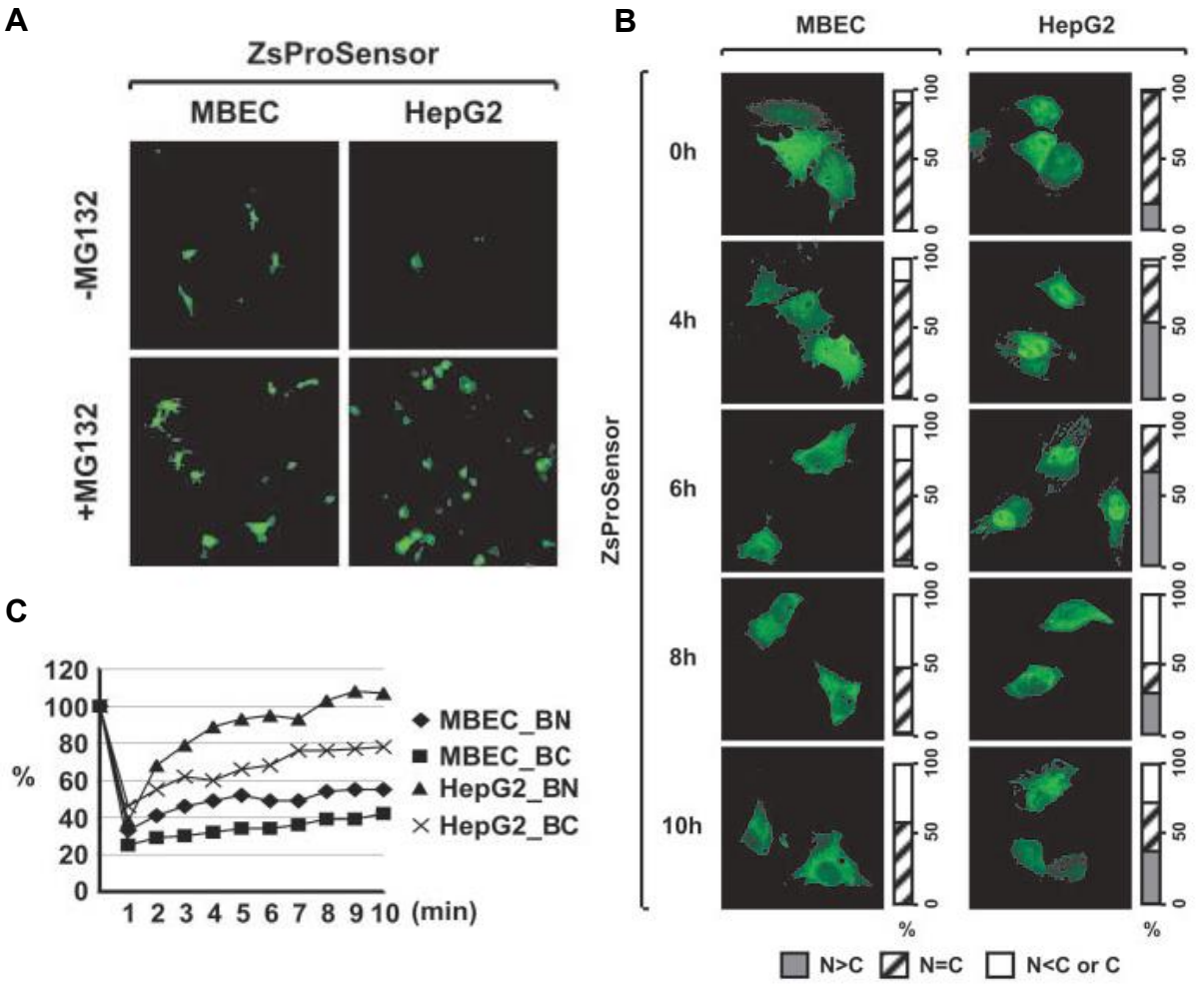

Figure 1.16 Reprinted with permission from Neefjes, J.; Dantuma, N. P. *Nature reviews. Drug discovery* **2004**, *3*, 58–69. Compartmentalization of proteasome activity in MBECs and HepG2 cells. (A) Treatment of cells with the proteasome inhibitor MG132 leads to stabilization of the ZsProSensor-1 protein. pZsProSensor-1 was transfected into MBECs or HepG2 cells cultured at normoxia. The cells were treated with dimethyl sulfoxide (MG132) or 10 M MG132 (MG132) for 8 h before fixation. Cells were observed with lower magnification. Representative images are shown. (B) Differential proteasome-mediated degradation of ZsProSensor-1 protein occurs in MBECs and HepG2 subcellular compartments. Cells were transfected with pZsProSensor-1 and cultured at normoxia. After treatment with 10 M MG132 for 8 h, the cells were fixed (0 h) or washed three times with culture medium to remove MG132 and then fixed at 4 h, 6 h, 8 h, or 10 h of incubation. Cells were analyzed by confocal microscopy, and representative images are presented. (C) FRAP analysis of cells transfected with pZsProSensor-1. Fluorescence before bleaching was considered 100%. Data are shown as the ratio between the fluorescence observed within the nuclear and cytoplasmic compartments or between cytoplasmic and nuclear compartments following bleaching of the nucleus or cytoplasm, respectively. The results presented are the average of the analysis of MBECs or HepG2 cells bleached in the nuclear compartment (MBEC_BN or HepG2_BN) or in the cytoplasm (MBEC_BC or HepG2_BC) after 4 h

endogenous proteasome activity, with the level of endogenous proteasome activity of HepG2 higher than MBEC. This has been documented previously.[88] Next, the authors used the ZsProSensor-1 to demonstrate compartmentalization of proteasome activity. MBEC and HepG2 cells were treated with MG132 for 8 hours, after which the cells were observed at various time points in the absence of inhibitor. Before the addition of MG132, 92% of MBEC cells had uniform expression of the ZsProSensor-1 biosensor (N = C). After removal of MG132, ZsProSensor-1 biosensor fluorescence decreased in the nucleus (N < C; 15%, 24%, and 52% at 4, 6, and 8 h, respectively). In the HepG2 cell line, before addition of MG132, fluorescence was evenly distributed throughout the cell (N = C) in 79% of the cells. However, after the addition of MG132, ZsProSensor-1 biosensor fluorescence decreased in the cytoplasm compared to the nucleus (N > C; 55% at 4 h and 67% at 6 h), although fluorescence was found mainly in the cytoplasm at later time frames (N < C; at 8 h, 49%; at 10 h, 28%) (Figure 1.16 (B)). These results are in agreement with other studies that demonstrate that during cell cycle progression proteasome activity is imported into the nucleus, with proteasome activity equilibrium occurring only after NEB.[89] Next, the diffusion of proteasome activity was investigated using FRAP (Fluorescence Recovery After Photobleaching). MBEC and HepG2 cells were first transfected with GFP to establish a baseline of fluorescence recovery. Fluorescence recovery was observed 4 to 5 minutes after photobleaching in both cell lines (Data not shown). Next, fluorescence recovery of MBEC and HepG2 cells transfected with the ZsProSensor-1 biosensor was investigated using FRAP. In the MBEC cell line fluorescence recovery was reduced, recovering only 50% over 10 minutes (Figure 1.16 (C)). In contrast, HepG2 cells recovered 80% of

[88] Brush, J. M.; Kim, K.; Sayre, J. W.; McBride, W. H.; Iwamoto, K. S. *International journal of radiation biology* **2009**, *85*, 483–94.
[89] (1) Wójcik, C.; DeMartino, G. N. *The International Journal of Biochemistry & Cell Biology* **2003**, *35*, 579–589. (2) Reits, E. a; Benham, a M.; Plougastel, B.; Neefjes, J.; Trowsdale, J. *The EMBO journal* **1997**, *16*, 6087–94.

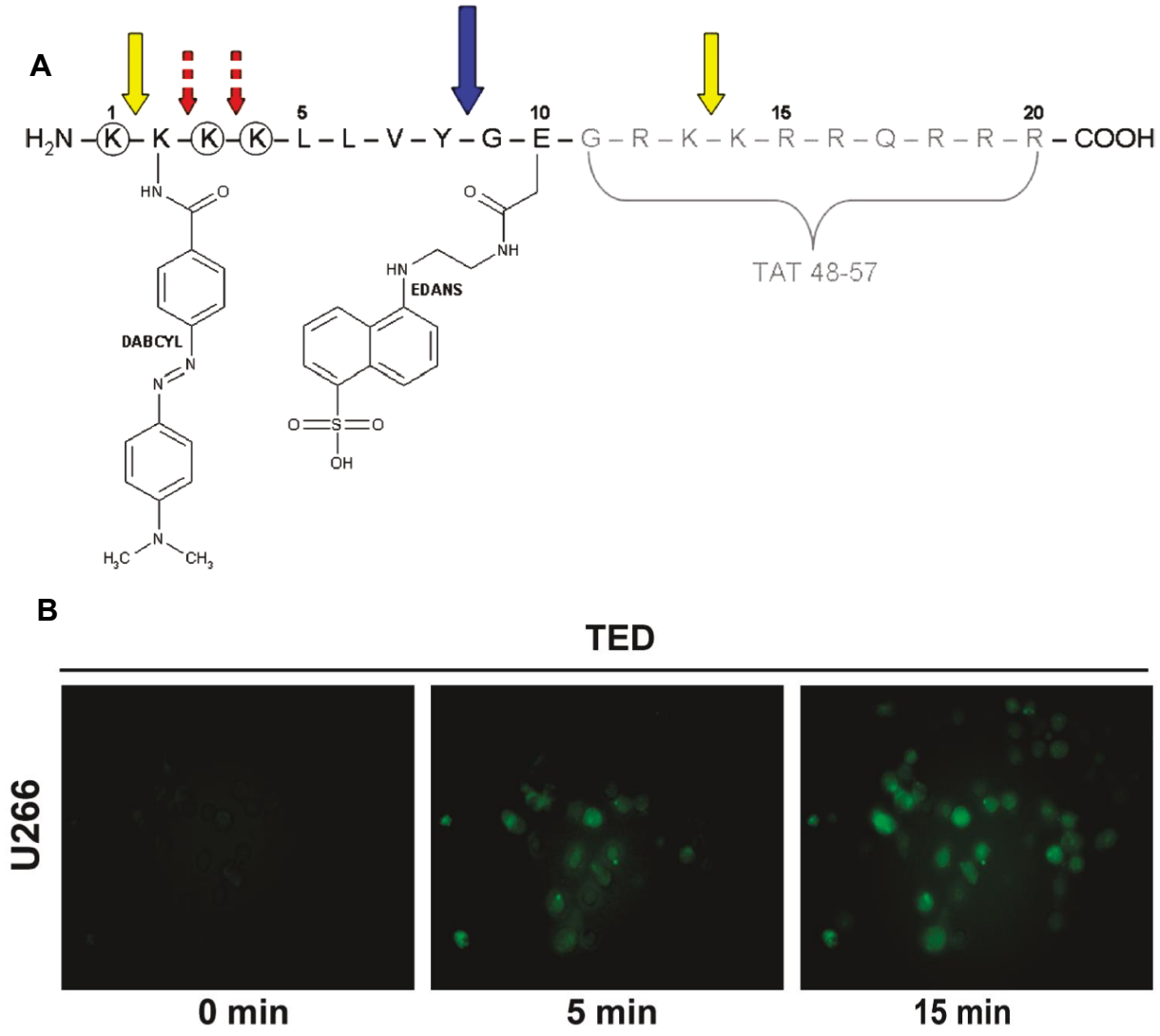

Figure 1.17 Reprinted with permission from Urru, S. a M.; Veglianese, P.; De Luigi, A.; Fumagalli, E.; Erba, E.; Gonella Diaza, R.; Carrà, A.; Davoli, E.; Borsello, T.; Forloni, G.; Pengo, N.; Monzani, E.; Cascio, P.; Cenci, S.; Sitia, R.; Salmona, M. *Journal of medicinal chemistry* **2010**, *53*, 7452–60. Copyright 2011 American Chemical Society. (A) Schematic structure of sensor (TED) for the β5 subunit of the proteasome. The blue arrow represents the preferred cleavage site. The yellow arrows represent secondary cleavage sites. The red dashed arrows represent amino acids in the D conformation to prevent cleavage. A TAT protein sequence was incorporated on the C-terminus to facilitate cytoplasmic delivery. (B) EDANS fluorescence was monitored over 15 minutes to observe fluorescence enhancement upon proteolysis after incubation with 17 μM TED.

fluorescence in the cytosolic fraction and 102% in the nucleus. These results demonstrate greater proteasome activity of the HepG2 cell line, along with a greater concentration of proteasome activity near the nucleus.

Although the ZsProSensor-1 was used to elucidate proteasome activity at various locations in the MBEC and HepG2 cell lines, it is difficult to label the sensor as a real-time assay of proteasome activity. First, the sensor provides an inverse readout of proteasome activity. If proteasome activity is present, no measurable fluorescent signal is observed. This can create a problem for measuring differences in proteasome activity due to ever decreasing amounts of EGFP, and hence, a decreasing fluorescent signal which is more difficult to measure. Also, no dynamic rage data was provided, so it is difficult to calculate the limit of detection for the assay. A third issue is the long time frame of the assay, which makes it difficult to apply to a wide variety of cellular processes. Very few enzymatic processes occur on a 10 hour long time scale, with many processes taking place in a few minutes, making use of this sensor unfeasible. Finally, unlike chemical probes which can be controlled via DMNB caging, no such control exists with the ZsProSensor-1 biosensor (see Discussion on DMNB caging in CURRENT CAPABILITIES OF PROTEIN KINASE BIOSENSORS).

Chemical probes are capable of overcoming the challenges associated with GFP-based proteasome biosensors. As an example of a chemical proteasome biosensor, a recent report describes the development of a chymotrypsin-like (proteasome β5 subunit) biosensor and its use intracellularly.[90] The TAT-EDANS-DABCYL (TED) biosensor was constructed based on a known consensus sequence for the β5-subunit of the proteasome, NH_2-LLVY-OH (Figure 1.17).

[90] Urru, S. a M.; Veglianese, P.; De Luigi, A.; Fumagalli, E.; Erba, E.; Gonella Diaza, R.; Carrà, A.; Davoli, E.; Borsello, T.; Forloni, G.; Pengo, N.; Monzani, E.; Cascio, P.; Cenci, S.; Sitia, R.; Salmona, M. *Journal of medicinal chemistry* **2010**, *53*, 7452–60.

A fluorophore/quencher FRET pair was included on either side of the cleavage site, using EDANS as the fluorophore and DABCYL as a non-fluorescent quencher. Since the consensus sequence for the β5 subunit is negatively charged and unlikely to reach the cytoplasm, a TAT sequence helps facilitate entry into the cytoplasm. N-terminal D-Lysine residues were also added to prevent proteolysis of the substrate by other proteases. The sensor (17 μM) was incubated with U266 cells to yield a fluorescent increase upon proteolysis. Unfortunately, no dynamic range was reported or intracellular experiments to quantitate intracellular chymotrypsin-like proteasome activity in U226 cells. Also, although this FRET pair did succeed in their manuscript, a FRET pair further in the red would be advantageous in future development.

A second report describes a chemical biosensor for the chymotrypsin-like activity of the proteasome.[91] This sensor **1.3** improves on the TED sensor in two main ways: (1) the photophysical properties of the fluorophore and (2) the addition of a DMNB caging group for control observer control of the assay (Scheme 1.1). The authors attached a long wavelength

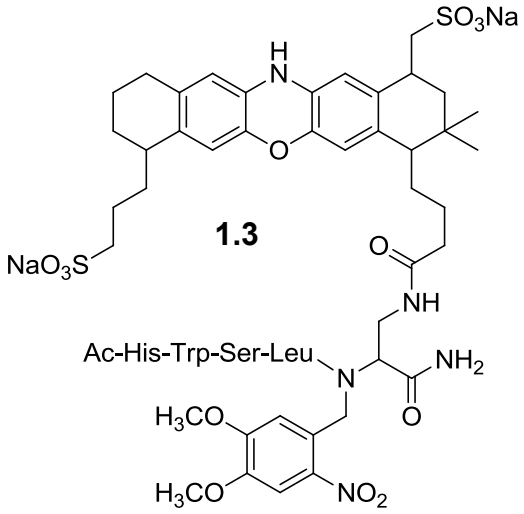

Scheme 1.1 Reprinted with permission from Wakata, A.; Lee, H.-M.; Rommel, P.; Toutchkine, A.; Schmidt, M.; Lawrence, D. S. *Journal of the American Chemical Society* **2010**, *132*, 1578–82. Copyright 2010 American Chemical Society. Structure of Chymotrypsin-like reporter of proteasome activity.

[91] Wakata, A.; Lee, H.-M.; Rommel, P.; Toutchkine, A.; Schmidt, M.; Lawrence, D. S. *Journal of the American Chemical Society* **2010**, *132*, 1578–82.

A

peptide	Flc increase	K_m (μM)	V_{max} (nmol/min · mg)	k_{cat}/K_m (M^{-1} s^{-1})
Ac-HWSL-Dap(Fl)	22.4-fold	56 ± 11	1.4 ± 0.2	300 ± 70
Ac-HWSL-Dab(Fl)	27.1-fold	80 ± 13	1.0 ± 0.1	150 ± 30
Ac-HWSL-Lys(Fl)	24.9-fold	81 ± 8	2.7 ± 0.2	390 ± 50
Ac-WHSL-Lys(Fl)	23.5-fold	73 ± 15	1.7 ± 0.3	280 ± 70

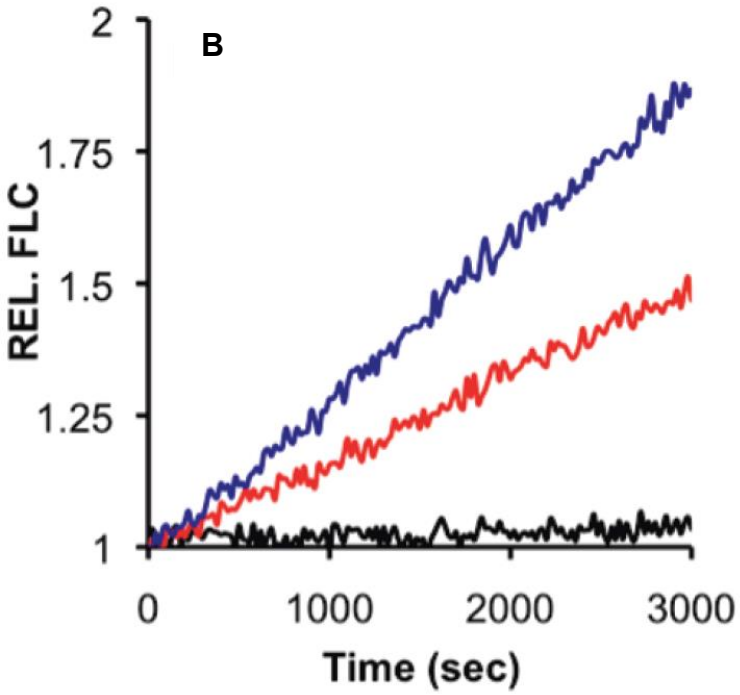

Figure 1.18 Reprinted with permission from Wakata, A.; Lee, H.-M.; Rommel, P.; Toutchkine, A.; Schmidt, M.; Lawrence, D. S. *Journal of the American Chemical Society* **2010**, *132*, 1578–82. Copyright 2010 American Chemical Society. (A) Table containing proteasome biosensor analogs, along with enzymatic data. (B) Peptide **1.3** (5.65 μM) treated with wild-type cell lysate (black), and preirradiated for 2 min (red) or 10 min (blue).

fluorophore (excitation 633 nm, emission 678 nm) with a high extinction coefficient (119,000 M^{-1} cm^{-1}).[92] These properties are much better than the EDANS fluorophore used for the TED sensor (excitation 335 nm, emission 493 nm, extinction coefficient 5,900 M^{-1} cm^{-1}). Additionally, a DMNB caging group was included to provide observer control of the assay. Along with the caged derivative in Scheme 1.1, the authors synthesized four noncaged analogs

[92] Toutchkine, A. PCT. Int. Appl., PCT/US2009/46238.

and fully characterized the enzymological properties of the substrates as well as their dynamic ranges, which are all over 20-fold (Figure 1.18(A)). Control of the biosensor using DMNB uncaging was also demonstrated using cell lysates. Peptide **1.3** (5.65 μM) was treated with wild-type yeast cell lysate containing active proteasome after irradiation for 0 min (black), 2 min (red) and 4 min (blue). As expected, differing amounts of substrate **1.3** were uncaged, resulting in a fluorescent enhancement. Although this biosensor has been applied to cell lysates, its use has yet to be demonstrated intracellularly.

CONCLUSIONS

Quantitation of enzyme activity is essential for understating signal transduction pathways. Many current techniques, such as western blotting or intracellular antibody labeling, quantitate enzyme expression levels while providing no assessment of enzyme activity. Current enzyme activity assays can be divided into two groups, each with unique advantages and disadvantages including: (1) GFP-based FRET sensors relying on polypeptide domains binding to a substrate as a mechanism of action and (2) chemical probes relying on bond cleavage, metal chelation, electrostatic interactions or environmentally-sensitive fluorophores as a mechanism of action. GFP-based FRET sensors are relatively easily transfected into a wide variety of cells, making them extremely useful to molecular biologists. However, GFP-based FRET sensors do have disadvantages including: (1) a lack of a large dynamic range for activity measurement and (2) the reliance on a large spectral window during confocal microscopy, limiting the number of possible readouts. Chemical probes provide the unique advantages of observer control (through

highly selective photodeprotection), large dynamic ranges (typically 10x (or more) larger than GFP-based FRET sensors), and a wide range of photophysical properties. Disadvantages associated with chemical probes include: (1) problems with cytoplasmic delivery of the probe and (2) difficulties with probe synthesis.

This thesis focuses on three main projects in development of chemical probes for PKA and proteasome activity. Chapter two describes the development of an assay for PKA including a large dynamic range. The assay relies on electrostatic interactions between a fluorophore labeled peptide and dark fluoresce quencher to realize large (up to 150-fold) enhancements in fluorescence. The assay is the applied to measure the subcellular distribution of PKA in mitochondria. Chapter three focuses on the development of a non-fluorescent dark quencher found to quench fluorophores with a broad range of photophysical properties, including many suitable for fluorescent microscopy. A previously identified quencher, Acid Blue 40, was chemically modified to include a carboxylic acid handle. The utility of carboxy Acid Blue 40 (cAB40) was demonstrated through construction of reporters of trypsinolysis and photolysis. Chapter four focuses on the synthesis and development of a unimolecular nanoparticle-based assay for PKA. The cAB40 quencher and a fluorescently labeled PKA substrate were attached to the surface of a silica nanoparticle (90 nm diameter). Upon phosphorylation a 2.2-fold fluorescent enhancement was observed. Chapter five focuses on the development of proteasome biosensors of the Caspase-like (Ca-L) and Chymotrypsin-like (Ch-L) catalytic activities of the proteasome. The fluorophore 5'-tetramethylrhodamine and cAB40 quencher were covalently attached to opposing ends of Ca-L and Ch-L consensus sequences. Selectivity of each substrate for each catalytic subunit was demonstrated. Overall, this body of work demonstrates substantial additions to the development of chemical probes for kinase and proteasome activity.

CHAPTER 2

SUBORGANELLE SENSING OF MITOCHONDRIAL cAMP-DEPENDENT PROTEIN KINASE ACTIVITY

(Reproduced with permission from Agnes, R. S.; Jernigan, F.; Shell, J. R.; Sharma, V.; Lawrence, D. S. *Journal of the American Chemical Society* **2010**, *132*, 6075–80.

INTRODUCTION

Protein kinases are a large enzyme family that has been implicated in nearly every cell-based behavior, from ATP generation to unrestrained growth and division.[1] These enzymes are linked by their ability to catalyze phosphoryl transfer from ATP to the hydroxyl moieties of serine, threonine, and/or tyrosine residues in proteins. A variety of factors limit protein kinase-catalyzed phosphorylation to intended protein targets: (a) the ability to phosphorylate serine/threonine or tyrosine, but only rarely both aliphatic and aromatic residues, (b) differential expression as a function of cell type, (c) recognition of specific amino acid sequences encompassing the hydroxyl phosphoryl acceptor moiety, and (d) localization to specific intracellular sites. The cAMP-dependent protein kinase (PKA) exhibits many of these attributes as a serine/threonine-specific protein kinase with a special preference for sequences of the general form Arg- Arg-Xaa-Ser/Thr-Xaa in protein substrates.[2] In addition, PKA is anchored to a variety of intracellular sites via coordination to A-kinase anchoring proteins (AKAPs), and thus

[1] Manning, G.; Whyte, D. B.; Martinez, R.; Hunter, T.; Sudarsanam, S. *Science* **2002**, *298*, 1912–1934.

[2] Shabb, J. B. *Chem. Rev.* **2001**, *101*, 2381–2411.

the biological consequences of its action are location-dependent.[3] For example, mitochondrial PKA is implicated in the regulation of apoptosis and ATP synthesis.[4] However, as is true for protein kinases in general, presumed intracellular PKA activity is commonly assessed in an indirect fashion: either by the mere presence of the enzyme (immunofluorescence or Western blots) or by the effect of small molecule modulators, such as inhibitors, on the phosphorylation of *presumed* PKA protein substrates. Unfortunately, these commonly employed methods do not furnish a direct measure of kinase activity. Fluorescent sensors have been used to directly and continuously assess kinase action.[5] However, these either display a limited dynamic range or employ fluorophores with photophysical properties (short $\lambda_{ex}/\lambda_{em}$,[6] small ε,[7] low Φ) that are incompatible (due to interference from autofluorescence) with cells, cell lysates, or organelles. With the latter limitation in mind, we report herein the application of a quenched fluorescence strategy[6] to create a kinase sensor of unprecedented dynamic range. Sensors with a large dynamic range can be used in relatively small quantities, thereby diminishing the likelihood of interference with ongoing biochemical processes (i.e., Observer Effect).[8] The favorable properties associated with the sensor have allowed us to assess the relative abundance of PKA in the major mitochondrial microenvironments (outer membrane, intermembrane space, and matrix).[9]

---

[3] Smith, F. D.; Langeberg, L. K.; Scott, J. D. *Trends Biochem. Sci.* **2006**, *31*, 316–323.

[4] Feliciello, A.; Gottesman, M. E.; Avvedimento, E. V. *Cell Signal.* **2005**, *17*, 279–87.

[5] Lawrence, D. S.; Wang, Q. *ChemBioChem* **2007**, *8*, 373–278.

[6] Sharma, V.; Agnes, R. S.; Lawrence, D. S. *J. Am. Chem. Soc.* **2007**, *129*, 2742–2743.

[7] Shults, M. D.; Imperiali, B. *J. Am. Chem. Soc.* **2003**, *125*, 14248–14249.

[8] Sharma, V.; Lawrence, D. S. *Angew. Chem., Int. Ed.* **2009**, *48*, 7290–7292.

[9] (1) Ma, Y.; Taylor, S. S. *J. Biol. Chem.* **2008**, *283*, 11743–11751. (2) Sardanelli, A. M.; Signorile, A.; Nuzzi, R.; Rasmo, D. D.; Technikova-Dobrova, Z.; Drahota, Z.; Occhiello, A.; Pica, A.; Papa, S. *FEBS Lett.* **2006**, *580*, 5690–

RESULTS AND DISCUSSION

The fluorophores described in this report are coumarin derivatives, which possess photophysical properties (Table 2.1) that are readily amenable to biological applications. Three coumarin-derivatized peptides (**2.1**-**2.3**, Scheme 2.1) of the general form coumarin-Aoc-GRTGRRFSYP-amide were prepared (where Aoc = aminooctanoic acid). These positively charged peptides were exposed to 47 different negatively charged dyes (End of Chapter, Table 2.2) with the expectation that complex formation would result in the quenching of coumarin fluorescence. In addition, we anticipated that PKA-catalyzed phosphorylation of coumarin-Aoc-GRTGRRFSYP-amide would promote association of the phosphorylated peptide with the 14-3-3τ domain,[10] thereby releasing the quenching dye and restoring fluorescence (Figure 2.1). The

sensor ($\lambda_{ex}/\lambda_{em}$)	fluorescent fold-increase	K_m (μM)	V_{max} (μmol/min·mg)
2.1 (420/475 nm)	152	2.2 ± 0.1	0.53 ± 0.03
2.2 (437/477 nm)	150	1.9 ± 0.1	0.34 ± 0.04
2.3 (450/490 nm)	28	6.2 ± 0.1	0.20 ± 0.09

Table 2.1 Photophysical properties, fluorescent-fold increase, K_m, and V_{max} for the PKA-catalyzed phosphorylation of sensors **2.1**-**2.3** (where Sensor = Fluorophore-Aoc-GRTGRRFSYP-amide). Kinetic properties were acquired in the presence of quencher **2.4** and the 14-3-3τ domain. See "Acquisition of apparent K_m and V_{max} values".

5696. (3) Chen, Q.; Lin, R. Y.; Rubin, C. S. *J. Biol. Chem.* **1997**, *272*, 15247–15257.(d) Schwoch, G.; Trinczek, B.; Bode, C. *Biochem. J.* **1990**, *270*, 181–188. (4) Ryu, H.; Lee, J.; Impey, S.; Ratan, R. R.; Ferrante, R. J. *Proc. Natl. Acad. Sci. U.S.A.* **2005**, *102*, 13915–13920.

[10] Yaffe, M. B.; Rittinger, K.; Volinia, S.; Caron, P. R.; Aitken, A.; Leffers, H.; Gamblin, S. J.; Smerdon, S. J.; Cantley, L. C. *Cell* **1997**, *91*, 961–971.

lead quencher dye for all three peptides proved to be Acid Green 27 (**2.4**) and the observed PKA-catalyzed changes in fluorescence in the presence of **2.4** are: peptide **2.1** (152-fold), peptide **2.2** (150-fold), and peptide **2.3** (28-fold) (Table 2.1). Given its large dynamic range and relatively high *V* max (Table 2.1), we decided to employ peptide **2.1** in all subsequent studies. We confirmed that phosphoryl transfer from ATP to the serine hydroxyl moiety of the peptide sensor is required for the observed fluorescent enhancement by examining analogues of the peptide substrate **2.1** and ATP. First, substitution of peptide **2.1** with its nonphosphorylatable Ala-for-Ser counterpart **2.5** fails to elicit a change in fluorescence (Figure 2.2D). Second, substitution of ATP with the corresponding thio-derivative, ATP(γ)S, dramatically reduces the rate of fluorescence

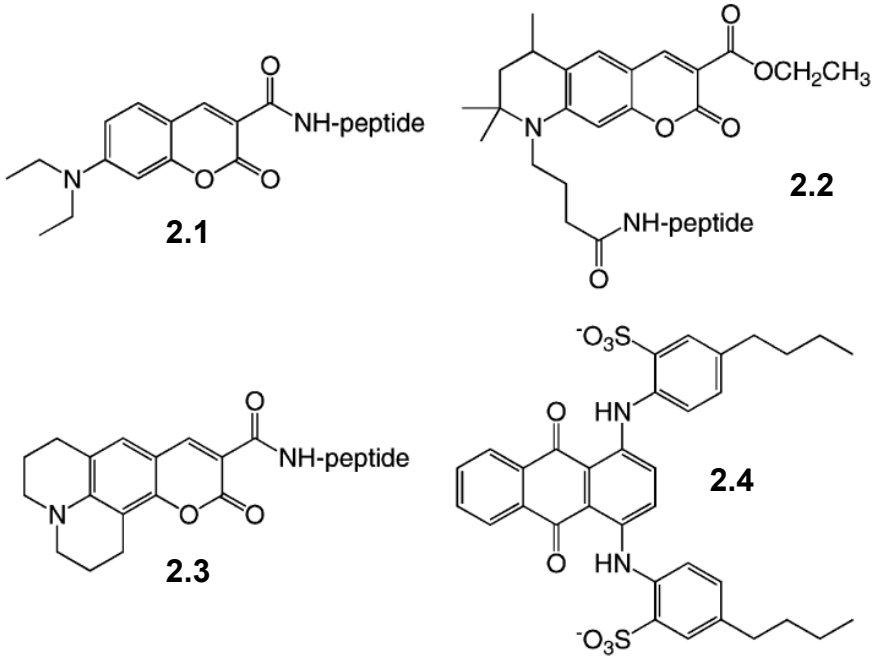

Scheme 2.1 Structures of the coumarin derivatives **1-3** of the general form fluorophore-Aoc-GRTGRRFSYP-amide. The fluorescent quencher Acid Green 27 (**4**) was identified from a library of 47 dyes (Table 2.9).

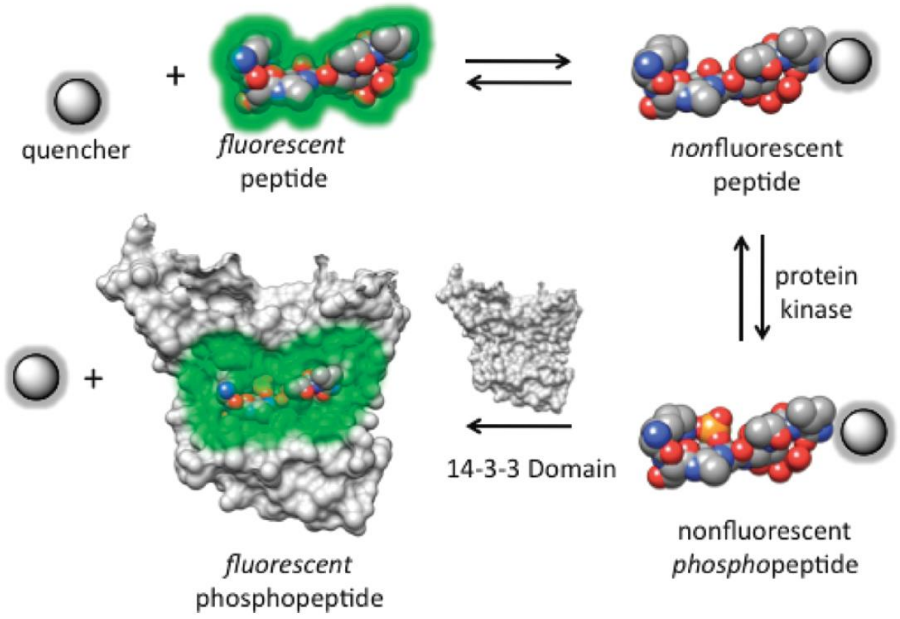

Figure 2.1 Protein Kinase-Catalyzed Phosphorylation of a Fluorescently Quenched Peptide Generates a Fluorescent Response in the Presence of the Phospho-Ser 14-3-3τ Binding Domain.

change (End of Chapter, Figure 2.3). ATP(γ)S is known to serve as a weak thiophosphoryl donor in protein kinase-catalyzed reactions.[11] Both 14-3-3τ and the fluorescent quencher, Acid Green 27 (**2.4**), are required for the large phosphorylation-induced fluorescence yield. In the absence of 14-3-3τ (but with quencher **2.4** present), no change in fluorescence is observed (End of Chapter, Figure 2.4). Furthermore, there exists a direct correlation between the relative amount of 14-3-3τ present and the observed phosphorylation-dependent fluorescent enhancement (End of Chapter, Figure 2.4). Surprisingly, in the absence of quencher **2.4** (but with 14-3-3τ present), there is a 50% *decrease* in observed fluorescence (End of Chapter, Figure 2.5). One possible explanation for the unexpected fluorescence decrease is the likely orientation of the 14-3-3τ- bound phosphopeptide **2.1** based on a previously described crystal

[11] (1) Zou, K.; Cheley, S.; Givens, R. S.; Bayley, H. *J. Am. Chem. Soc.* **2002**, *124*, 8220–8229. (2) Anderson, M. P.; Berger, H. A.; Rich, D. P.; Gregory, R. J.; Smith, A. E.; Welsh, M. J. *Cell* **1991**, *67*, 775–784.

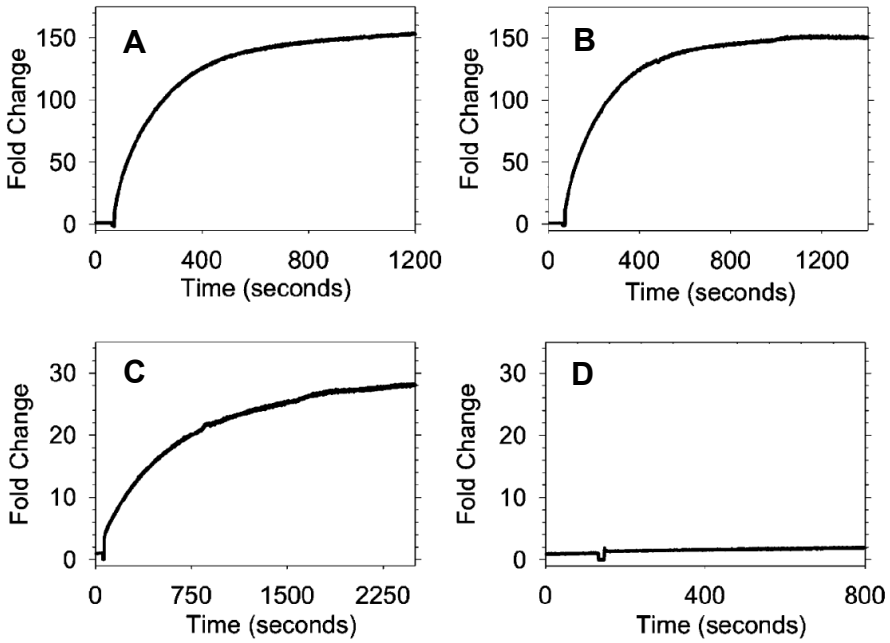

Figure 2.2 Fluorescence change as a function of incubation time of the PKA-catalyzed phosphorylation of sensors (A) **2.1**, (B) **2.2**, (C) **2.3**, and (D) a nonphosphorylatable Ala-for-Ser control peptide **2.5** (coumarin-Aoc GRTGRRFAYP-amide). Experiments were conducted in the presence of fluorescent quencher (**4**) and 14-3-3τ domain.

structure.[12] The N-terminus of the peptide, when complexed with the 14-3-3τ domain, is positioned adjacent to two tryptophan residues (Figure 2.6). We,[13] as well as others,[14] have shown that tryptophan can serve as a fluorescent quencher. 14-3-3τ domain-mediated quenching of coumarin-phosphopeptide fluorescence is intriguing since it suggests that removal of the tryptophan residues in the 14-3-3τ domain could furnish fluorescence fold changes even larger than those observed in this study. We examined the underlying assumption that the negatively charged quencher **2.4** engages the positively charged peptide substrate via electrostatic interactions. A small library of Arg to Ala substituted peptide analogues were prepared and K_D

[12] Rittinger, K.; Budman, J.; Xu, J.; Volinia, S.; Cantley, L. C.; Smerdon, S. J.; Gamblin, S. J.; Yaffe, M. B. *Mol. Cell* **1999**, *4*, 153 166.

[13] Lee, H. M.; Priestman, M. A.; Lawrence, D. S. *J. Am. Chem. Soc.* **2010**, *132*, 1446–1447.

[14] Doose, S.; Neuweiler, H.; Sauer, M. *ChemPhysChem* **2005**, *6*, 2277–2285.

values were acquired for each of these with Acid Green 27, using fluorescence quenching as an indicator of complex formation. As is clear from Table 2.2, the quenching phenomenon is Arg residue-dependent, with the apparent K_D displaying an approximate two orders of magnitude loss for every Arg replaced by an Ala. The effect is independent of the site of the Ala-for-Arg substitution (cf. **2.6** vs **2.7** vs **2.8**), implying a diffuse electrostatic interaction between the negatively charged dye and the peptide substrate. Job plot analysis revealed the formation of a 1:1 complex between **2.1** and **2.4** (Figure 2.7). The large fluorescent dynamic range of the PKA-catalyzed phosphorylation of peptide **2.1** furnishes a sensitive measure of kinase activity. The catalytic activity of PKA at a concentration as low as 160 pM can be detected as demonstrated by the plot of initial rate versus PKA concentration (Figure 2.8). Figure 2.8 provides a standard curve for assessing "PKA activity equivalents" in biological systems. Although the indispensable nature of the PKA signaling pathway in mitochondrial physiology is beyond dispute,[4] its

Peptide	Peptide Sequence	K_D (μM)
2.1	Cou-Aoc-GRTGRRFSYP-amide	0.04 ± 0.07
2.6	Cou-Aoc-G**A**TGRRFSYP-amide	1.6 ± 0.3
2.7	Cou-Aoc-GRTG**A**RFSYP-amide	2.7 ± 0.6
2.8	Cou-Aoc-GRTGR**A**FSYP-amide	1.8 ± 0.2
2.9	Cou-Aoc-G**A**TGR**A**FSYP-amide	130 ± 80
2.10	Cou-Aoc-G**A**TG**A**RFSYP-amide	130 ± 65
2.11	Cou-Aoc-GRTG**AA**FSYP-amide	130 ± 70
2.12	Cou-Aoc-G**A**TG**AA**FSYP-amide	>200

Table 2.2 K_D Values of Sensor **2.1** and Various Ala-for-Arg Analogues (**2.6**-**2.12**) of Sensor **2.1**, with the Fluorescent Quencher **2.4**. See "Acquisition of Apparent K_D Values for **2.4** with Peptides **2.1** and **2.6**-**2.12**" in the Material and Methods section for experimental details.

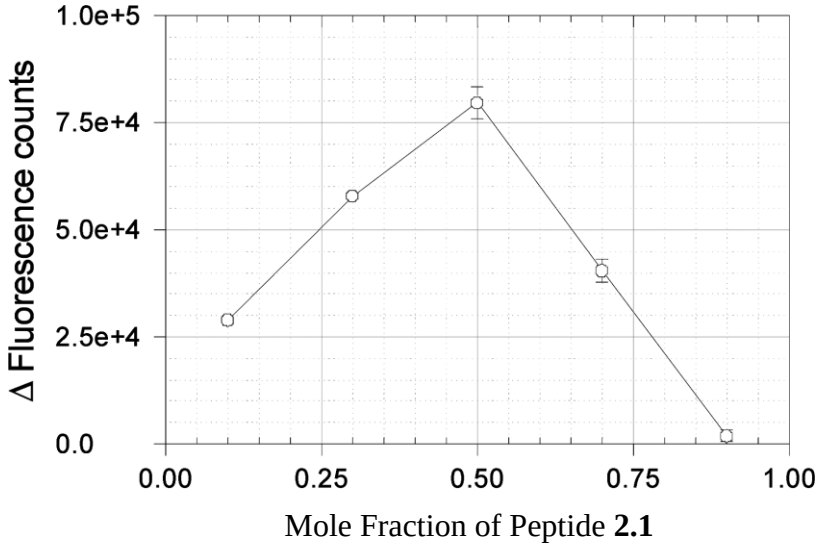

Figure 2.7 Fluorescence change as a function of mole fraction of sensor **2.1**. See "Job Plot for Determination of Stoichiometry" in the Material and Methods section for experimental details.

suborganelle location within the mitochondria (i.e., matrix, intermembrane space, and/or on the outer membrane oriented toward the cytoplasm; Figure 2.9) is enigmatic. Orr and colleagues demonstrated (via electron microscopy) that type-II PKA is primarily associated with the outer membrane of mitochondria in male germ cells.[15] Indeed, a major mitochondrial A-kinase anchoring protein (AKAP121 in mice and AKAP149 in humans), and its splice variants, position PKA on the cytoplasmic face of the outer membrane.[9(c)] Proteolysis of this AKAP[16] appears to promote apoptosis by releasing PKA from the outer membrane, which is known to promote antiapoptotic behavior.[17] By contrast, Schwoch et al showed (via electron microscopy) that both

[15] Lieberman, S. J.; Wasco, W.; MacLeod, J.; Satir, P.; Orr, G. A. *J. Cell Biol.* **1988**, *107*, 1809–1816.

[16] (1) Yoo, H.; Cha, H. J.; Lee, J.; Yu, E. O.; Bae, S.; Jung, J. H.; Sohn, I.; Lee, S. J.; Yang, K. H.; Woo, S. H.; Seo, S. K.; Park, I. C.; Kim, C. S.; Jin, Y. W.; Ahn, S. K. *Oncol. Rep.* **2008**, *19*, 1577–1582. (2) Carlucci, A.; Adornetto, A.; Scorziello, A.; Viggiano, D.; Foca, M.; Cuomo, O.; Annunziato, L.; Gottesman, M.; Feliciello, A. *EMBO J.* **2008**, *27*, 1073–1084.

[17] (1) Affaitati, A.; Cardone, L.; de Cristofaro, T.; Carlucci, A.; Ginsberg, M. D.; Varrone, S.; Gottesman, M. E.; Avvedimento, E. V.; Feliciello, A. *J. Biol. Chem.* **2003**, *278*, 4286–4294. (2) Harada, H.; Becknell, B.; Wilm, M.; Mann, M.; Huang, L. J.; Taylor, S. S.; Scott, J. D.; Korsmeyer, S. J. *Mol. Cell* **1999**, *3*, 413–422.

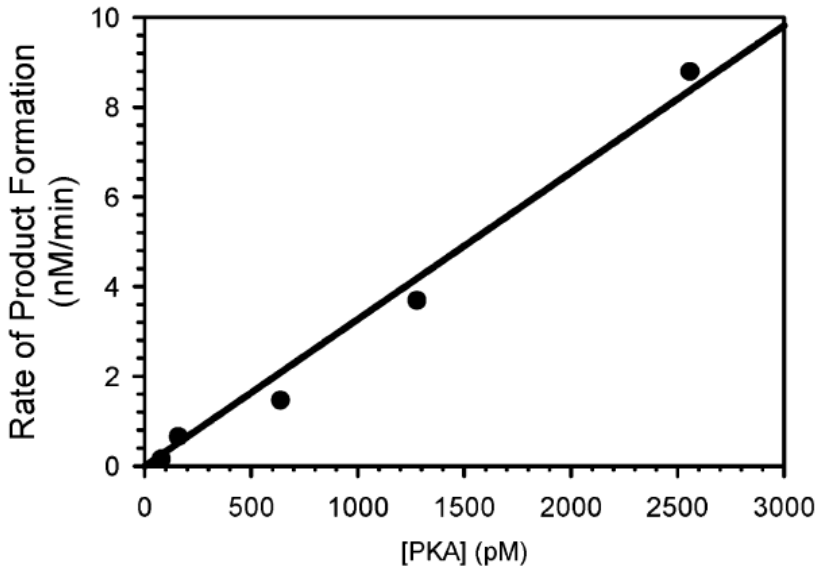

Figure 2.8 Reaction rate (nM of phosphopeptide formation/min) as a function of PKA concentration (pM).

types-I and -II PKA are primarily associated with the mitochondrial matrix/inner membrane in mitochondria isolated from a wide variety of organs.[9(d)] Matrix localization of PKA has also been observed in neuronal mitochondria.[9e] Papa and his colleagues found that PKA is associated with the inner membrane of bovine heart mitochondria.[18] Furthermore, these investigators reported a detailed electron microscopic analysis of rat heart mitochondria and concluded that more than 90% of all mitochondrial-bound PKA is present in the inner mitochondrial compartment.[9(b)] However, an additional complication, not described by these studies, is the enzymatic reach of PKA. In particular, the majority of mitochondrial proteins are nuclear encoded and thus must be imported from the cytoplasm. Consequently, although a variety of mitochondrial proteins are phosphorylated in a cAMP-dependent fashion, they may suffer PKA-catalyzed phosphorylation during import (e.g., at the outer membrane) and thus prior to being embedded within their final destination (e.g., in the matrix).[18] In short, the mitochondrial location of known PKA substrates

[18] Papa, S.; Sardanelli, A. M.; Scacco, S.; Technikova-Dobrova, Z. *FEBS Lett.* **1999**, *444*, 245–249.

Figure 2.9 Strategy for assessing PKA activity on the outer membrane (blue), in the intermembrane space (red), and in the matrix (yellow). PKA activity of intact mitochondria (**A**) is due to enzyme present on the outer membrane and in the intermembrane space. Trypsinized (i) mitochondria (**B**) lack outer membrane proteins and thus only intermembrane space PKA is present. Sonicated (ii) mitochondria (**C**) furnishes enzyme from all three compartments and thus represents total mitochondrial PKA.

is not necessarily a valid indicator of microenvironmental PKA activity. Finally, the active form of PKA (C subunit), which is released from the inactive holoenzyme (R2C2) upon exposure to cAMP, can diffuse through membranes.[19] Therefore, the suborganelle location of the holoenzyme (as determined by electron microscopy) does not necessarily recapitulate the location of the active form of the enzyme. With these factors in mind, we turned our attention to the suborganelle analysis of cAMP-activated PKA in isolated bovine heart mitochondria. Perhaps the most obvious approach for assessing PKA activity as a function of mitochondrial microenvironment is purification of the enzyme from the outer membrane, the intermembrane space, and the matrix. However, such a strategy is not practical for both structural and technological reasons. The holoenzyme resides as an AKAP-bound membrane-associated species on the outer membrane and likely, in an analogous AKAP-dependent fashion, at the inner membrane. Unfortunately, even if it were feasible to isolate and purify the outer and inner membrane components, it would not be clear which direction the enzyme is facing in the intact mitochondrion (i.e., an outer membrane bound species could be oriented outward toward the

[19] Harootunian, A. T.; Adams, S. R.; Wen, W.; Meinkoth, J. L.; Taylor, S. S.; Tsien, R. Y. *Mol. Biol. Cell* **1993**, *4*, 993–1002.

cytoplasm or inward toward the intermembrane space). An alternative approach might involve the cAMP-induced release of the C subunit and its subsequent isolation from the extra-mitochondrial, intermembrane space, and matrix regions. However, as demonstrated with bovine heart mitochondria, the standard technique used to expose the contents of the intermembrane space (digitonin treatment) results in some disruption of the matrix as well, leading to contamination of the intermembrane space contents with components from the matrix.[20] Therefore, we resorted to the strategy depicted in Figure 2.8. We reasoned that exposure of intact mitochondria to cAMP should activate PKA located on the outer membrane as well as any PKA present in the intermembrane space (i.e., inner leaflet of the outer membrane and/or outer leaflet of the inner membrane). The mitochondrial outer membrane contains a channel-forming protein-based complex (porin; also known as the voltage-dependent anion channel) that allows small molecules (<5000 molecular weight) to passively diffuse between the extra-mitochondrial environment and the intermembrane space.[21] We expected that, in addition to cAMP, our PKA sensor **2.1** and quencher **2.4** should be able to freely migrate into and out of the intermembrane space and thus report any PKA activity (by contrast, the inner membrane blocks access to the matrix of externally added cAMP[22]). This approach avoids the use of digitonin and thus should prevent contamination by the unintended release of matrix contents. In short, cAMP-treated mitochondria should furnish outer membrane *and* inter membrane space PKA activity. Furthermore, since trypsin digests only outward-facing outer membrane mitochondrial proteins,[9(a)] we expected that cAMP-exposed *trypsin*-treated mitochondria should provide only

[20] Burnette, B.; Batra, P. P. *Anal. Biochem.* **1985**, *145*, 80–86.

[21] Alberts, B.; Johnson, A.; Lewis, J.; Raff, M.; Roberts, K.; Walter, P. *Molecular Biology of the Cell*, Reference ed.; Garland Science: New York, 2007; pp 818.

[22] Acin-Perez, R.; Salazar, E.; Kamenetsky, M.; Buck, J.; Levin, L. R.; Manfredi, G. *Cell Metab.* **2009**, *9*, 265–276.

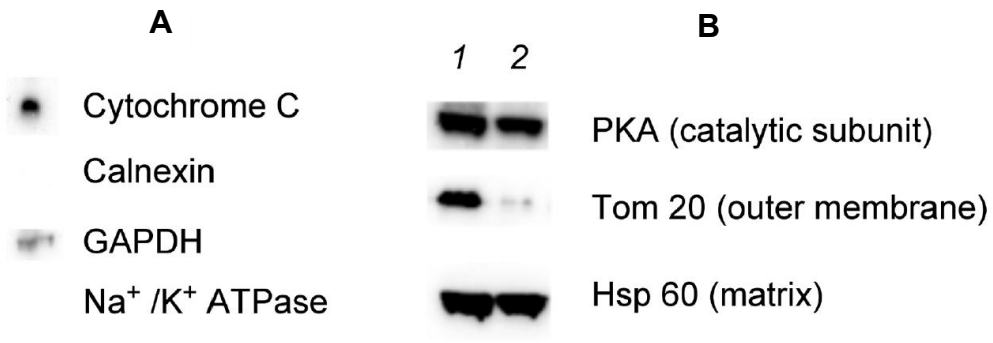

Figure 2.10 Assessment of mitochondrial purity and extent of trypsinolysis by Western blot analysis. (A) The mitochondrial preparation was examined for the presence of ER (calnexin), plasma membrane (Na+/K+-ATPase), and cytoplasmic (glyceraldehyde phosphate dehydrogenase) proteins. A minimal amount of cytoplasmic contamination is observed. (B) Trypsin digestion of intact mitochondria. Untreated mitochondria (lane 1) and mitochondria treated with trypsin for 1 h at 37 °C (lane 2) were analyzed by Western blot for Hsp 60 and Tom 20, matrix and outer membrane markers, respectively, and the PKA catalytic subunit. Complete loss of Tom 20 upon trypsin exposure implies extensive trypsinolysis of the outer membrane surface. Complete retention of Hsp 60 implies that the mitochondrial matrix is preserved upon exposure to trypsin.

intermembrane space PKA activity (Figure 2.9). Finally, mitochondrial structural integrity is completely disrupted by sonication, and thus mitochondria treated in this fashion should yield, upon cAMP exposure, total mitochondrial PKA activity. These three activities can then be used to assign relative PKA activity to the three separate mitochondrial microenvironments. The purity of mitochondria isolated from bovine heart was assessed via Western blot analysis using antibodies against proteins that are localized to mitochondrial (cytochrome C) and nonmitochondrial sites, including the endoplasmic reticulum (calnexin), the plasma membrane (Na+/K+ ATPase), and the cytosol (GAPDH) (Figure 2.10A). The results demonstrate that the mitochondrial preparation is not contaminated with proteins from other membranes or the ER and displays only minimal contamination from the cytoplasm. Mitochondrial structural integrity

(intactness) was assessed as previously described[23] and found to be greater than 90% (data not shown). Intact mitochondria, upon exposure to cAMP, exhibit an initial rate of PKA activity equivalent to 29 (4 pg PKA/μg mitochondria. By contrast, in the absence of cAMP, phosphorylation activity is minimal (Figure 2.11); demonstrating that sensor **2.1** is phosphorylated in a cAMP dependent fashion. Indeed, previous studies have shown that active-site directed sequences, similar to the sequence employed in sensor **2.1**, are highly selective for PKA.[24] Finally, we have found that H-89, a PKA inhibitor, blocks the phosphorylation of sensor **2.1** by mitochondrial preparations (Figure 2.12). These results are consistent with the notion that peptide **2.1** serves as a selective PKA sensor. As noted above (Figure 2.9), we expected that the PKA activity associated with intact mitochondria would be a combination of enzyme present on the outer membrane and enzyme oriented into the intermembrane space. We addressed this possibility by treating mitochondria with trypsin, which should selectively hydrolyze the outer membrane proteins exposed to the external milieu (Figure 2.10B), but not hydrolyze matrix- or intermembrane space-embedded proteins. Indeed, an outer membrane marker (TOM 20) is completely digested in trypsin-treated mitochondria, whereas a matrix marker (Hsp 60) is unperturbed. Previous studies with trypsin-exposed mitochondria demonstrated that an intermembrane space marker is protected against proteolysis as well.[9(a)] Subsequent analysis of PKA activity (cAMP exposure) in trypsin-treated mitochondria revealed a drop in PKA activity from 24 (4 pg PKA/μg mitochondria to 10 (1 pg PKA/μg mitochondria, implying a 1:1.4 ratio of intermembrane space: outer membrane (external) PKA. Finally, mitochondria were sonicated to

[23] (1) Wharton, D. C.; Tzagoloff, A. *Methods Enzymol.* **1967**, *10*, 245–250. (2) Rice, J. E.; Lindsay, J. G. In *Subcellular Fractionation*; Graham, J. M., Rickwood, D., Eds.; IRL Press: Oxford, England, 1997; pp 107-142.

[24] (1) Su, J.; Bringer, M. R.; Ismagilov, R. F.; Mrksich, M. *J. Am. Chem. Soc.* **2005**, *127*, 7280–7281. (2) Min, D. H.; Su, J.; Mrksich, M. *Angew. Chem., Int. Ed.* **2004**, *43*, 5973–5977. (3) He, Y.; Yeung, E. S. *Electrophoresis* **2003**, *24*, 101–108.

completely disrupt their structural integrity, thereby exposing all mitochondria-associated PKA, including any matrix-embedded enzyme. Total mitochondrial PKA activity (cAMP treatment) is equivalent to 165 ± 24 pg PKA/μg mitochondria, approximately 5.7 times greater than that observed with intact mitochondria. These values suggest that the relative distribution of PKA activity in the matrix (165 ± 24 pg PKA/ μg mitochondria - 24 ± 4 pg PKA/μg mitochondria = *141 pg PKA/μg mitochondria*), the intermembrane space (*10 ± 1 pg PKA/μg* mitochondria), and the outer membrane (24 ± 4 pg PKA/μg mitochondria - 10 ± 1 pg PKA/μg mitochondria = *14 pg PKA/μg* mitochondria) in bovine heart mitochondria is 85 : 6 : 9, respectively. The latter compares favorably with the electron microscopy work of Papa and colleagues,[18] who reported that 90% of the PKA present in mitochondria is found the matrix and the intermembrane space. However, our analysis could be complicated by endogenous protein phosphatases if they are present in different amounts in the three distinct mitochondrial compartments. Consequently, an analogous series of experiments were conducted in the presence of a phosphatase inhibitor cocktail. The experimentally determined ratio (79 : 8 : 13) of matrix/intermembrane space/outer membrane PKA activity corresponds to that acquired in the absence of phosphatase inhibitors. In summary, we have developed a protein kinase sensing system with a robust dynamic range and used it to characterize the compartmentalized location of PKA activity in mitochondria. Given the important role of PKA in mediating the dynamics of mitochondrial biochemistry, the ability to monitor protein kinase activity should prove useful in assessing the mitochondrial response from both healthy individuals and from patients with mitochondrial-based disorders.[25]

MATERIALS AND METHODS

[25] Carlucci, A.; Lignitto, L.; Feliciello, A. *Trends Cell. Biol.* **2008**, *18*, 604–613.

General reagents and solvents were purchased from Fisher or Sigma-Aldrich. Novasyn TGR Resin and all natural Fmoc-protected amino acids were purchased from EMD Biosciences Inc. HCTU [1H-benzotriazolium-1-[bis(dimethylamino)methylene]-5-chloro-hexafluorophosphate (1),3-oxide] was purchased from Peptides International (Louisville, KY, U.S.A.). Fluorescent dyes (7-(diethylamino)coumarin-3-carboxylic acid, Coumarin 343 [11-oxo-2,3,6,7-tetrahydro-1*H*,5*H*,11*H*-pyrano[2,3-*f*]pyrido[3,2,1-*ij*]quinoline-10-carboxylic acid], and Atto 425-NHS ester were purchased from Sigma-Aldrich. Fmoc-aminooctanoic acid (Fmoc-Aoc-OH) was purchased from Advanced ChemTech (Louisville, KY, U.S.A.). Bovine heart mitochondria was purchased from MitoSciences, and trypsin (sequencing grade) and PKA were purchased from Promega. The antibodies against the PKA catalytic subunit, Tom 20, and Hsp60 were purchased from BD Biosciences, and the goat antimouse secondary antibody was purchased from Santa Cruz Biotechnology. Total mitochondrial protein was quantified using the BCA protein assay (Pierce). Immunoblots were performed using Snap i.d. (Millipore), and visualized using an AlphaInnotech FluorChem FC2 imager. The intactness of the isolated mitochondria was assessed via a previously described protocol.[30,31] PKA murine catalytic subunit (cat.) plasmid and the GST-14-3-3τ plasmid were generous gifts from Dr. Susan Taylor and Dr. Alistair Aitken, respectively.

Synthesis of Fluorophore-Labeled PKA Substrates. Peptides were synthesized using standard Fmoc solid-phase synthesis on a Prelude peptide synthesizer (Protein Technologies Inc., Tucson, AZ, U.S.A.). Novasyn TGR resin was swelled for 30 min in dichloromethane (DCM) before synthesis. Amino acids were then sequentially coupled using 5.0 equiv of amino acid, 4.9 equiv of HCTU, 20 equiv of diisopropylethylamine (DIPEA) in *N*,*N*dimethylformamide (DMF) (2 × 5

min) followed by DMF wash (6 × 30 s). The Fmoc-protecting group was removed using 20% piperidine in DMF (2 × 2.5 min) followed by a DMF wash (6 × 30 s). The free N-terminal amine was used for subsequent on-resin fluorophore labeling. Fluorescent dyes diethylcoumarin and Coumarin 343 were coupled to the N-terminal amine using 5.0 equiv of fluorophore, 4.9 equiv of HCTU, 20 equiv of DIPEA in DMF (1× 60 min). Atto425-NHS ester was coupled using 1.0 equiv of dye and 20 equiv of DIPEA in DMF (1 × 60 min). The resin was washed (3× DMF, IPA, DCM) and then cleaved and deprotected using a 95:2.5:2.5 trifluoroacetic acid (TFA)/H2O/triisopropylsilane (TIPS). The peptides were isolated via filtration, precipitated with ice-cold ether, and centrifuged to isolate the precipitate. The precipitates were air-dried, dissolved in DMSO, and purified using HPLC (3% to 40% acetonitrile gradient against water with 0.1% TFA over 40 min). The peak corresponding to the peptide was collected, freeze-dried, and characterized by electrospray ionization mass spectrometry: **2.1** Cou-Aoc-GRTGRRFSYP-amide [Exact Mass calculated: 1579.84, found: 1580.84 (M + H)+], **2.2** Atto425-Aoc-GRTGRRFSYP-amide [Exact Mass calculated: 1719.98, found: 1720.97 (M + H)+], **2.3** Cou343-Aoc-GRTGRRFSYP-amide [Exact Mass calculated: 1603.82, found: 1604.85 (M + H)+], **2.5** Cou-Aoc-GRTGRRFAYP-amide [Exact Mass calculated: 1562.8, found: 782.6 $(M + 2H)^{2+}$, 522.2 $(M + 3H)^{3+}$], **2.6** Cou-Aoc-GATGRRFSYP- amide [Exact Mass calculated: 1494.69, found: 1495.80 $(M + H)^{+}$], **2.7** Cou-Aoc-GRTGARFSYP-amide [Exact Mass calculated: 1494.69, found: 1495.77 $(M + H)^{+}$], **2.8** Cou-Aoc-GRTGRAFSYP-amide [Exact Mass calculated: 1495.69, found: 1495.78 $(M + H)^{+}$], **2.9** Cou-Aoc-GATGRAFSYP-amide [Exact Mass calculated: 1409.58, found: 1409.72 $(M + H)^{+}$], **2.10** Cou-Aoc-GATGARFSYP-amide [Exact Mass calculated: 1409.58, found: 1409.73 $(M + H)^{+}$], **2.11** Cou-Aoc-GRTGAAFSYP-amide [Exact Mass calculated: 1409.58, found: 1409.72 $(M + H)^{+}$], and **12** Cou-

Aoc-GATGAAFSYP-amide [Exact Mass calculated: 1323.6, found: 1324.5 $(M + H)^+$].

Identification of Lead Quencher Dye 2.4 The concentration of peptide 1 was adjusted using a molar excitation coefficient of 60,000 M-1 cm-1 at 430 nm. GST-tagged 14-3-3τ (purified to a single band at 56 KDa on 12.5% SDS PAGE) was dialyzed four times in 50 mM Tris pH 7.5, prior to use, and its concentration was determined using the Bradford assay. Concentrations of each of the 47 assembled dyes (See Table 2.9) were adjusted on the basis of weight. PKA enzyme (2.08 mg/mL) was purchased from Promega. Peptide **2.1** (1 μM) was incubated with 10 μM GST-tagged 14-3-3τ, 1 mM ATP, 2 mM DTT, 5 mM $MgCl_2$, and 50 mM Tris-HCl at pH 7.5, in a quartz 96-well plate (Hellma). Each dye was added to a separate well at 5 μM. PKA (10 nM) was added to each well, and the enzyme-dependent increase in fluorescence (λex 420 nm, λem 475 nm) was determined with a plate reader (Molecular Devices Spectra Max Gemini EM). Dyes D1, D6, D18, D33, and D39 showed >2-fold enhancements in fluorescence.

Phosphorylation of Sensor 2.1 and Dephosphorylation of Phospho Sensor Peptide PKA-catalyzed phosphorylation of sensor **2.1** was performed using the conditions in "Optimization of Enzyme-Dependent Fold-Change" described below. The mass of the resulting phosphorylated peptide was found to be 830.6 $(M + 2H)^{2+}$, 554.1 $(M + 3H)^{3+}$ (Exact Mass calculated 1658.8). The phosphorylated lead peptide was dephosphorylated using Protein Phosphatase 1 (NEB) in the presence of 50 mM HEPES pH 7.5, 100 mM NaCl, 2 mM DTT, 0.01% Brij 35, and 1 mM $MnCl_2$. The mass of the resulting dephosphorylated peptide was found to be 789.5 $(M + 2H)^{2+}$ (Exact Mass calculated 1577.8).

Acquisition of Apparent K_m and V_{max} Values Phosphorylation dependent increase in coumarin fluorescence intensity of peptides **2.1**-**2.3** was monitored on a Photon Technology QM-1 spectrofluorimeter at 30 °C. Standard curves were used to correlate fluorescence intensity with concentration of product formed. For generating the standard curve, various substrate concentrations were incubated, in duplicate, with 5 nM PKA at 25 °C over 30 h (in the presence of 320 μM dye, 20 μM 14-3-3τ, 1 mM ATP, 5 mM $MgCl_2$, 2 mM DTT, and 50 mM Tris HCl pH 7.5). The fluorescence intensity after complete phosphorylation was plotted against concentration, and parameters obtained from a linear regression of the data were used to convert the fluorescence intensity to product concentration. For determining the initial velocities, different concentrations of the peptide substrate was equilibrated with 20 μM 14-3-3τ, 1 mM ATP, 5 mM $MgCl_2$, 2 mM DTT, in 50 mM Tris buffer pH 7.5, for 10 min. PKA (5 nM) was added, and the reaction progress curves were obtained. Reaction rates were determined from the slope under conditions where 5-8% substrate had been converted to product in duplicate (typically from 200 to 300 s). The resulting slopes (initial velocity, Vo) for each of the progress curves were plotted versus the concentration of substrate. A nonlinear regression analysis (SigmaPlot version 8.02 software) was used to fit the data to the rectangular hyperbola model.

Optimization of Enzyme-Dependent Fold-Change Peptide **2.1** (1 μM) was incubated with 1 mM ATP, 2 mM DTT, 5 mM $MgCl_2$, 50 mM Tris-HCl at pH 7.5, in different wells of a quartz 96-well plate. To each well, were added systematically varied concentrations of dye **2.4** (0-600 μM) and GST-tagged 14-3-3τ (0-40 μM) followed by 10 nM PKA. Enzyme-dependent enhancement in fluorescence (λ_{ex} 420 nm, λ_{em} 475 nm) was determined with a plate reader (Molecular Devices Spectra Max Gemini EM). The maximum fluorescence increase was

observed with 320 μM dye **2.4** and 20 μM GST-tagged 14-3-3τ. These optimized conditions were used to assay peptides **2.1**-**2.3** using a Photon Technology QM-4 spectrofluorimeter. The enzyme-dependent fold changes obtained under these conditions are reported in Table 2.1 and are shown in Figure 2.3.

Acquisition of Apparent K_D Values for 4 with Peptides 2.1 and 2.6-2.12. Varying concentrations of **2.4** ranging from 0.02 to 200 μM, were added to 1 μM of the coumarin-labeled peptides in 100 mM Tris HCl pH 7.5 buffer. Fluorescence data (λ_{ex} 420 nm, λ_{em} 475 nm) was acquired using a Photon Technology QM-4 spectrofluorimeter at 30 °C. Correction for the inner filter effect was made as previously reported.[26] Molar absorbtivities (λ_{ex} 420 nm, λ_{em} 475 nm) were calculated from single absorbance spectra at [**2.4**]) 16 μM. After correcting for the inner filter effect, the percentage of quench was plotted against the concentration of the dye. Concentration of the dye-peptide complex was determined on the basis of the change in fluorescence emission intensity. The data were fit using the nonlinear regression mode of SigmaPlot ver.8.02. The calculated K_D values are reported in Table 2.5.

Job Plot for Determination of Stoichiometry. Fluorescence emission (λex 420 nm, λem 475 nm) of varying concentrations of peptide **2.1** (0.2, 0.6, 1.0, 1.4, 1.8 μM) and dye **2.4** (65% purity) (1.8, 1.4, 1, 0.6, 0.2 μM) at a fixed total concentration of 2 μM was acquired in duplicate, on a Photon Technology QM-4 spectrofluorimeter at 30 °C (Figure 2.6).

Mitochondria-Based Experiments. A standard curve for PKA concentration versus activity was generated using 1 μM peptide **2.1**, 32 μM dye **2.4**, 10 μM 14-3-3τ, 1 mM ATP, 5 mM

[26] Levine, R. L. *Clin. Chem.* **1977**, *23*, 2292–2301.

$MgCl_2$, 2 mM DTT, 1 mM cAMP, in 50 mM Tris HCl at pH 7.5. Assays were conducted in duplicate at two concentrations of total mitochondria protein (14 μg and 55 μg) using intact mitochondria (MitoSciences), trypsin-treated mitochondria (mitochondria samples incubated with 1:50 trypsin/total mitochondrial protein for 1 h at 37 °C, followed by treatment with 20-fold excess of soybean trypsin inhibitor) and sonicated mitochondria, [mitochondria sonicated (Ultrasonic Processor, Tekmar, Cincinnati, OH, U.S.A.) for 30 s on ice]. Initial rates were converted into pg of active PKA per μg of mitochondria using the standard curve. Rates in the presence of Ser/Thr phosphatase inhibitor cocktail (P2850 Sigma) were acquired at the recommended 1:100 dilution.

Trypsin Treatment of Mitochondria. Mitochondria were incubated with trypsin (1:50 trypsin/total mitochondrial protein) for 1 h at 37 °C followed by treatment with a 20-fold excess of soybean trypsin inhibitor. The outcome of the trypsin digestion was validated by Western blot using an outer membrane marker, Tom 20, and a matrix marker, Hsp60.

Western Blot Analyses. Twenty micrograms of total protein was loaded onto 4-12% bis-tris-polyacrylamide gels, separated by electrophoresis, and electroblotted onto PVDF membranes. The membranes were then blocked in 0.5% nonfat dry milk followed by incubation with the appropriate primary antibody (C subunit of PKA 1:1000, Tom 20 1:1000, and Hsp60 1:5000) for 10 min. The membranes were then washed three times with 0.1% Tween-20 in PBS followed by incubation with a goat antimouse secondary antibody conjugated to horseradish peroxidase (1:2000) for 10 min. The membranes were washed with 0.1% Tween-20 in PBS (3×), PBS (3×), and 0.5% NaCl (3×) and detection of horseradish peroxidase performed using the ECL Plus

reagent (GE).

Table 2.3 Library of quencher dyes. Phosphorylation-induced fluorescence fold changes of peptide **1** in the presence of the quencher dyes (non-optimized conditions).

Dye	Name	Fold Change
D1	Acid Green 27	3.95
D2	Acid Blue 40	1.36
D3	Evans Blue	1.88
D4	Acid Alizarin Violet N	1.53
D5	Acid Blue 80	1.57
D6	Reactive Blue 2	2.51
D7	N,N-dimethylnitrosoaniline	1.21
D8	Cresol Red	1.47
D9	Phenol Red	1.2
D10	Methyl Orange	1.18
D11	Bromophenol Blue	1.49
D12	BUFFER	1.16
D13	Xylene Cyanol FF	1.15
D14	Disperse Yellow 3	1.15
D15	Ethyl Orange	1.27
D16	Methylene Blue	1.14
D17	Brilliant Blue R	1.16
D18	Eriochrome Black T	2.04
D19	Alizarin Red	1.31
D20	Malachite Green oxalate	1.16
D21	Phenolphthalein	1.17
D22	Carminic Acid	1.15
D23	Nuclear Fast Red	1.16
D24	Acid Fuchsin	1.18
D25	Acridine Orange	1.17
D26	Acridine Yellow G	1.11
D27	Aniline Blue WS	1.2
D28	Azure A	1.13
D29	Azure B bromide	1.12
D30	Basic Fuchsin	1.17
D31	Bismark Brown Y	1.17
D32	Brilliant Yellow	1.65
D33	Bromocresol Purple	2.33
D34	Chlorazol Black E	1.2
D35	Chlorophenol Red	1.2
D36	Chrysoidine Y	1.16
D37	Erythrosin	1.17
D38	Ethyl Violet	1.14
D39	Naphthol Blue Black	2.27
D40	Methylthymol Blue	1.31

D41	Methyl Violet	1.14
D42	Ponceau S	1.24
D43	Rose Bengal	1.2
D44	Rosolic Acid	1.16
D45	Safranin O	1.18
D47	Tartrazine	1.18
D48	Trypan Blue	1.55

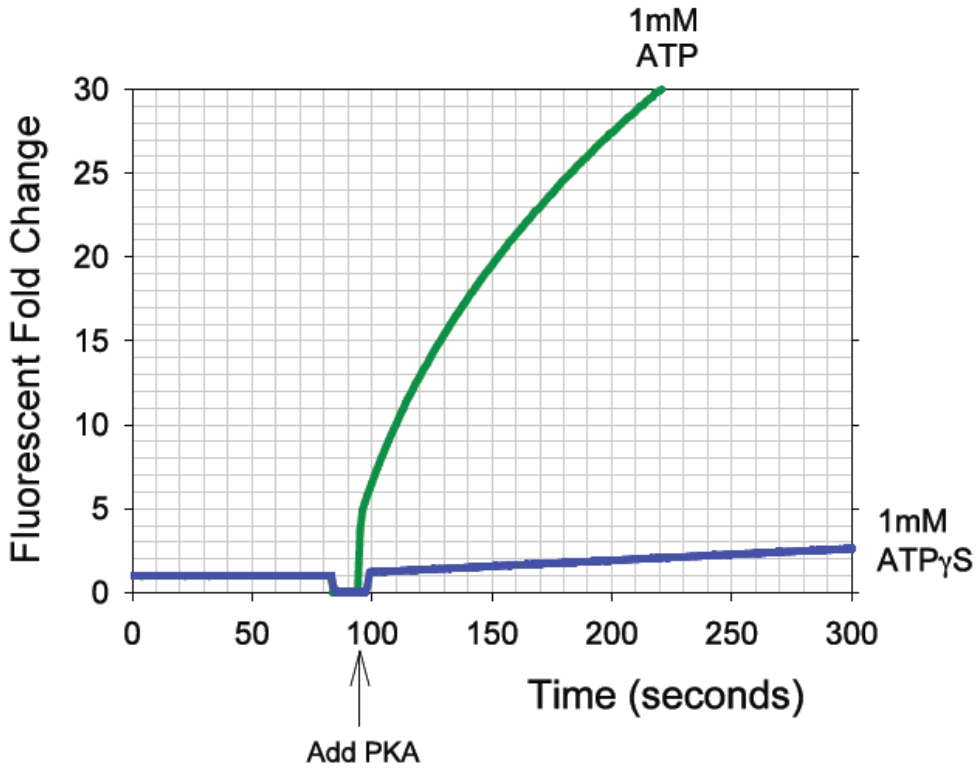

Figure 2.3 ATP(γ)S serves as a weak ATP analog in the PKA-catalyzed thiophosphorylation of peptide **2.1**. Experiments were performed with 10 μM 14-3-3, 5 mM $MgCl_2$, 2 mM DTT, 50 mM Tris HCl at pH 7.5, 1 μM peptide **2.1**, and 30 μM **2.4** in the presence of 1 mM ATP or 1 mM ATP(γ)S. 0.5 nM PKA was added after 100 s and the reaction progress was monitored and plotted as fold change verses time. The kinase reaction was significantly slower with ATP(γ)S, however the peptide was thiophosphorylated under these conditions. Mass found m/z 1673.2 (calculated m/z 1673.8).

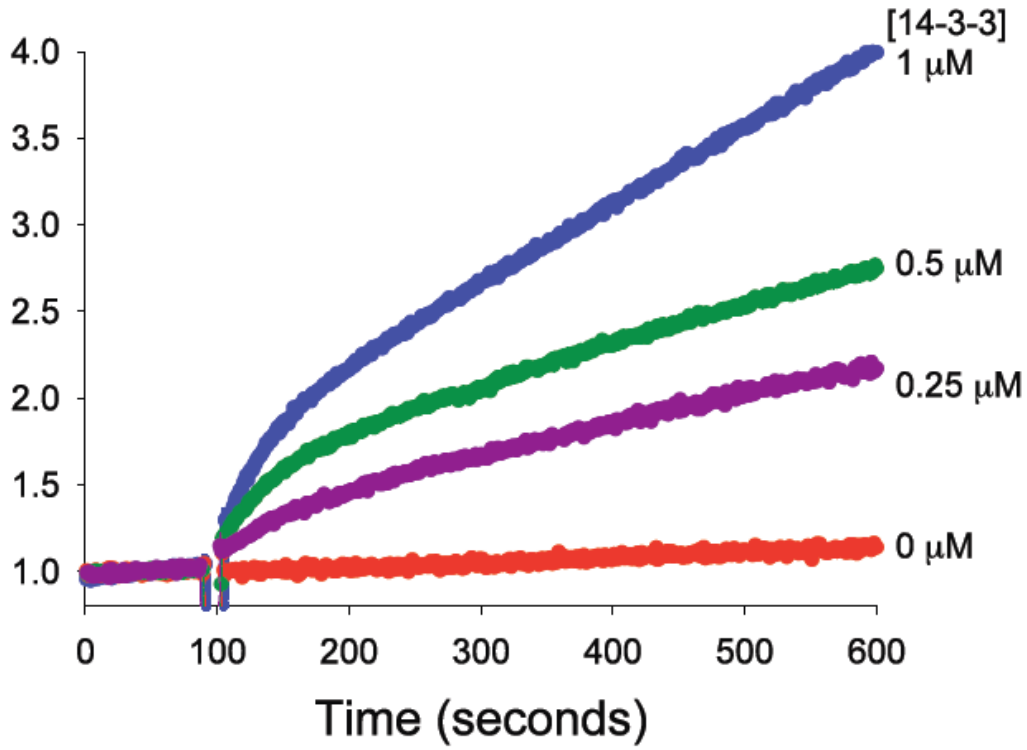

Figure 2.4 Fluorescence fold-change as a function of time in the absence (0 μM) and presence of 14-3-3. Experiments were performed with 5 mM $MgCl_2$, 2 mM DTT, 50 mM Tris HCl at pH 7.5, 1 μM peptide, 30 μM **2.4**, 1 mM ATP, and varying concentrations of 14- 3-3. 0.5 nM PKA was added at 100 s to initiate the reaction.

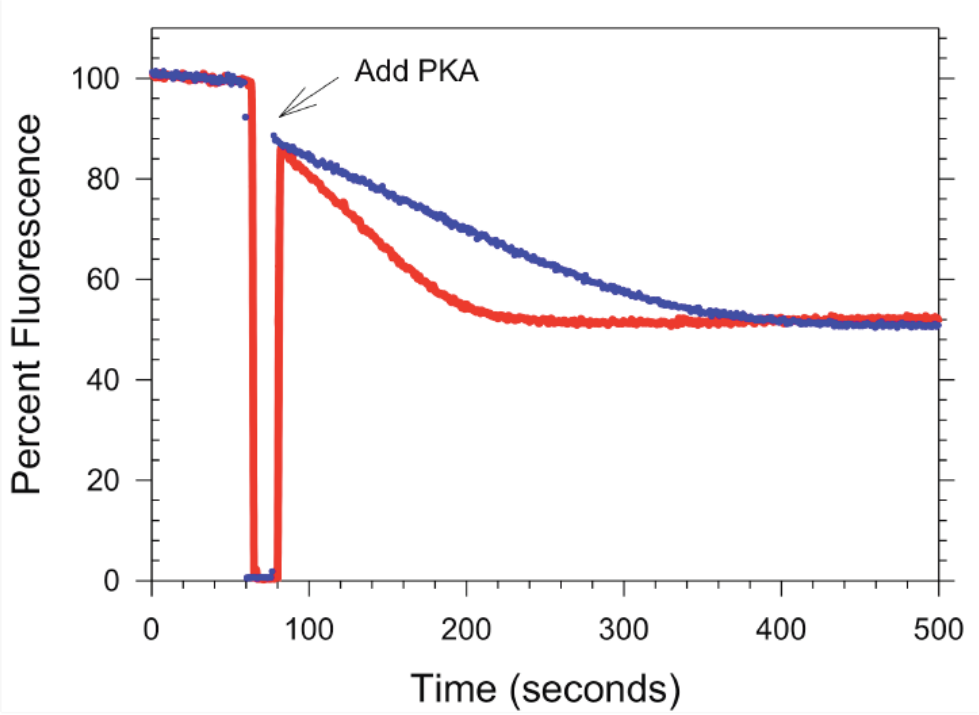

Figure 2.5 Fluorescence fold change as a function of time in the absence of fluorescent quencher **2.4.** Experiments were performed with 10 μM 14-3-3, 5 mM $MgCl_2$, 2 mM DTT, 50 mM Tris HCl at pH 7.5, 1 μM peptide **1**, 1 mM ATP, and two different concentrations of PKA [1 nM (blue curve) and 2 nM (red curve)] to initiate the reaction.

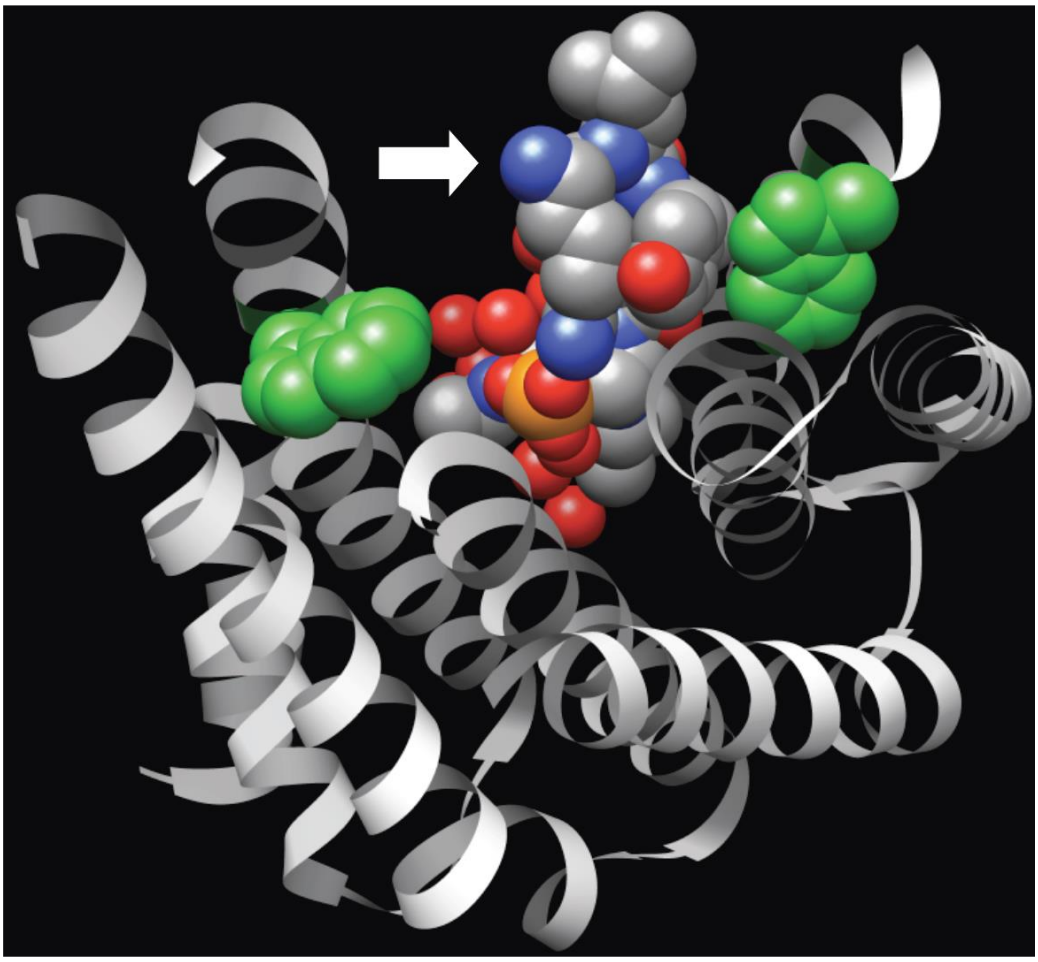

Figure 2.6 3-dimensional structure of a 14-3-3 domain/phosphopeptide complex**.** The tryptophan residues of the 14-3-3 domain are highlighted in lime green, whereas the remainder of the 14-3-3 domain is shown as a grey cartoon. The N-terminus of the phosphopeptide is indicated with an arrow. Coordinates were downloaded from the Protein Data Bank (PDB ID 1QJA).

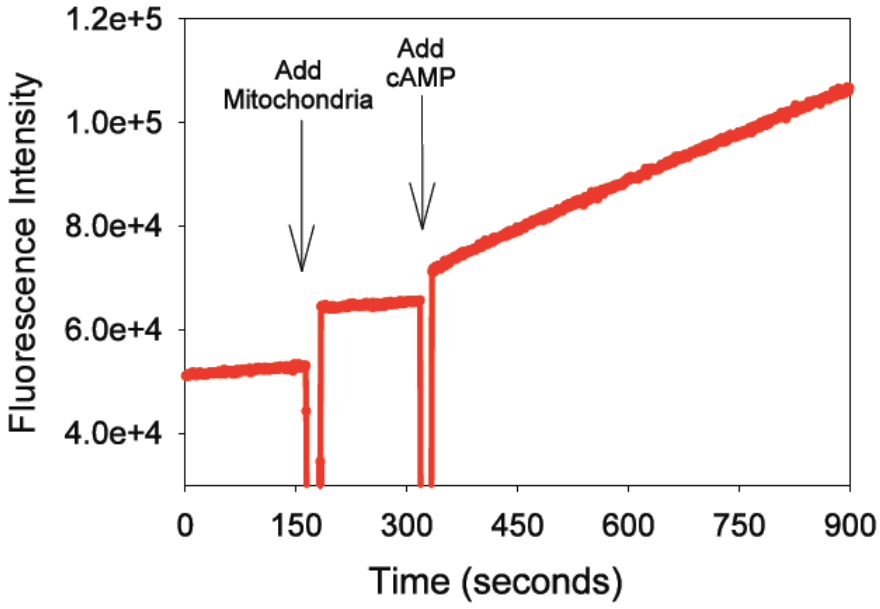

Figure 2.11 Mitochondrial-driven fluorescence enhancement is cAMP-dependent. Experiments were performed using 1 mM ATP, 5 mM $MgCl_2$, 2 mM DTT in 50 mM Tris HCl at pH 7.5, 1 μM peptide sensor **2.1**, 30 μM **2.4**, and 10 μM 14-3-3 incubated for 2 min, after which time 0.22 mg/mL of total mitochondrial lysate was added. After incubating for another 2 min, 1 mM cAMP was added. The reaction progress was monitored and plotted as fluorescence intensity versus time.

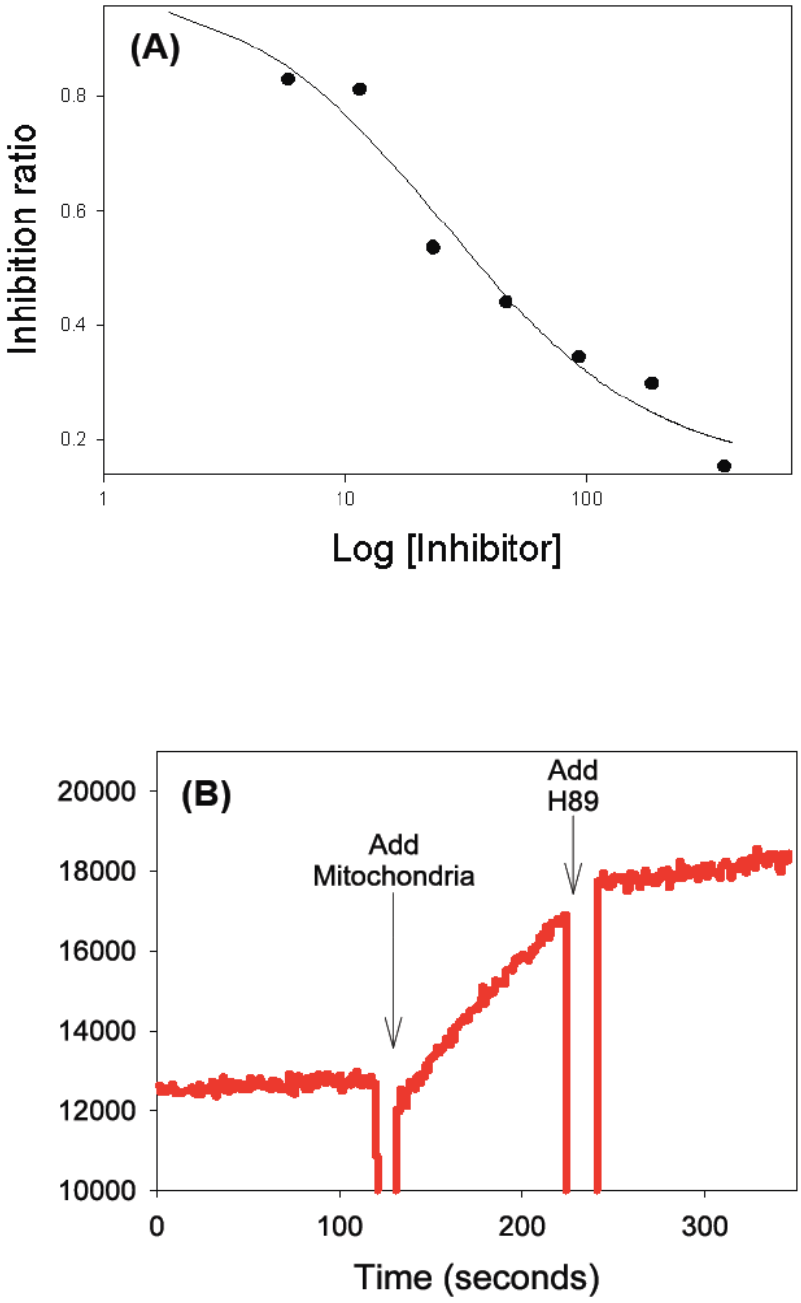

Figure 2.12 The PKA inhibitor H-89 blocks the fluorescent enhancement driven by (A) the C subunit (IC_{50} = 26 ± 9 μM) and (B) by cAMP-treated mitochondria. The experiments were performed under standard conditions (1 mM ATP, 5 mM MgCl2, 2 mM DTT, 1 μM peptide **2.1**,10 μM 14-3-3, 30 μM **2.4**, 50mM Tris HCl at pH 7.5). For the experiments shown in (B), mitochondria were added after a 2 min pre-incubation. H-89 was subsequently introduced following a second 2 min incubation.

CHAPTER 3

A BROAD SPECTRUM DARK QUENCHING DYE: CONSTRUCTION OF TRYPSIN AND PHOTOLABILE FLUORESCENT REPORTERS

INTRODUCTION

A wide variety of fluorescent biosensors have been described for a host of biomolecules, including nucleic acid sequences,[1] proteases,[2] kinases,[3] metal ions,[4] and other stimuli. Typically, fluorescent biosensors are designed containing a fluorescent donor species coupled to an acceptor species capable of modulating the biosensors' fluorescence in response to stimuli. Many biosensors commonly employ a design motif whereby the excitation energy of one fluorophore is transferred to a second fluorophore, which emits light at a longer wavelength than that of the initially excited species. An alternative strategy employs a single fluorophore/quencher motif that furnishes a profluorescent species. The latter exhibits a fluorescent change when acted upon by biomolecules that separate the fluorophore from the quencher. The "relief from fluorescent quenching" strategy takes up only half of the spectral window space of conventional Förster

---

[1] (1) Tyagi, S. and Kramer, F. R. *Nat. Biotech.* **1996**, *14*, 303-308. (2) Tyagi, S., Marras, S. A. E. and Kramer, F. R. *Nat. Biotech.* **2000**, *18*, 1191.

[2] (1) Ogawa, M., Kosaka, N., Longmire, M., Urano, Y., Choyke, P. L. and Kobayashi, H. *Mol. Pharm.* **2009**, *6*, 386-395. (2) Wakata, A., Lee, H.-M., Rommel, P., Toutchkine, A., Schmidt, M. and Lawrence, D. S. *J. Am. Chem. Soc.*, **2010**, *132*, 1578-82.

[3] (1) Ting, A. Y., Kain, K. H., Klemke, R. L. and Tsien, R. Y. *Proc. Natl. Acad. Sci*. **2001**, *98*, 15003-8. (2) Violin, J. D., Zhang, J., Tsien, R. Y. and Newton, A. C. *J. Cell Biol.* **2003**, *161*, 899-909.

[4] (1) Sikdar, A.; Roy, S.; Haldar, K.; Sarkar, S.; Panja, S. S. *Journal of fluorescence* **2013**. (2) Gong, Y.-J.; Zhang, X.-B.; Zhang, C.-C.; Luo, A.-L.; Fu, T.; Tan, W.; Shen, G.-L.; Yu, R.-Q. *Anal. Chem.* **2012**, *84*, 10777–84.

resonance energy transfer (FRET) sensors. This is especially useful for microscopy-based experiments, where multiple readouts, using several different channels, are common. Additional potential advantages associated with relief-from-quenching constructs are that (1) only a single fluorophore is required, thereby reducing the expense of synthesis and (2) enhanced structural flexibility since it is not dependent upon the use of a limited set of functional FRET fluorophore-fluorophore pairs. However, these potential advantages are only available if the quencher enjoys a broad wavelength spectrum that can accept excited state energy from a wide variety of fluorophores.

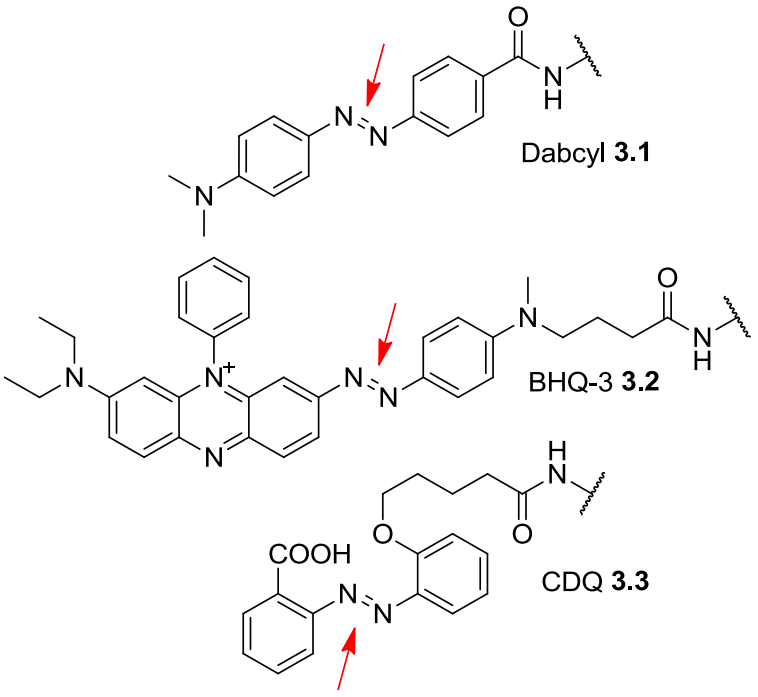

Scheme 3.1 Structures of the dark quenchers Dabcyl **3.1**, Black Hole Quencher 3 **3.2**, and CDQ **3.3**. The red arrow indicates an azo bond subject to reduction, which eliminates the ability of the compound to serve as a dark fluorescence quencher.

For example, two commonly used dark quenchers include **3.1** Dabcyl (4-(4'-dimethylaminophenylazo)benzoic acid, λ_{max} = 425 nm, QR (Quenching Range) = 375 – 500 nm) and Dansyl (4-(4'-dimethylaminoazobenzene-4'-sulfonyl, λ_{max} = 339 nm, QR = 300 – 400 nm).

Dabcyl is commonly used as a FRET quencher of the fluorophore EDANS (5-[(2-aminoethyl)amino]naphthalene-1-sulfonic acid; λ_{ex} = 430 nm, λ_{em} = 479 nm).[5] However, the absorption maxima of Dabcyl and Dancyl are shorter than 500 nm, which limits their usefulness to blue and green fluorophores with emissions of < 500 nm for through space fluorescence quenching. This limits the usefulness of Dabcyl and Dansyl to fluorophores not applicable to fluorescence microscopy.

Other dark quenchers are limited to specific ranges within the red or near infrared spectra window for through space quenching mechanisms. The combined Black Hole Quencher (BHQ) family covers the visible and near-IR spectral range, relying on a FRET mechanism.[6] This family includes BHQ-0 (λ_{max} = 495 nm, quenching range (QR) = 430 – 520 nm), BHQ-1 (λ_{max} = 534 nm, QR = 480 – 580 nm), BHQ-2 (λ_{max} = 579, QR = 559 – 670 nm), BHQ-3 **3.2** (λ_{max} = 672, QR = 620 – 730 nm).[7] As noted, each quencher has an approximately 110 nm spectral window where the quencher is capable of through space fluorescence quenching. As well as containing limited spectral window for through space quenching, BHQ quenchers contain (like Dabcyl and Dansyl mentioned above) an azo moiety that is subject to reduction. This has been demonstrated to abolish fluorescent quenching in the reductive environment of the cell (Figure 3.1).[8] Leriche et al. successfully applied the susceptibility of azo bonds to reduction to the synthesis of a FRET–based biosensor of capsase-3 activity that included the quencher CDQ **3.3** ((4-hydroxy-2-

[5] Matayoshi, E. D.; Wang, G. T.; Krafft, G. a; Erickson, J. *Science* **1990**, *247*, 954–8.

[6] Marras, S. a E.; Kramer, F. R.; Tyagi, S. *Nucleic acids research* **2002**, *30*, e122.

[7] Biosearch Technologies. Black Hole Quencher Dyes: The Inescapable Solution. https://www.biosearchtech.com/support/applications/dyes-from-biosearch-technologies/black-hole-quencher%C2%AE-dyes (accessed March, 15 2013).

[8] (1) Linder, K. E.; Metcalfe, E.; Nanjappan, P.; Arunachalam, T.; Ramos, K.; Skedzielewski, T. M.; Marinelli, E. R.; Tweedle, M. F.; Nunn, A. D.; Swenson, R. E. *Bioconjugate Chem.* **2011**, *22*, 1287–97. (2) Chung, K. T.; Stevens, S. E.; Jr., Cerniglia, C. *Crit. Rev. Microbiol.* **1992**, *18*, 175–190. (3) Leriche, G.; Budin, G.; Darwich, Z.; Weltin, D.; Mély, Y.; Klymchenko, A. S.; Wagner, A. Chem. Comm. **2012**, *48*, 3224–6.

methoxy-phenylazo) benzoic acid). Upon addition of the reducing agent dithionite, the CDQ quencher lost its ability to quench fluorescence.

In addition to the BHQ quencher family, the QSY family of dark fluorescent quenchers has been found to quench a series of fluorophores in the visible and near IR range via through space mechanisms.[9] This quencher family includes QSY-35 (λ_{max} = 475 nm, QR = 430 – 520 nm), QSY-7 (λ_{max} = 560 nm, QR = 500 – 600 nm), QSY-9 (λ_{max} = 562, QR = 500 – 600 nm), and QSY-21 (λ_{max} = 661 nm, QR = 575 – 700 nm).[10] QSY quenchers have similar spectral windows as the BHQ series for through space energy transfer of between 100 - 125 nm. Although the QSYs lack an azo functionality and are thus not subject to undesired reduction, they are also much less synthetically accessible than the BHQs.

While the BHQ and QSY quencher series have the ability to quench fluorophores over the entire visible spectral range, careful selection of the fluorophore/quencher pair is necessary to ensure effective quenching. Our aim was to identify a dark fluorescent quencher effective with a wide range of fluorophores and apply this to the construction of multicolored protease substrates. We describe herein a dark fluorescent quencher that is effective over a wide wavelength range, thereby enabling the construction of multicolored family of protease substrates.

RESULTS

We've recently identified a host of fluorescent quenchers for several fluorophores by

[9] Life Technologies. Molecular Probes nonfluorescent quenchers and photosensitizers. http://www.invitrogen.com/site/us/en/home/References/Molecular-Probes-The-Handbook/tables/Molecular-Probes-nonfluorescent-quenchers-and-photosensitizers.html (accessed March, 15 2013).

[10] Marcotte, P. a; Richardson, P. L.; Richardson, P. R.; Guo, J.; Barrett, L. W.; Xu, N.; Gunasekera, A.; Glaser, K. B. *Anal. Biochem.* **2004**, *332*, 90–9.

screening a library of 47 negatively charged dyes with fluorophore substituted, positively charged peptides.[11] The strategy employs electrostatics to rapidly screen and assess quenching efficacy of dye-quencher/fluorophore pairs. Several of the lead dye-quenchers (e.g. acid green 27, bromocresol purple, naphthol blue black, Acid Blue 40 **3.4** etc.) possess a broad-spectrum absorbance, thereby rendering their application to fluorophores that emit in the visible and near-IR range. We chose Acid Blue 40 (AB40) **3.4** as our lead, prepared a carboxylic acid-containing derivative (cAB40 **3.7**), and used the latter to construct profluorescent protease and photolabile sensors.

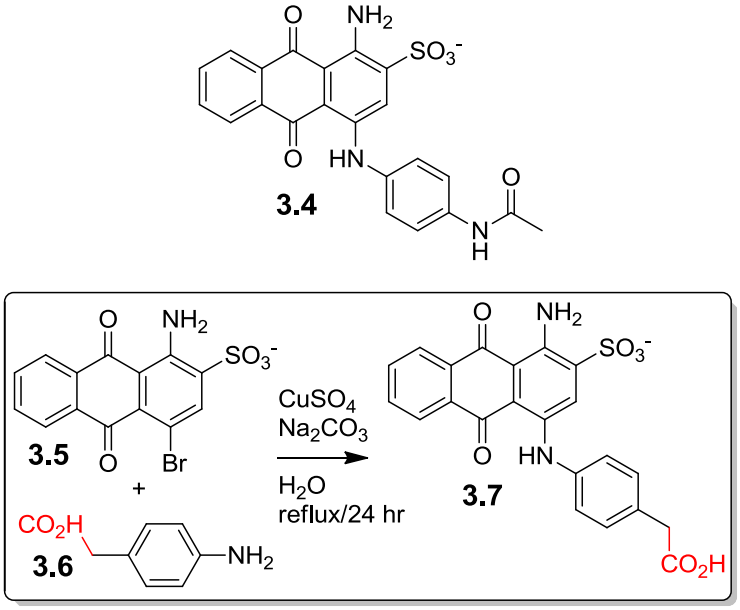

Scheme 3.2 Structure of Acid Blue 40 (AB40) **3.4** and synthesis of carboxy Acid Blue 40 (cAB40) **3.7**.

Readily available phenylacetic acid derivative **3.6** was converted to the 4-amiophenyl acetic acid derivative **3.7** via Ullman coupling with bromaminic acid **3.5** (Scheme 3.2).[12]

[11] Agnes, R. A.; Jernigan, F. E.; Sharma, V.; Shell, J. R.; Lawrence, D. S. J. Am. Chem. Soc. **2010**, 132, 6075-6080.

[12] Weyler, S.; Baqi, Y.; Hillmann, P.; Kaulich, M.; Hunder, A. M.; Müller, I. A.; Müller, C. E. *Bioorg. Med. Chem. Lett.* **2008**, *18*, 223-227.

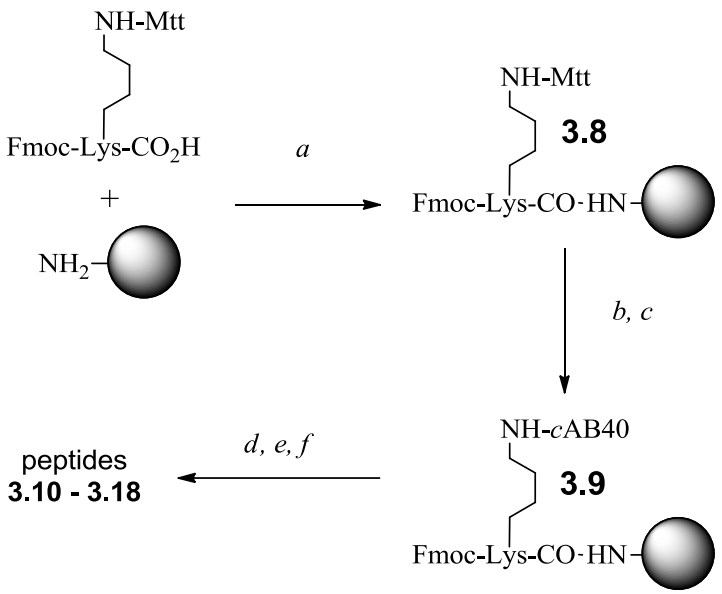

Scheme 3.3. Solid phase synthesis of protease sensors **3.10** - **3.17** and photolabile reporter **3.18**. *a*. HCTU/DIPEA/DMF. *b*. 7% TFA/7% TIS/84% CH_2Cl_2. *c*. 1.1 eq. cAB40/1.0 eq. HCTU/20 eq. piperidine/DMF. *d*. 20% piperidine/DMF. *e*. Fmoc-amino acid coupling (repeat steps *d* and *e* for subsequent couplings). *f*. 95% TFA/2.5% TIPS/2.5% H_2O.

Briefly, **3.5** and **3.6** were heated to reflux for 24 h in aqueous $CuSO_4$ and $NaHCO_3$. Any unreacted **3.6** was removed by washing the cooled reaction mixture with CH_2Cl_2. Following purification via flash chromatography the desired compound **3.7** was acquired in 37% yield. Using **3.7**, Trypsin substrates and a photolabile reporter were synthesized. First, Fmoc-Lys(Mtt)-OH was coupled to the Novasyn TGR-Resin to afford **3.8** (Scheme 3.3). Second, the 4-methyltrityl (Mtt) protected amine was deprotected and acylated with HCTU [1H-benzotriazolium-1 [bis(di-methylamino)-methylene]-5-chloro-hexafluoro-phosphate (1),3-oxide]-activated cAB40 **3.7** to furnish **3.9**. Third, trypsin substrates **3.10** - **3.17** were prepared by sequentially coupling Fmoc-Arg-OH and Fmoc-Gly-OH to **3.9** via solid phase peptide synthesis. The photosensitive reporter **3.18** was constructed in an analogous fashion by sequentially coupling the photolabile 4-[4-[1-(Fmoc)Ethyl]-2-Methoxy-5-Nitrophenoxy]Butanoic Acid

Substrate/Cassette	λ_{max} Excitation	λ_{max} Emission	Fold Enhancement upon Trypsinolysis or Photolysis	Quenching efficiency	Förster Distance (Å)
(**3.10**) DEAC-GRK(cAB40)-amide	430	479	22.5 ± 3.9	95.6	48
(**3.11**) Cou343-GRK(cAB40)-amide	445	490	6.2 ± 1.0	83.9	74
(**3.12**) FAM-GRK(cAB40)-amide	494	520	6.5 ± 0.3	84.6	55
(**3.13**) TAM-GRK(cAB40)-amide	565	580	75.0 ± 7.6	98.7	69
(**3.14**) Atto610-GRK(cAB40)-amide	610	635	77.3 ± 5.0	98.7	75
(**3.15**) Atto700-GRK(cAB40)-amide	681	714	18.2 ± 1.2	94.5	61
(**3.16**) TAM-GRK(BHQ-2)-amide	565	580	64.0 ± 5.0	98.4	48
(**3.17**) TAM-GRK(QSY-7)-amide	565	580	75.4 ± 3.3	98.7	55
(**3.18**) TAM-G-Ø-K(cAB40)-amide	565	580	109.5 ± 6.2	99.1	69

Table 3.1 Photophysical properties of the trypsin substrates **3.10** – **3.17** and the photolabile reporter **3.18**. Fold enhancement upon trypsinolysis or photolysis and the substrate percent quench is also included.

(Fmoc-Ø-OH) and Fmoc-Gly-OH. Fluorophores were condensed to the peptide N-terminus and the resultant products simultaneously deprotected and cleaved from the resin with 95% trifluoroacetic acid (TFA). An array of fluorophores that cover the entire visible spectrum up to the near IR were employed for peptides **3.10** - **3.15**, including diethylaminocoumarin (DEAC; λ_{ex} = 430 nm, λ_{em} = 479 nm), coumarin 343 (Cou343; λ_{ex} = 445 nm, λ_{em} = 490 nm), fluorescein (FAM; λ_{ex} = 494 nm, λ_{em} = 520 nm), tetramethylrhodamine (TAM; λ_{ex} = 565 nm, λ_{em} = 580 nm), atto610 (λ_{ex} = 610 nm, λ_{em} = 635 nm), and atto700 (λ_{ex} = 681 nm, λ_{em} = 714 nm) (Figure 3.1).

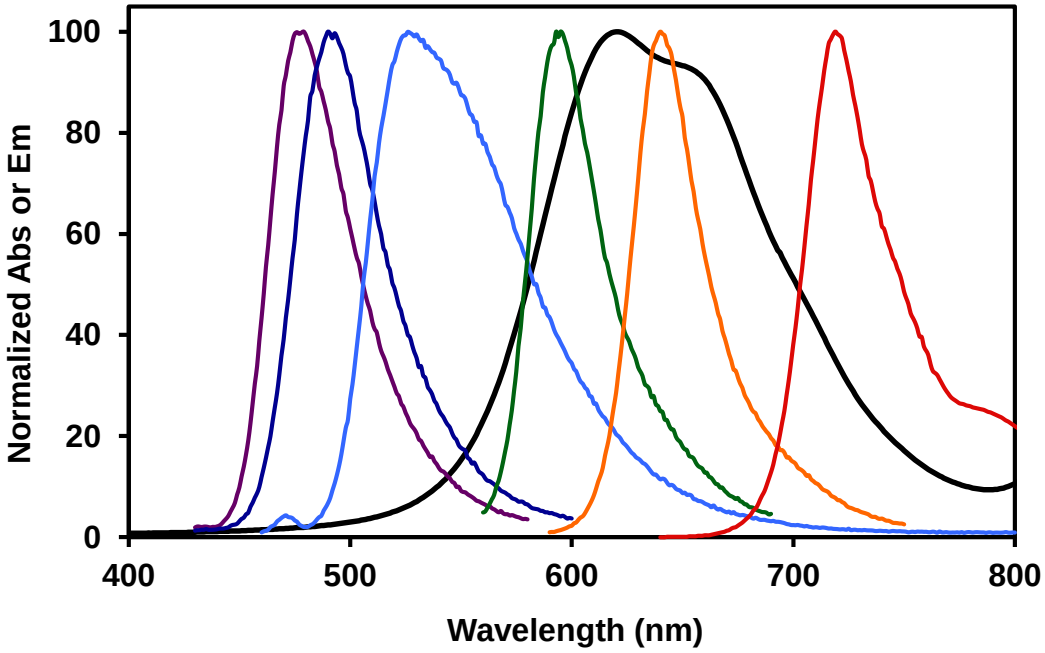

Figure 3.1 AB40 absorbance spectrum (black) and the emission spectra of DEAC (purple), Cou343 (navy blue), FAM (light blue), TAM (green), atto610 (orange), and atto700 (red).

Following synthesis, peptides **3.10** - **3.17** were treated with trypsin and fluorescent enhancements were observed. As is evident from Table 1, large enhancements in fluorescence were obtained for TAM (75-fold), atto610 (77-fold), DEAC (22.5-fold), and atto700 (18.2-fold) peptides. By contrast, the observed increase in fluorescence intensity for the shorter wavelength fluorophores Cou343 (6.2-fold), and FAM (6.5-fold) although significant, are more modest. The

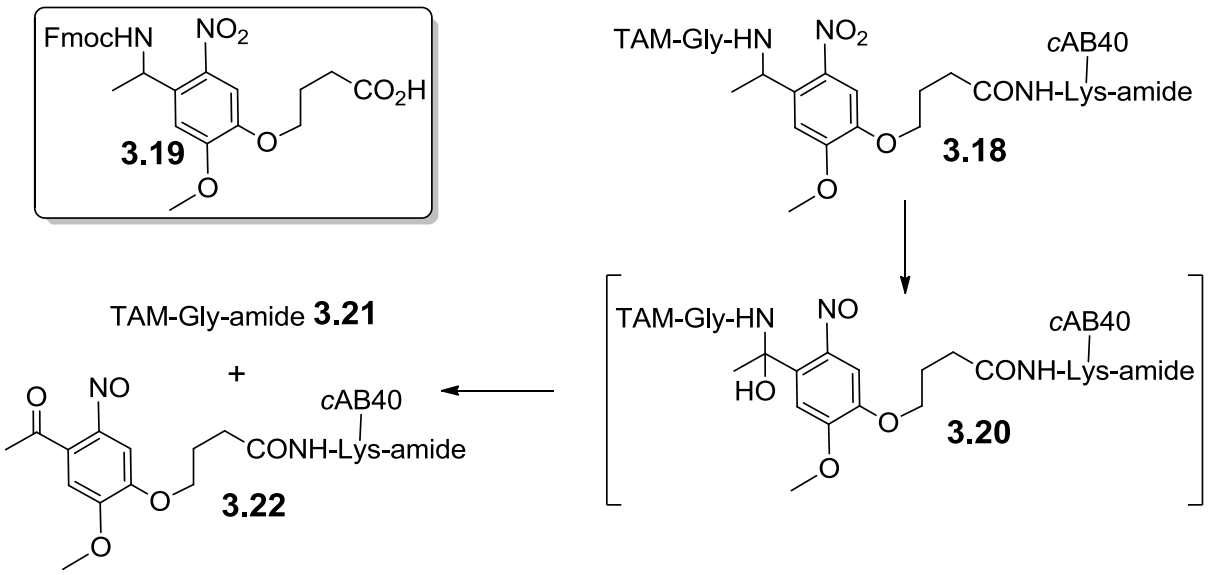

Scheme 3.4 Photolysis of TAM-G-Ø-K(cAB40)-amide **18**. Illumination at 360 nm induces the well-established transfer of one of the oxygens of the nitro functionality to the nearby benzylic position. The intermediate hemiaminal decomposes, generating two fragments, one with the now highly fluorescent TAM fluorophore and the other with the AB40 quenching partner.

fluorescent fold change of the photolabile cassette **3.18** was also determined. Irritation at 360 nm induces the well-established transfer of one of the oxygens of the nitro functionality to the nearby benzylic position creating the hemiaminal **3.20** (Scheme 3.4). The intermediate hemiaminal **3.20** decomposes, generating two fragments, one with the now highly fluorescent TAM fluorophore (**3.21)** and the other with the AB40 quenching partner (**3.22**). Photocleavage of **3.18** was complete within 2 minutes of illumination, delivering a greater than 100-fold fluorescent enhancement (Figure 3.2). A word of caution is in order with respect to the fluorescent enhancements reported in this study and elsewhere, particularly with regard to profluorescent reporters. We found it challenging to remove the last traces of free fluorophore, which could dramatically alter the observed fluorescence enhancement.

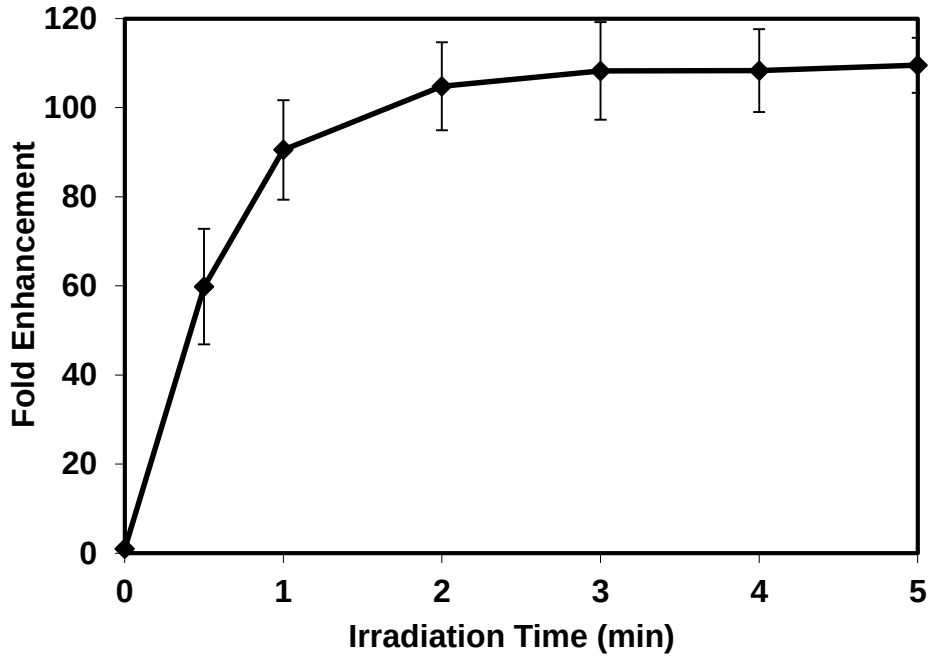

Figure 3.2 Fluorescent enhancement of TAM-G-PL-K(AB40)-amide (**3.17**) as a function of photolysis time.

Förster distances for peptides **3.10** – **3.18** were calculated using the PhotochemCAD software suite (Table 3.1).[13] The fluorophore emission and AB40 absorbance spectra were collected and imported into the software package. A refractive index for 1:1 DMSO/H_2O was used along with a κ^2 value of 2/3, indicative of free molecular rotation.[14] The DEAC and cAB40 pair displays the shortest Förster distance (48 Å) whereas the atto610/cAB40 pair exhibits the longest (75 Å). FRET radii were also calculated for the commercially available quenchers QSY-7 and BHQ-2 (with TAM as the fluorophore) and found to be 48 Å and 55 Å, respectively. The TAM/cAB40 pair displays a Förster distance (69 Å) that compares favorably to the values for QSY-7 and BHQ-2. Quenching efficiency was also calculated from the fluorescent fold change data for each substrate. The quenching efficiency value for the TAM-GRK(AB40)-amide

[13] (1) Du, H.; Fuh, R.-C. A.; Li, J.; Corkan, L. A.; Lindsey, J. S. *Photochem. Photobiol.* **1998**, *68*, 141-142. (2) Dixon, J. M.; Taniguchi, M.; Lindsey, J. S. *Photochem. Photobiol.* **2005**, *81*, 212-213.

[14] LeBel, R. G.; Goring, D. A. I. *J. Chem. Eng. Data* **1962**, *7*, 100-101.

substrate **3.13** were found to compare favorably with BHQ-2 substrate **3.16** and QSY-7 substrate **3.17**.

Next, we chose to investigate the absorbance spectra of substrates with minimal (**3.10**), slight (**3.11**), and complete (**3.13**) overlap with the cAB40 quencher. The substrate absorption spectra (Fl-GRK(cAB40)-amide) was compared with peptides lacking the fluorophore (NH_2-GRK(cAB40)-amide) or quencher (Fl-GRK(NH_2)-amide). Additionally, the fluorophore and quencher absorbance spectra were combined to create a single additive spectrum. The absorbance spectrum of substrate **3.10** displayed changes in absorbance in comparison with the combined spectra of peptides DEAC-GRK(NH_2)-amide **3.23** and NH_2-GRK(AB40)-amide **3.24** (Figure 3.3). A red shift in the shape of the cAB40 peak was evident, as well as blue shift in the fluorophore excitation from 450 to 437 nm was observed. Like substrate **3.10**, the absorbance spectrum of substrate **3.11** displayed changes in comparison with the absorbance spectrum of

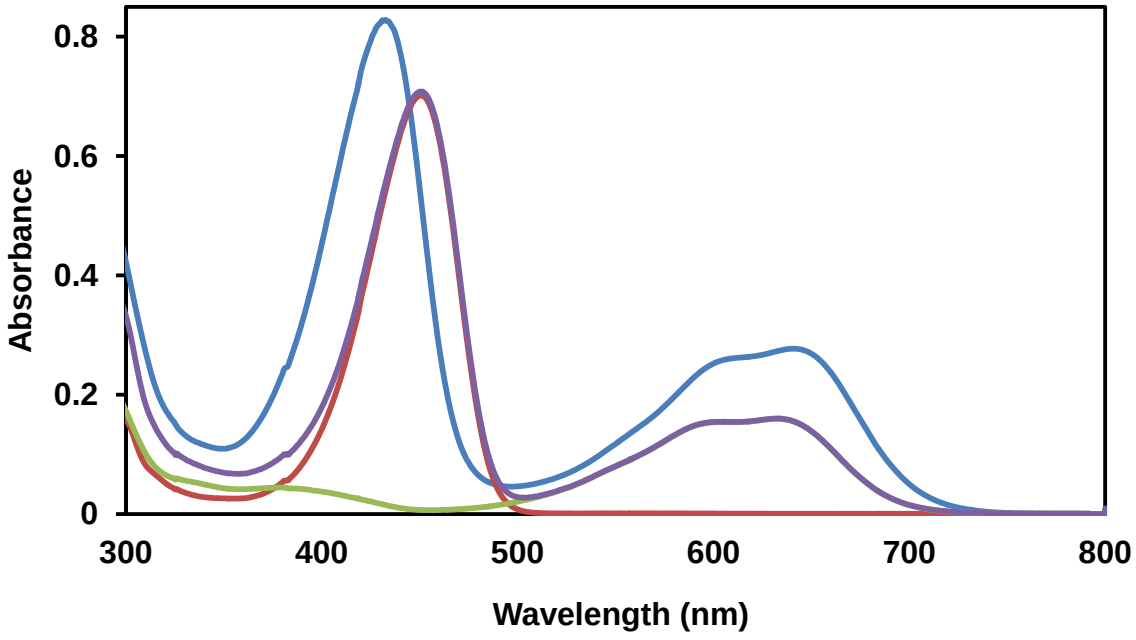

Figure 3.3 Absorbance spectrum of substrate DEAC-GRK(cAB40)-amide **3.10** (Blue), DEAC-GRK(NH_2)-amide **3.23** (Red), NH_2-GRK(AB40)-amide **3.24** (Green), as well as an additive spectrum of **3.23** and **3.24** (Purple).

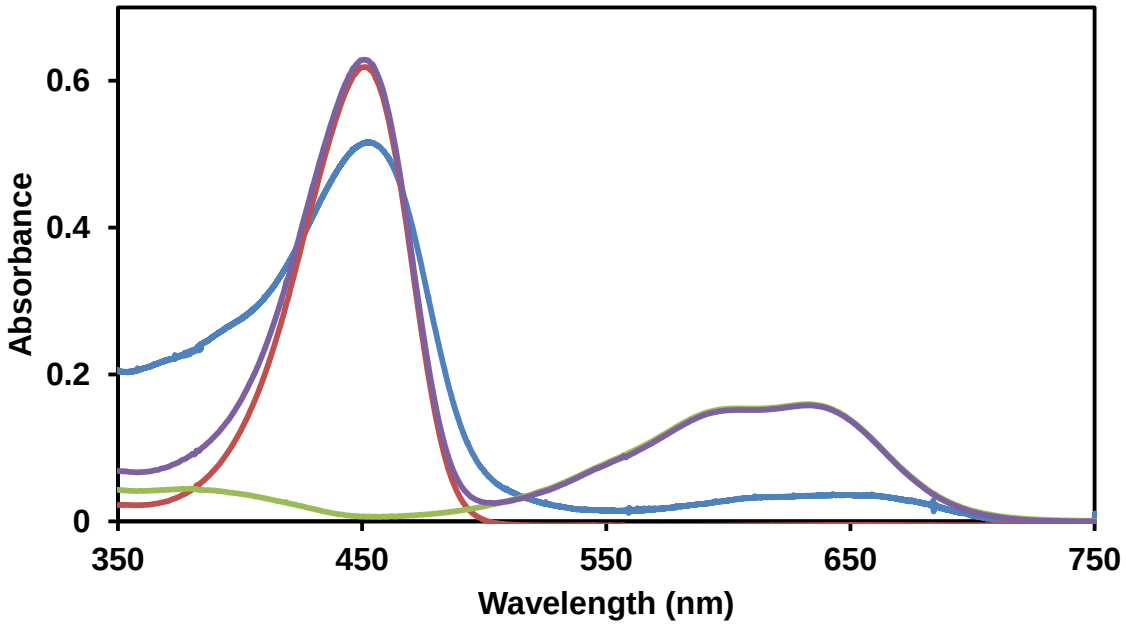

Figure 3.4 Absorbance spectrum of substrate Cou343-GRK(cAB40)-amide **3.11** (Blue), Cou343-GRK(NH_2)-amide **3.25** (Red), NH_2-GRK(AB40)-amide **3.24** (Green), as well as an additive spectra of **3.25** and **3.24** (Purple).

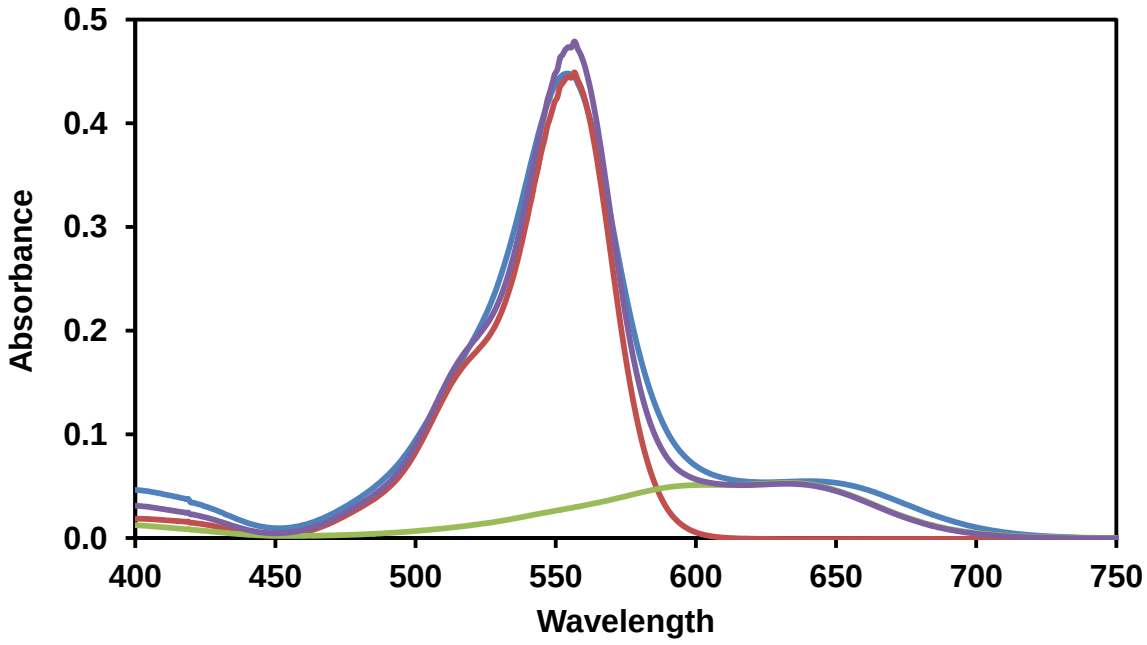

Figure 3.5 Absorbance spectrum of substrate TAM-GRK(cAB40)-amide **3.13** (Blue), TAM-GRK(NH_2)-amide **3.26** (Red), NH_2-GRK(AB40)-amide **3.24** (Green), as well as an additive spectra of **3.26** and **3.24** (Purple).

peptides Cou343-GRK(NH_2)-amide **3.25** and NH_2-GRK(AB40)-amide **3.24** (Figure 3.4). A largeincrease in molar absorptivity in the 300 - 400 nm range as well as a decrease in the 500 - 600 nm range is evident. The absorbance spectrum of substrate **3.13** displayed few changes in comparison with peptides TAM-GRK(NH_2)-amide **3.26** and NH_2-GRK(AB40)-amide **3.24** (Figure 3.5).

Next, we chose to investigate external effects such as viscosity, on the fluorescence of the substrates. Increased viscosity attenuates interaction between the fluorophore and quencher, decreasing the rate at which a donor and acceptor can collide and transfer energy or electrons, thereby decreasing quenching.[13,15] With this in mind, we compared the viscosity dependent fluorescence of substrates **3.10** (DEAC-GRK(cAB40)-amide), **3.11** (Cou343-GRK(AB40)-amide), and **3.13** (TAM-GRK(AB40)-amide) with respect to peptides lacking the cAB40 quencher (peptides DEAC-GRK(NH_2)-amide **3.19**, Cou343-GRK(NH_2)-amide **3.21**, and TAM-GRK(NH_2)-amide) **3.22** (Figure 3.6). In preforming the experiment with coumarin derivatives, it is important to include the unquenched coumarin fluorophore, since coumarin fluorescence is known to be effected by changes in viscosity.[16] The normalized fluorescence change of substrate **3.10** shows increasing fluorescence as a function of viscosity over peptide **3.23** (20-fold). This is approximately similar to the fluorescence change observed from trypsinolysis (22.5-fold). Substrate **3.11** displays a fluorescence change over the background at lower weight percentages of PEG400, however this effect is not observed at higher viscosities. Substrate **3.13** displays no effect to increases in viscosity.

Environmental effects were further investigated with the addition of Hydroxypropyl Beta

[15] Wakata, A.; Cahill, S. M.; Blumenstein, M.; Gunby, R. H.; Jockusch, S.; Marti, A. a; Cimbro, B.; Gambacorti-Passerini, C.; Donella-Deana, A.; Pinna, L. A; Turro, N. J.; Lawrence, D. S. *Org. Lett.* **2008**, *10*, 301–4.

[16] (1) Wagner, B. D. *Molecules (Basel, Switzerland)* **2009**, *14*, 210–37. (2) Choi, J. Y.; Park, E. J.; Chang, S. H.; Kang, T. J. *Bulletin of the Korean Chemical Society* **2009**, *30*, 1452–1458.

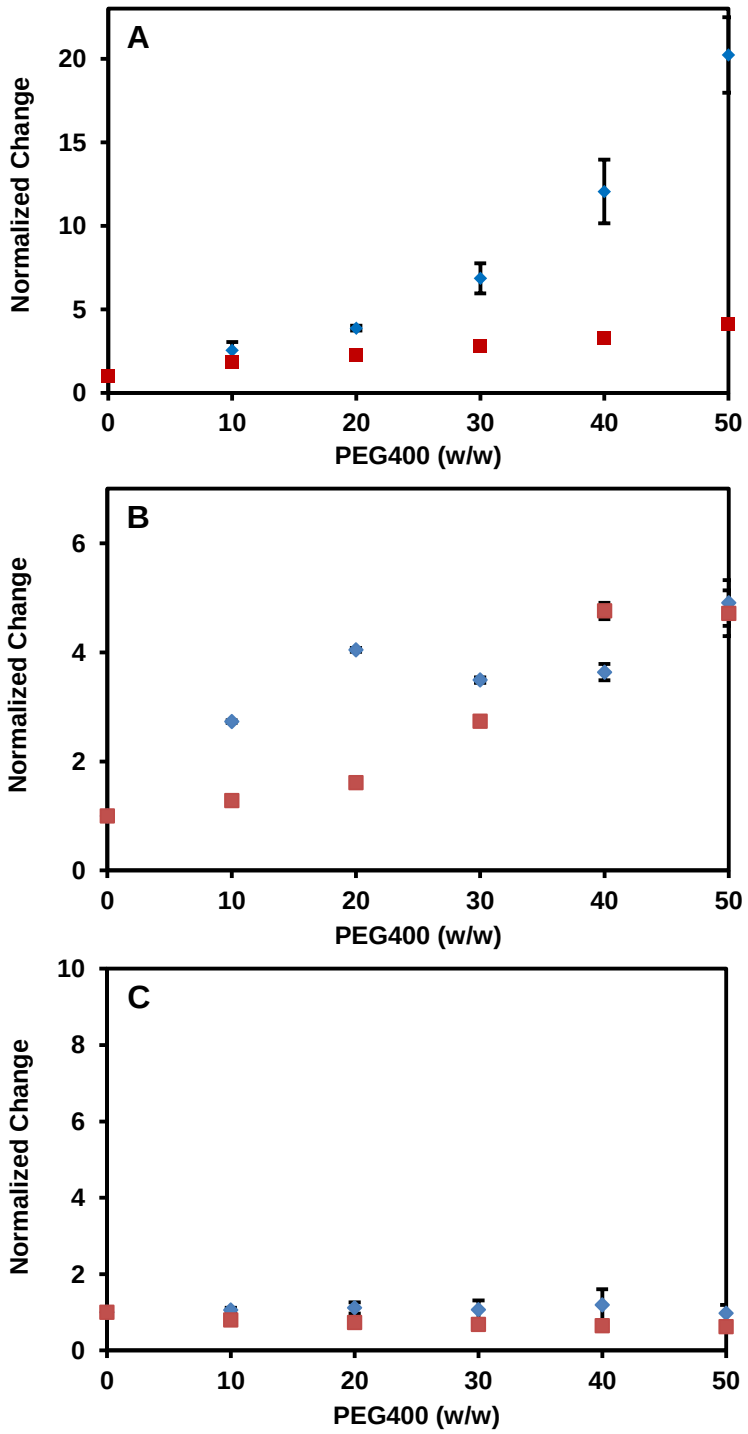

Figure 3.6 Normalized viscosity dependent fluorescence change of substrates DEAC-GRK(cAB40)-amide **3.10** (A, Blue Diamond), Cou343-GRK(AB40)-amide **3.11** (B, Blue Diamond), and TAM-GRK(cAB40)-amide **3.13** (C, Blue Diamond) versus substrates DEAC-GRK(NH_2)-amide **3.23** (A, Red Square), Cou343-GRK(NH_2)-amide **3.25** (B, Red Square), and TAM-GRK(NH_2)-amide **3.26** (C, Red Square). Error bars are present for each measurement, however they may be too tight to observe.

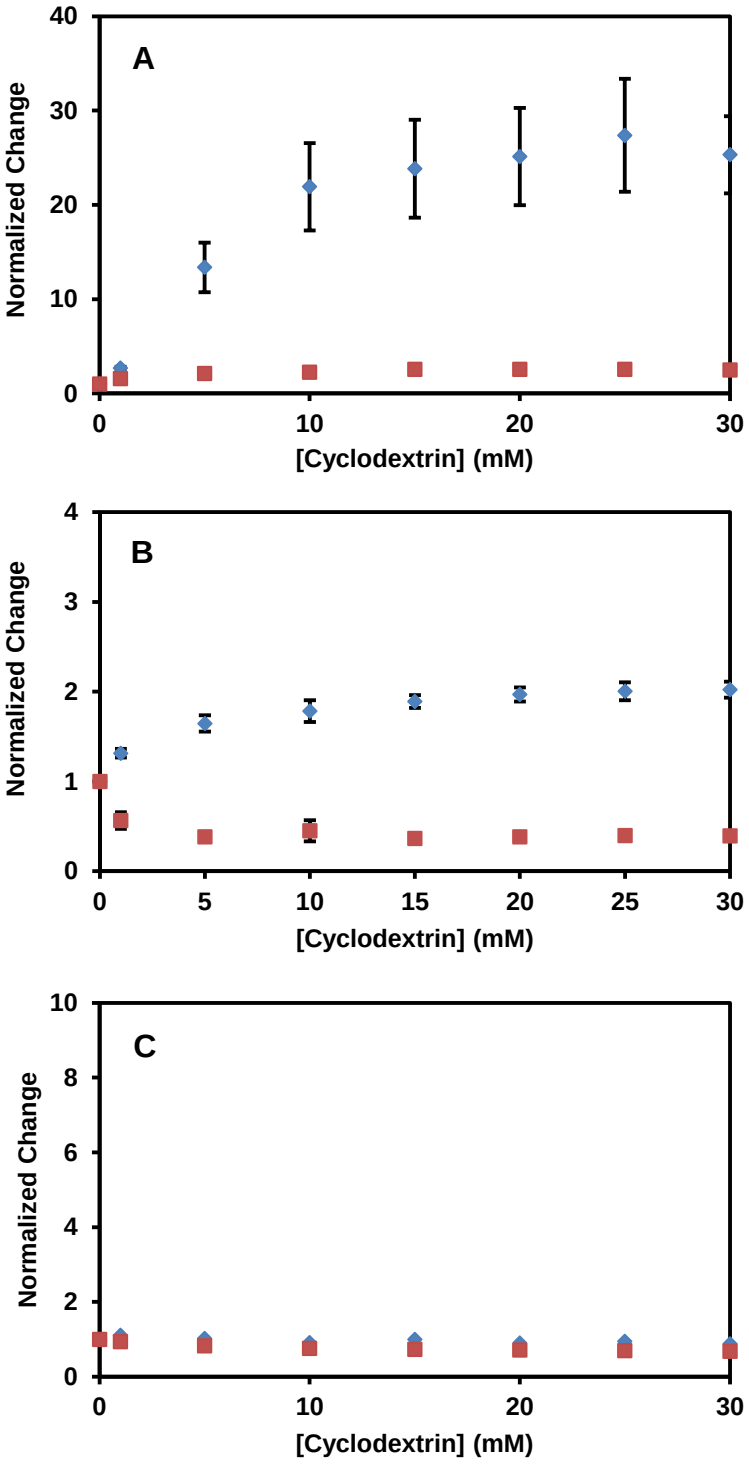

Figure 3.7 Normalized Hydroxypropylbetacyclodextrin (HP-β-CD) dependent fluorescence change of substrates DEAC-GRK(cAB40)-amide **3.10** (A, Blue Diamond), Cou343-GRK(AB40)-amide **3.11** (B, Blue Diamond), and TAM-GRK(cAB40)-amide **3.13** (C, Blue Diamond) versus substrates DEAC-GRK(NH_2)-amide **3.23** (A, Red Square), (Cou343-GRK(NH_2)-amide) **3.25** (B, Red Square), and (TAM-GRK(NH_2)-amide) **3.26** (C, Red Square). Error bars are present for each measurement, however they may be too tight to observe.

Cyclodextrin (HP-β-CD) to peptides **3.10**, **3.11**, and **3.13**. HP-β-CD has been demonstrated to bind coumarins[17] and TAMRA[18] to form supramolecular inclusion complexes. Therefore, the addition of HP-β-CD should work to prevent the interaction of the fluorophore and quencher and relieve quenching in a similar manner as increasing viscosity. With this in mind, we compared the HP-β-CD concentration dependent fluorescence of peptide substrates **3.10**, **3.11**, and **3.13** with the corresponding peptides **3.23**, **3.25**, and **3.26** which lack the cAB40 quencher (Figure 5). The fluorescence of substrate **3.10** dramatically increases as a function of HP-β-CD concentration over the baseline fluorescence observed by substrate **3.23** (25-fold). Substrate **3.11** does show an increase of 1.5-fold in the normalized fluorescence change over the baseline of peptide **3.25**, but this fails to match the enhancement upon trypsinolysis of 6.2-fold. The fluorescence of substrate **3.13** shows no effect to HP-β-CD.

DISCUSSION

The dark quencher cAB40 serves as an efficient broad spectrum quencher in protease substrates using a wide variety fluorophores relevant in fluorescence microscopy. Protease substrates with a wide variety of photophysical properties are effectively quenched, with fluorescence increases upon proteolysis of 75-fold and 100-fold in the case of photolysis. As is clear from Figure 3.1, AB40 absorbance displays significant overlap with the emission signals of TAM, atto610, and to a somewhat lesser extent with atto700, which is consistent with a FRET-

[17] (1) Chakraborty, A.; Seth, D.; Chakrabarty, D.; Sarkar, N. *Spectrochimica acta. Part A, Molecular and biomolecular spectroscopy* **2006**, *64*, 801–8. (2) Ghosh, S.; Mondal, S. K.; Sahu, K.; Bhattacharyya, K. (3) Karnik, N. A.; Prankerd, R. J.; Perrin, J. H. *Chirality* **1991**, *3*, 124–128. *The journal of physical chemistry. A* **2006**, *110*, 13139–44. (4) Velic, D.; Knapp, M.; Köhler, G. *J. Mol. Struct.* **2001**, *598*, 49–56.

[18] Nguyen, T.; Joshi, N. S.; Francis, M. B. *Bioconjugate Chem.*, **2006**, *17*, 869–72.

based quenching mechanism. Curiously, although there is minimal overlap between the emission of DEAC with the cAB40 absorbance spectrum, nonetheless this species displays a trypsin-mediated fluorescent enhancement analogous to that of the atto700 derivative **3.15**. In light of this, we chose to further investigate the mechanism and delivery of quenching.

Dark quenchers can modulate fluorescence through two processes consisting of (1) electron transfer mechanisms or (2) energy transfer mechanisms.[19] Electron transfer involves the transfer of an electron either to or from a ground or excited state donor, resulting in a return to the ground state. Energy transfer mechanisms consist of nonradiative (1) Dexter or (2) Förster energy transfer. The Dexter energy transfer mechanism requires an overlap of frontier molecular orbitals preceding electron exchange, which results in acceptor excitation and donor relaxation.[20] FRET occurs via an overlap of dipolar electric fields that precede energy transfer. After dipole overlap occurs, energy transfer proceeds from an excited state fluorophore to an acceptor through resonance of oscillating electronic dipoles.[21] The acceptor then undergoes relaxation via radiative or non-radiative processes.

Additionally, each quenching mechanism is affected by changes in molecular diffusion, which can affect the mechanism for electron or energy delivery. Delivery processes from donor to acceptor can be divided into three types: (1) the formation of donor/acceptor complex continuously held as a pair (ie static quenching), (2) a diffusional related processes that helps associate the donor and acceptor (ie dynamic quenching), or (3) a conductor that facilities energy or electron transfer between the donor and acceptor. The formation of a ground state

[19] Turro, N. J., Ramamurthy, V., Scaiano, J. C. Modern Molecular Photochemistry of Organic Molecules. Sausalito, Calif.: University Science Books, 2010.

[20] Dexter, D. L. *J. Phys. Chem.* **1953**, *21*, 836.

[21] T. Förster, *Fluorenzenz Organische Verbindungen.* Vandenhoech and Ruprecht: Göttingen, **1951**.

donor/acceptor complex that exists before photon absorption is termed "static quenching". A hallmark of static quenching is an altered fluorophore absorbance spectrum because donor/acceptor interactions occur in the ground state, and are hence visible to the observer.[22] Diffusional related energy or electron delivery processes that occur in the excited state are termed "dynamic quenching". Dynamic quenching requires the excited state donor and acceptor enter into close proximity for quenching to occur. Because of this, dynamic quenching is susceptible to external effects such as temperature or viscosity. The third delivery mechanism requires a conductive tether capable of transporting energy or electrons (e.g. the through bond energy transfer mechanism[23]).

Due to the large fluorophore emission/quencher absorbance overlap of the TAMRA/cAB40 pair, we expected a FRET based mechanism to primarily be responsible for the high quenching efficiency as is observed in BHQ and QSY quencher series. However, electron transfer or Dexter energy transfer could still be possible. We expected to observe some degree of ground state complex formation (or static quenching) for each substrate, since the fluorophore and quencher are covalently bound, and unable to freely diffuse apart. The absorbance spectra of substrates **3.10** and **3.11** indicate the presence of a static quenching mechanism due to the changes in absorbance (Figure 3.3, 3.4). However, substrate **3.13** displays only minor changes in absorbance indicating the lack of a static quenching mechanism (Figure 3.5).

The effects of PEG400 and HP-β-CD were investigated for evidence of dynamic quenching. The viscosity (22.5 fold) and HP-β-CD (25 fold) normalized fluorescent increases of substrate **3.10** approximately matches the 22.5-fold enhancement observed from trypsinolysis (Figure 4A, 5A). This indicates the presence of a diffusional related delivery mechanism of

[22] Lakowicz J. R.: Principles of Fluorescence Spectroscopy. 3rd ed. New York: Kluwer Academic/Plenum, 2006.

[23] Fan, J.; Hu, M.; Zhan, P.; Peng, X. *Chem. Soc.Rev.* **2013**, *42*, 29–43.

energy transfer (i.e. dynamic quenching). The environmental effects of increasing viscosity and HP-β-CD of substrate **3.11** are somewhat ambiguous. Increasing viscosity does not produce an increase over the baseline fluorescence provided by **3.21** but not to the extent seen during trypsinolysis (6-fold) (Figure 3.7B). Substrate **3.13** shows no effect to viscosity and HP-β-CD (Figure 4C, 5C). Both substrate **3.11** and **3.13** demonstrate the absence of a dynamic quenching mechanism.

Overall, the absorbance, viscosity, and HP-β-CD experiments allow us to determine the mechanism of energy delivery in each substrate. Substrate **3.10** is likely a combination of static and dynamic quenching due to the changes observed in the absorbance spectrum of the substrate (likely static quenching) and the relief of quenching due to the environmental effects of viscosity and HP-β-CD (likely dynamic quenching).[24] The lack of large changes in the absorbance of substrate **3.13**, as well as the absence of changes in normalized fluorescence upon exposure to PEG400 or HP-β-CD, indicates a lack of a static or dynamic quenching mechanism. Due to this, we believe energy transfer occurs via a radiative energy transfer mechanism, whereby quenching occurs via fluorophore emission preceding quencher absorption. This is somewhat different than a Förster resonance energy transfer mechanism, where energy transfer is nonradiative and occurs through resonance of electronic dipoles in the excited state,[19] although there is some debate over this issue.[25] Since the photophysical properties of substrate **3.11** fall between that of **3.10** and **3.13**, energy delivery could be occurring as a combination of mechanisms. However, we know quenching in substrates **3.10** and **3.11** occurs via a static mechanism due to the observed changes in absorbance spectrum.

[24] Birks, J. B.; Salete, M.; Leite, S. C. P. *Journal of Physics B: Atomic and Molecular Physics* **1970**, *3*, 417–424.

[25] (1) Andrews, D. L.; Bradshaw, D. S. *European Journal of Physics* **2004**, *25*, 845–858. (2) Andrews, D. L. *Chemical Physics* **1989**, *135*, 195–201.

CONCLUSIONS

cAB40 is an effective broad-spectrum dark quencher of a variety of fluorophores, enabling it to be used in the construction of multi-colored protease sensors, as well as a reporter of photolysis (with up to a 100- fold increases fluorescence observed). Although bond cleavage-induced fluorescent enhancement varies by fluorophore, the most pronounced changes are observed with fluorophores possessing emission spectra commonly employed in microscopy. The cAB40 quencher was shown to have different mechanisms of energy delivery for various fluorophores, due to changes observed in absorbance spectra, and differing responses to increased viscosity and concentrations of Hydroxypropyl Beta Cyclodextrin (HP-β-CD). Substrate **3.10** was shown to have large changes in absorbance spectra (relative to peptides containing solely DEAC or cAB40) and found to be no longer quenched with increasing viscosity and concentrations of HP-β-CD. These results point to combined dynamic and static mechanism for delivery of energy from the fluorophore to the quencher. Substrate **3.13** showed only minor changes in its absorbance spectrum and no effect upon exposure to increasing viscosity and concentrations of HP-β-CD. This leads us to believe energy transfer occurs in this case due to a radiative energy transfer mechanism. Overall, this work represents an easily synthesized dark quencher capable of quenching a broad spectrum of fluorophores, which can be used in the construction of protease substrates and other probes for bioimaging.

MATERIALS AND METHODS

General Procedures General reagents and solvents were purchased from Fisher or Sigma-Aldrich. Novasyn TGR Resin, Fmoc-Lys(Mtt)-OH (N-α-Fmoc-N-ε-4-methyltrityl-L-lysine)**,** and all Fmoc protected natural amino acids were purchased from EMD Biosciences Inc. HCTU [1H-benzotriazolium-1 [bis(dimethylamino)methylene]-5-chloro-hexafluorophosphate (1),3-oxide] was purchased from Peptides International (Louisville, KY, U.S.A.). TAM (5-carboxytetramethylrhodamine), and FAM (5-carboxyfluorescein) were purchased from Chempep, Inc. (Wellington, Fl, U.S.A). DECou (7-(diethylamino)coumarin-3-carboxylic acid), Cou343 ([11-oxo-2,3,6,7-tetrahydro-1H,5H,11H-pyrano[2,3-f]pyrido[3,2,1-ij]quinoline-10-carboxylic acid), atto610 NHS-ester, and atto700 NHS-ester were purchased from Sigma-Aldrich. Fmoc-Photolabile Linker (Fmoc-Ø-OH) **3.19** (4-{4-[1-(9-fluorenylmethyloxycarbonyl)ethyl]-2-methoxy-5-nitrophenoxy}butanoic acid) was purchased from Advanced ChemTech (Louisville, KY, U.S.A.). Flash Chromatography was performed on a Biotage (Charlotte, N.C., U.S.A.) Isolera One System using a 120 gram C18 reverse phase column. Trypsin from bovine pancreas was purchased from Sigma-Aldrich.

Synthesis of *c*AB40 3.7 The sodium salt of bromaminic acid **3.5** (1-amino-4-bromo-9,10-dihydro-9,10-dioxo-2-anthracenesulfonic acid sodium salt**,** 0.500 g, 1.23 mmol), 4-aminophenylacetic acid **3.6** (0.166 g, 1.1 mmol), sodium carbonate (0.197 g, 1.58 mmol), copper (II) sulfate (28 mg, 0.179 mmol) and water (50 mL) were added to a 100 mL flask. The color of the solution turned from a bright red to a dark blue after stirring and heating the mixture to reflux for 24 h, indicating product formation. The aqueous mixture was washed with dichloromethane (DCM) (3 x 50 mL) and the solvent removed via rotary evaporation. The resulting solid was dissolved in methanol, filtered, and the solvent removed via rotary evaporation. The furnished

solid was purified via reverse-phase flash chromatography using an acetonitrile to water gradient (3% to 95%) over 30 min to furnish the desired material as a dark blue solid in 37.2% yield. ^{1}H NMR (400 MHz, DMSO-d_6) δ 9.62 (broad, 5H), 8.212 (t, J = 9.2 Hz, 1H), 8.208 (t, J = 8.8 Hz, 1H), 8.044 (s, 1H), 7.787 (t, J = 3.2 Hz, 1H), 7.787 (t, J = 4.4Hz, 1H), 7.236 (d, J = 8.4 Hz, 2H), 7.240 (d, J = 8.4 Hz, 2H), 3.611 (s, 2H), 2.537 (s, 1H); ^{13}C NMR (100 MHz, $CDCl_3$) δ 182.506, 181.971, 172.859, 144.138, 142.695, 141.011, 137.861, 134.155, 133.613, 133.202, 132.858, 131.349, 130.815, 126.090, 126.017, 123.034, 122.735, 111.513, 109.543; HRMS (ESI-) m/z calc'd for $C_{22}H_{15}N_2O_7S^-$ [M^-]: 451.0605, m/z found: 451.0607.

Synthesis of Fluorophore/Dye-labeled Peptides Peptides were synthesized using standard Fmoc solid-phase synthesis on a Prelude peptide synthesizer (Protein Technologies Inc., Tucson, AZ, U.S.A.). Novasyn TGR resin was swelled for 30 min in DCM before synthesis. Fmoc-Lys(Mtt)-OH was then coupled using 5.0 equiv AA, 4.9 equiv of HCTU, 20 equiv of diisopropylethylamine (DIPEA) in N,N-dimethylformamide (DMF) (2 × 5 min) followed by a DMF wash (6 × 30 s). The Lys 4-methyltrityl protecting group was then deprotected using 7% TFA/7% TIS/86% DCM. The deprotected side chain amine was then acylated using 1.1 equiv *c*AB40, 1.0 equiv HCTU, and 20.0 equiv DIPEA in DMF (2 x 2 h). The Fmoc-protecting group was removed using 20% piperidine in DMF (2 × 2.5 min) followed by a DMF wash (6 × 30 s). Fmoc-Arg-OH and Fmoc-Gly-OH were then to the free N-terminus of the peptide using the conditions described for the coupling and deprotection of Fmoc-Lys(Mtt)-OH. In the case of **14**, the Fmoc-Ø-OH photolabile amino acid was coupled instead of Fmoc-Arg-OH. The N-terminal Fmoc was then removed using 20% piperidine in DMF (2 × 2.5 min) and fluorophores were coupled using one of two methods. (1) The fluorophores DECou, Cou343, 5'-FAM, TAM, and

ROX were coupled to the N-terminal amine using 5.0 equiv of fluorophore, 4.9 equiv of HCTU, and 20 equiv of DIPEA in DMF (1× 60 min) followed by a wash (3× DMF, IPA, DCM). (2) The fluorophores atto610-NHS ester and atto700-NHS ester were coupled using 1.0 mg of dye and 20 equiv of DIPEA in DMF (1 × 60 min) followed by a wash (3X DMF, IPA, DCM). The synthesis of peptides **15**, **17**, and **18** followed the exact same procedure as above, but the Mtt protecting group deprotection and cAB40 coupling was skipped. The synthesis of peptide **16** followed the exact same procedure as above, but fluorophore coupling was skipped to leave a free N-terminal amine. After synthesis was complete, the peptide was cleaved from the resin and deprotected using a 95:2.5:2.5 TFA:H_2O:triisopropylsilane (TIPS) cleavage cocktail. The peptides were isolated via filtration, precipitated with ice-cold ether, and centrifuged. The precipitates were air-dried, dissolved in DMSO, and purified using HPLC (3% to 95% acetonitrile to water gradient with 0.1% TFA over 30 min using a 25 cm x 21.2 mm C18 column). Peptides **3.10** – **3.18** were collected, freeze-dried, and characterized by matrix-assisted laser desorption/ionization mass spectrometry (Matrix: alpha cyano-4-hydroxycinnaminic acid, mono-isotopic): DECou-GRK(AB40)-amide **3.10** [Exact Mass calculated: 1035.391, found: 1035.355 $(M+H)^+$], Cou343-GRK(AB40)-amide **3.11** [Exact Mass calculated: 1059.391, found: 1059.351 $(M+H)^+$], FAM-GRK(AB40)-amide **3.12** [Exact Mass calculated: 1150.349, found: 1150.333 $(M+H)^+$], TAM-GRK(AB40)-amide **3.13** [Exact Mass calculated: 1205.451, found: 1205.476 $(M+H)^+$], atto610-GRK(AB40)-amide **3.14** [Exact Mass calculated: 1165.529, found: 1165.556 $(M+H)^+$], atto700-GRK(AB40)-amide **3.15** [The structure of atto700 has not been published, exact mass could not be calculated, found: 1340.512], TAM-GRK(BHQ2)-amide **3.16** [Exact Mass calculated: 1259.575, found: 1259.606 $(M+H)^+$], TAM-GRK(QSY7)-amide **3.17** [Exact Mass calculated: 1410.613, found: 1410.612 $(M+H)^+$], TAM-G-Ø -K(AB40)-amide **3.18**

[Exact Mass calculated: 1329.456, found: 1329.427 $(M+H)^+$]. Peptides **3.23** – **3.25** were collected, freeze-dried, and were characterized by positive electrospray ionization quadrupole mass spectrometry (ESI^+-QMS): DEAC-GRK(NH_2)-amide **3.23** [Exact Mass calculated: 602.3, found: 602.3 $(M+H)^+$], NH_2-GRK(cAB40)-amide **3.24** [Exact Mass calculated: 793.3, found: 793.3 $(M+H)^+$], Cou343-GRK(NH_2)-amide **3.25** [Exact Mass calculated: 626.3, found: 626.3 $(M+H)^+$], TAM-GRK(NH_2)-amide **3.26** [Exact Mass calculated: 771.4, found: 771.4 $(M+H)^+$].

Photolysis Protocol The photolabile peptide **3.16** (1 μM) was incubated in a 1:1 solution of DMSO/H_2O containing 1 mM dithiothreitol and 25 mM Tris pH 7.4 buffer. An aliquot was removed to collect a base line fluorescence measurement using a Photon Technology QM-4 spectrofluorimeter (Birmingham, NJ). The aliquot was returned to stock solution and mixed thoroughly. The sample was then photolyzed using 290 nm to 390 nm (365 nm maximum light intensity) light by an Oriel Hg arc lamp (power supply model 69907 with a 200 Watt Hg lamp, NewPort, North Billerica, MA) using a UG.1 UV bandpass filter (Newport, North Billerica, MA) at various time points at room temperature. After the photolysis period, an aliquot was removed and the fluorescence of the photolyzed material determined. This cycle was repeated until three consecutive fluorescence measurements remained constant to establish a maximum fluorescence enhancement.

Trypsin Protocol Peptides **3.7** – **3.14** (1 μM) were incubated in 25 mM Tris pH 7.4 buffer containing 1 mM dithiothreitol in a 200 μL quartz cuvette at 30 ˚C. After 5 min, a fluorescent baseline was collected using a Photon Technology QM-4 spectrofluorimeter (Birmingham, NJ).

Once a stable baseline had been established, 2 µL of trypsin (50 µM) was added and the fluorescence enhancement was monitored.

Characterization Data

Mass Spectrometry Data

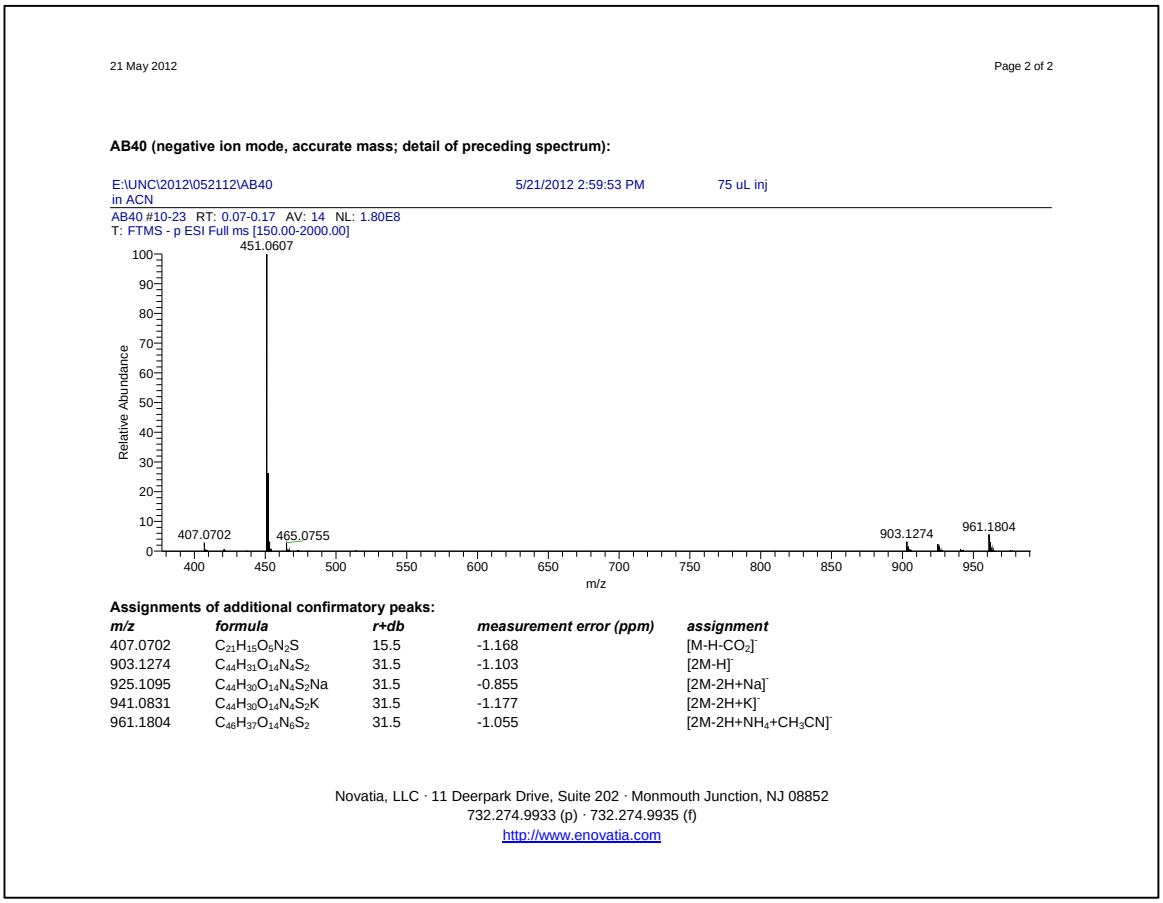

Figure 3.8: HRMS of cAB40 **3.7**: m/z calc'd for $C_{22}H_{15}N_2O_7S^-$ [M-]: 451.0605, m/z found: 451.0607.

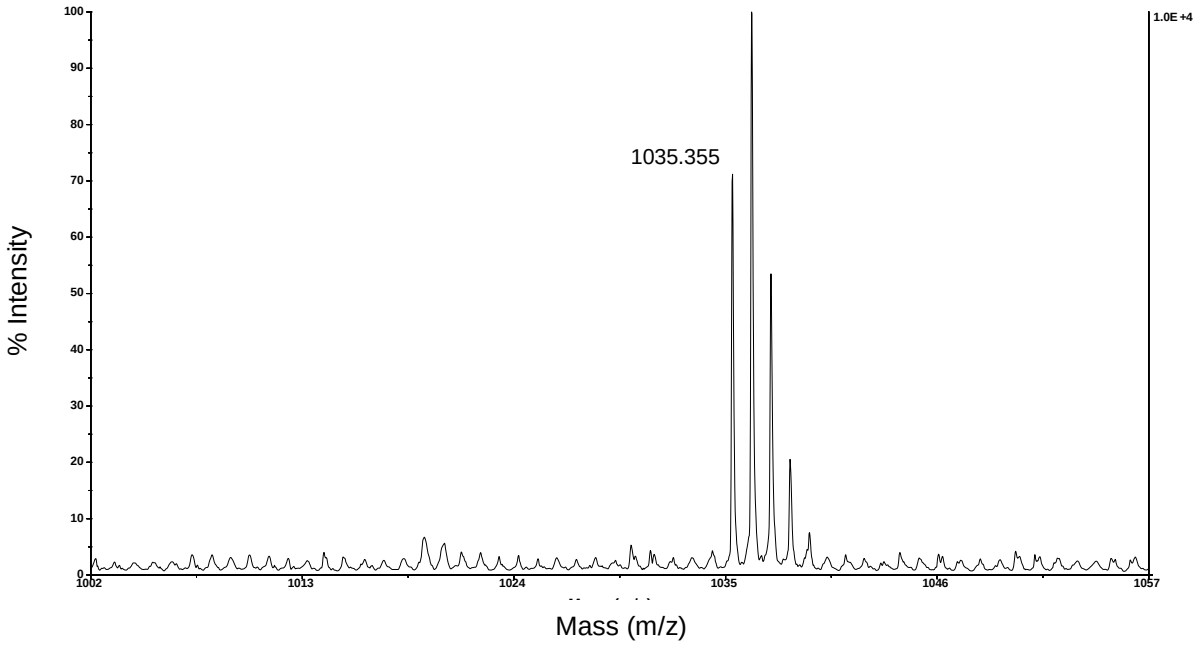

Figure 3.9: MALDI-TOF (alpha cyano-4-hydroxycinnaminic acid, mono-isotopic) of DECou-GRK(AB40)-amide **3.10**: m/z calc'd for $C_{50}H_{57}N_{11}O_{12}S$ $[M+H]^+$: 1035.391, m/z found: 1035.355.

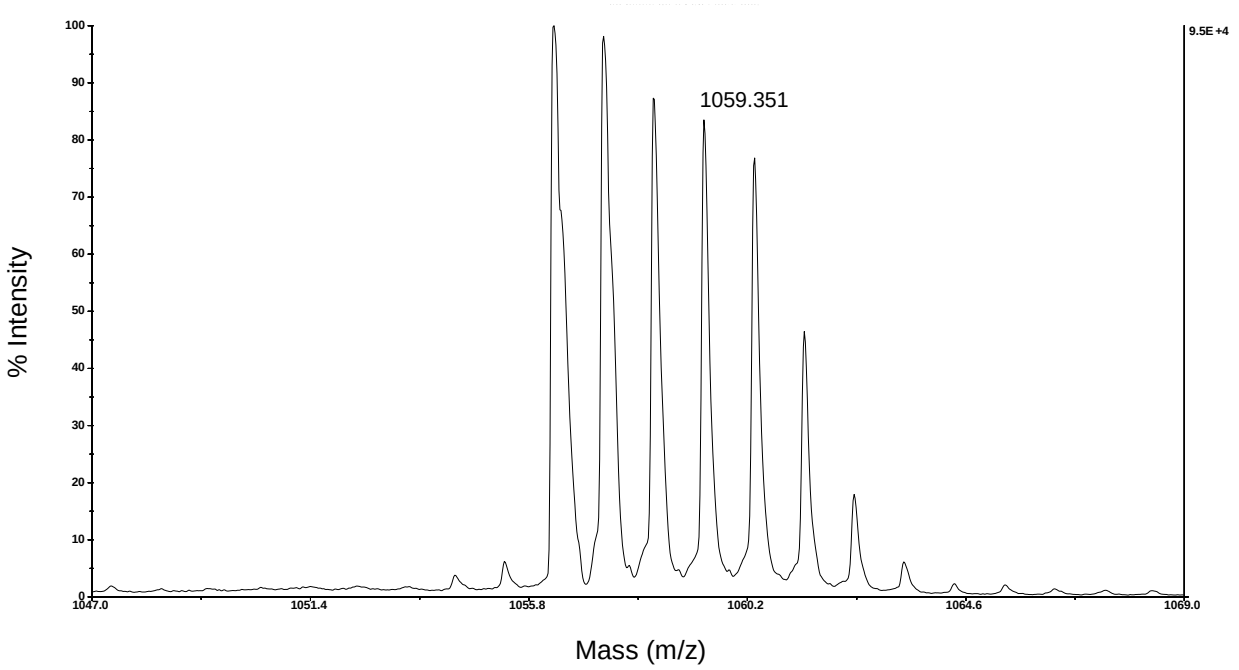

Figure 3.10: MALDI-TOF (alpha cyano-4-hydroxycinnaminic acid, mono-isotopic) of Cou343-GRK(AB40)-amide **3.11**: m/z calc'd for $C_{50}H_{57}N_{11}O_{12}S$ $[M+H]^+$: 1059.391, m/z found: 1059.351

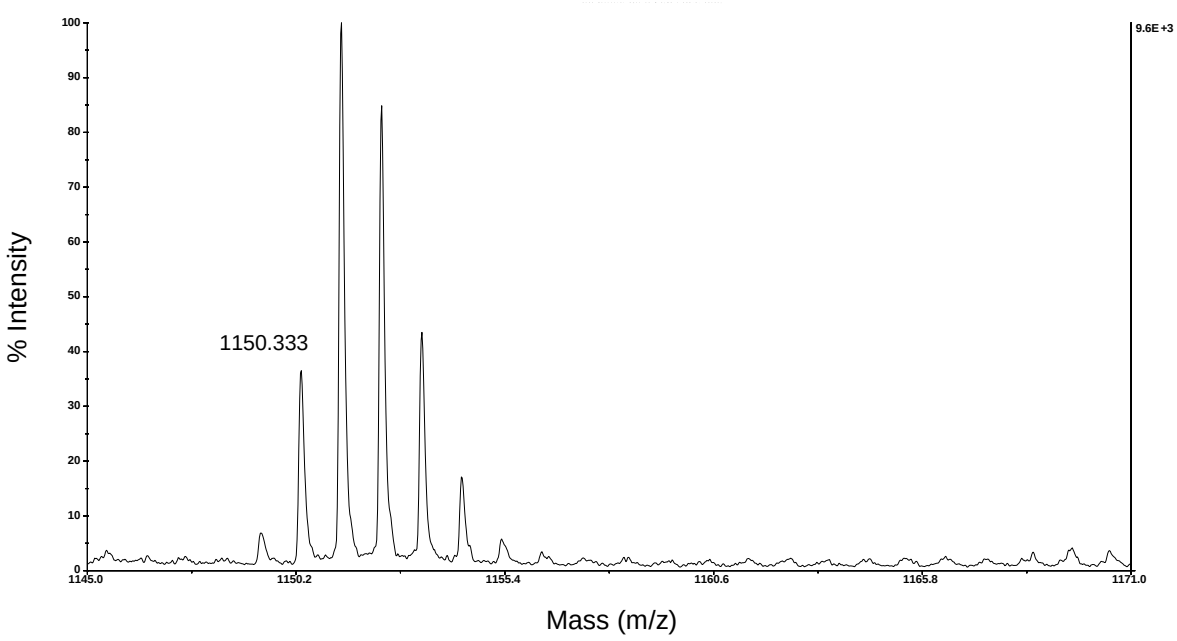

Figure 3.11: MALDI-TOF (alpha cyano-4-hydroxycinnaminic acid, mono-isotopic) of FAM-GRK(AB40)-amide **3.12**: m/z calc'd for $C_{57}H_{54}N_{10}O_{15}S$ $[M+H]^+$: 1150.349, m/z found: 1150.333.

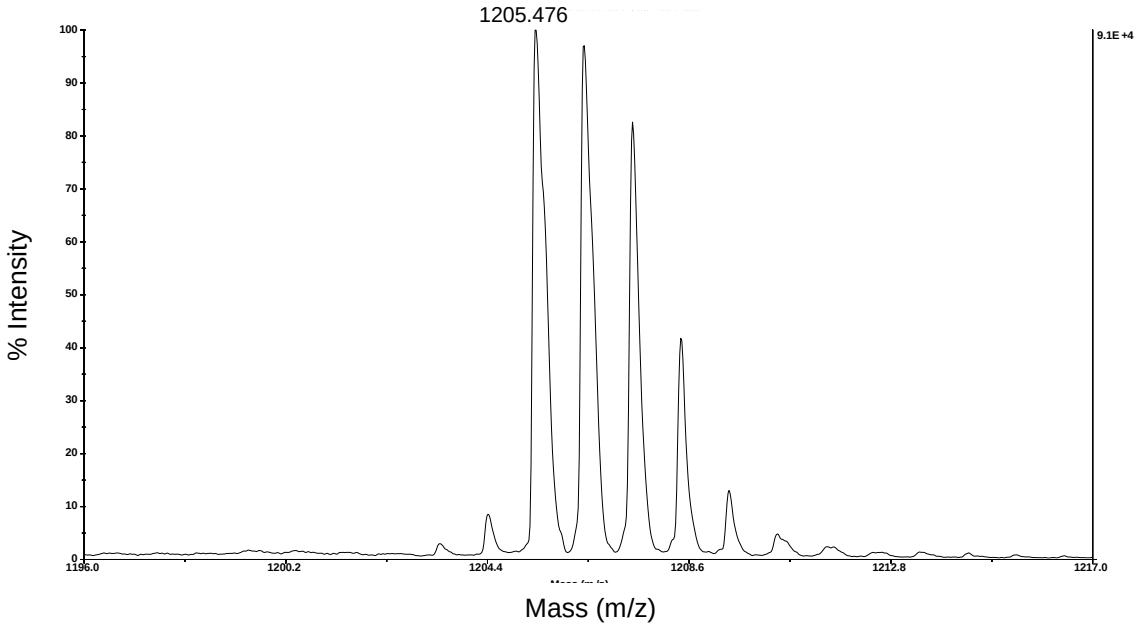

Figure 3.12: MALDI-TOF (alpha cyano-4-hydroxycinnaminic acid, mono-isotopic) of TAM-GRK(AB40)-amide **3.13**: m/z calc'd for $C_{61}H_{65}N_{12}O_{13}S$ $[M+H]^+$: 1205.451, m/z found: 1205.476.

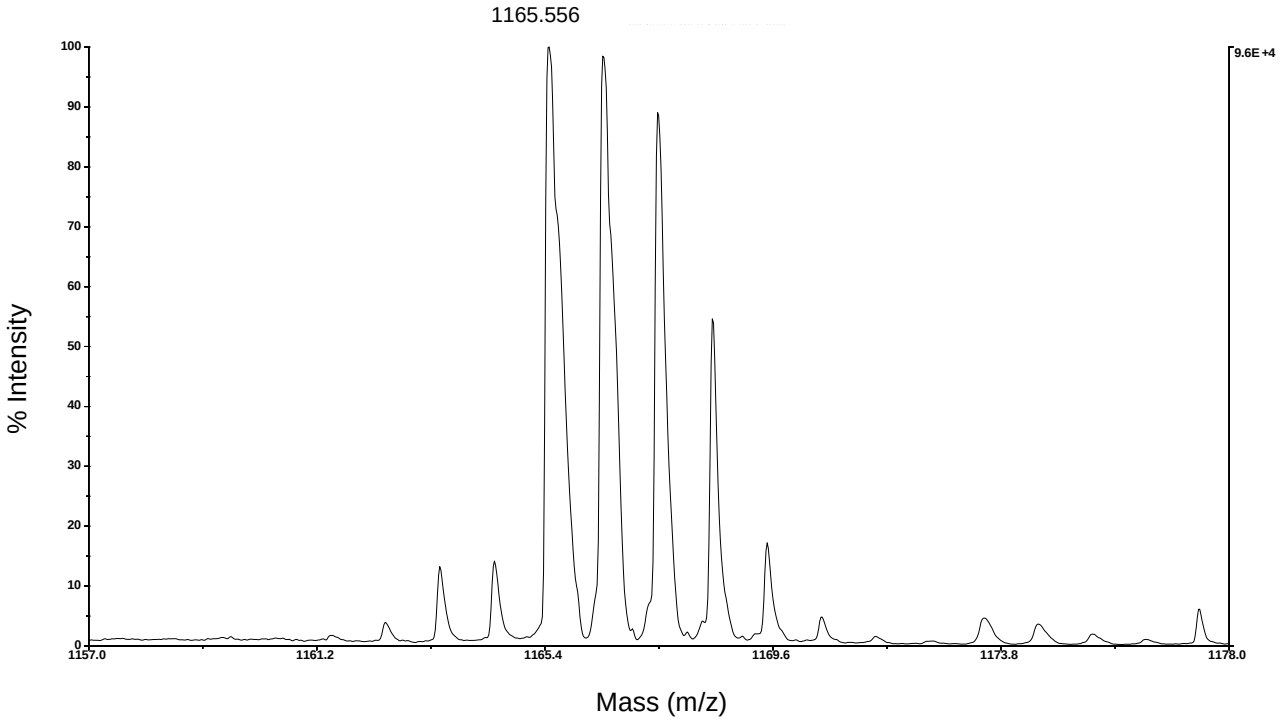

Figure 3.13: MALDI-TOF (alpha cyano-4-hydroxycinnaminic acid, mono-isotopic) of atto610-GRK(AB40)-amide **3.14**: m/z calc'd for $C_{61}H_{73}N_{12}O_{10}S$ $[M+H]^+$: 1165.529, m/z found: 1165.556.

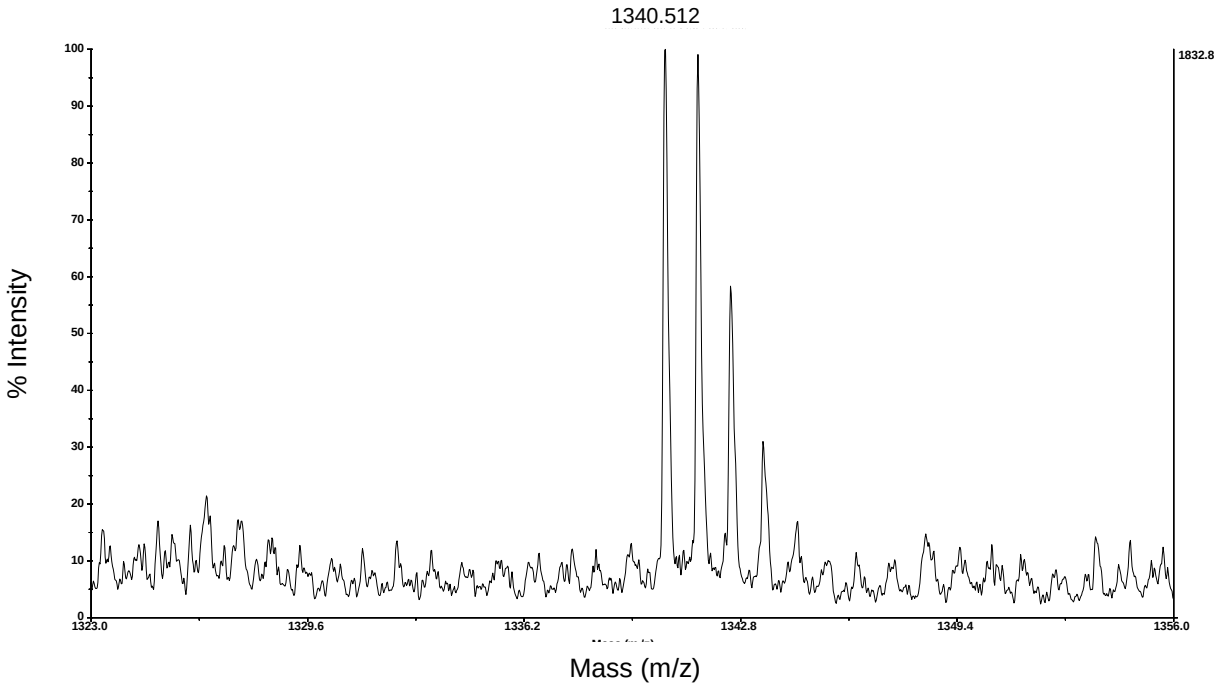

Figure 3.14: MALDI-TOF (alpha cyano-4-hydroxycinnaminic acid, mono-isotopic) of atto700-GRK(AB40)-amide **3.15**: Unable to calculate exact mass due to unpublished atto 700 structure, m/z found: 1340.512.

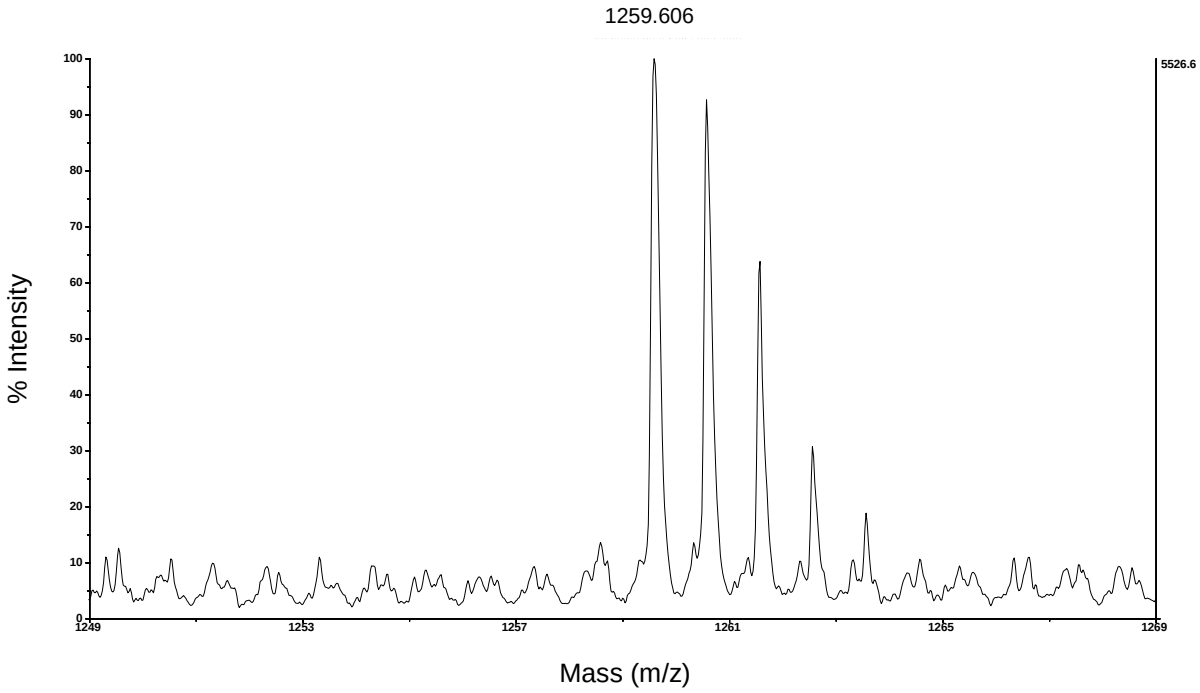

Figure 3.15: MALDI-TOF (alpha cyano-4-hydroxycinnaminic acid, mono-isotopic) of TAM-GRK(BHQ2)-amide **3.16**: m/z calc'd for $C_{128}H_{150}N_{31}O_{22}$ $[M+H]^+$: 1259.575, m/z found: 1259.606.

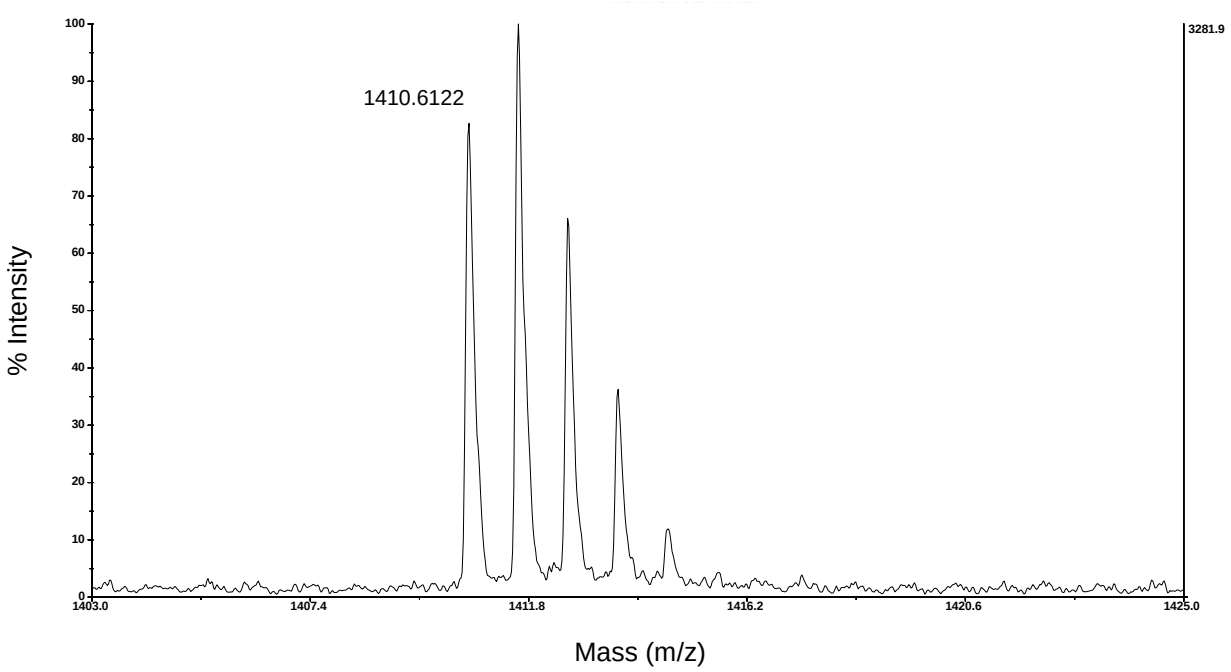

Figure 3.16: MALDI-TOF (alpha cyano-4-hydroxycinnaminic acid, mono-isotopic) of TAM-GRK(QSY7)-amide **3.17**: m/z calc'd for $C_{78}H_{84}N_{13}O_{11}S$ $[M+H]^+$: 1410.613, m/z found: 1410.612.

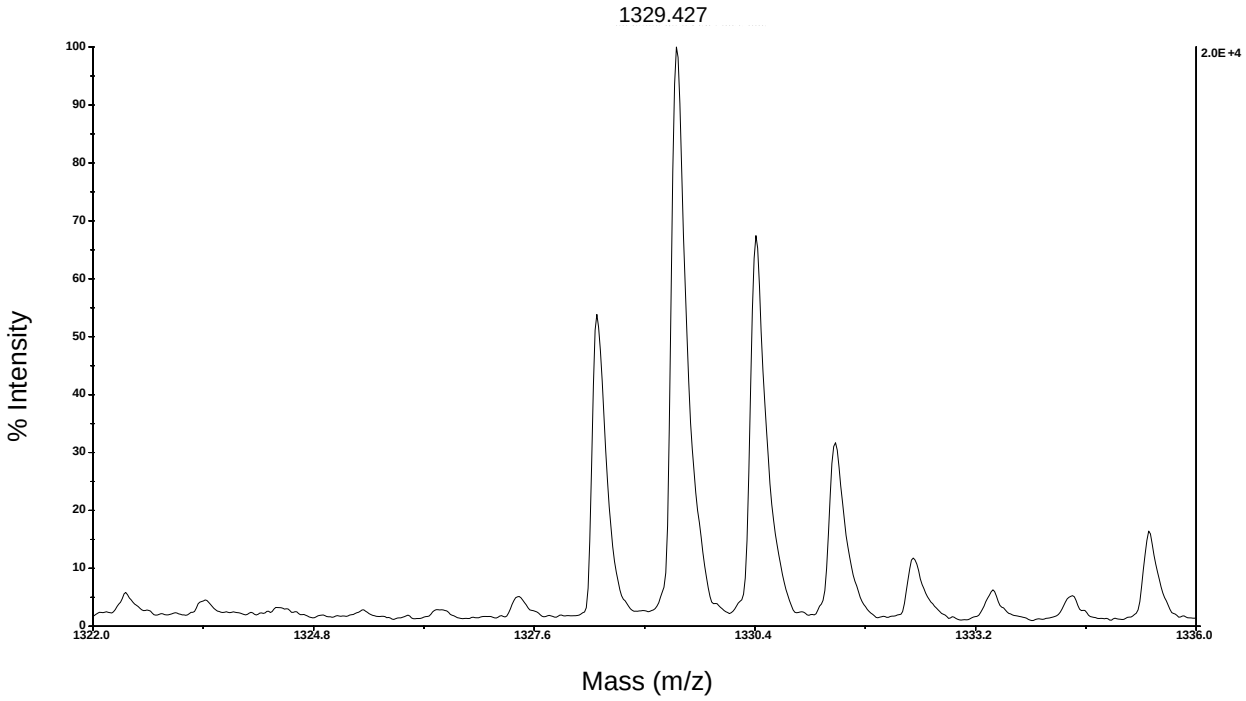

Figure 3.17: MALDI-TOF (alpha cyano-4-hydroxycinnaminic acid, mono-isotopic) of TAM-G-Ø-K(AB40)-amide **3.18**: m/z calc'd for $C_{78}H_{84}N_{13}O_{11}S$ $[M+H]^+$: 1329.456, m/z found: 1329.427.

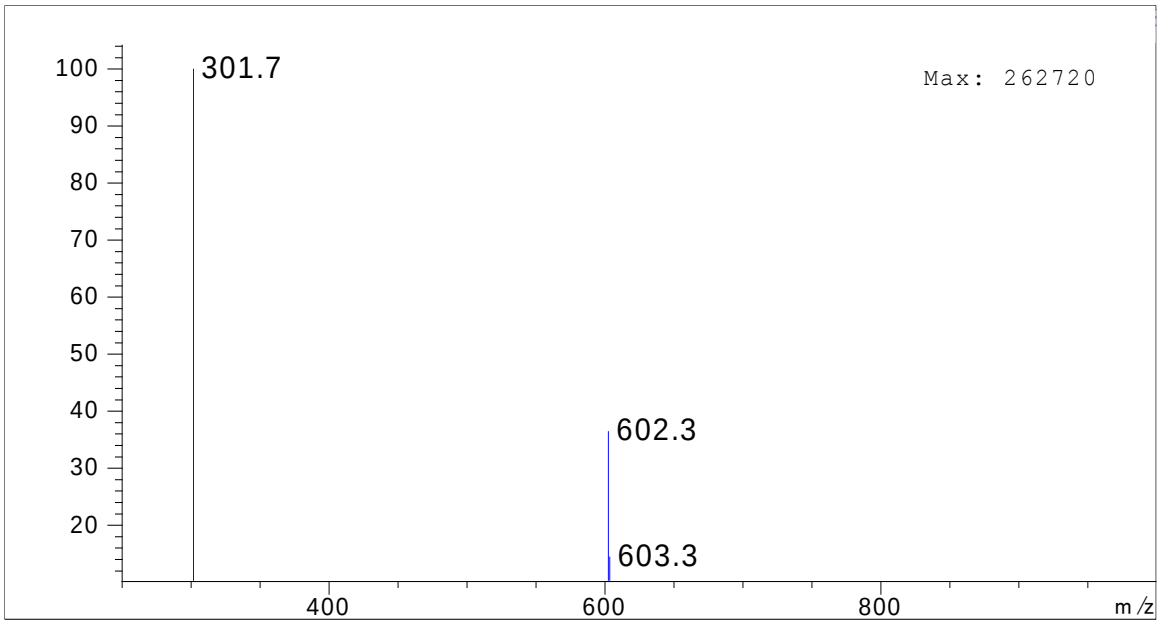

Figure 3.18: ESI(+)-QMS of DEAC-GRK(NH_2)-amide **3.23**: m/z calc'd for $C_{28}H_{44}N_9O_6^+$ $[M]^+$: 602.3, m/z found: 602.3.

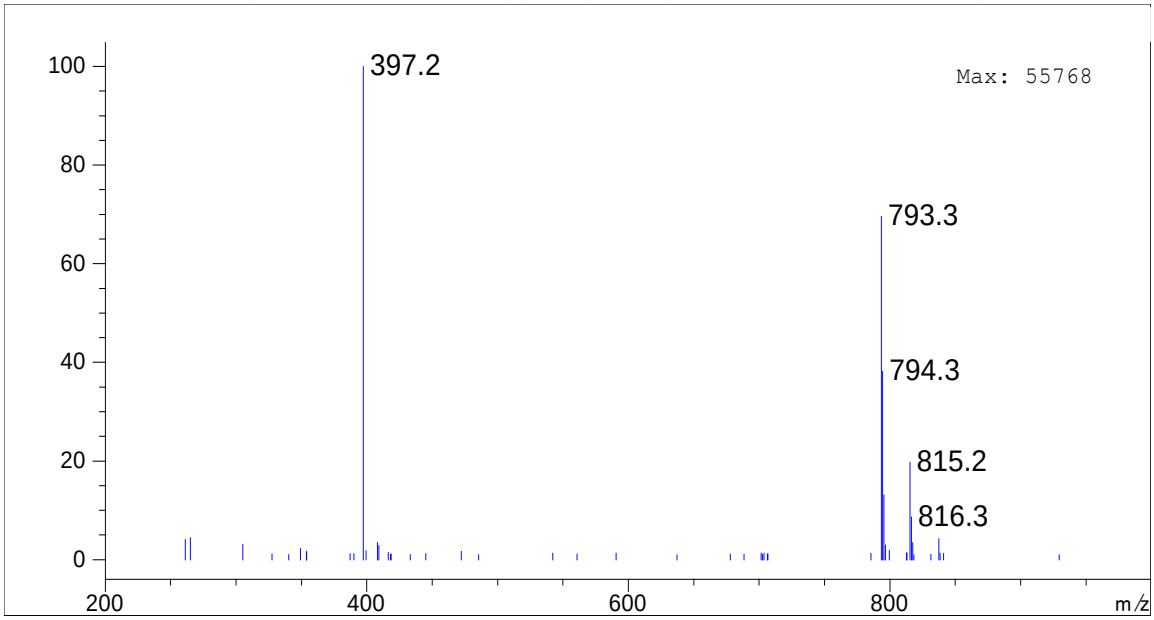

Figure 3.19: ESI(+)-QMS of NH_2-GRK(cAB40)-amide **3.24**: m/z calc'd for $C_{36}H_{45}N_{10}O_9S^+$ $[M]^+$: 793.3, m/z found: 793.3

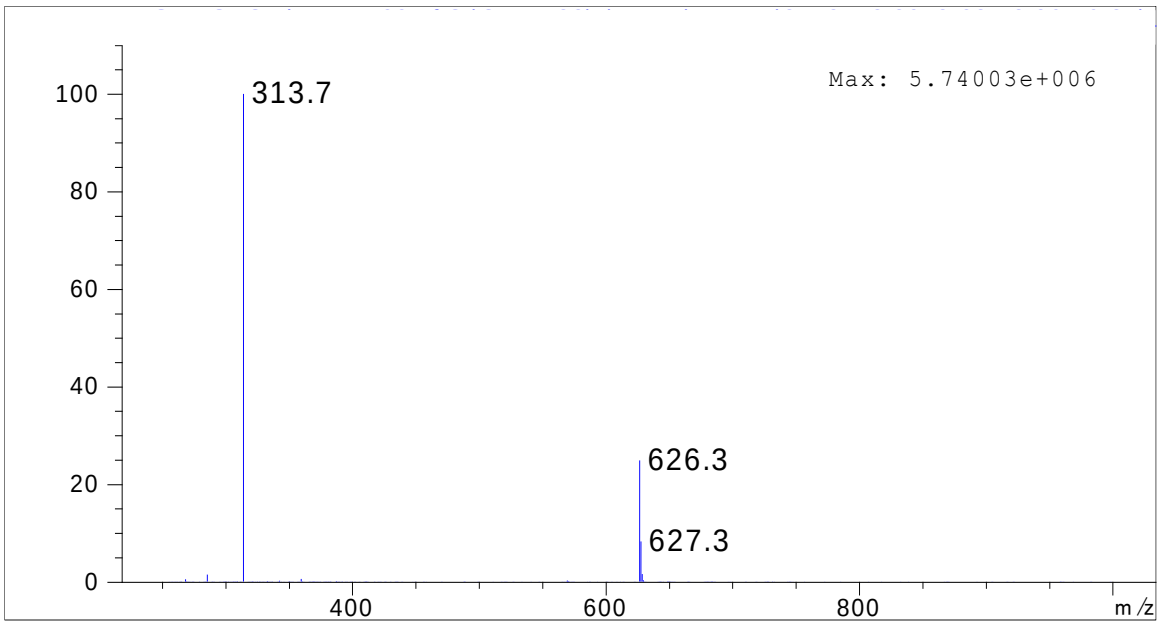

Figure 3.20: ESI(+)-QMS of Cou343-GRK(NH_2)-amide **3.25**: m/z calc'd for $C_{30}H_{44}N_9O_6^+$ $[M]^+$: 626.3, m/z found: 626.3.

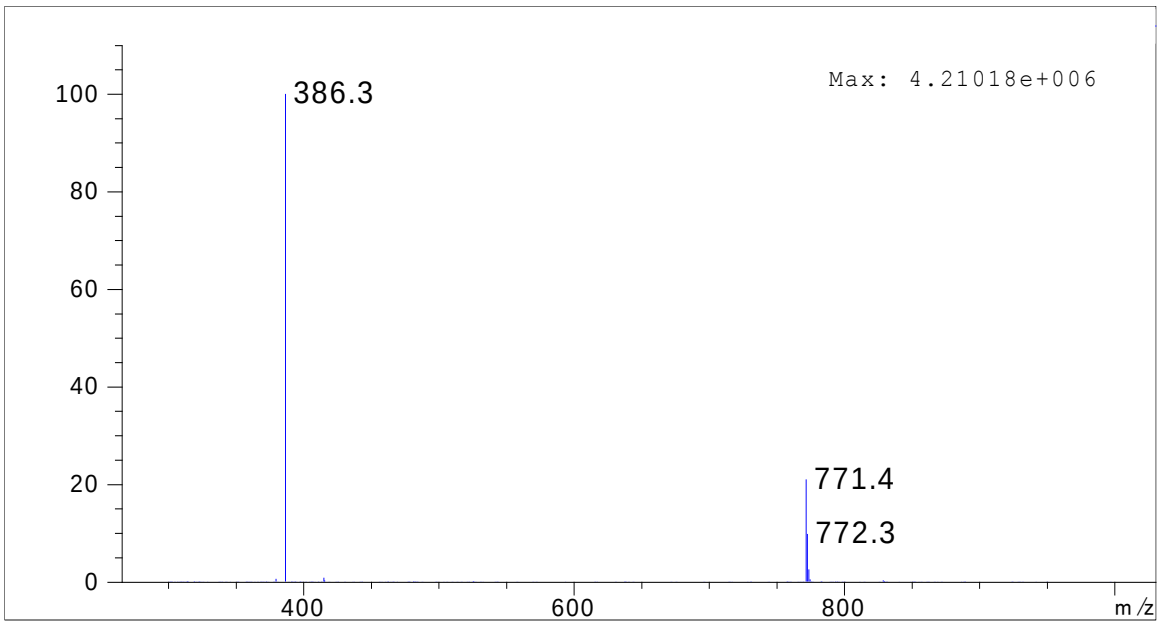

Figure 3.21: ESI(+)-QMS of TAM-GRK(NH_2)-amide **3.26**: m/z calc'd for $C_{39}H_{51}N_{10}O_7^+$ $[M]^+$: 771.4, m/z found: 771.4.

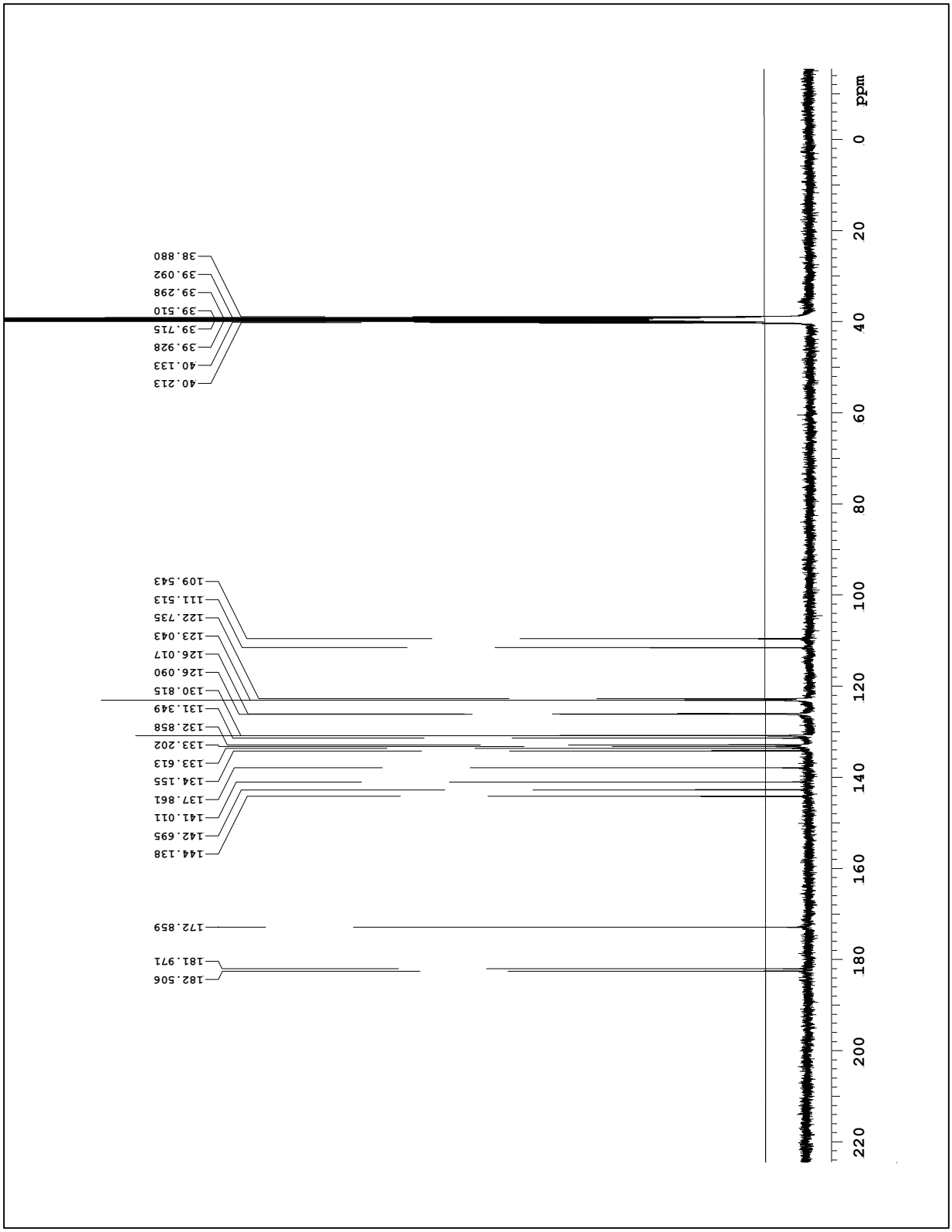

Figure 3.22: ^{13}C NMR (400 MHz, $CDCl_3$) of *c*AB40 **3.7**

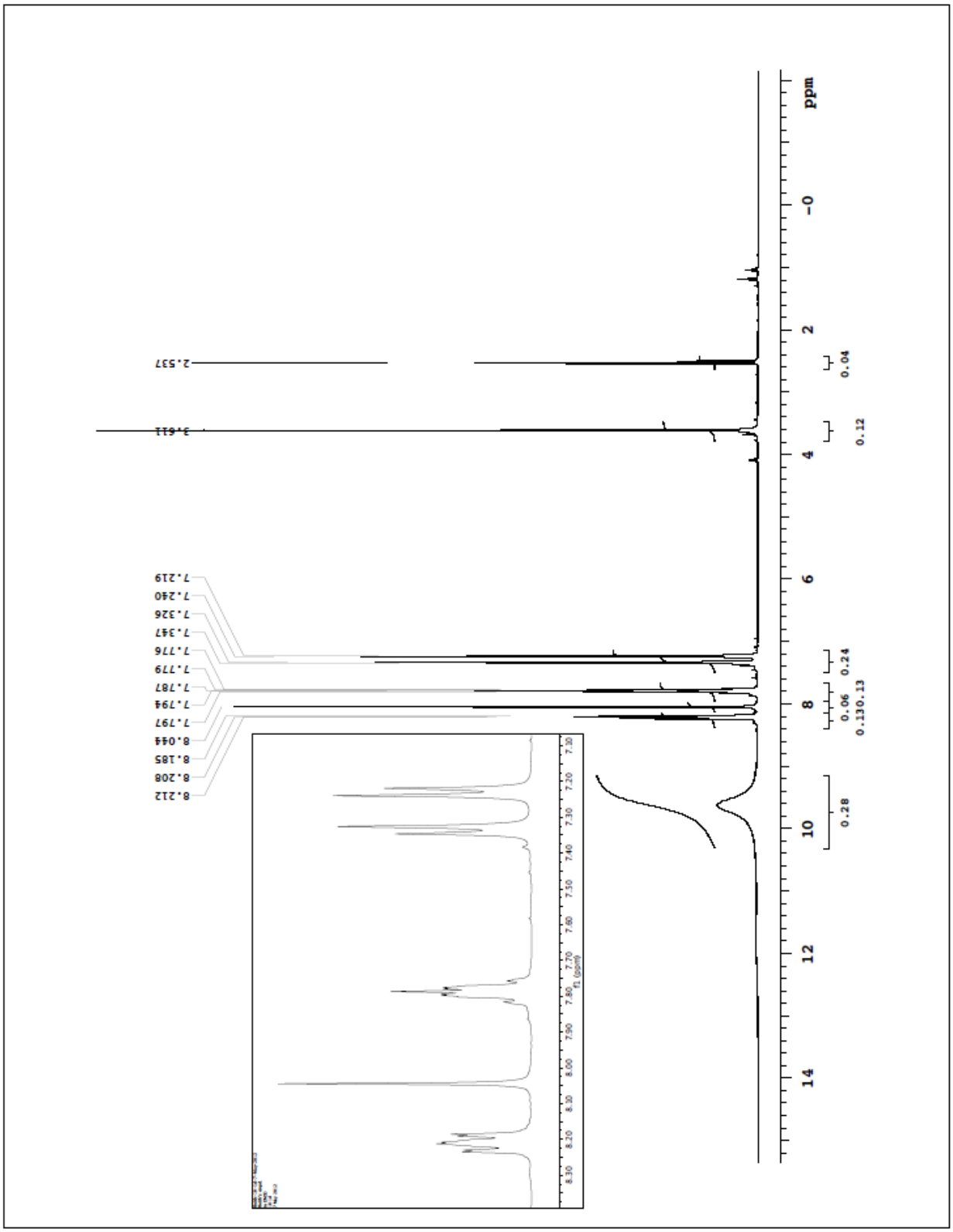

Figure 3.23: ^{1}H NMR (400 MHz, DMSO-d_6) of *c*AB40 **3.4**

Assessments of Purity

Assessments of purity of DECou-GRK(AB40)-amide 3.10

Figure 3.24: RP-HPLC injection of DECou-GRK(AB40)-amide **3.10** on a 250 mm x 4.6 mm, 5µm C18 column. The injection was monitored at 220 nm using a 0 - 97% linear acetonitrile to water gradient over 35 min. A small amount of DMSO was present in the sample, which eluted at 3 min.

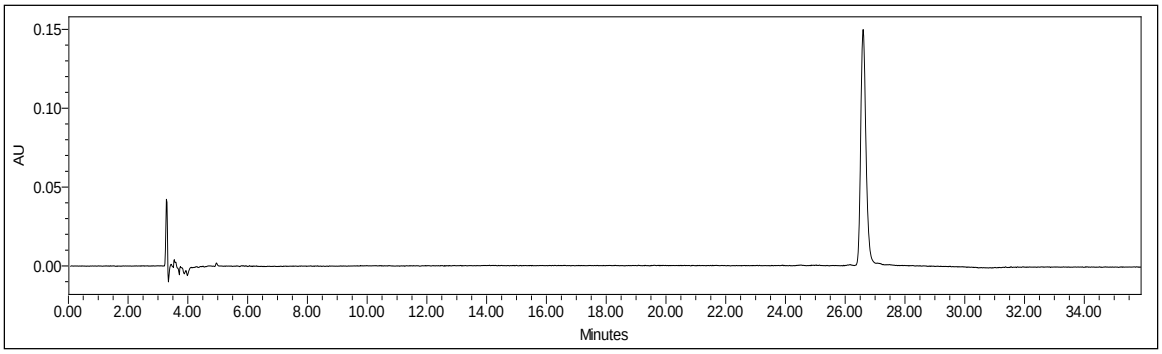

Figure 3.25: RP-HPLC injection of DECou-GRK(AB40)-amide **3.10** on a Restek Viva 50 mm x 2.1 mm, 5µm C4 column. The injection was monitored at 220 nm using a 0 – 97% linear acetonitrile to water gradient over 20 min.

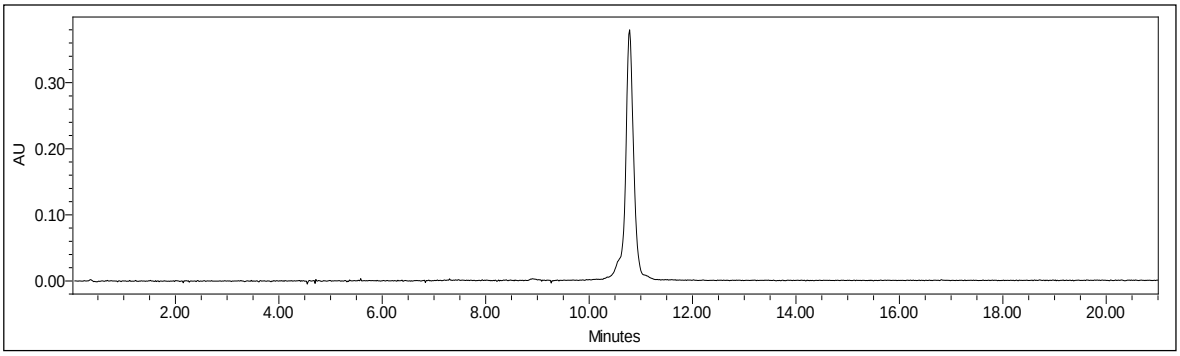

Assessments of purity of Cou343-GRK(AB40)-amide 3.11

Figure 3.26: RP-HPLC injection of Cou343-GRK(AB40)-amide **3.11** on an Alltech Apollo 250 mm x 4.6 mm, 5µm C18 column. The injection was monitored at 220 nm using a 0 - 97% linear acetonitrile to water gradient over 35 min.

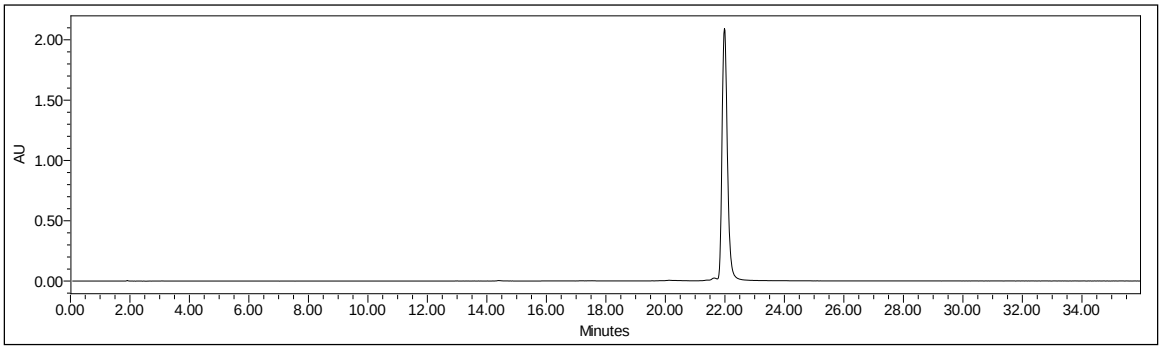

Figure 3.27: RP-HPLC injection of Cou343-GRK(AB40)-amide **3.11** on a Restek Viva 50mm x 2.1 mm, 5µm C4 column. The injection was monitored at 220 nm using a 0 – 97% linear acetonitrile to water gradient over 20 min.

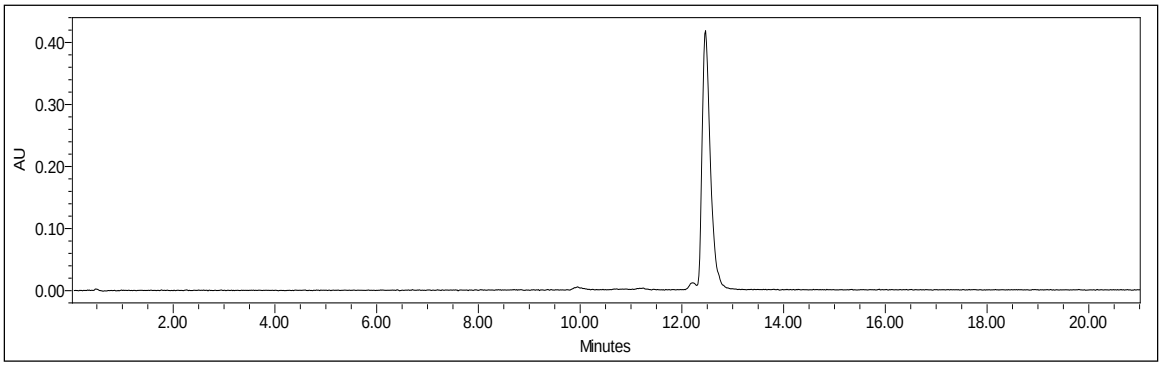

Assessments of purity of FAM-GRK(AB40)-amide 3.12

Figure 3.28: RP-HPLC injection of FAM-GRK(AB40)-amide **3.12** on an Alltech Apollo 250 mm x 4.6 mm, 5µm C18 column. The injection was monitored at 220 nm using a 0 - 97% linear acetonitrile to water gradient over 35 min. DMSO was present in the sample, which eluted at 3 min.

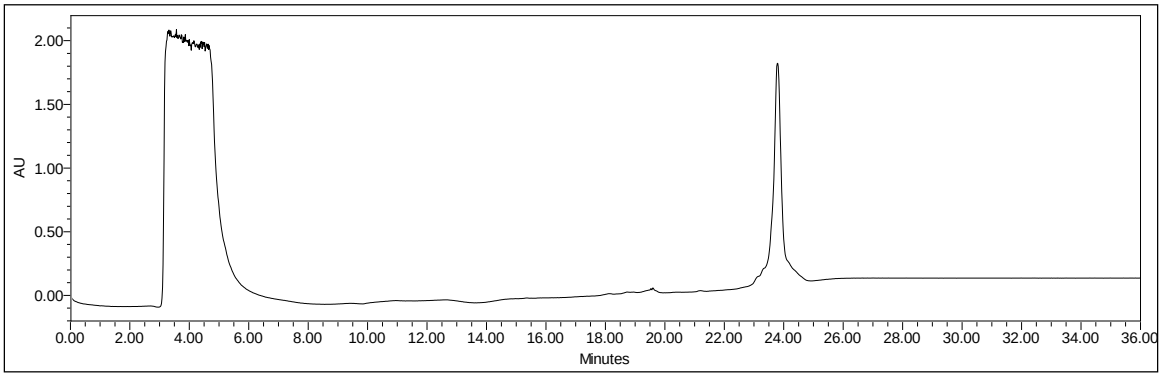

Figure 3.29: RP-HPLC injection of FAM-GRK(AB40)-amide **3.12** on a Restek Viva 50 mm x 2.1 mm, 5µm C4 column. The injection was monitored at 220 nm using a 0 – 97% linear acetonitrile to water gradient over 20 min.

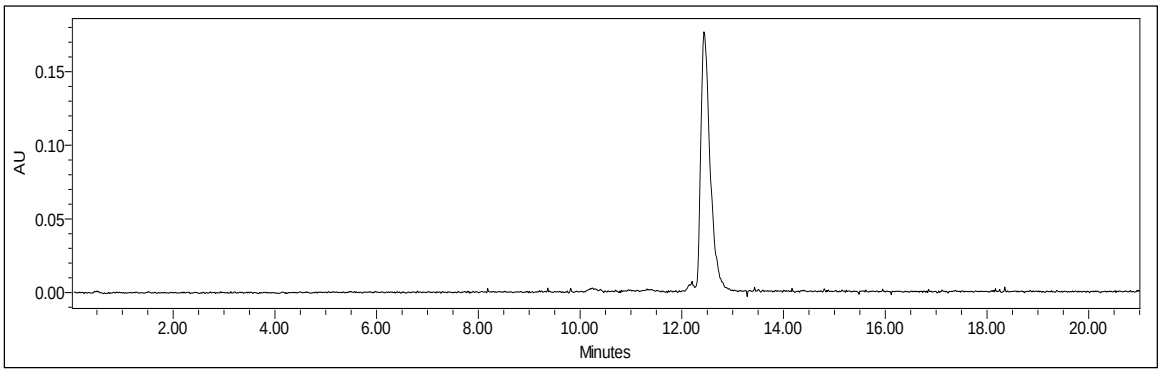

Assessments of purity of TAM-GRK(AB40)-amide 3.13

Figure 3.30: RP-HPLC injection of TAM-GRK(AB40)-amide **3.13** on an Alltech Apollo 250 x 4.6 mm, 5µm C18 column. The injection was monitored at 220 nm using a 0 - 97% linear acetonitrile to water gradient over 35 min.

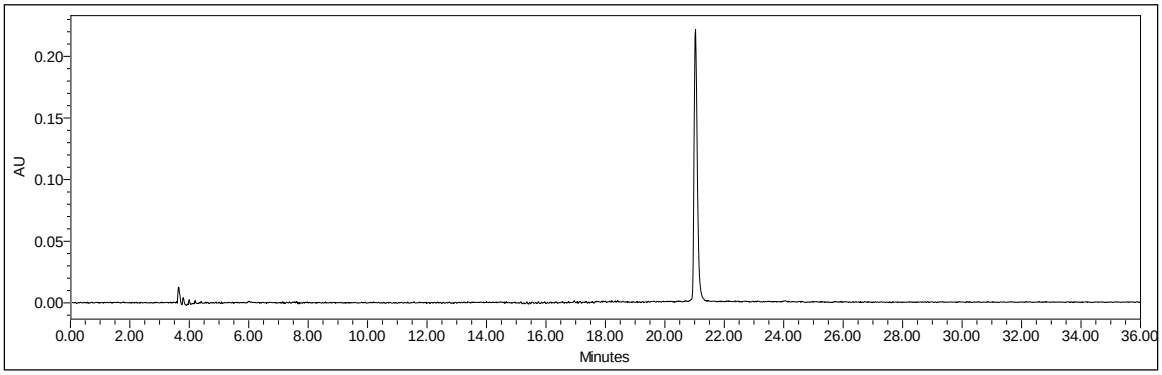

Figure 3.31: RP-HPLC injection of TAM-GRK(AB40)-amide **3.13** on a Restek Viva 50 x 2.1 mm, 5µm C4 column. The injection was monitored at 220 nm using a 0 – 97% linear acetonitrile to water gradient over 30 min.

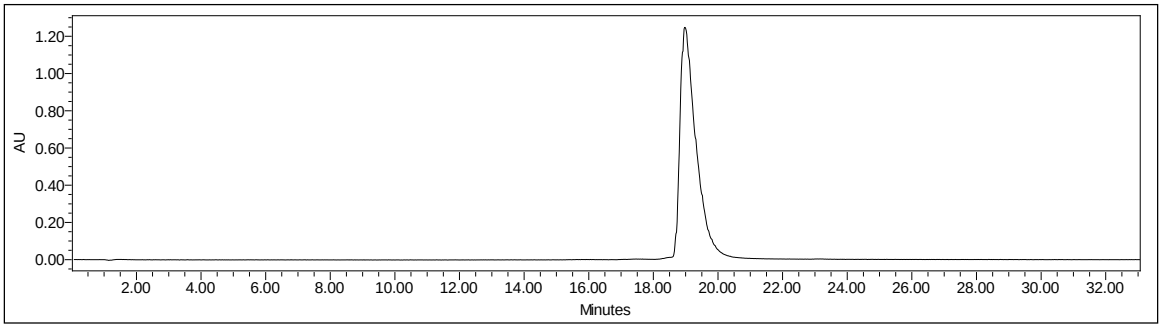

Assessments of purity of atto610-GRK(AB40)-amide 3.14

Figure 3.32: RP-HPLC injection of atto610-GRK(AB40)-amide **3.14** on an Alltech Apollo 250 x 4.6 mm, 5µm C18 column. The injection was monitored at 220 nm using a 0 - 97% linear acetonitrile to water gradient over 35 min.

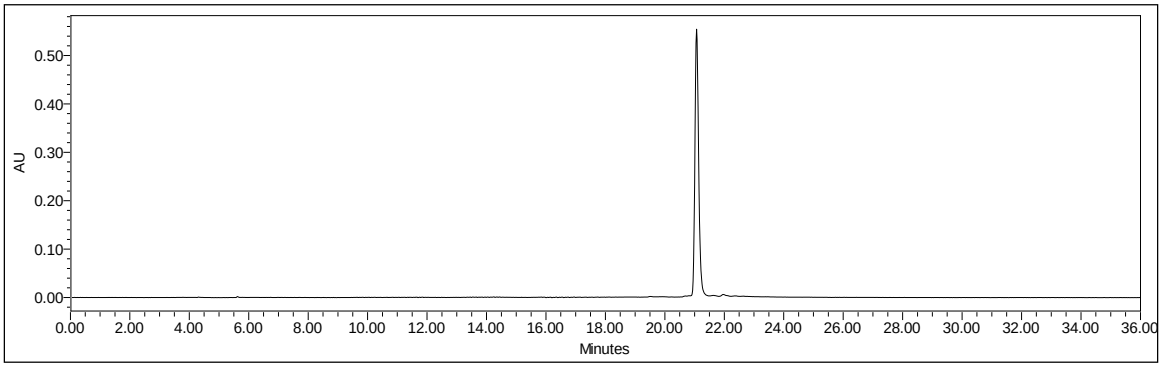

Figure 3.33: RP-HPLC injection of atto610-GRK(AB40)-amide **3.14** on a Restek Viva 50 mm x 2.1 mm, 5µm C4 column. The injection was monitored at 220 nm using a 0 – 97% linear acetonitrile to water gradient over 30 min.

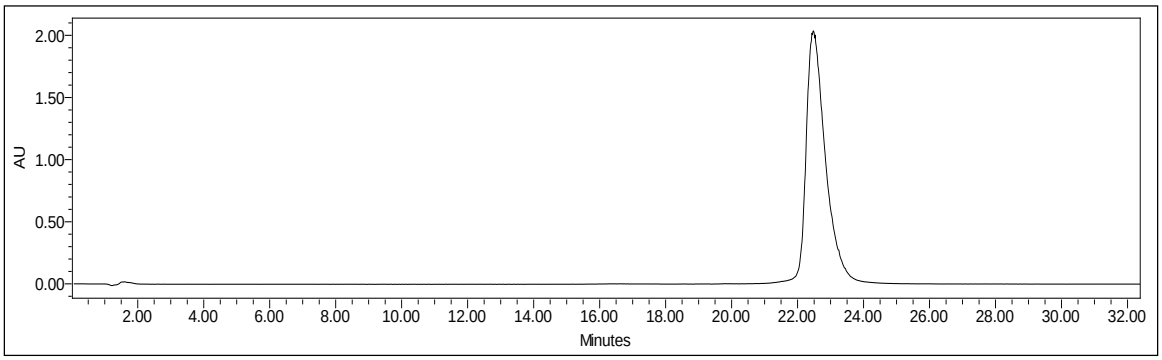

Assessments of purity of atto700-GRK(AB40)-amide 3.15

Figure 3.34: RP-HPLC injection of atto700-GRK(AB40)-amide **3.15** on an Alltech Apollo 250 mm x 4.6 mm, 5µm C18 column. The injection was monitored at 220 nm using a 0 - 97% linear acetonitrile to water gradient over 35 min.

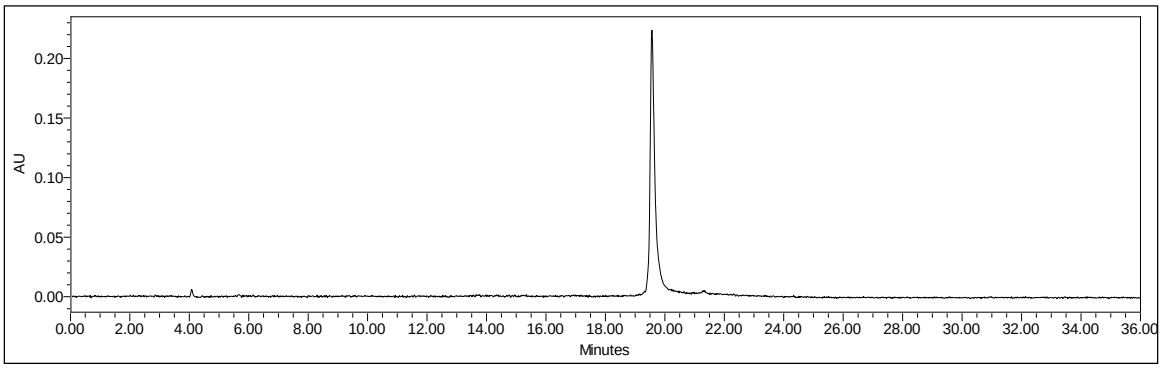

Figure 3.35: RP-HPLC injection of atto700-GRK(AB40)-amide **3.15** on a Restek Viva 50 mm x 2.1 mm, 5µm C4 column. The injection was monitored at 220 nm using a 0 – 97% linear acetonitrile to water gradient over 30 min.

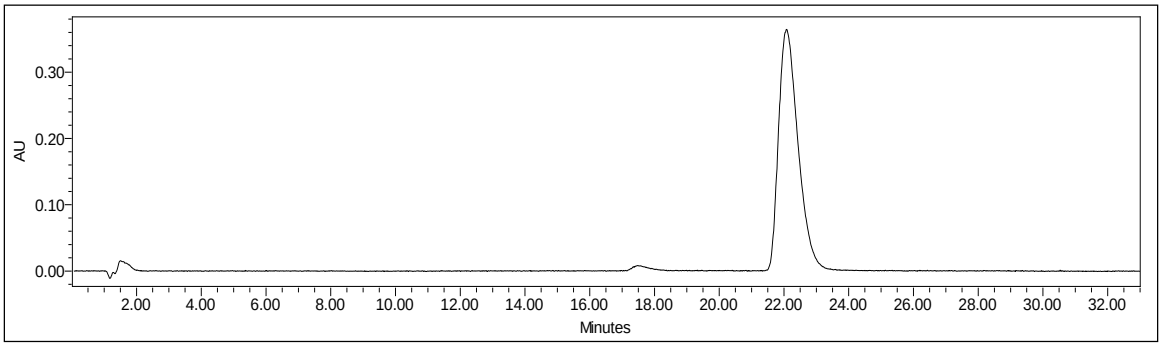

Assessments of purity of TAM-GRK(BHQ-2)-amide 3.16

Figure 3.36: RP-HPLC injection of TAM-GRK(BHQ-2)-amide **3.16** on an Alltech Apollo 250 mm x 22 mm, 5µm C18 column. The injection was monitored at 220 nm using a 0 - 97% linear acetonitrile to water gradient over 90 min. DMSO was present in the sample, which eluted at 7 min.

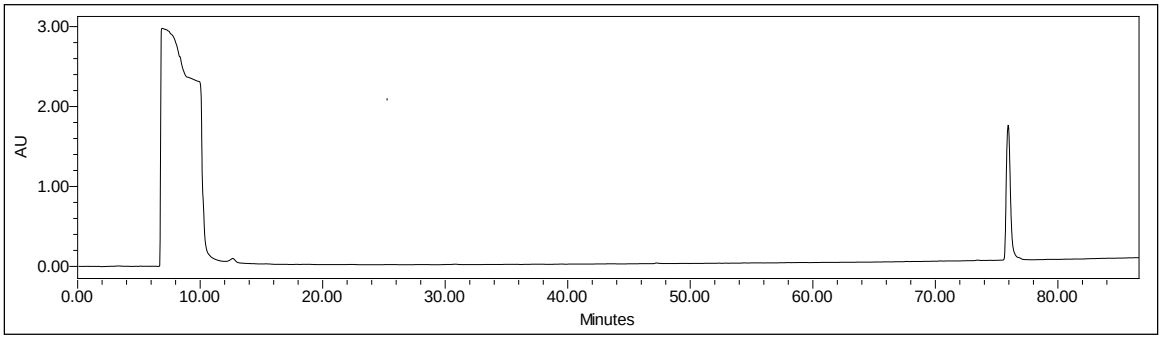

Figure 3.37: RP-HPLC injection of TAM-GRK(BHQ-2)-amide **3.16** on a Restek Viva 50 mm x 2.1 mm, 5 µm C4 column. The injection was monitored at 220 nm using a 0 – 97% linear acetonitrile to water gradient over 30 min.

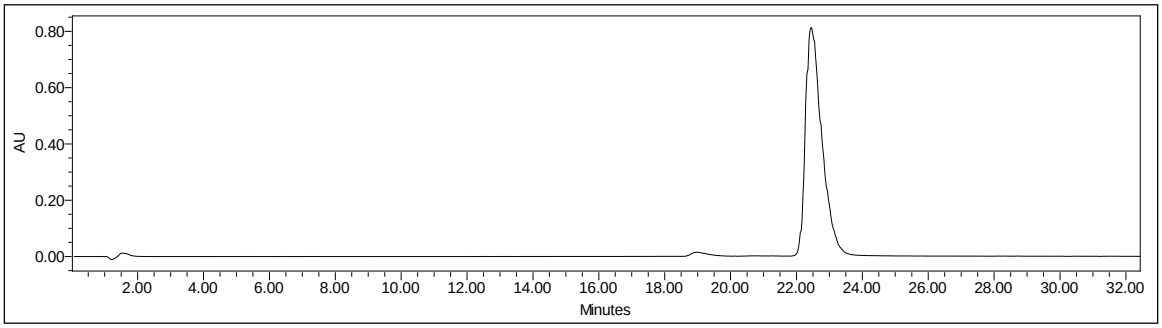

Assessments of purity of TAM-GRK(QSY7)-amide 3.17

Figure 3.38: RP-HPLC injection of TAM-GRK(QSY7)-amide **3.17** on an Alltech Apollo 250 mm x 22 mm, 5 µm C18 column. The injection was monitored at 220 nm using a 0 - 97% linear acetonitrile to water gradient over 90 min. DMSO was present in the sample, which eluted at 7 min.

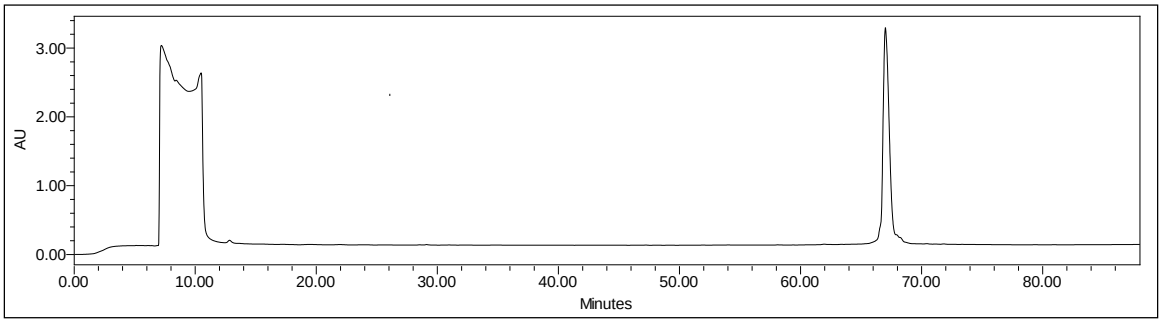

Figure 3.39: RP-HPLC injection of TAM-GRK(QSY7)-amide **3.17** on a Restek Viva 50 mm x 2.1 mm, 5 µm C4 column. The injection was monitored at 220 nm using a 0 – 97% linear acetonitrile to water gradient over 30 min.

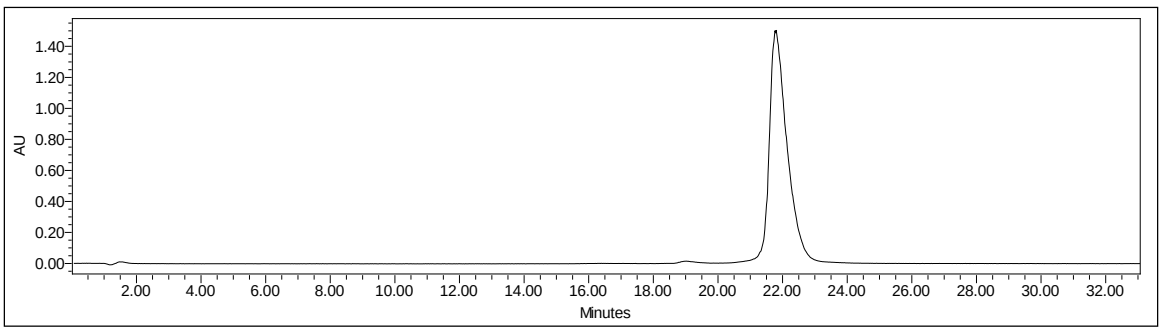

Assessments of purity of TAM-G-PL-K(AB40)-amide 3.18

Figure 3.40: RP-HPLC injection of TAM-G-PL-K(AB40)-amide **3.18** on an Alltech Apollo 250 mm x 4.6 mm, 5µm C18 column. The injection was monitored at 220 nm using a 0 - 97% linear acetonitrile to water gradient over 35 min.

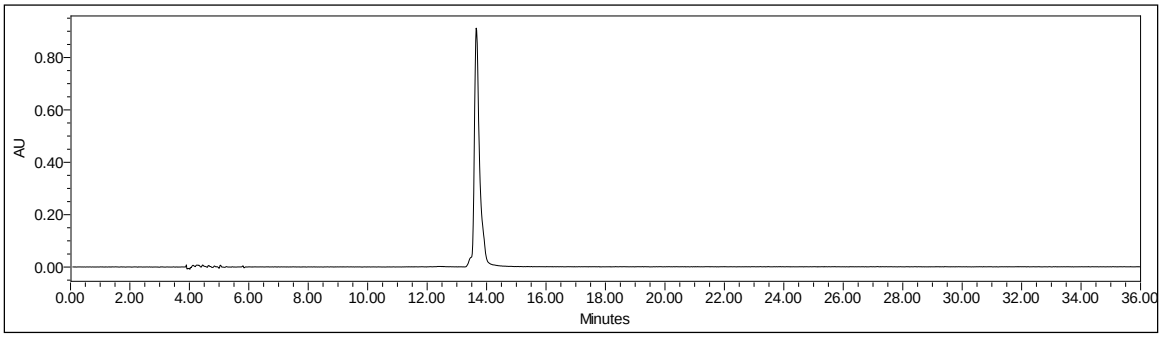

Figure 3.41: RP-HPLC injection of TAM-G-PL-K(AB40)-amide **3.18** on a Restek Viva 50 mm x 2.1 mm, 5µm C4 column. The injection was monitored at 220 nm using a 0 – 97% linear acetonitrile to water gradient over 20 min.

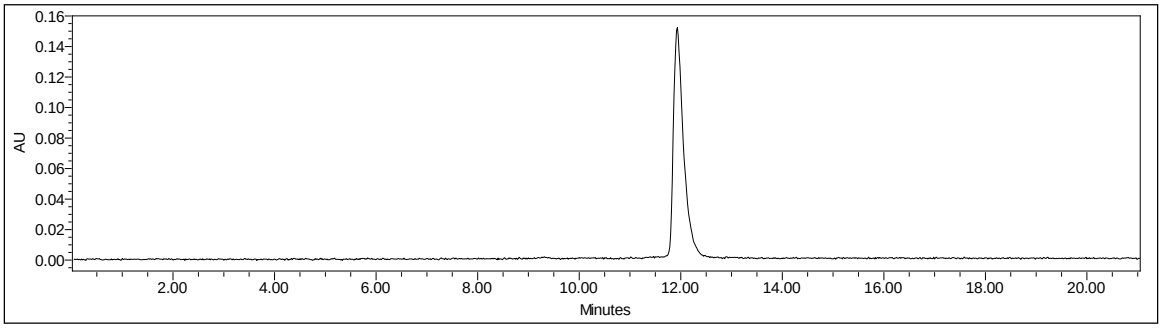

Assessments of purity of DEAC-GRK(NH_2)-amide 3.23

Figure 3.42: RP-HPLC injection of DEAC-GRK(NH_2)-amide **3.23** on an Alltech Apollo 50 mm x 2.1 mm, 5µm C18 column. The injection was monitored at 220 nm using a 0 - 97% linear acetonitrile to water gradient over 12 min.

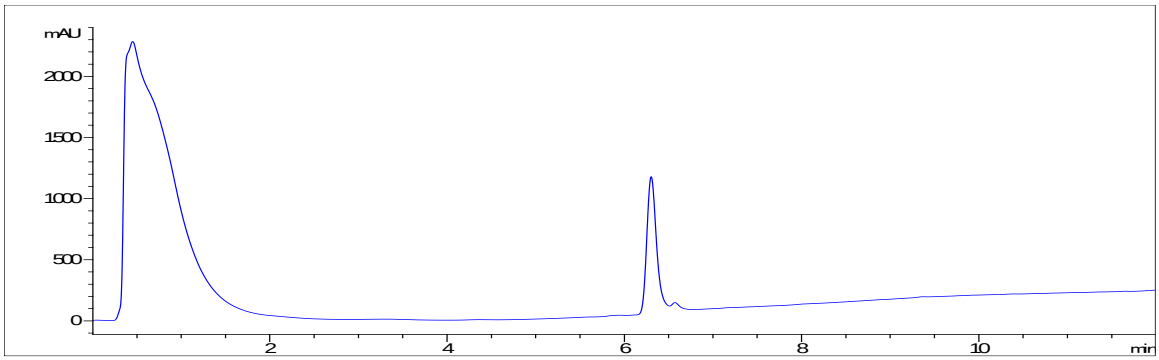

Figure 3.43: RP-HPLC injection of TAM-G-PL-K(AB40)-amide **3.23** on a Restek Viva 50 mm x 2.1 mm, 5µm C4 column. The injection was monitored at 220 nm using a 0 – 97% linear acetonitrile to water gradient over 12 min.

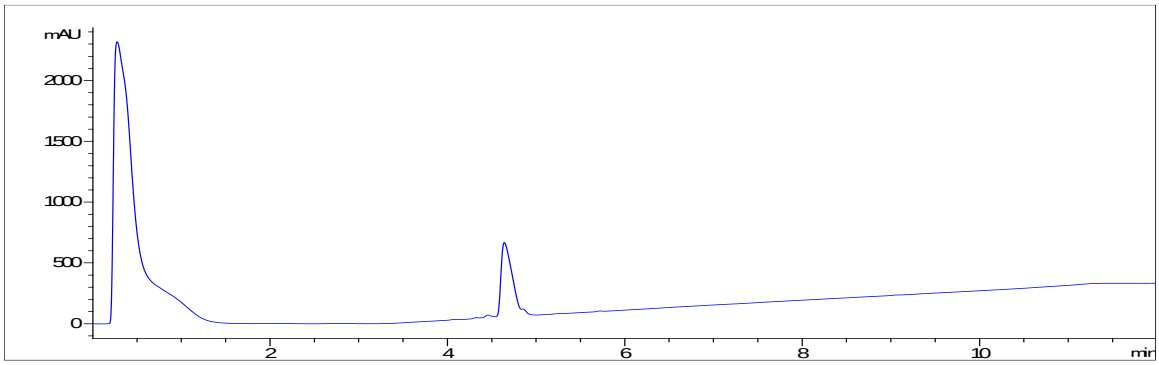

Assessments of purity of NH_2-GRK(cAB40)-amide 3.24

Figure 3.44: RP-HPLC injection of NH_2-GRK(cAB40)-amide **3.24** on an Alltech Apollo 50 mm x 2.1 mm, 5µm C18 column. The injection was monitored at 220 nm using a 0 - 97% linear acetonitrile to water gradient over 12 min.

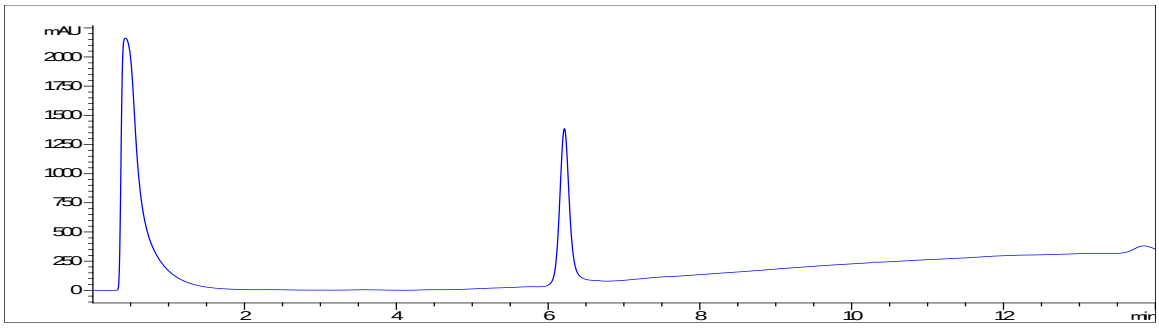

Figure 3.45: RP-HPLC injection of NH_2-GRK(cAB40)-amide **3.24** on a Restek Viva 50 mm x 2.1 mm, 5µm C4 column. The injection was monitored at 220 nm using a 0 – 97% linear acetonitrile to water gradient over 12 min.

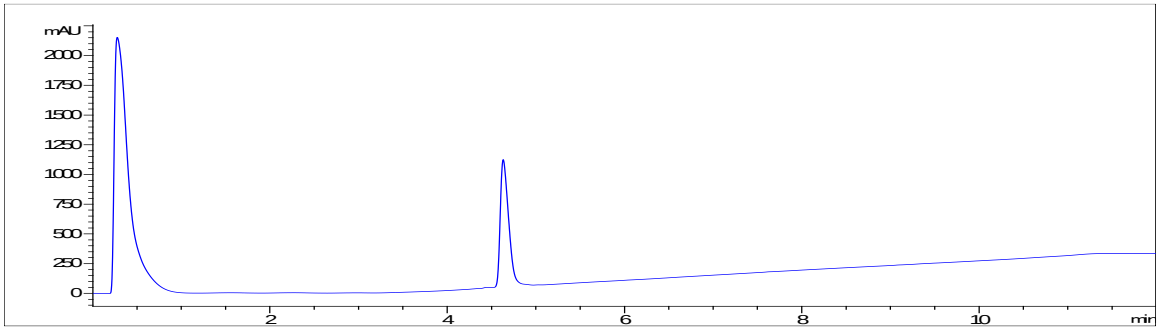

Assessments of purity of Cou343-GRK(NH_2)-amide 3.25

Figure 3.46: RP-HPLC injection of Cou343-GRK(NH_2)-amide **3.25** on an Alltech Apollo 50 mm x 2.1 mm, 5µm C18 column. The injection was monitored at 220 nm using a 0 - 97% linear acetonitrile to water gradient over 12 min.

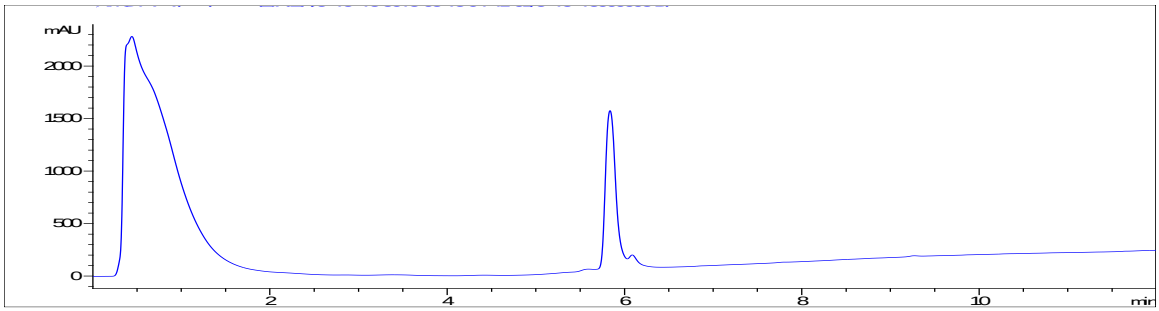

Figure 3.47: RP-HPLC injection of Cou343-GRK(NH_2)-amide **3.25** on a Restek Viva 50 mm x 2.1 mm, 5µm C4 column. The injection was monitored at 220 nm using a 0 – 97% linear acetonitrile to water gradient over 12 min.

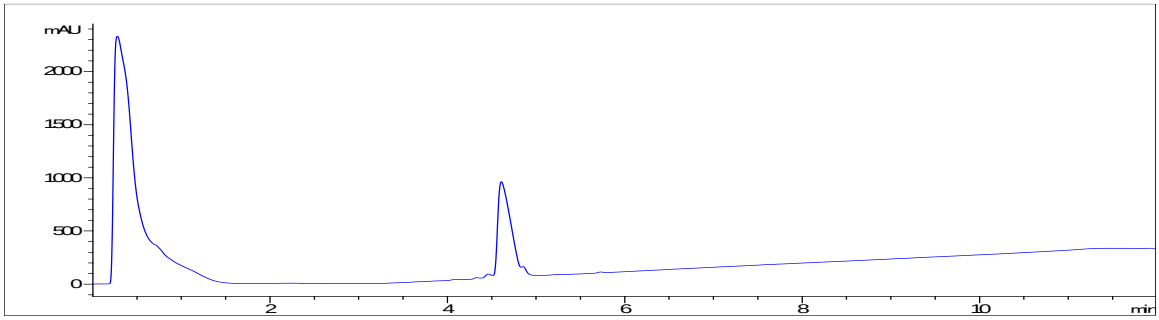

Assessments of purity of TAM-GRK(NH_2)-amide 3.26

Figure 3.48: RP-HPLC injection of TAM-GRK(NH_2)-amide **3.26** on an Alltech Apollo 50 mm x 2.1 mm, 5µm C18 column. The injection was monitored at 220 nm using a 0 - 97% linear acetonitrile to water gradient over 12 min.

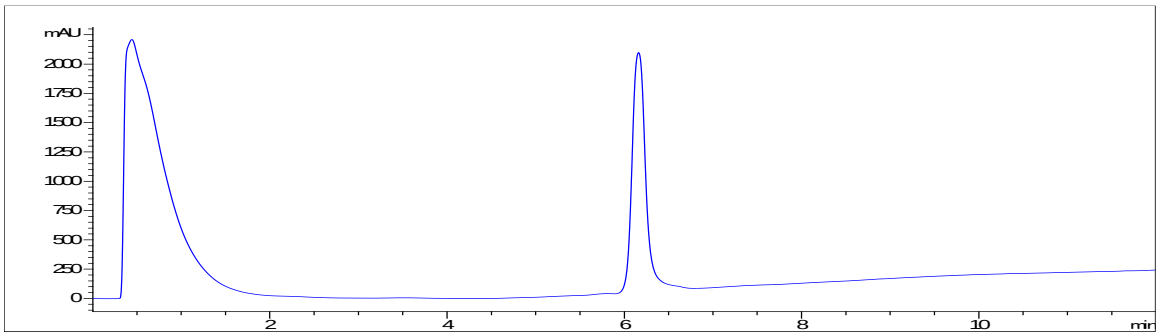

Figure 3.49: RP-HPLC injection of TAM-GRK(NH_2)-amide **3.27** on a Restek Viva 50 mm x 2.1 mm, 5µm C4 column. The injection was monitored at 220 nm using a 0 – 97% linear acetonitrile to water gradient over 12 min.

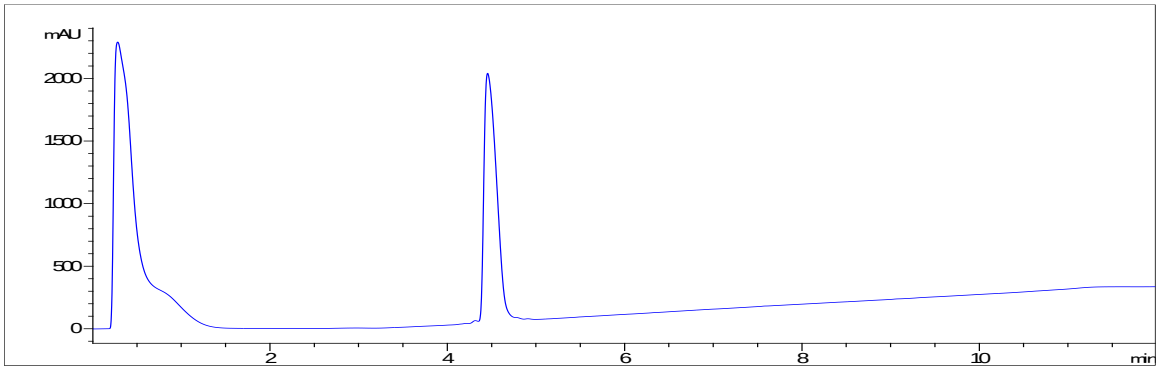

CHAPTER 4

CONSTRUCTION OF A NANOPARTICLE-BASED SENSOR FOR cAMP-DEPENDENT PROTEIN KINASE ACTIVITY

(Reproduced with permission from unpublished results from Jernigan, F. E., Oien, N., Priestman, M., Sharma, V., Agnes, R., and Lawrence, D. S.)

INTRODUCTION

Protein kinases play a large role in the regulation of cellular processes via phosphorylation including mitosis,[1] proliferation,[2] survival,[3] death,[4] and metabolism.[5] Many of these processes are regulated in a spatial fashion with precise control required for many cellular functions. For examples, the cyclic-AMP dependent protein kinase (PKA) is intimately related in the regulation of cell death and survival near the mitochondria.[6] For the study of PKA's role in apoptosis, we have previously developed a kinase

[1] (1) Lapenna, S.; Giordano, A. *Nature reviews. Drug discovery* **2009**, *8*, 547–66. (2) Strebhardt, K. *Nature reviews. Drug discovery* **2010**, *9*, 643–60.

[2] Romeo, Y.; Zhang, X.; Roux, P. P. *The Biochemical journal* **2012**, *441*, 553–69.

[3] Horbinski, C.; Chu, C. T. *Free radical biology & medicine* **2005**, *38*, 2–11.

[4] Orrenius, S. *Toxicology letters* **2004**, *149*, 19–23.

[5] Michel, J. J. C.; Scott, J. D. *Annual review of pharmacology and toxicology* **2002**, *42*, 235–57.

[6] See discussion and references in Chapter 1: Introduction.

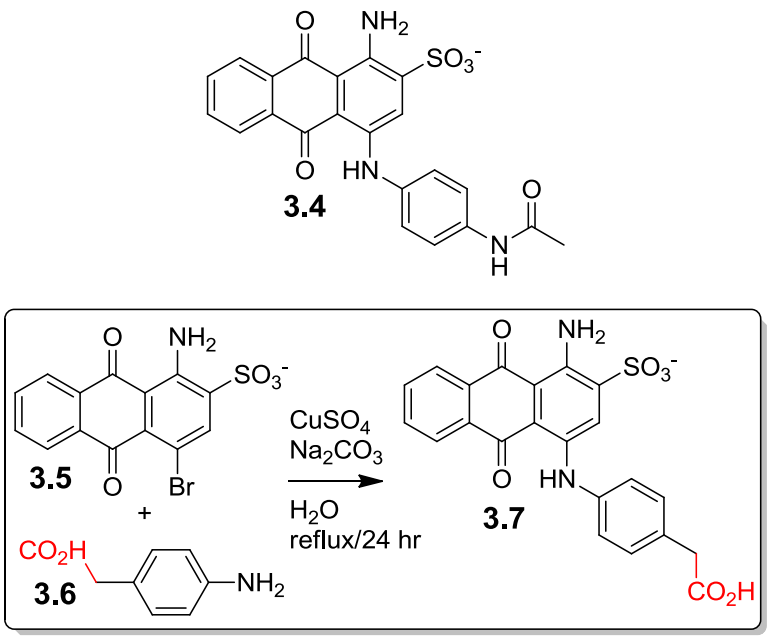

Scheme 3.2 Reproduced from Chapter 3 of this work. Structure of Acid Blue 40 (AB40) **3.4** and synthesis of carboxy Acid Blue 40 (cAB40) **3.7**.

sensor which includes an extraordinary dynamic range.[7] This sensor was used to elucidate the suborganellular distribution of mitochondrial PKA activity in fractionated mitochondria. But the system suffers from three major drawbacks that limit its use intracellularly: (1) the photophysical properties of the fluorophores used are not ideal for microscopy, (2) the reliance on multiple chemical components (i.e. binding a 14-3-3τ domain) to produce a fluorescence enhancement, and (3) delivery of the biosensor to cytoplasm and/or the surface of the mitochondria. Modifying the photophysical properties of the sensor should be as simple as changing the fluorophore and rescreening the resulting peptide against a series of dyes to find a sensor that displays a large fluorescent enhancement upon phosphorylation. However, removing the 14-3-3τ dependence is a larger problem. One way to solve the problem may be covalently attaching 14-3-3τ to a fluorescently labeled PKA consensus sequence, along with the attachment of a quencher. The

[7] Agnes, R. S.; Jernigan, F.; Shell, J. R.; Sharma, V.; Lawrence, D. S. *Journal of the American Chemical Society* **2010**, *132*, 6075–80.

quencher Acid Blue 40 has been modified to include a carboxylic acid capable of covalent attachment (Scheme 3.2). Another method would include screening a variety of quenchers for 14-3-3τ-independent behavior. This is the more attractive solution, since the chemistry of 14-3-3τ-independent sensor would be more straightforward. Yet even if the biosensor synthesis is straightforward, delivery to the cytoplasm also remains a major issue. Luckily, much work has been described in this area. Cytoplasmic delivery of biomolecules has been accomplished using the HIV-1 TAT sequence,[8] mitochondrial-penetrating peptides,[9] lipid anchors[10] and nanoparticles.[11] Using one of these four methods, cytoplasmic delivery of our unimolecular PKA biosensor should be possible. Following this direction, we have made significant progress towards the construction of a unimolecular PKA sensor for intracellular use.

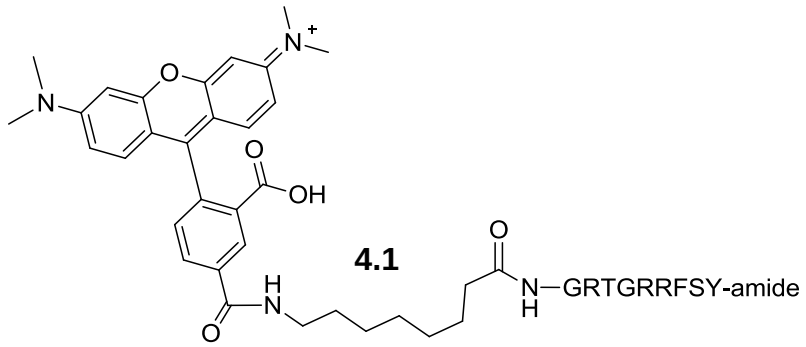

Scheme 4.1 Structure of TAMRA labeled PKA substrate. Peptide contains a PKA consensus sequence with a 5'-TAMRA fluorophore attached to the N-terminus via an aminooctanoic acid linker.

[8] (1) Fröbel, J.; Rose, P.; Müller, M. *Philosophical transactions of the Royal Society of London. Series B, Biological sciences* **2012**, *367*, 1029–46. (2) Sawant, R.; Torchilin, V. *Molecular bioSystems* **2010**, *6*, 628–40.

[9] (1) Kelley, S. O.; Stewart, K. M.; Mourtada, R. *Pharmaceutical research* **2011**, *28*, 2808–19. (2) Pereira, M. P.; Kelley, S. O. *Journal of the American Chemical Society* **2011**, *133*, 3260–3. (3) Horton, K. L.; Pereira, M. P.; Stewart, K. M.; Fonseca, S. B.; Kelley, S. O. *Chembiochem : a European journal of chemical biology* **2012**, *13*, 476–85.

[10] Rajendran, L.; Udayar, V.; Goodger, Z. V. *Trends in pharmacological sciences* **2012**, *33*, 215–22.

[11] (1) Elsabahy, M.; Wooley, K. L. *Chemical Society reviews* **2012**, *41*, 2545–61. (2) Kamaly, N.; Xiao, Z.; Valencia, P. M.; Radovic-Moreno, A. F.; Farokhzad, O. C. *Chemical Society reviews* **2012**, *41*, 2971–3010.

RESULTS AND DISCUSSION

The most important steps toward intracellular use of the PKA biosensor relies on: (1) removing the dependence on 14-3-3τ to produce a fluorescent enhancement and (2) improving the photophysical properties of the fluorophore. We chose the fluorophore 5'-TAMRA (TAM) since it is red-shifted and relatively bright when compared with fluorophores of the previous system coumarin-based "deep quench" system (see Chapter 2). A TAM labeled substrate was synthesized using solid phase peptide synthesis, including a PKA consensus sequence, an

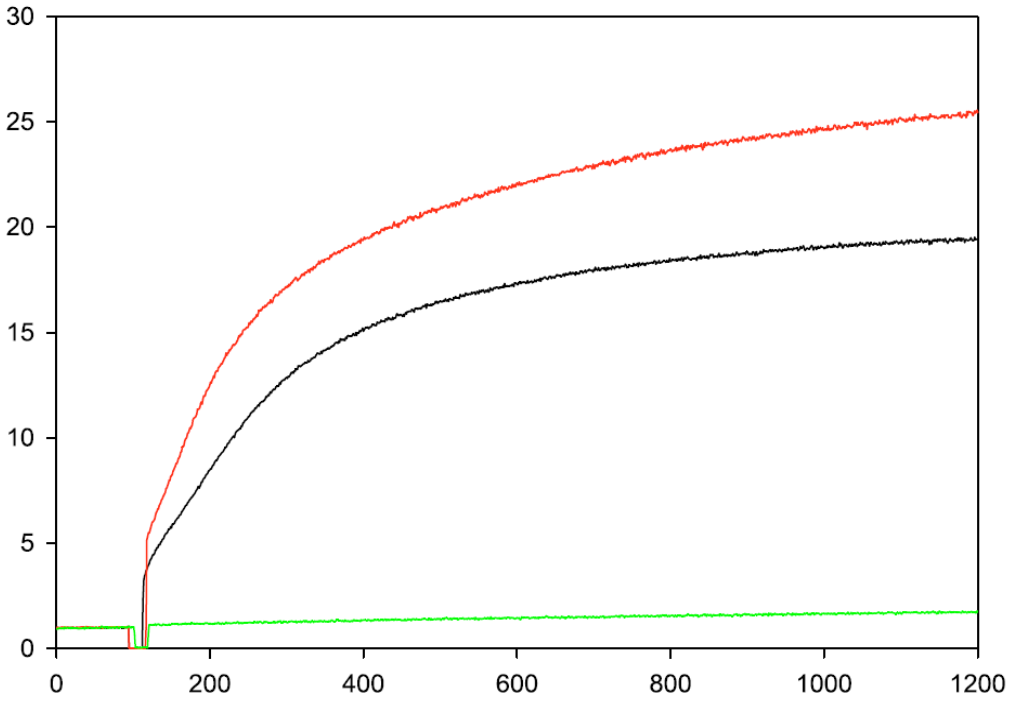

Figure 4.1 PKA sensor fold enhancements using the quencher Acid Blue 40. Assay in the presence of 150 mM KCl buffer containing Tris pH 7.4 Buffer (Red), 1 mM KCl buffer containing Tris pH 7.4 Buffer (Black), 150 mM KCl buffer containing Tris pH 7.4 Buffer in the presence of H-89 (100 μM).

aminooctanoic acid linker, and TAM attached to the N-terminus (Scheme 4.1). A C-terminal proline, which is required for binding to the 14-3-3τ domain was not included. This peptide was screened in the presence of 48 negatively charged dyes (Table 2.3) for 14-3-3τ independent behavior. Of these 48 dyes, the quenchers Acid Blue 40 and Aniline Blue yielded the largest fluorescent enhancement upon phosphorylation (respectively, 12-fold and 14-fold). Thorough further development of the assay, we were able to increase the fold enhancement to 25-fold (Figure 4.1). This was accomplished by optimization of the $MgCl_2$ concentration (changed from 5 mM to 1 mM, which is more physiologically relevant) and increased purification of the substrate peptide. We observed slowly decreasing fold enhancements as the peptide aged. However, purification via reverse-phase HPLC would restore the fold enhancement back to the maximum observed immediately after the synthesis of the peptide.

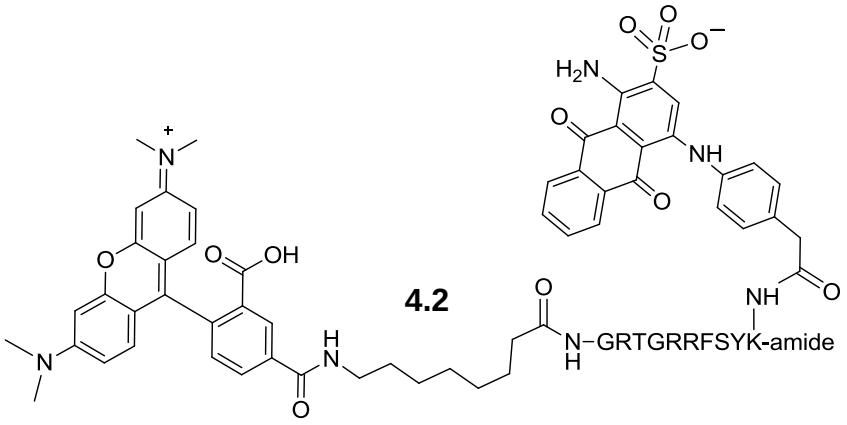

Scheme 4.2 Structure of PKA biosensor peptide including cAB40. The PKA consensus sequence was modified to include an N-terminal aminooctanoic acid covalently attached to the fluorophore TAMRA and C-terminal lysine covalently attached to the fluorescent Quencher AB40.

We then attempted to attach the dye to the peptide directly, anticipating that phosphorylation of the peptide would still produce a fluorescent enhancement. Since the modification of Acid Blue 40 to an analog capable of covalent attachment had been previously

accomplished (see chapter 3 of this work), a peptide containing the TAMRA and cAB40 was synthesized (Scheme 4.3). However, when this peptide was phosphorylated, no fluorescent enhancement was observed. Although this result was not completely unexpected, it is unsurprising since the overlap between the TAMRA emission and fluorophore (Figure 3.4),

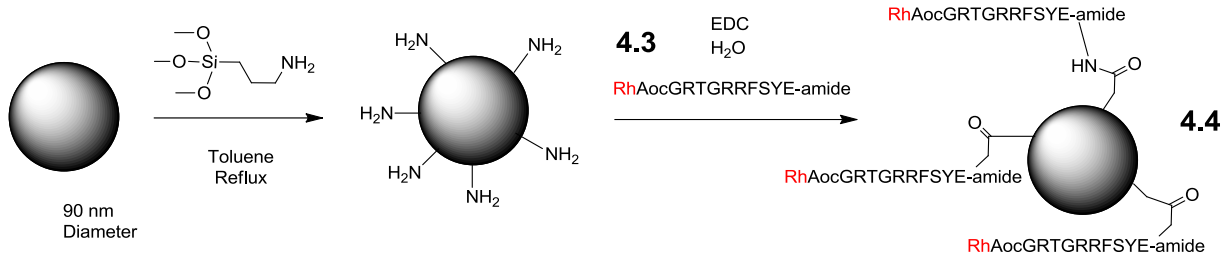

Scheme 4.3 Labeling of 90 nm silica nanoparticles with a fluorescent PKA substrate. Silica nanoparticles (90 nm diameter) were first amine derivatized by refluxing with 3-aminopropyltrimethoxysilane in toluene. Amines were then acylated using a modified fluorescent PKA substrate.

making the mechanism of quenching likely due to a through space mechanism. Since the cAB40 quencher and TAMRA fluorophore are attached to the peptide (where distances are measured in angstroms), perhaps they are not capable moving far enough away to create any noticeable change in quenching after phosphorylation. We hypothesized the TAMRA fluorophore and AB40 quencher would be required to be placed further apart to produce any noticeable change in fluorescence after phosphorylation.

Many strategies exist for increasing the distance between the PKA substrate and cAB40 quencher. We chose to pursue a strategy of covalent attachment to amine functionalized silica nanoparticles and hypothesized that this would allow a population of TAMRA labeled peptides to move further away from the cAB40 quencher, and enable the system to produce a fluorescent enhancement despite covalent attachment. As an added benefit, nanoparticles have the added

advantage of improved cytoplasmic delivery.[11] However, before constructing a nanoparticle containing both the fluorescent substrate and cAB40 quencher, we chose to investigate the interaction of silica nanoparticles labeled with a TAMRA labeled PKA substrate with free AB40 **3.4**. Nanoparticles were synthesized by first derivatizing the surface of silica nanoparticles (90 nm diameter) to contain free amines using 3-aminopropyltrimethoxysilane (Scheme 4.4). Free amines on the nanoparticle surface were then acylated with carboxy derivatized PKA substrate **4.3** using EDC in H_2O to yield the PKA substrate-labeled nanoparticles **4.4**.

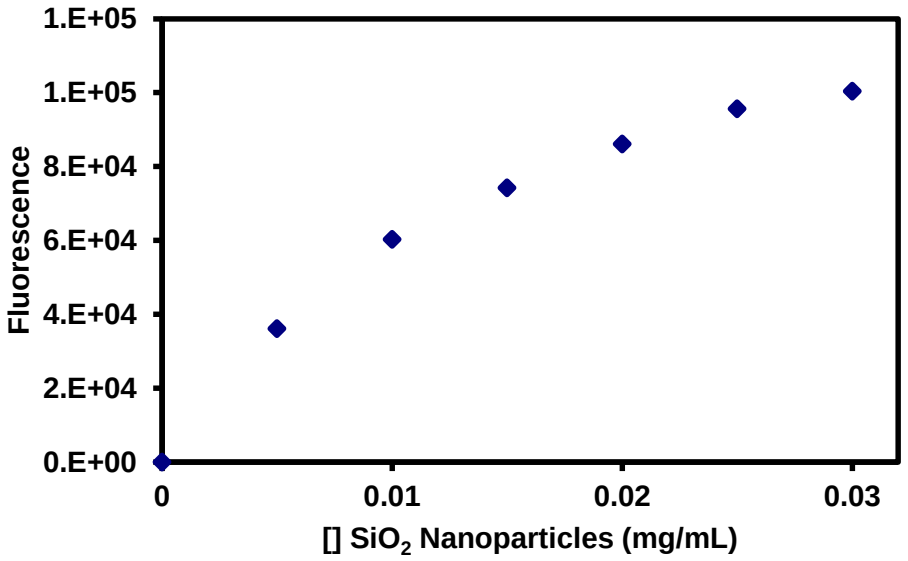

Figure 4.2 Beer's law plot of PKA-labeled SiO_2 Nanoparticles. The fluorescence was measured an increasing concentrations of nanoparticles. Error bars are present, however they may be too small to observe.

Initially, we were concerned about TAMRA self-quenching on the silica nanoparticle surface. Nanoparticles **4.4** were diluted to various concentrations in buffer and the fluorescence was measured (Figure 4.2). At increasing concentration of nanoparticles, fluorescence does not increase linearly, indicating what is likely self-quenching. This is to be expected as TAMRA is known to self-quench at high concentrations. However, at lower concentrations, the fluorescence

does appear to increase linearly. Next, quenching of PKA substrate-labeled nanoparticles **4.4** upon addition of AB40 **3.4** was investigated (Table 4.1). Quenching of the PKA substrate-labeled nanoparticles **4.4** (0.005 mg/mL) increased upon each addition of AB40 **3.4**, with a maximum 22-fold quench at 48 uM AB40 **3.4**. While a 22-fold quench is not as deep as the system with free PKA substrate, if half the fluorescence could be recovered upon phosphorylation, the system would be very promising.

[] AB40 **3.4** (μM)	% quench	Fold Quench
0	0	1.0
6	74	3.9
12	83	6.0
18	88	8.5
24	90	10.0
32	92	12.6
36	93	14.9
42	95	18.3
48	95	21.7

Table 4.1 Quenching observed after addition of AB40 quencher to PKA-substrate labeled nanoparticles in buffer.

To create a unimolecular system, we attached both the modified PKA substrate **4.3** and the cAB40 quencher **3.7** to the surface of 90 nm silica nanoparticles (Scheme 4.5). First, the surface of silica nanoparticles (90 nm diameter) was derivatized to contain free amines using 3-aminopropyltrimethoxysilane. As we were unsure what concentration of cAB40 on the surface would create an optimum fluorescence upon phosphorylation, a 32-member combinatorial library was constructed by varying the concentration of PKA substrate and cAB40 with respect

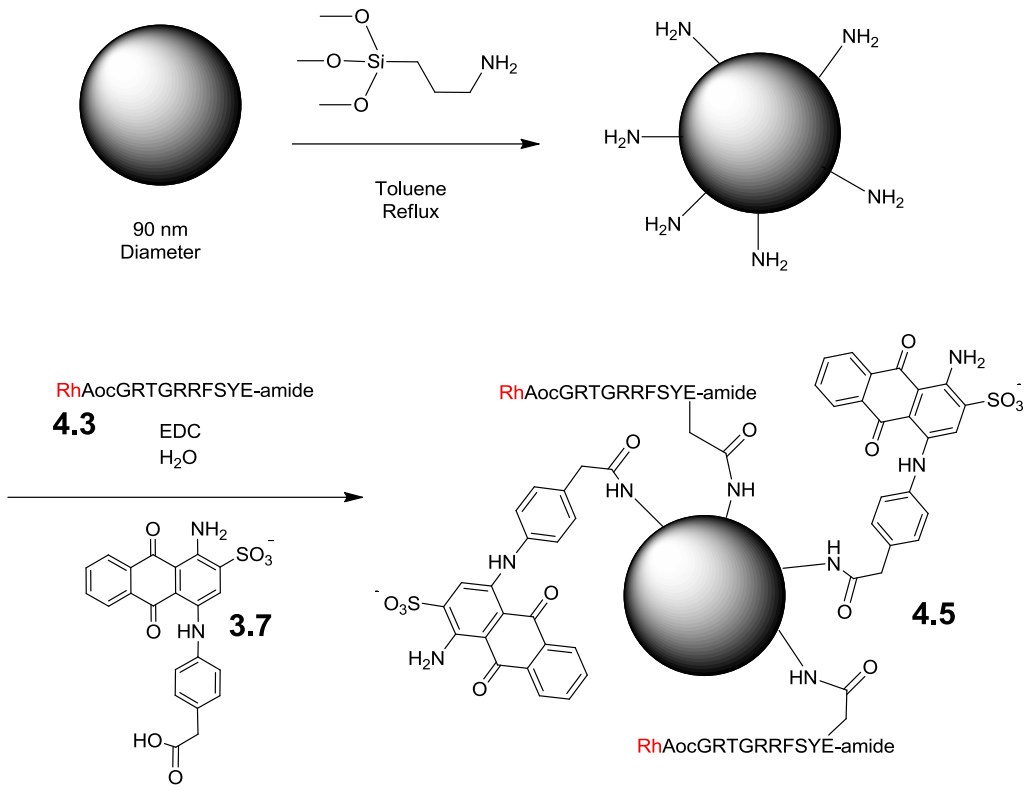

Scheme 4.4 Construction of Unimolecular PKA sensor **4.5**. Silica nanoparticles (90 nm diameter) were first amine derivatized by refluxing with 3-aminopropyltrimethoxysilane in toluene. Amines were then acylated using a modified fluorescent PKA substrate **4.3** and the quencher cAB40 **3.7**.

to the number of free amines present on the surface of 1 mg of nanoparticles (see Materials and Methods). Nanoparticles were then screened for the highest fluorescent enhancement upon phosphorylation. The 300:10:1 (quencher : PKA substrate : amine) and 240:10:1 (quencher : PKA substrate : amine) ratios had the largest dynamic range of 2.2-fold and 2.1-fold, respectively. To prove the fluorescent enhancement was enzyme dependent, the assay was run in the presence and absence of PKA, and showed an enchantment only in the presence of enzyme (Figure 4.3).

While a 2.2-fold enhancement is greater than most GFP-based fluorescent reporters (see introduction) it is not as dramatic as the 35-fold enhancement we observed with the free PKA

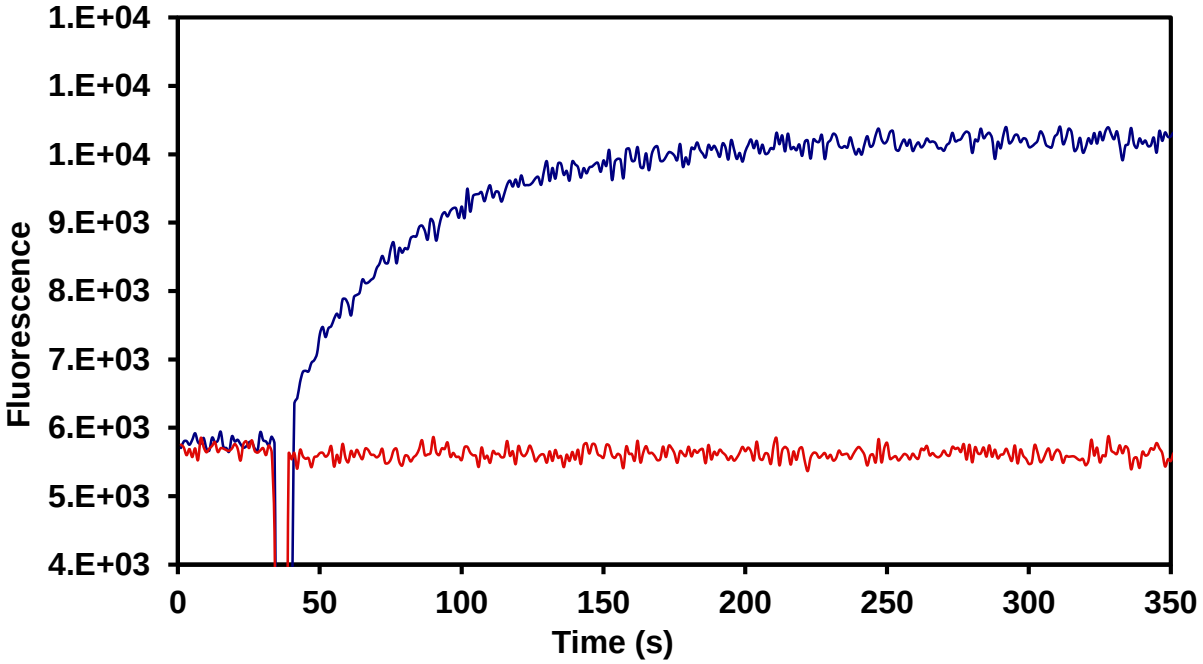

Figure 4.3 Fluorescent enhancement of 240:10:1 (quencher **3.7**: PKA substrate **4.3** : nanoparticle amine) SiO_2 nanoparticles in the presence (Blue) and absence of PKA (Red). Assay was initiated via PKA addition at 40s.

substrate **4.2** and the AB40 quencher **3.4**. With a 2.2-fold fluorescence enhancement, it is questionable whether the sensor could be used for sensitive measurements of PKA activity. With this in mind, we tested the sensitivity of the 300:10:1 (quencher **3.7** : PKA substrate **4.3** : amine) sensor. The sensor appears to be concentration dependent (Figure 4.4). While the biosensor does display enzyme dependence, its utility has only been demonstrated *in vitro*. In biological samples, thousands of various cellular components could limit the fluorescent response. As a result, we chose to demonstrate the effects of high salt concentrations which we thought could potentially disrupt the interaction between the fluorescent substrate and quencher. The fluorescent enhancement of the 300:10:1 (quencher : PKA substrate : amine) PKA biosensor was investigated at high salt concentrations (Figure 4.5). High salt concentration did have an effect on the fluorescent enhancement of the assay, reducing the fluorescent enhancement upon

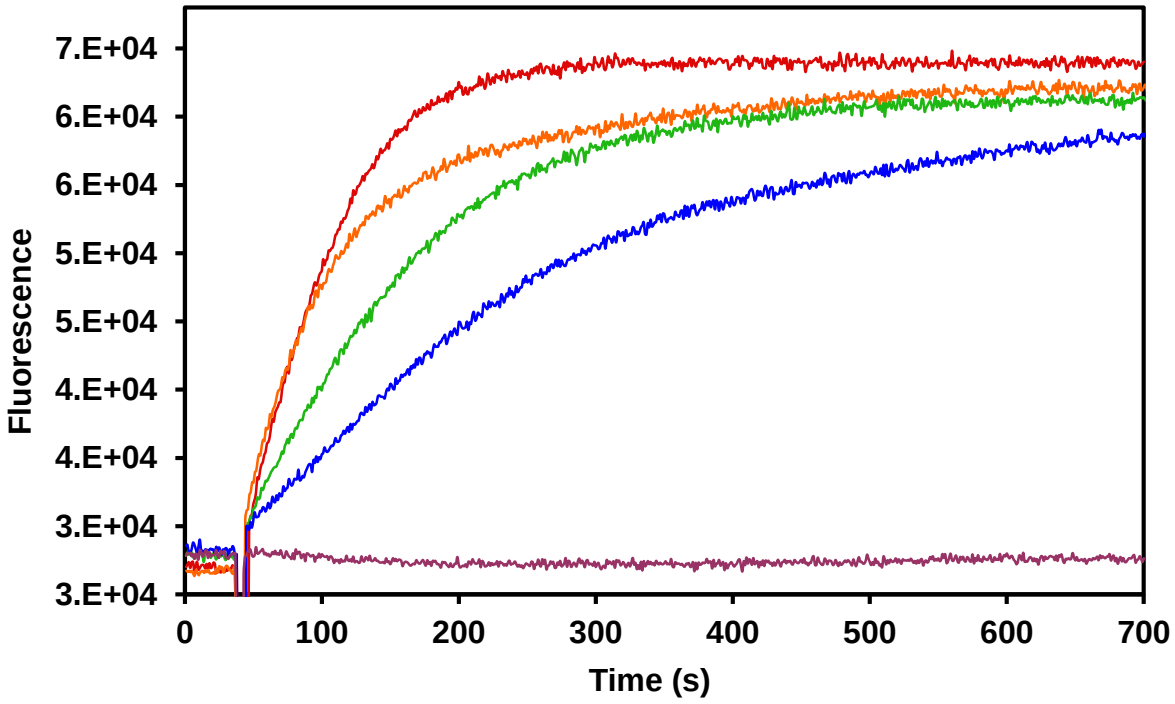

Figure 4.4 Fluorescent enhancements of the 300:10:1 (quencher **3.4** : PKA substrate **4.6**: nanoparticle amine) sensor at 20 nM (Red), 15 nM (Orange), 10 nM (Green), 5 nM (Blue), and 0 nM (Purple) of PKA. PKA-C addition initiated the reaction at 30 seconds.

phosphorylation from 2.2-fold (1 mM KCl) to 1.8-fold (150 mM KCl) to 1.4-fold (300 mM KCl). While this is disappointing, it is not unexpected, since the PKA substrate peptide and AB40 quencher are both highly charged, making interference from high salt concentrations likely.

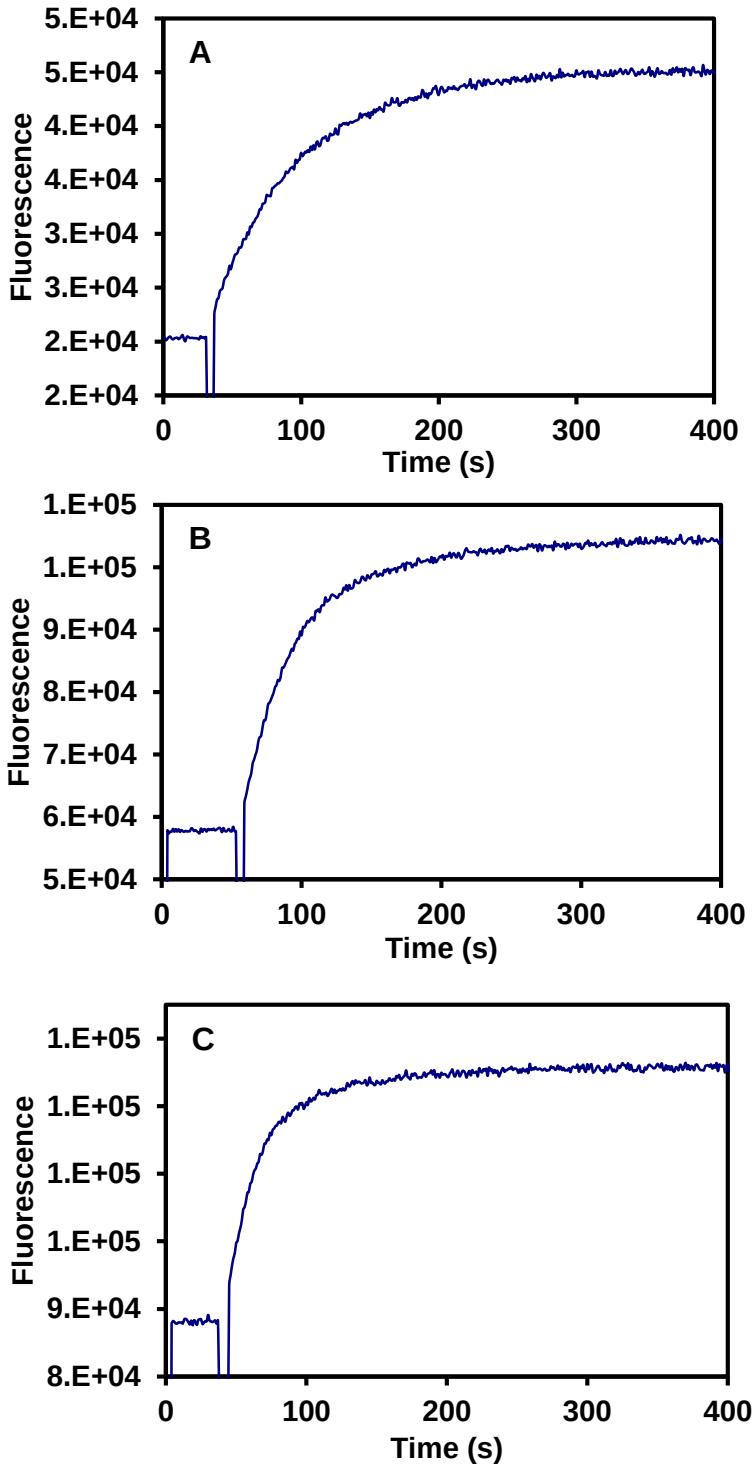

Figure 4.5 PKA nanoparticle (300 : 10 : 1, Quencher : Peptide : Amine) assays performed with 1 mM KCl (A, 2.2-fold), 150 mM KCl (B, 1.8-fold), and 300 mM KCl (C, 1.4-fold) containing Tris pH 7.4 buffer.

CONCLUSIONS

Significant progress has been made toward the creation of a unimolecular sensor for PKA activity. The synthesis and purification of the SiO_2 nanoparticle biosensor is relatively straight-forward. The biosensor shows enzyme-dependent fluorescent enhancements using a robust fluorophore with good photophysical properties. High concentrations of salt do have a negative effect, but do not completely eliminate the fluorescent response, suggesting further experiments with biological samples may be successful. As an additional benefit, the nanoparticle-based structure should facilitate delivery to the cytoplasm. However, further development of this assay is necessary before intracellular use should be attempted, particularly to further increase the robustness of the fluorescent response upon phosphorylation.

MATERIALS AND METHODS

General reagents and solvents were purchased from Fisher or Sigma-Aldrich. Novasyn TGR Resin, Fmoc-Lys(Mtt)-OH (N-α-Fmoc-N-ε-4-methyltrityl-L-lysine)**,** and all Fmoc protected natural amino acids were purchased from EMD Biosciences Inc. HCTU [1H-benzotriazolium-1 [bis(dimethylamino)methylene]-5-chloro-hexafluorophosphate (1),3-oxide] and Fmoc-Aoc-OH (N-α-Fmoc-octanoic acid) was purchased from Peptides International (Louisville, KY, U.S.A.). 5'-TAMRA (5-carboxytetramethylrhodamine) was purchased from Chempep, Inc. (Wellington, Fl, U.S.A). Flash Chromatography was performed on a Biotage (Charlotte, N.C., U.S.A.) Isolera One System using a 120 gram C18 reverse phase column. The catalytic subunit of the cyclic-AMP dependent Protein Kinase was purchased from Promega. Bulk silica nanoparticles (90 nm

in diameter) and 3-aminopropyltrimethoxysilane (APTMS) were purchased from Sigma-Aldrich.

Peptide Synthesis. (Including Rhodamine PKA Substrate RhAocGRTGRRFSY-amide and modified substrate RhAocGRTGRRFSYE-amide) The peptide was synthesized using standard Fmoc solid-phase synthesis on a Prelude peptide synthesizer (Protein Technologies Inc., Tucson, AZ, U.S.A.). Briefly, Novasyn TGR resin was swelled for 30 min in DCM before synthesis. The first Fmoc-protected AA was then coupled using 5.0 equiv AA, 4.9 equiv of HCTU, 20 equiv of diisopropylethylamine (DIPEA) in N,N-dimethylformamide (DMF) (2 × 5 min) followed by a DMF wash (6 × 30 s). The Fmoc-protecting group was removed using 20% piperidine in DMF (5 × 2.5 min) followed by a DMF wash (6 × 30 s). The remaining amino acids were then to the free N-terminus of the peptide using the conditions described for the coupling and deprotection of Fmoc-Tyr-OH. The N-terminal Fmoc was then removed using 20% piperidine in DMF (5 × 2.5 min) and the 5-TAM fluorophore was coupled using 5.0 equiv of fluorophore, 4.9 equiv of HCTU, and 20 equiv of DIPEA in DMF (1× 60 min) followed by a wash (3× DMF, IPA, DCM). After fluorophore coupling, the peptides were cleaved from the resin and deprotected using a 95:2.5:2.5 TFA:H_2O:triisopropylsilane (TIPS) cleavage cocktail. The peptides were isolated via filtration, precipitated with ice-cold ether, and centrifuged. The precipitates were air-dried, dissolved in DMSO, and purified using HPLC (3% to 95% acetonitrile to water gradient with 0.1% TFA over 30 min using a 250 mm x 21.2 mm C18 column). The peak corresponding to the peptide was collected, freeze-dried, and characterized by electrospray ionization mass spectrometry: TAM-Aoc-GRTGRRFSY-amide **1** [Exact Mass calculated: 1651.85, found: 826.9 $(M+2H)^{2+}$], TAM-Aoc-GRTGRRFSYK(AB40)-amide **2** [Exact Mass calculated: 2211.99, found: 1107.2 $(M+2H)^{2+}$], TAM-Aoc-GRTGRRFSYE-amide **3** [Exact Mass calculated: 1779.88,

found: 890.8 $(M+2H)^{2+}$].

Synthesis of Nanoparticle-based PKA sensor. A 32-member combinatorial library was constructed with various concentrations of peptide **4.3** and quencher **3.4**, and 1 mg/mL amine functionalized SiO_2 nanoparticles (90 nm). Nanoparticles (1 mg/mL, 50 mL) were refluxed with 3-aminopropyltrimethoxysilane (2 mL, 8.5 mmol) in toluene overnight. The nanoparticles were then washed with MeOH (3x) and then DMF (3x). The number of amines per mg of nanoparticles was determined using the Kaiser test followed by quantitation via absorbance at 570 nm. Following the quantitation of amines, a 32-member library was constructed by varying the ratio of Quencher **3.4** and Peptide **4.3** to the number of amines contained in 1 mg of nanoparticles. An example reaction (10 : 1 : 1) would include 1 mM Quencher **3.4**, 100 μM Peptide **4.3**, and 100 μM free nanoparticle amine in 1 mL DMF. Also included would be 20 eq. PyBOP, 20 eq. HOBT, and 100 eq. DIPEA (with respect to free amine concentration). After shaking overnight, each reaction would be washed (3 x DMF) then resuspended in H_2O (1 mL).

Quencher **3.7** : Peptide **4.3** : Nanoparticle Amine								
1 Peptide : 1 Amine			10 Peptide : 1 Amine			100 Peptide : 1 Amine		
Quencher **3.7**	Peptide **4.3**	NP Amine	Quencher **3.7**	Peptide **4.3**	NP Amine	Quencher **3.7**	Peptide **4.3**	NP Amine
10	1	1	10	10	1	10	100	1
20	1	1	20	10	1	20	100	1
40	1	1	40	10	1	40	100	1
80	1	1	80	10	1	80	100	1
160	1	1	160	10	1	160	100	1
240	1	1	240	10	1	240	100	1
360	1	1	360	10	1	360	100	1
480	1	1	480	10	1	480	100	1

Table 4.2 Unimolecular PKA biosensor library constructed by varying the concentration of Quencher **3.4** and Peptide **4.3** versus the number of free amines determined via the Kaiser test.

The Cyclic-AMP Dependent Protein Kinase Assay. Peptide **4.1** or **4.2** (1 μM) was incubated with 1 mM ATP, 1 mM DTT, 1 mM $MgCl_2$, 1 mM KCl, and 25 mM Tris-HCl at pH 7.4 in a quartz cuvette. To the cuvette including peptide **4.1** or **4.2** (1 μM), the dye Acid Blue 40 **3.4** (30 μM) was added followed by 10 nM PKA. Additional assays were performed with peptide **4.1**, including an assay including 150 mM KCl and 100 μM of the PKA inhibitor H-89. To the cuvette including peptide **4.2**, no dye was added followed by 10 nM PKA. Enzyme-dependent enhancement in fluorescence (λ_{ex} 550 nm, λ_{em} 580 nm) was determined with each system using a Photon Technology QM-4 spectrofluorimeter (Birmingham, NJ).

Quenching Quantitation using substrate-labeled Nanoparticles. Nanoparticles (**4.4**, 0.005 mg/mL) were incubated with 1 mM ATP, 1 mM DTT, 1 mM $MgCl_2$, 1 mM KCl, and 25 mM Tris-HCl (total volume 196 μL) at pH 7.4 in a quartz cuvette. Acid Blue 40 was added in 6 μM increments (0.5 μL per addition to 200 uL final volume, 2.4 mM stock solution). Fluorescence (λ_{ex} 550 nm, λ_{em} 580 nm) was determined using a Photon Technology QM-4 spectrofluorimeter (Birmingham, NJ).

The Nanoparticle-based cyclic-AMP Dependent Protein Kinase Assay. Nanoparticles (**4.5**) (0.005 mg/mL) were incubated with 1 mM ATP, 1 mM DTT, 1 mM $MgCl_2$, 1 mM KCl, and 25 mM Tris-HCl at pH 7.4 in a quartz cuvette. The catalytic subunit of PKA (0 to 20 nM) was added to initiate the reaction. Additional assays were performed with the nanoparticles, including an assay including 150 mM and 300 mM KCl (Figure 4.11). Enzyme-dependent enhancement in fluorescence (λ_{ex} 550 nm, λ_{em} 580 nm) was determined with each system using a Photon Technology QM-4 spectrofluorimeter (Birmingham, NJ).

CHAPTER 5

SYNTHESIS AND DEVELOPMENT OF FLUORESCENT BIOSENSORS FOR THE PROTEASOME

INTRODUCTION

It has become clear that the future of cancer chemotherapy rests in the inhibition of entire abnormal pathways via multiple inhibitors as part of a chemotherapy cocktail.[1] As abnormal signal transduction via the ubiquitin-proteasome system is a known to play a role in numerous cancers,[2] proteasome inhibitors have been included in various cocktails. For example, a chemotherapy cocktail currently under investigation consist of inhibitors of the proteasome and histone deacetylases (HDAC).[3] While this inhibitor cocktail has been demonstrated to be

[1] Grant, S. *Best practice & research. Clinical haematology* **2008**, *21*, 629–37.

[2] (1) Grande, E.; Earl, J.; Fuentes, R.; Carrato, A. *Expert review of anticancer therapy* **2012**, *12*, 457–67. (2) Dalla Via, L.; Nardon, C.; Fregona, D. *Future medicinal chemistry* **2012**, *4*, 525–43. (3) Rahimi, N. *Molecular cancer therapeutics* **2012**, *11*, 538–48. (4) Yang, H.; Zonder, J. A.; Dou, Q. P. *Expert opinion on investigational drugs* **2009**, *18*, 957–71.

[3] (1) Emanuele, S.; Lauricella, M.; Carlisi, D.; Vassallo, B.; D'Anneo, a; Di Fazio, P.; Vento, R.; Tesoriere, G. *Apoptosis : an international journal on programmed cell death* **2007**, *12*, 1327–38. (2) Hideshima, T.; Chauhan, D.; Richardson, P.; Mitsiades, C.; Mitsiades, N.; Hayashi, T.; Munshi, N.; Dang, L.; Castro, A.; Palombella, V.; Adams, J.; Anderson, K. C. *The Journal of biological chemistry* **2002**, *277*, 16639–47. (3) Catley, L.; Weisberg, E.; Kiziltepe, T.; Tai, Y.; Hideshima, T.; Neri, P.; Tassone, P.; Atadja, P.; Chauhan, D.; Munshi, N. C.; Anderson, K. C. **2006**, *108*, 3441–3449. (4) Place, R. F.; Noonan, E. J.; Giardina, C. *Biochemical pharmacology* **2005**, *70*, 394–406. (5) Dai, Y.; Chen, S.; Kramer, L. B.; Funk, V. L.; Dent, P.; Grant, S. *Clinical cancer research : an official journal of the American Association for Cancer Research* **2008**, *14*, 549–58.

effective, little is known about the mechanism of action. Partly this is due to the lack of readily available tools to monitor the activities of HDACs and the ubitiquin-proteasome system. Due to this, new assays capable of monitoring multiple catalytic activities of the ubiquitin-proteasome system should be a high priority in the field. It is important that the assays be continuous, capable of use in parallel and, eventually, intracellularly using confocal microscopy. Also, the assays must be capable of observer control via a photolabile protecting group (see Introduction for an in depth discussion). In this preliminary study, we chose to focus work on the development of biosensors for the Chymotrypsin-like (Ch-L) and Caspase-like activities (Ca-L) of the ubiquitin-proteasome system using a robust fluorophore compatible with confocal microscopy.

It is important to understand the complexity of proteasome and the difficulties associated with proteasome assay development. As discussed in Chapter 1, the 19S subunit of the proteasome contains three catalytic activities as a part of three different subunits: (1) the β2 subunit trypsin-like activity (T-L), (2) the β5 subunit Ch-L activity, and (3) the β1 subunit Ca-L activity.[4] Each active site is thought to be allosterically regulated,[5] and the effect of one inhibitor on the other active sites is unknown, although there is some debate over this issue.[6] Due to this, each subunit must be monitored simultaneously using an assay with different consensus sequence specificity. As discussed above (see Chapter 1), substrate recognition by the 19S proteasomal subunit occurs via an ubitiquin tag which is critically important for usual proteasome function. At first it was unclear whether peptide substrates of the proteasome would

[4] (1) Finley, D. *Annual review of biochemistry* **2009**, *78*, 477–513. (2) Marques, A. J.; Palanimurugan, R.; Matias, A. C.; Ramos, P. C.; Dohmen, R. J. *Chemical reviews* **2009**, *109*, 1509–36.

[5] Kisselev, A. F.; Akopian, T. N.; Castillo, V.; Goldberg, A. L. *Molecular cell* **1999**, *4*, 395–402.

[6] Schmidtke, G.; Emch, S.; Groettrup, M.; Holzhutter, H. G. *The Journal of biological chemistry* **2000**, *275*, 22056–63.

function as substrates unless tagged with ubitiquin and recognized by the 19S regulatory particle. Fortunately, while ubitiquin tags are necessary in some cases for substrate recognition, the 26S proteasome has been found to degrade nonubiquitylated, unstructured proteins in an ATP-independent fashion.[7] It has also been demonstrated that unstructured proteins are capable of entering the catalytic channel of the 26S proteasomal subunit via the C-terminus or N-terminus.[8] Nonubiquitylated, unstructured peptides should enter the 26S particle of the proteasome via the C-terminus or N-terminus and rapidly be cleaved.

Fluorescent assays have previously been developed for each activity of the proteasome, yet each contains distinct disadvantages. Commercially available Ch-L[9] and Ca-L[10] proteasome assays included blue fluorophores not ideal for confocal microscopy. Further work has been done in the development of a Ch-L substrate using a far red fluorophore suitable for microscopy.[11] However, the Ca-L and T-L fluorescent substrates included Tryptophan or Histidine as a quencher and may not be applicable across the visible spectrum. In this work, we aimed to create Ca-L and Ch-L substrates with robust fluorophores while including a quenching moiety relevant

---

[7] (1) Baugh, J. M.; Viktorova, E. G.; Pilipenko, E. V. *Journal of molecular biology* **2009**, *386*, 814–27. (2) Liu, C.-W.; Li, X.; Thompson, D.; Wooding, K.; Chang, T.; Tang, Z.; Yu, H.; Thomas, P. J.; DeMartino, G. N. *Molecular cell* **2006**, *24*, 39–50.

[8] Berko, D.; Tabachnick-Cherny, S.; Shental-Bechor, D.; Cascio, P.; Mioletti, S.; Levy, Y.; Admon, A.; Ziv, T.; Tirosh, B.; Goldberg, A. L.; Navon, A. *Molecular cell* **2012** Oct 3, 1–11.

[9] (1) Wong, D. J.; Nuyten, D. S. A.; Regev, A.; Lin, M.; Adler, A. S.; Segal, E.; van de Vijver, M. J.; Chang, H. Y. *Cancer research* **2008**, *68*, 369–78. (2) Huang, L.; Ho, P.; Chen, C.-H. *FEBS letters* **2007**, *581*, 4955–9. (3) Filimonenko, M.; Stuffers, S.; Raiborg, C.; Yamamoto, A.; Malerød, L.; Fisher, E. M. C.; Isaacs, A.; Brech, A.; Stenmark, H.; Simonsen, A. *The Journal of Cell Biology* **2007**, *179*, 485–500. (4) Gomez, A. M.; Vrolix, K.; Martínez-Martínez, P.; Molenaar, P. C.; Phernambucq, M.; van der Esch, E.; Duimel, H.; Verheyen, F.; Voll, R. E.; Manz, R. a; De Baets, M. H.; Losen, M. *Journal of immunology (Baltimore, Md. : 1950)* **2011**, *186*, 2503–13. (5) Sharma, M.; Burré, J.; Südhof, T. C. *Science translational medicine* **2012**, *4*, 147ra113.

[10] (1) Brooks, A. D.; Jacobsen, K. M.; Li, W.; Shanker, A.; Sayers, T. J. *Molecular cancer research : MCR* **2010**, *8*, 729–38. (2) Cali, J. J.; Niles, A.; Valley, M. P.; O'Brien, M. A.; Riss, T. L.; Shultz, J. *Expert opinion on drug metabolism & toxicology* **2008**, *4*, 103–20.

[11] Wakata, A.; Lee, H.-M.; Rommel, P.; Toutchkine, A.; Schmidt, M.; Lawrence, D. S. *Journal of the American Chemical Society* **2010**, *132*, 1578–82.

across the visible spectrum.

RESULTS AND DISCUSSION

In this chapter, we describe the synthesis and specificity of proteasome sensors for the Ca-L and Ch-L subunit of the proteasome. A previously described Ch-L biosensor[11] included excellent photophysical properties, proteasome-subunit specificity, and a large dynamic range. However, the Ch-L biosensor relied on tryptophan or histidine, which may not quench other fluorophores necessary to visualize all three catalytic activities of the proteasome. Instead, we applied our recently described dark quencher cAB40 (**3.4**, see chapter 3) which is known to deeply quench a wide variety of fluorophores. We chose the fluorophore 5'-TAMRA (5'-carboxytetramethylrhodamine) as it is appropriate for microscopy (typically includes long $\lambda_{ex}/\lambda_{em}$, large ε, and high Φ). 5'-TAMRA derivatives were synthesized for all preliminary work due to the expense of Atto or Dylight fluorophores.

By applying known consensus sequences for the proteasomal subunit activities, a library was constructed using glycine as a linker to lysine residue acylated with fluorophore or quencher. Three optimized consensus sequences for each activity are:

1) Trypsin-like (β2 subunit): NH_2-LRR-COOH[12]
2) Caspase-like (β1 subunit): NH_2-nLPnLD-COOH[13]
3) Chymotrypsin-like (β5 subunit) : NH_2-HHSL-COOH[14]

[12] Bogyo, M.; Shin, S.; McMaster, J. S.; Ploegh, H. L. *Chemistry & Biology* **1998**, *5*, 307–320.

[13] Kisselev, A. F.; Garcia-Calvo, M.; Overkleeft, H. S.; Peterson, E.; Pennington, M. W.; Ploegh, H. L.; Thornberry, N. a; Goldberg, A. L. *The Journal of biological chemistry* **2003**, *278*, 35869–77.

Using these consensus-sequences, trypsin-like (β2 subunit) fluorescent substrates were synthesized including a 5'-TAMRA (TAM) fluorophore attached to the N-terminus and cAB40 **3.4** attached to the C-terminus via a C-terminal lysine as well as the reverse. Glycines (n = 0, 1, 2) were added as a linker between the acylated lysine and the consensus sequence (Table 5.1). As stated in the introduction, less structured substrates are known to freely diffuse into the 20S catalytic particle, bypassing the regulatory machinery of the proteasome.

At this point, we decided to focus on the development of Ch-L and Ca-L biosensors, and chose to forgo work on the T-L activity biosensor. While all sixteen Ch-L and Ca-L biosensors

Substrate	Chymotrypsin-like (Ch-L)	Caspase-like (Ca-L)	Trypsin-like (T-L)
5.1	**AB40**-HHSLK(**TAM**)-amide	**AB40**-nLPnLDK(**TAM**)-amide	**AB40**-LRRK(**TAM**)-amide
5.2	**AB40**-HHSLGK(**TAM**)-amide	**AB40**-nLPnLDGK(**TAM**)-amide	**AB40**-LRRGK(**TAM**)-amide
5.3	**AB40**-HHSLGGK(**TAM**)-amide	**AB40**-nLPnLDGGK(**TAM**)-amide	**AB40**-LRRGGK(**TAM**)-amide
5.4	**AB40**-GHHSLGK(**TAM**)-amide	**AB40**-GnLPnLDGK(**TAM**)-amide	**AB40**-GLRRGK(**TAM**)-amide
5.5	**TAM**-HHSLK(**AB40**)-amide	**TAM**-nLPnLDK(**AB40**)-amide	**TAM**-LRRK(**AB40**)-amide
5.6	**TAM**-HHSLGK(**AB40**)-amide	**TAM**-nLPnLDGK(**AB40**)-amide	**TAM**-LRRGK(**AB40**)-amide
5.7	**TAM**-HHSLGGK(**AB40**)-amide	**TAM**-nLPnLDGGK(**AB40**)-amide	**TAM**-LRRGGK(**AB40**)-amide
5.8	**TAM**-GHHSLGK(**AB40**)-amide	**TAM**-GnLPnLDGK(**AB40**)-amide	**TAM**-GLRRGK(**AB40**)-amide

Table 5.1 24-member library of sensors synthesized for the proteasome. Glycine linkers were added to increase flexibility of substrate and decrease secondary structure of peptide. 5'-TAMRA and cAB40 were added to each consensus sequence at the N-terminal amine and C-terminal lysine as well a second substrate in reverse to construct a 32-member library.

were substrates for the corresponding activity of the proteasome, we found that Ca-L and Ch-L substrates **5.5**, **5.6**, and **5.7** had the highest specific activities and corresponding fluorescent enhancements (Table 5.2). We decided to focus on these six substrates. In attempting to obtain the K_m and V_{max} we discovered the solubility of the substrates is low at concentrations above 10

[14] Harris, J.; Alper, P.; Li, J.; Rechsteiner, M.; Backes, B. *Chemistry & biology* **2001**, *8*.

μM make the concentrations of substrate necessary for accurate K_m and V_{max} values unattainable. Therefore, instead of collecting K_m and V_{max} data, we found the specific activity of each substrate near our working substrate concentration (2.5 μM). For Ch-L activity, substrates Ch-L **5.5** and Ch-L **5.7** had the best specific activities around 0.110 nmol/min/mg enzyme. The fluorescent enhancement upon proteolysis (fold) for Ch-L **7** was 10-fold higher making it the better overall biosensor. However, as was the case in chapter 3, we found the fold enhancements are a function of the purity of the substrate. This suggests that Ch-L **5.7** could be less pure, and

Peptide	**Specific Activity (nmol/min/mg enzyme)**			**Fluorescent enhancement upon proteolysis (fold)**		
	1 μM	2.5 μM	5 μM	1 μM	2.5 μM	5 μM
Ch-L **5.5**	0.065 ± 0.003	0.114 ± 0.003	0.138 ± 0.006	33.5 ± 1.0	34.1 ± 0.7	30.4 ± 0.7
Ch-L **5.6**	0.039 ± 0.001	0.073 ± 0.001	0.103 ± 0.001	43.0 ± 2.2	40.5 ± 1.8	37.7 ± 2.0
Ch-L **5.7**	0.067 ± 0.002	0.110 ± 0.001	0.162 ± 0.003	47.0 ± 4.0	44.8 ± 1.7	41.3 ± 2.3
Ca-L **5.5**	1.16 ± 0.016	1.12 ± 0.033	0.78 ± 0.03	29.3 ± 1.9	25.1 ± 0.5	23.4 ± 0.5
Ca-L **5.6**	0.14 ± 0.005	0.13 ± 0.004	0.13 ± 0.01	33.7 ± 0.9	27.8 ± 0.7	20.5 ± 0.2
Ca-L **5.7**	0.55 ± 0.017	0.44 ± 0.018	0.33 ± 0.02	15.7 ± 0.7	14.5 ± 0.7	13.3 ± 0.5

Table 5.2 Specific activities and fluorescent enhancements upon proteolysis of Ch-L and Ca-L biosensors. K_m and V_{max} data could not be obtained due to lack of solubility at high concentrations of substrate.

equally as capable as Ch-L **5.5**. For Ca-L activity, biosensor **5.5** is clearly the best substrate, having the highest specific activity, as well as large fluoresce enhancements upon proteolysis.

Using Ca-L and Ch-L substrates **5.5**, **5.6**, and **5.7**, we calculated the IC_{50} (μM) of four inhibitors known to be specific for certain catalytic subunits of the 20S proteasome at constant biosensor concentration (2.5 μM). We used the proteasome subunit specific inhibitors:

(1) Ac-APnLD-H[15] for Caspase-like activity

(2) Epoxomicin[16] for Chymotrypsin-like activity

(3) MG132[17] for both the Caspase-like and Chymotrypsin-like activities

(4) Lactacystin[18] for the Chymotrypsin-like and Trypsin-like activities

The IC_{50} (μM) for each inhibitor was calculated for each peptide substrate (Table 5.3). The Ca-L inhibitor Ac-APnLD-H shows selectivity for our Ca-L substrates over Ch-L, with the IC_{50} of our optimized Ch-L **5.7** substrate around 100 μM and the Ca-L substrates all over 100 uM. Epoxomicin (specific for Ch-L activity) demonstrates selectivity for the Ch-L substrates **5.5**, **5.6**, and **5.7** which are all near 0.02 μM with Ca-L substrates all over 10 μM. The Ca-L and Ch-L inhibitor MG132 inhibits the Ch-L (near 0.01 μM) substrates substantially better than the Ca-L (near 40 μM) activity. The Ch-L and T-L subunit specific inhibitor Lactacystin demonstrates selectivity for Ch-L **5.5**, **5.6**, and **5.7** over substrates Ca-L **5.5**, **5.6**, and **5.7**. Our substrates demonstrate the selectivity that should be observed with each inhibitor.

[15] Kisselev, A. F.; Garcia-Calvo, M.; Overkleeft, H. S.; Peterson, E.; Pennington, M. W.; Ploegh, H. L.; Thornberry, N. a; Goldberg, A. L. *The Journal of biological chemistry* **2003**, *278*, 35869–77.

[16] Meng, L.; Mohan, R.; Kwok, B. H. B.; Elofsson, M.; Sin, N.; Crews, C. M. *Proceedings of the National Academy of Sciences* **1999**, *96*, 10403–10408.

[17] (1) Han, Y. H.; Moon, H. W. A. J. I. N.; You, B. O. R. A.; Park, W. O. O. H. *Oncology Reports* **2009**, *22*, 215–221. (2) Bogyo, M.; Shin, S.; McMaster, J. S.; Ploegh, H. L. *Chemistry & Biology* **1998**, *5*, 307–320. (3) Chen, B.; Ma, Y.; Meng, R.; Xiong, Z.; Zhang, C.; Chen, G.; Zhang, A.; Dong, Y. *Acta Biochimica et Biophysica Sinica* **2010**, *42*, 253–258.

[18] (1) Fenteany, G.; Standaert, R.; Lane, W.; Choi, S.; Corey, E.; Schreiber, S. *Science* **1995**, *268*, 726–731. (2) Nagamitsu, T.; Sunazuka, T.; Tanaka, H.; Ōmura, S.; Sprengeler, P. A.; Smith, A. B. *Journal of the American Chemical Society* **1996**, *118*, 3584–3590.

Peptide	IC_{50} (μM)			
	Ac-APnLD-H	Epoxomicin	MG132	Lactacystin
Ch-L **5.5**	>>>100	0.024 ± 0.001	0.013 ± 0.003	1.65 ± 0.19
Ch-L **5.6**	>100	0.018 ± 0.001	0.009 ± 0.001	1.61 ± 0.08
Ch-L **5.7**	>100	0.044 ± 0.001	0.021 ± 0.008	2.44 ± 0.11
Ca-L **5.5**	94.9 ± 9.8	>10	40.6 ± 2.1	>25
Ca-L **5.6**	8.7 ± 2.3	>10	9.6 ± 2.4	>25
Ca-L **5.7**	109 ± 15.6	>10	41.3 ± 4.3	>25

Table 5.3 IC_{50} (μM) values of four subunit specific proteasome inhibitors in the presence of biosensor substrate (2.5 μM).

CONCLUSIONS

Proteasome assays have been synthesized and developed for the Ch-L and Ca-L catalytic activities of the proteasome. The assays rely on the fluorophore 5'-TAMRA, a robust fluorophore with good photophysical properties, and the broad spectrum cAB40 quencher **3.7** to produce a fluorescent enhancement upon cleavage by the proteasome. Substrate specificity was demonstrated for either the Ca-L or Ch-L subunit of the proteasome. This is promising, as a multicolored sensor could be constructed by simply substituting a far red fluorophore on the Ca-L substrate along with cAB40 **3.7**. The T-L substrate needs further attention but it should be straightforward to characterize its fluorescence enhancement and proteasome subunit specificity. As with the Ca-L substrate, a robust green fluorophore could easily be substituted for 5'-TAMRA on the T-L substrate. With different fluorophores on all three subunit specific substrates, the three catalytic activities of the proteasome could be monitored simultaneously.

MATERIALS AND METHODS

General Procedures General reagents and solvents were purchased from Fisher or Sigma-Aldrich. Novasyn TGR Resin, Fmoc-Lys(Mtt)-OH (N-α-Fmoc-N-ε-4-methyltrityl-L-lysine)**,** and all Fmoc protected natural amino acids were purchased from EMD Biosciences Inc. HCTU [1H-benzotriazolium-1 [bis(dimethylamino)methylene]-5-chloro-hexafluorophosphate (1),3-oxide] was purchased from Peptides International (Louisville, KY, U.S.A.). 5'-TAMRA (5'-carboxytetramethylrhodamine) was purchased from Chempep, Inc. (Wellington, Fl, U.S.A). Proteasome inhibitors and the 20S proteasome were purchased from BostonBiochem.

Peptide Synthesis Peptides were synthesized using standard Fmoc solid-phase synthesis on a Prelude peptide synthesizer (Protein Technologies Inc., Tucson, AZ, U.S.A.). Novasyn TGR resin was swelled for 30 min in DCM before synthesis. Fmoc-Lys(Mtt)-OH was then coupled using 5.0 equiv AA, 4.9 equiv of HCTU, 20 equiv of diisopropylethylamine (DIPEA) in N,N-dimethylformamide (DMF) (2 × 5 min) followed by a DMF wash (6 × 30 s). The Lys 4-methyltrityl protecting group was then deprotected using 7% TFA/7% TIS/86% DCM. The deprotected side chain amine was then acylated using 1.1 equiv cAB40, 1.0 equiv HCTU, and 20.0 equiv DIPEA in DMF (2 x 2 h). The Fmoc-protecting group was removed using 20% piperidine in DMF (2 × 2.5 min) followed by a DMF wash (6 × 30 s). Peptide chain elongation was performed using the conditions described for the coupling and deprotection of Fmoc-Lys(Mtt)-OH. The N-terminal Fmoc was then removed using 20% piperidine in DMF (2 × 2.5

min) and 5'-TAMRA was coupled using 5.0 equiv of fluorophore, 4.9 equiv of HCTU, and 20 equiv of DIPEA in DMF (1× 60 min) followed by a wash (3× DMF, IPA, DCM). After fluorophore coupling, the peptide was cleaved from the resin and deprotected using a 95:2.5:2.5 TFA: H_2O: triisopropylsilane (TIPS) cleavage cocktail. The peptides were isolated via filtration, precipitated with ice-cold ether, and centrifuged. The precipitates were air-dried, dissolved in DMSO, and purified twice using HPLC ((1) 3% to 95% acetonitrile to water gradient with 0.1% TFA over 30 min using a 250 mm x 21.2 mm C4 column) followed by (2) 3% to 95% acetonitrile to water gradient with 0.1% TFA over 30 min using a 250 mm x 21.2 mm C18 column). The peak corresponding to the peptide was collected, freeze-dried, and characterized by electrospray ionization mass spectrometry: TAM-nLPnLDK(AB40)-amide Ca-L **5.5** [Exact Mass calculated: 1428.6, found: 715.0 $(M+2H)^{2+}$], TAM-nLPnLDGK(AB40)-amide Ca-L **5.6** [Exact Mass calculated: 1472.6, found: 737.05 $(M+2H)^{2+}$], TAM-nLPnLDGGK(AB40)-amide Ca-L **5.7** [Exact Mass calculated: 1542.6, found: 772.1 $(M+2H)^{2+}$], TAM-HHSLK(AB40)-amide Ch-L **5.5** [Exact Mass calculated: 1463.6, found: 732.7 $(M+2H)^{2+}$], TAM-HHSLGK(AB40)-amide Ch-L **5.6** [Exact Mass calculated: 1521.6, found: 761.7 $(M+2H)^{2+}$], TAM-HHSLGGK(AB40)-amide Ch-L **5.7** [Exact Mass calculated: 1580.6, found: 791.5 $(M+2H)^{2+}$].

Specific Activity and Fluorescent Enhancement Assays Specific activities and fluorescent enhancements were calculated for all six Ch-L and Ca-L peptides. Biosensor substrates (1, 2.5 and 5 μM) were incubated in a pH 8.0 buffer containing 20 mM HEPES, 0.5 mM EDTA, and 0.035% w/v SDS. Once the plate reader (Molecular Devices Spectra Max Gemini EM) had reached equilibration, 20S proteasome was added (47 nM) and the fluorescence monitored. After

three assays, the specific activity and fold enhancement upon proteolysis was calculated for each substrate.

Inhibitor IC_{50} value determination IC_{50} values were determined using specific commercially available proteasome inhibitors for each Ca-L and Ch-L substrate. Each peptide substrate (Ch-L **5.5**, **5.6**, **5.7** and Ca-L **5.5**, **5.6**, **5.7**) was incubated with six concentrations of Ac-APnLD-H, Epoxomicin, MG132, and Lactacystin. The concentrations of each inhibitor used depended on the published IC_{50} value of the inhibitor, with three concentrations above and below the published IC_{50} value. Specifically, peptide substrate (2.5 μM) was incubated with six differed concentrations of inhibitor at 37 °C in pH 8.0 buffer containing 20 mM HEPES, 0.5 mM EDTA, and 0.035% w/v SDS. Proteasome (37 nM, purified rabbit 20S proteasome) was added and the reaction was monitored via fluorescence. Upon completion of the reaction at various inhibitor concentrations, kinetic data was entered into Sigmaplot and fit to a dose response curve to generate IC_{50} values for each inhibitor/substrate pair.

BIBLIOGRAPHY

Acin-Perez, R.; Salazar, E.; Kamenetsky, M.; Buck, J.; Levin, L. R.; Manfredi, G. *Cell Metab.* **2009**, *9*, 265–276.

Adams, S. R.; Harootunian, A. T.; Buechler, Y. J.; Taylor, S. S.; Tsien, R. Y. *Nature* **1991**, *349*, 694–7.

Affaitati, A.; Cardone, L.; de Cristofaro, T.; Carlucci, A.; Ginsberg, M. D.; Varrone, S.; Gottesman, M. E.; Avvedimento, E. V.; Feliciello, A. *The Journal of biological chemistry* **2003**, *278*, 4286–94.

Agnes, R. S.; Jernigan, F.; Shell, J. R.; Sharma, V.; Lawrence, D. S. *Journal of the American Chemical Society* **2010**, *132*, 6075–80.

Alberts, B.; Johnson, A.; Lewis, J.; Raff, M.; Roberts, K.; Walter, P. *Molecular Biology of the Cell*, Reference ed.; Garland Science: New York, 2007; pp 818.

An, B.; Goldfarb, R. H.; Siman, R.; Dou, Q. P. *Cell death and differentiation* **1998**, *5*, 1062–75.

Ananthanarayanan, B.; Fosbrink, M.; Rahdar, M.; Zhang, J. *The Journal of biological chemistry* **2007**, *282*, 36634–41.

Anderson, M. P.; Berger, H. A.; Rich, D. P.; Gregory, R. J.; Smith, A. E.; Welsh, M. J. *Cell* **1991**, *67*, 775–784.

Andrews, D. L. *Chemical Physics* **1989**, *135*, 195–201.

Andrews, D. L.; Bradshaw, D. S. *European Journal of Physics* **2004**, *25*, 845–858.

Aye-Han, N.-N.; Ni, Q.; Zhang, J. *Current opinion in chemical biology* **2009**, *13*, 392–7.

Balakrishnan, S.; Zondlo, N. J. *Journal of the American Chemical Society* **2006**, *128*, 5590–1.

Baugh, J. M.; Viktorova, E. G.; Pilipenko, E. V. *Journal of molecular biology* **2009**, *386*, 814–27.

Berko, D.; Tabachnick-Cherny, S.; Shental-Bechor, D.; Cascio, P.; Mioletti, S.; Levy, Y.; Admon, A.; Ziv, T.; Tirosh, B.; Goldberg, A. L.; Navon, A. *Molecular cell* **2012** Oct 3, 1–11.

Biosearch Technologies. Black Hole Quencher Dyes: The Inescapable Solution. https://www.biosearchtech.com/support/applications/dyes-from-biosearch-technologies/black-hole-quencher%C2%AE-dyes (accessed March, 15 2013).

Birks, J. B.; Salete, M.; Leite, S. C. P. *Journal of Physics B: Atomic and Molecular Physics* **1970**, *3*, 417–424.

Blagosklonny, M. V.; Wu, G. S.; Omura, S.; El-Deiry, W. S. *Biochemical and biophysical research communications* **1996**, *227*, 564–9.

Bogyo, M.; Shin, S.; McMaster, J. S.; Ploegh, H. L. *Chemistry & Biology* **1998**, *5*, 307–320.

Bórquez, D. a; González-Billault, C. *Biological research* **2011**, *44*, 35–41.

Brooks, A. D.; Jacobsen, K. M.; Li, W.; Shanker, A.; Sayers, T. J. *Molecular cancer research : MCR* **2010**, *8*, 729–38.

Brush, J. M.; Kim, K.; Sayre, J. W.; McBride, W. H.; Iwamoto, K. S. *International journal of radiation biology* **2009**, *85*, 483–94.

Burnette, B.; Batra, P. P. *Anal. Biochem.* **1985**, *145*, 80–86.

Cali, J. J.; Niles, A.; Valley, M. P.; O'Brien, M. A.; Riss, T. L.; Shultz, J. *Expert opinion on drug metabolism & toxicology* **2008**, *4*, 103–20.

Calleja, V.; Alcor, D.; Laguerre, M.; Park, J.; Vojnovic, B.; Hemmings, B. a; Downward, J.; Parker, P. J.; Larijani, B. *PLoS biology* **2007**, *5*, e95.

Carlucci, A.; Adornetto, A.; Scorziello, A.; Viggiano, D.; Foca, M.; Cuomo, O.; Annunziato, L.; Gottesman, M.; Feliciello, A. *EMBO J.* **2008**, *27*, 1073–1084.

Carlucci, A.; Lignitto, L.; Feliciello, A. *Trends Cell. Biol.* **2008**, *18*, 604–613.

Carmony, K. C.; Lee, D.-M.; Wu, Y.; Lee, N.-R.; Wehenkel, M.; Lee, J.; Lei, B.; Zhan, C.-G.; Kim, K.-B. *Bioorganic & medicinal chemistry* **2012**, *20*, 607–13.

Carrillo, L. D.; Krishnamoorthy, L.; Mahal, L. K. *Journal of the American Chemical Society* **2006**, *128*, 14768–9.

Cataldi, A. *Current pharmaceutical design* **2010**, *16*, 1387–95.

Catley, L.; Weisberg, E.; Kiziltepe, T.; Tai, Y.; Hideshima, T.; Neri, P.; Tassone, P.; Atadja, P.; Chauhan, D.; Munshi, N. C.; Anderson, K. C. **2006**, *108*, 3441–3449.

Chakraborty, A.; Seth, D.; Chakrabarty, D.; Sarkar, N. *Spectrochimica acta. Part A, Molecular and biomolecular spectroscopy* **2006**, *64*, 801–8.

Chen, B.; Ma, Y.; Meng, R.; Xiong, Z.; Zhang, C.; Chen, G.; Zhang, A.; Dong, Y. *Acta Biochimica et Biophysica Sinica* **2010**, *42*, 253–258.

Chen, C.-A.; Yeh, R.-H.; Lawrence, D. S. *Journal of the American Chemical Society* **2002**, *124*, 3840–1.

Chen, C.-A.; Yeh, R.-H.; Yan, X.; Lawrence, D. S. *Biochimica et biophysica acta* **2004**, *1697*, 39–51.

Chen, J. *Circulation* **2002**, *105*, 2766–2771.

Chen, J.; Tung, C.-H.; Mahmood, U.; Ntziachristos, V.; Gyurko, R.; Fishman, M. C.; Huang, P. L.; Weissleder, R. *Circulation* **2002**, *105*, 2766–71.

Chen, Q.; Lin, R. Y.; Rubin, C. S. *J. Biol. Chem.* **1997**, *272*, 15247–15257.(d) Schwoch, G.; Trinczek, B.; Bode, C. *Biochem. J.* **1990**, *270*, 181–188.

Chung, K. T.; Stevens, S. E.; Jr., Cerniglia, C. *Crit. Rev. Microbiol.* **1992**, *18*, 175–190.

Clarke, P. R.; Zhang, C. *Nature reviews. Molecular cell biology* **2008**, *9*, 464–77.

Cochran, J. C.; Sontag, C. a; Maliga, Z.; Kapoor, T. M.; Correia, J. J.; Gilbert, S. P. *The Journal of biological chemistry* **2004**, *279*, 38861–70.

Coux, O.; Tanaka, K.; Goldberg, a L. *Annual review of biochemistry* **1996**, *65*, 801–47.

Dahlmann, B. *BMC biochemistry* **2007**, *8 Suppl 1*, S3.

Dai, Y.; Chen, S.; Kramer, L. B.; Funk, V. L.; Dent, P.; Grant, S. *Clinical cancer research : an official journal of the American Association for Cancer Research* **2008**, *14*, 549–58.

Dai, Z.; Dulyaninova, N. G.; Kumar, S.; Bresnick, A. R.; Lawrence, D. S. *Chemistry & biology* **2007**, *14*, 1254–60.

Dalla Via, L.; Nardon, C.; Fregona, D. *Future medicinal chemistry* **2012**, *4*, 525–43.

Dalton, W. S. *Seminars in oncology* **2004**, *31*, 3–9; discussion 33.

Deshayes, S.; Morris, M. C.; Divita, G.; Heitz, F. *Cellular and molecular life sciences : CMLS* **2005**, *62*, 1839–49.

Dexter, D. L. *J. Phys. Chem.* **1953**, *21*, 836.

DiPilato, L. M.; Cheng, X.; Zhang, J. *Proceedings of the National Academy of Sciences of the United States of America* **2004**, *101*, 16513–8.

Diviani, D.; Scott, J. D. *Journal of cell science* **2001**, *114*, 1431–7.

Dixon, J. M.; Taniguchi, M.; Lindsey, J. S. *Photochem. Photobiol.* **2005**, *81*, 212-213.

Doose, S.; Neuweiler, H.; Sauer, M. *ChemPhysChem* **2005**, *6*, 2277–2285.

Du, H.; Fuh, R.-C. A.; Li, J.; Corkan, L. A.; Lindsey, J. S. *Photochem. Photobiol.* **1998**, *68*, 141-142.

Durocher, D.; Taylor, I. a; Sarbassova, D.; Haire, L. F.; Westcott, S. L.; Jackson, S. P.; Smerdon, S. J.; Yaffe, M. B. *Molecular cell* **2000**, *6*, 1169–82.

Edgington, L. E.; Verdoes, M.; Bogyo, M. *Current opinion in chemical biology* **2011**, *15*, 798–805.

Ellis-Davies, G. C. R. *Nature methods* **2007**, *4*, 619–28.

Elsabahy, M.; Wooley, K. L. *Chemical Society reviews* **2012**, *41*, 2545–61.

Emanuele, S.; Lauricella, M.; Carlisi, D.; Vassallo, B.; D'Anneo, a; Di Fazio, P.; Vento, R.; Tesoriere, G. *Apoptosis : an international journal on programmed cell death* **2007**, *12*, 1327–38.

Emonet, T.; Cluzel, P. *Proceedings of the National Academy of Sciences of the United States of America* **2008**, *105*, 3304–9.

Engels, J.; Schlaeger, E. J. *Journal of Medicinal Chemistry* **1977**, *20*, 907–911.

Fan, J.; Hu, M.; Zhan, P.; Peng, X. *Chem. Soc.Rev.* **2013**, *42*, 29–43.

Feliciello, A.; Gottesman, M. E.; Avvedimento, E. V. *Cellular signaling* **2005**, *17*, 279–87.

Fenteany, G.; Standaert, R.; Lane, W.; Choi, S.; Corey, E.; Schreiber, S. *Science* **1995**, *268*, 726–731.

Filimonenko, M.; Stuffers, S.; Raiborg, C.; Yamamoto, A.; Malerød, L.; Fisher, E. M. C.; Isaacs, A.; Brech, A.; Stenmark, H.; Simonsen, A. *The Journal of Cell Biology* **2007**, *179*, 485–500.

Finley, D. *Annual review of biochemistry* **2009**, *78*, 477–513.

Förster, A.; Masters, E. I.; Whitby, F. G.; Robinson, H.; Hill, C. P. *Molecular cell* **2005**, *18*, 589–99.

Freeman, R.; Finder, T.; Gill, R.; Willner, I. *Nano letters* **2010**, *10*, 2192–6.

Fröbel, J.; Rose, P.; Müller, M. *Philosophical transactions of the Royal Society of London. Series B, Biological sciences* **2012**, *367*, 1029–46.

Fujioka, A.; Terai, K.; Itoh, R. E.; Aoki, K.; Nakamura, T.; Kuroda, S.; Nishida, E.; Matsuda, M. *The Journal of biological chemistry* **2006**, *281*, 8917–26.

Geng, F.; Wenzel, S.; Tansey, W. P. *Annual review of biochemistry* **2012**, *81*, 177–201.

Goldberg, A. L.; Cascio, P.; Saric, T.; Rock, K. L. *Molecular immunology* **2002**, *39*, 147–64.

Gomez, A. M.; Vrolix, K.; Martínez-Martínez, P.; Molenaar, P. C.; Phernambucq, M.; van der Esch, E.; Duimel, H.; Verheyen, F.; Voll, R. E.; Manz, R. a; De Baets, M. H.; Losen, M. *Journal of immunology (Baltimore, Md. : 1950)* **2011**, *186*, 2503–13.

Gong, Y.-J.; Zhang, X.-B.; Zhang, C.-C.; Luo, A.-L.; Fu, T.; Tan, W.; Shen, G.-L.; Yu, R.-Q. *Anal. Chem.* **2012**, *84*, 10777–84.

Grande, E.; Earl, J.; Fuentes, R.; Carrato, A. *Expert review of anticancer therapy* **2012**, *12*, 457–67.

Grant, D. M.; Zhang, W.; McGhee, E. J.; Bunney, T. D.; Talbot, C. B.; Kumar, S.; Munro, I.; Dunsby, C.; Neil, M. A.; Katan, M.; French, P. M. W. *Biophysical journal* **2008**, *95*, L69–71.

Grant, S. *Best practice & research. Clinical haematology* **2008**, *21*, 629–37.

Groll, M.; Bajorek, M.; Köhler, a; Moroder, L.; Rubin, D. M.; Huber, R.; Glickman, M. H.; Finley, D. *Nature structural biology* **2000**, *7*, 1062–7.

Han, Y. H.; Moon, H. W. A. J. I. N.; You, B. O. R. A.; Park, W. O. O. H. *Oncology Reports* **2009**, *22*, 215–221.

Harada, H.; Becknell, B.; Wilm, M.; Mann, M.; Huang, L. J.; Taylor, S. S.; Scott, J. D.; Korsmeyer, S. J. *Molecular cell* **1999**, *3*, 413–22.

Harootunian, A. T.; Adams, S. R.; Wen, W.; Meinkoth, J. L.; Taylor, S. S.; Tsien, R. Y. *Mol. Biol. Cell* **1993**, *4*, 993–1002.

Harris, J.; Alper, P.; Li, J.; Rechsteiner, M.; Backes, B. *Chemistry & biology* **2001**, *8*.

He, Y.; Yeung, E. S. *Electrophoresis* **2003**, *24*, 101–108.

Hideshima, T.; Chauhan, D.; Richardson, P.; Mitsiades, C.; Mitsiades, N.; Hayashi, T.; Munshi, N.; Dang, L.; Castro, A.; Palombella, V.; Adams, J.; Anderson, K. C. *The Journal of biological chemistry* **2002**, *277*, 16639–47.

Horbinski, C.; Chu, C. T. *Free radical biology & medicine* **2005**, *38*, 2–11.

Horton, K. L.; Pereira, M. P.; Stewart, K. M.; Fonseca, S. B.; Kelley, S. O. *Chembiochem : a European journal of chemical biology* **2012**, *13*, 476–85.

Hu, E.; Demmou, L.; Cauli, B.; Gallopin, T.; Geoffroy, H.; Harris-Warrick, R. M.; Paupardin-Tritsch, D.; Lambolez, B.; Vincent, P.; Hepp, R. *Cerebral cortex (New York, N.Y. : 1991)* **2011**, *21*, 708–18.

Huang, L.; Ho, P.; Chen, C.-H. *FEBS letters* **2007**, *581*, 4955–9.

Jaffer, F. a; Kim, D.-E.; Quinti, L.; Tung, C.-H.; Aikawa, E.; Pande, A. N.; Kohler, R. H.; Shi, G.-P.; Libby, P.; Weissleder, R. *Circulation* **2007**, *115*, 2292–8.

Janmey, P.; McCulloch, C. *Annual review of biomedical engineering* **2007**, *9*, 1–34.

Kamaly, N.; Xiao, Z.; Valencia, P. M.; Radovic-Moreno, A. F.; Farokhzad, O. C. *Chemical Society reviews* **2012**, *41*, 2971–3010.

Karnik, N. A.; Prankerd, R. J.; Perrin, J. H. *Chirality* **1991**, *3*, 124–128. *The journal of physical chemistry. A* **2006**, *110*, 13139–44.

Kelley, S. O.; Stewart, K. M.; Mourtada, R. *Pharmaceutical research* **2011**, *28*, 2808–19.

Kikuchi, K.; Hashimoto, S.; Mizukami, S.; Nagano, T. *Organic letters* **2009**, *11*, 2732–5.

Kisselev, A. F.; Akopian, T. N.; Castillo, V.; Goldberg, A. L. *Molecular cell* **1999**, *4*, 395–402.

Kisselev, A. F.; Akopian, T. N.; Woo, K. M.; Goldberg, A. L. **1999**, *274*, 3363–3371.

Kisselev, A. F.; Garcia-Calvo, M.; Overkleeft, H. S.; Peterson, E.; Pennington, M. W.; Ploegh, H. L.; Thornberry, N. a; Goldberg, A. L. *The Journal of biological chemistry* **2003**, *278*, 35869–77.

Kiyokawa, E.; Aoki, K.; Nakamura, T.; Matsuda, M. *Annual review of pharmacology and toxicology* **2011**, *51*, 337–58.

Kobayashi, H.; Choyke, P. L. *Accounts of chemical research* **2011**, *44*, 83–90.

Kozloff, K. M.; Quinti, L.; Patntirapong, S.; Hauschka, P. V.; Tung, C.-H.; Weissleder, R.; Mahmood, U. *Bone* **2009**, *44*, 190–8.

Lakowicz J. R.: Principles of Fluorescence Spectroscopy. 3rd ed. New York: Kluwer Academic/Plenum, 2006.

Lapenna, S.; Giordano, A. *Nature reviews. Drug discovery* **2009**, *8*, 547–66.

Lawrence, D. S. *Current opinion in chemical biology* **2005**, *9*, 570–5.

Lawrence, D. S.; Wang, Q. *Chembiochem : a European journal of chemical biology* **2007**, *8*, 373–8.

Lawrence, D. S.; Wang, Q. *ChemBioChem* **2007**, *8*, 373–278.

LeBel, R. G.; Goring, D. A. I. *J. Chem. Eng. Data* **1962**, *7*, 100-101.

Lee, C.; Prakash, S.; Matouschek, A. *The Journal of biological chemistry* **2002**, *277*, 34760–5.

Lee, H. M.; Priestman, M. A.; Lawrence, D. S. *J. Am. Chem. Soc.* **2010**, *132*, 1446–1447.

Lee, H.-M.; Larson, D. R.; Lawrence, D. S. *ACS chemical biology* **2009**, *4*, 409–27.

Leriche, G.; Budin, G.; Darwich, Z.; Weltin, D.; Mély, Y.; Klymchenko, A. S.; Wagner, A. Chem. Comm. **2012**, *48*, 3224–6.

Levine, R. L. *Clin. Chem.* **1977**, *23*, 2292–2301.

Li, H.; Hah, J.; Lawrence, D. S. *Journal of the American Chemical Society* **2008**, *130*, 10474–5.

Li, X.; Zhao, X.; Fang, Y.; Jiang, X.; Duong, T.; Fan, C.; Huang, C. C.; Kain, S. R. *The Journal of biological chemistry* **1998**, *273*, 34970–5.

Lieberman, S. J.; Wasco, W.; MacLeod, J.; Satir, P.; Orr, G. A. *J. Cell Biol.* **1988**, *107*, 1809–1816.

Life Technologies. Molecular Probes nonfluorescent quenchers and photosensitizers. http://www.invitrogen.com/site/us/en/home/References/Molecular-Probes-The-Handbook/tables/Molecular-Probes-nonfluorescent-quenchers-and-photosensitizers.html (accessed March, 15 2013).

Lin, C.-W.; Jao, C. Y.; Ting, A. Y. *Journal of the American Chemical Society* **2004**, *126*, 5982–3.

Linder, K. E.; Metcalfe, E.; Nanjappan, P.; Arunachalam, T.; Ramos, K.; Skedzielewski, T. M.; Marinelli, E. R.; Tweedle, M. F.; Nunn, A. D.; Swenson, R. E. *Bioconjugate Chem.* **2011**, *22*, 1287–97.

Liu, C.-W.; Li, X.; Thompson, D.; Wooding, K.; Chang, T.; Tang, Z.; Yu, H.; Thomas, P. J.; DeMartino, G. N. *Molecular cell* **2006**, *24*, 39–50.

Lopes, U. G.; Erhardt, P.; Yao, R.; Cooper, G. M. *The Journal of biological chemistry* **1997**, *272*, 12893–6.

Loving, G. S.; Sainlos, M.; Imperiali, B. *Trends in biotechnology* **2010**, *28*, 73–83.

Luković, E.; González-Vera, J. a; Imperiali, B. *Journal of the American Chemical Society* **2008**, *130*, 12821–7.

Ma, Y.; Taylor, S. S. *J. Biol. Chem.* **2008**, *283*, 11743–11751.

Manning, G.; Whyte, D. B.; Martinez, R.; Hunter, T.; Sudarsanam, S. *Science* **2002**, *298*, 1912–1934.

Marcotte, P. a; Richardson, P. L.; Richardson, P. R.; Guo, J.; Barrett, L. W.; Xu, N.; Gunasekera, A.; Glaser, K. B. *Anal. Biochem.* **2004**, *332*, 90–9.

Marques, A. J.; Palanimurugan, R.; Matias, A. C.; Ramos, P. C.; Dohmen, R. J. *Chemical reviews* **2009**, *109*, 1509–36.

Marras, S. A. E.; Kramer, F. R.; Tyagi, S. *Nucleic acids research* **2002**, *30*, e122.

Matayoshi, E. D.; Wang, G. T.; Krafft, G. a; Erickson, J. *Science* **1990**, *247*, 954–8.

Mayer, G.; Heckel, A. *Angewandte Chemie (International ed. in English)* **2006**, *45*, 4900–21.

McBride, H. M.; Neuspiel, M.; Wasiak, S. *Current biology : CB* **2006**, *16*, R551–60.

McNeil P. L. *Current Protocol in Cell Biology* **2001**, Chapter 20:Unit 20.1.

Meng, L.; Mohan, R.; Kwok, B. H. B.; Elofsson, M.; Sin, N.; Crews, C. M. *Proceedings of the National Academy of Sciences* **1999**, *96*, 10403–10408.

Meyer, B. S.; Rademann, J. *The Journal of biological chemistry* **2012**, *11*. in press.

Michel, J. J. C.; Scott, J. D. *Annual review of pharmacology and toxicology* **2002**, *42*, 235–57.

Min, D. H.; Su, J.; Mrksich, M. *Angew. Chem., Int. Ed.* **2004**, *43*, 5973–5977.

Morris, M. C. *Cell biochemistry and biophysics* **2010**, *56*, 19–37.

Morris, M. C.; Deshayes, S.; Heitz, F.; Divita, G. *Biology of the cell / under the auspices of the European Cell Biology Organization* **2008**, *100*, 201–17.

Murakami, Y.; Matsufuji, S.; Kameji, T.; Hayashi, S.; Igarashi, K.; Tamura, T.; Tanaka, K.; Ichihara, A. *Nature* **1992**, *360*, 597–9.

Nagamitsu, T.; Sunazuka, T.; Tanaka, H.; Ōmura, S.; Sprengeler, P. A.; Smith, A. B. *Journal of the American Chemical Society* **1996**, *118*, 3584–3590.

Neefjes, J.; Dantuma, N. P. *Nature reviews. Drug discovery* **2004**, *3*, 58–69.

Nguyen, T.; Joshi, N. S.; Francis, M. B. *Bioconjugate Chem.,* **2006**, *17*, 869–72.

Ogawa, M., Kosaka, N., Longmire, M., Urano, Y., Choyke, P. L. and Kobayashi, H. *Mol. Pharm.* **2009**, *6*, 386-395.

Orrenius, S. *Toxicology letters* **2004**, *149*, 19–23.

Papa, S.; Sardanelli, a M.; Scacco, S.; Technikova-Dobrova, Z. *FEBS letters* **1999**, *444*, 245–9.

Pazos, E.; Vázquez, O.; Mascareñas, J. L.; Vázquez, M. E. *Chemical Society reviews* **2009**, *38*, 3348–59.

Pereira, M. P.; Kelley, S. O. *Journal of the American Chemical Society* **2011**, *133*, 3260–3.

Perroy, J.; Pontier, S.; Charest, P. G.; Aubry, M.; Bouvier, M. *Nature methods* **2004**, *1*, 203–8.

Pickart, C. M.; Cohen, R. E. *Nature reviews. Molecular cell biology* **2004**, *5*, 177–87.

Pidoux, G.; Taskén, K. *Journal of molecular endocrinology* **2010**, *44*, 271–84.

Place, R. F.; Noonan, E. J.; Giardina, C. *Biochemical pharmacology* **2005**, *70*, 394–406.

Poras, H.; Duquesnoy, S.; Dange, E.; Pinon, A.; Vialette, M.; Fournié-Zaluski, M.-C.; Ouimet, T. *The Journal of biological chemistry* **2012**, *287*, 20221–30.

Portbury, A. L.; Ronnebaum, S. M.; Zungu, M.; Patterson, C.; Willis, M. S. *Journal of molecular and cellular cardiology* **2012**, *52*, 526–37.

Quesada, V.; Ordóñez, G. R.; Sánchez, L. M.; Puente, X. S.; López-Otín, C. *Nucleic acids research* **2009**, *37*, D239–43.

Rahimi, N. *Molecular cancer therapeutics* **2012**, *11*, 538–48.

Rajendran, L.; Udayar, V.; Goodger, Z. V. *Trends in pharmacological sciences* **2012**, *33*, 215–22.

Reits, E. a; Benham, a M.; Plougastel, B.; Neefjes, J.; Trowsdale, J. *The EMBO journal* **1997**, *16*, 6087–94.

Reyes-Turcu, F. E.; Ventii, K. H.; Wilkinson, K. D. *Annual review of biochemistry* **2009**, *78*, 363–97.

Rhee, H.-W.; Choi, S. J.; Yoo, S. H.; Jang, Y. O.; Park, H. H.; Pinto, R. M.; Cameselle, J. C.;

Rhee, H.-W.; Lee, S. H.; Shin, I.-S.; Choi, S. J.; Park, H. H.; Han, K.; Park, T. H.; Hong, J.-I. *Angewandte Chemie (International ed. in English)* **2010**, *49*, 4919–23.

Rice, J. E.; Lindsay, J. G. In *Subcellular Fractionation*; Graham, J. M., Rickwood, D., Eds.; IRL Press: Oxford, England, 1997; pp 107-142.

Rittinger, K.; Budman, J.; Xu, J.; Volinia, S.; Cantley, L. C.; Smerdon, S. J.; Gamblin, S. J.; Yaffe, M. B. *Mol. Cell* **1999**, *4*, 153 166.

Rogers, S.; Wells, R.; Rechsteiner, M. *Science (New York, N.Y.)* **1986**, *234*, 364–8.

Romeo, Y.; Zhang, X.; Roux, P. P. *The Biochemical journal* **2012**, *441*, 553–69.

Ryu, H.; Lee, J.; Impey, S.; Ratan, R. R.; Ferrante, R. J. *Proc. Natl. Acad. Sci. U.S.A.* **2005**, *102*, 13915–13920.

Sandoval, F. J.; Roje, S.; Han, K.; Chung, D. S.; Suh, J.; Hong, J.-I. *Journal of the American Chemical Society* **2009**, *131*, 10107–12.

Sardanelli, A. M.; Signorile, A.; Nuzzi, R.; Rasmo, D. D.; Technikova-Dobrova, Z.; Drahota, Z.; Occhiello, A.; Pica, A.; Papa, S. *FEBS Lett.* **2006**, *580*, 5690–5696.

Saucerman, J. J.; Zhang, J.; Martin, J. C.; Peng, L. X.; Stenbit, A. E.; Tsien, R. Y.; McCulloch, A. D. *Proceedings of the National Academy of Sciences of the United States of America* **2006**, *103*, 12923–8.

Sawant, R.; Torchilin, V. *Molecular bioSystems* **2010**, *6*, 628–40.

Schmidtke, G.; Emch, S.; Groettrup, M.; Holzhutter, H. G. *The Journal of biological chemistry* **2000**, *275*, 22056–63.

Schwarze, S. R.; Hruska, K. a; Dowdy, S. F. *Trends in cell biology* **2000**, *10*, 290–5.

Scott, J. D.; Newton, A. C. *BMC biology* **2012**, *10*, 61.

Shabb, J. B. *Chem. Re*v. **2001**, *101*, 2381–2411.

Sharma, M.; Burré, J.; Südhof, T. C. *Science translational medicine* **2012**, *4*, 147ra113.

Sharma, V.; Agnes, R. S.; Lawrence, D. S. *Journal of the American Chemical Society* **2007**, *129*, 2742–3.

Sharma, V.; Lawrence, D. S. *Angew. Chem., Int. Ed.* **2009**, *48*, 7290–7292.

Sharma, V.; Wang, Q.; Lawrence, D. S. *Biochimica et biophysica acta* **2008**, *1784*, 94–9.

Shults, M. D.; Carrico-Moniz, D.; Imperiali, B. *Analytical biochemistry* **2006**, *352*, 198–207.

Shults, M. D.; Imperiali, B. *Journal of the American Chemical Society* **2003**, *125*, 14248–9.

Sikdar, A.; Roy, S.; Haldar, K.; Sarkar, S.; Panja, S. S. *Journal of fluorescence* **2013**.

Skalhegg BS and Tasken K. *Front Biosci* **2000,** 5, D678–D693,.

Smith, F. D.; Langeberg, L. K.; Scott, J. D. *Trends Biochem. Sci.* **2006**, *31*, 316–323.

Snyder, E. L.; Dowdy, S. F. *Expert opinion on drug delivery* **2005**, *2*, 43–51.

Soderling, S. H.; Beavo, J. *Current opinion in cell biology* **2000**, *12*, 174–9.

Strebhardt, K. *Nature reviews. Drug discovery* **2010**, *9*, 643–60.

Su, J.; Bringer, M. R.; Ismagilov, R. F.; Mrksich, M. *J. Am. Chem. Soc.* **2005**, *127*, 7280–7281.

Sun, H.; Low, K. E.; Woo, S.; Noble, R. L.; Graham, R. J.; Connaughton, S. S.; Gee, M. a; Lee, L. G. *Analytical chemistry* **2005**, *77*, 2043–9.

Sunahara, R. K.; Dessauer, C. W.; Gilman, A. G. *Annual review of pharmacology and toxicology* **1996**, *36*, 461–80.

T. Förster, *Fluorenzenz Organische Verbindungen.* Vandenhoech and Ruprecht: Göttingen, **1951**.

Tasken K, Skalhegg BS, Tasken KA, Solberg R, Knutsen HK, Levy FO, Sandberg M, Orstavik S, Larsen T, Johansen AK, Vang T, Schrader HP, Reinton NT, Torgersen KM, Hansson V, and Jahnsen T. *Adv Second Messenger Phosphoprotein Res* **1997**, *1*, 191–204.

Taskén, K.; Aandahl, E. M. *Physiological reviews* **2004**, *84*, 137–67.

Ting, A. Y., Kain, K. H., Klemke, R. L. and Tsien, R. Y. *Proc. Natl. Acad. Sci*. **2001**, *98*, 15003-8.

Toutchkine, A. PCT. Int. Appl., PCT/US2009/46238.

Tremblay, M. S.; Lee, M.; Sames, D. *Organic letters* **2008**, *10*, 5–8.

Tremblay, M. S.; Zhu, Q.; Martí, A. a; Dyer, J.; Halim, M.; Jockusch, S.; Turro, N. J.; Sames, D. *Organic letters* **2006**, *8*, 2723–6.

Turk, B.; Turk, D. S. A.; Turk, V. *The EMBO journal* **2012**, *31*, 1630–43.

Turro, N. J., Ramamurthy, V., Scaiano, J. C. Modern Molecular Photochemistry of Organic Molecules. Sausalito, Calif.: University Science Books, 2010.

Tyagi, S. and Kramer, F. R. *Nat. Biotech.* **1996**, *14*, 303-308.

Tyagi, S., Marras, S. A. E. and Kramer, F. R. *Nat. Biotech.* **2000**, *18*, 1191.

Urru, S. a M.; Veglianese, P.; De Luigi, A.; Fumagalli, E.; Erba, E.; Gonella Diaza, R.; Carrà, A.; Davoli, E.; Borsello, T.; Forloni, G.; Pengo, N.; Monzani, E.; Cascio, P.; Cenci, S.; Sitia, R.; Salmona, M. *Journal of medicinal chemistry* **2010**, *53*, 7452–60.

Veldhuyzen, W. F.; Nguyen, Q.; McMaster, G.; Lawrence, D. S. *Journal of the American Chemical Society* **2003**, *125*, 13358–9.

Velic, D.; Knapp, M.; Köhler, G. *J. Mol. Struct.* **2001**, *598*, 49–56.

Violin, J. D., Zhang, J., Tsien, R. Y. and Newton, A. C. *J. Cell Biol.* **2003**, *161*, 899-909.

Votano, J. R.; Parham, M.; Hall, L. H.; Kier, L. B.; Hall, L. M. *Chemistry & biodiversity* **2004**, *1*, 1829–41.

Wagner, B. D. *Molecules (Basel, Switzerland)* **2009**, *14*, 210–37. (b) Choi, J. Y.; Park, E. J.; Chang, S. H.; Kang, T. J. *Bulletin of the Korean Chemical Society* **2009**, *30*, 1452–1458.

Wakata, A., Lee, H.-M., Rommel, P., Toutchkine, A., Schmidt, M. and Lawrence, D. S. *J. Am. Chem. Soc.*, **2010**, *132*, 1578-82.

Wakata, A.; Cahill, S. M.; Blumenstein, M.; Gunby, R. H.; Jockusch, S.; Marti, A. a; Cimbro, B.; Gambacorti-Passerini, C.; Donella-Deana, A.; Pinna, L. A; Turro, N. J.; Lawrence, D. S. *Org. Lett.* **2008**, *10*, 301–4.

Wakata, A.; Lee, H.-M.; Rommel, P.; Toutchkine, A.; Schmidt, M.; Lawrence, D. S. *Journal of the American Chemical Society* **2010**, *132*, 1578–82.

Wang, Q.; Cahill, S. M.; Blumenstein, M.; Lawrence, D. S. *Journal of the American Chemical Society* **2006**, *128*, 1808–9.

Wang, Q.; Lawrence, D. S. *Journal of the American Chemical Society* **2005**, *127*, 7684–5.

Webb, M. R. *Molecular bioSystems* **2007**, *3*, 249–56.

Webb, M. R.; Corrie, J. E. *Biophysical journal* **2001**, *81*, 1562–9.

Webb, M. R.; Reid, G. P.; Munasinghe, V. R. N.; Corrie, J. E. T. *Biochemistry* **2004**, *43*, 14463–71.

Weissman, A. M.; Shabek, N.; Ciechanover, A. *Nature reviews. Molecular cell biology* **2011**, *12*, 605–20.

Weyler, S.; Baqi, Y.; Hillmann, P.; Kaulich, M.; Hunder, A. M.; Müller, I. A.; Müller, C. E. *Bioorg. Med. Chem. Lett.* **2008**, *18*, 223-227.

Wharton, D. C.; Tzagoloff, A. *Methods Enzymol.* **1967**, *10*, 245–250.

Whitby, F. G.; Masters, E. I.; Kramer, L.; Knowlton, J. R.; Yao, Y.; Wang, C. C.; Hill, C. P. *Nature* **2000**, *408*, 115–20.

Wójcik, C.; DeMartino, G. N. *The International Journal of Biochemistry & Cell Biology* **2003**, *35*, 579–589.

Wong, D. J.; Nuyten, D. S. A.; Regev, A.; Lin, M.; Adler, A. S.; Segal, E.; van de Vijver, M. J.; Chang, H. Y. *Cancer research* **2008**, *68*, 369–78.

Wunder, A.; Tung, C.-H.; Müller-Ladner, U.; Weissleder, R.; Mahmood, U. *Arthritis and rheumatism* **2004**, *50*, 2459–65.

Yaffe, M. B.; Rittinger, K.; Volinia, S.; Caron, P. R.; Aitken, A.; Leffers, H.; Gamblin, S. J.; Smerdon, S. J.; Cantley, L. C. *Cell* **1997**, *91*, 961–971.

Yaffe, M. B.; Rittinger, K.; Volinia, S.; Caron, P. R.; Aitken, A.; Leffers, H.; Gamblin, S. J.; Smerdon, S. J.; Cantley, L. C. *Cell* **1997**, *91*, 961–971.

Yang, H.; Zonder, J. A.; Dou, Q. P. *Expert opinion on investigational drugs* **2009**, *18*, 957–71.

Yang, H.; Zonder, J. A.; Dou, Q. P. *Expert opinion on investigational drugs* **2009**, *18*, 957–71.

Yeh, R.-H.; Yan, X.; Cammer, M.; Bresnick, A. R.; Lawrence, D. S. *The Journal of biological chemistry* **2002**, *277*, 11527–32.

Yoo, H.; Cha, H. J.; Lee, J.; Yu, E. O.; Bae, S.; Jung, J. H.; Sohn, I.; Lee, S. J.; Yang, K. H.; Woo, S. H.; Seo, S. K.; Park, I. C.; Kim, C. S.; Jin, Y. W.; Ahn, S. K. *Oncol. Rep.* **2008**, *19*, 1577–1582.

Yudushkin, I.; Schleifenbaum, A.; Kinkhabwala, A.; Neel, B. G.; Schultz, C.; Bastiaens, P. I. H. *Science* **2007**, *315*, 115–9.

Zhang, J.; Allen, M. D. *Molecular bioSystems* **2007**, *3*, 759–65.

Zhang, J.; Hupfeld, C. J.; Taylor, S. S.; Olefsky, J. M.; Tsien, R. Y. *Nature* **2005**, *437*, 569–73.

Zhang, J.; Ma, Y.; Taylor, S. S.; Tsien, R. Y. *Proceedings of the National Academy of Sciences of the United States of America* **2001**, *98*, 14997–5002.

Zheng, X.; Ruas, J. L.; Cao, R.; Salomons, F. a; Cao, Y.; Poellinger, L.; Pereira, T. *Molecular and cellular biology* **2006**, *26*, 4628–41.

Zondlo, S. C.; Gao, F.; Zondlo, N. J. *Journal of the American Chemical Society* **2010**, *132*, 5619–21.

Zou, K.; Cheley, S.; Givens, R. S.; Bayley, H. *J. Am. Chem. Soc.* **2002**, *124*, 8220–8229.

Zungu, M.; Schisler, J. C.; Essop, M. F.; McCudden, C.; Patterson, C.; Willis, M. S. *The American journal of pathology* **2011**, *178*, 4–11.